

Cal Poly

Caltech



UC Irvine

UCLA

**UC Santa
Barbara**

USC

RISK AND RESISTANCE MODELS OF GAS PIPELINE AND SEISMIC VULNERABILITY OF GAS STORAGE FACILITIES

**Yi Peng, Yousef Bozorgnia, Wadie Chalgham, Ali Mosleh, Jennifer
Donahue, Wenyang Zhang**

Natural Hazards Risk and Resiliency Research Center
University of California, Los Angeles

Douglas Honegger

D.G. Honegger Consulting, Arroyo Grande, CA, USA

Francois Ayello, Justin Gossard, Shane Finneran

DNV, Oakland, CA, USA

UCLA Project Principal Investigators:
Yousef Bozorgnia and Ali Mosleh

A report on research supported by California Energy Commission

Report GIRS-2023-10

DOI: 10.34948/N3T887

University of California, Los Angeles (headquarters)



Natural Hazards Risk & Resiliency Research Center
The B. John Garrick Institute for the Risk Sciences

RESISTANCE MODEL OF GAS PIPELINE AND SEISMIC VULNERABILITY OF GAS STORAGE FACILITIES

**Yi Peng, Yousef Bozorgnia, Wadie Chalgham, Ali Mosleh, Jennifer Donahue,
Wenyang Zhang**

Natural Hazards Risk and Resiliency Research Center
University of California, Los Angeles

Douglas Honegger

D.G. Honegger Consulting, Arroyo Grande, CA, USA

Francois Ayello, Justin Gossard, Shane Finneran

DNV, Oakland, CA, USA

UCLA Project Principal Investigators:
Yousef Bozorgnia and Ali Mosleh

A report on research conducted with support from California
Energy Commission

Report GIRS-2023-10
DOI: 10.34948/N3T887

Natural Hazards Risk & Resiliency Research Center
The B. John Garrick Institute for the Risk Sciences
University of California, Los Angeles (Headquarters)

September 2023

EXECUTIVE SUMMARY

This report presents the quantification of seismic risk for natural gas pipelines and gas storage facilities, as well as the development and application of the final product of the project: a user-friendly risk analysis software tool for estimating the probabilities of pipeline failure. The software reads pre-computed earthquake hazard estimates and predicts pipeline failure probabilities using the developed fragility database and risk model, enabling informed decisions on pipeline maintenance and management.

Firstly, a resistance model is developed for the quantification of seismic risk. The development of the resistance model began by establishing generic modeling approaches for surface faulting, liquefaction and landslide movements. Non-linear pipe-soil interaction finite element analyses (FEA) were conducted to assess the sensitivity of pipeline response to geohazard characteristics (such as displacement amplitude, direction of displacement) and pipeline characteristics (such as pipe diameter, thickness).

Using the results of the sensitivity analyses, we ranked each parameter from the most important to least important and performed 551,789 nonlinear pipe-soil interaction FEA using ANSYS software. These simulations took into account relevant soil and pipeline variables, such as length of pipeline exposed to ground movement, the direction of ground movement, soil strength, depth of burial, pipe diameter, pipe wall thickness, etc. The simulation results were compiled in a comprehensive fragility database, from which Bayesian network models of experienced pipe strains were created. Meanwhile, fracture resistance analysis using a well-established fracture model is used to evaluate the maximum strain the pipeline can survive. The experienced strain model and allowable strain model were then combined to predict a probability of failure of pipelines subjected to fault displacement, soil liquefaction and landslides. Finally, we incorporated the interaction between geohazards and other hazards, such as corrosion, to further refine the risk analysis.

The last part of the report explains the seismic vulnerability of pipelines and gas storage facilities, the risk model software, and the end-user guide of risk tools. We present an overall description of the free, open source, software platform for natural gas infrastructure risk assessment. The operational concept of the software platform allows users to (1) conduct risk assessment at different levels of complexity and sophistication, depending on the needs and objectives of the analysis; and (2) use the platform as decision support system for gas infrastructure proactive risk management, tracking and use of leading risk indicators, and (3) develop or upload new models and data if desired. Lastly, we provide a step-by-step guide and examples of how to run various analyses and use different risk management features of the software.

ACKNOWLEDGEMENTS

Support for this research project was provided by the California Energy Commission, Pacific Gas & Electric Company, and Southern California Gas Company. The support of these organizations is greatly appreciated. The opinions, findings, conclusions, or recommendations expressed in this publication are those of the authors and do not necessarily reflect the views of the study sponsors, the Natural Hazards Risk and Resiliency Research Center, or the Regents of the University of California.

Massive computations for this project were carried out on the supercomputers of The Texas Advanced Computing Center (TACC). Cooperations of the University of Texas DesignSafe and TACC are greatly appreciated. ANSYS donated numerous software licenses and also provided technical support. Cooperation of ANSYS is gratefully acknowledged.

TABLE OF CONTENTS

EXECUTIVE SUMMARY	I
ACKNOWLEDGEMENTS	II
TABLE OF CONTENTS	III
LIST OF FIGURES	V
LIST OF TABLES	XI
1 INTRODUCTION	1
2 PIPELINE PROPERTIES RELEVANT TO CALIFORNIA GAS TRANSMISSION PIPELINES	2
3 CHARACTERIZING PIPE-SOIL INTERACTION FOR FINITE ELEMENT ANALYSIS	4
3.1 DEPTH OF SOIL COVER	4
3.2 SOIL WEIGHT	5
3.3 SOIL PARTICLE SIZE DISTRIBUTION AND SOIL STRENGTH	5
3.4 AXIAL RESTRAINT INTERFACE FRICTION FACTOR	6
3.5 CHARACTERIZING GENERIC SOIL STRENGTH FOR CALIFORNIA	6
4 FINITE ELEMENT ANALYSIS PROCEDURE	17
4.1 GENERIC MODELING APPROACH FOR SURFACE FAULTING	19
4.2 GENERIC MODELLING APPROACH FOR LATERAL DISPLACEMENT	28
5 EXPERIENCED STRAIN MODEL FOR FAULT DISPLACEMENT	31
5.1 SENSITIVITY ANALYSIS FOR FAULT DISPLACEMENT	31
5.1.1 <i>Pipeline Response Sensitivity to Steel Type</i>	34
5.1.2 <i>Pipeline Response Sensitivity to Pipe Diameter</i>	36
5.1.3 <i>Pipeline Response Sensitivity to Pipe Wall Thickness</i>	37
5.1.4 <i>Pipeline Response Sensitivity to Internal Pressure</i>	38
5.1.5 <i>Pipeline Response Sensitivity to Pipeline Depth of Soil Cover</i>	39
5.1.6 <i>Pipeline Response Sensitivity to Levels of Soil Restraint</i>	40
5.1.7 <i>Pipeline Response Sensitivity to Soil Coefficient</i>	42
5.1.8 <i>Pipeline Response Sensitivity to Soil Unit Weight</i>	43
5.1.9 <i>Pipeline Response Sensitivity to Fault Displacement Direction</i>	44
5.2 GAS PIPELINE STRAIN EXPERIENCED BAYESIAN MODEL FOR FAULT DISPLACEMENT	48
5.2.1 <i>Fault Crossing Model Inputs for Fault Displacement</i>	48
5.2.2 <i>Gas Pipeline Strain Experienced Bayesian Model for Fault Displacement</i>	49
6 EXPERIENCED STRAIN MODEL FOR LANDSLIDES AND LIQUEFACTION	51
6.1 SENSITIVITY ANALYSIS FOR LATERAL DISPLACEMENT	51
6.1.1 <i>Pipeline Response Sensitivity to Steel Type</i>	52
6.1.2 <i>Pipeline Response Sensitivity to Pipe Diameter</i>	54
6.1.3 <i>Pipeline Response Sensitivity to Pipe Wall Thickness</i>	55
6.1.4 <i>Pipeline Response Sensitivity to Internal Pressure</i>	56
6.1.5 <i>Pipeline Response Sensitivity to Depth of Soil Cover</i>	57
6.1.6 <i>Pipeline Response Sensitivity to Levels of Soil Restraint</i>	58
6.1.7 <i>Pipeline Response Sensitivity to Soil Coefficient</i>	60
6.1.8 <i>Pipeline Response Sensitivity Soil Unit Weight</i>	61
6.1.9 <i>Pipe Soil Interactions – Movement Direction Angle</i>	62
6.1.10 <i>Pipeline Sensitivity to the Length of Pipe Exposed to Displacement</i>	62

6.2	GAS PIPELINE STRAIN EXPERIENCED BAYESIAN MODEL FOR LANDSLIDE & LIQUEFACTION	64
6.2.1	<i>Gas Pipeline Strain Experienced Bayesian Model Inputs for Lateral Displacement</i>	64
6.2.2	<i>Gas Pipeline Strain Experienced Bayesian Model for Lateral Displacement</i>	65
7	PIPELINE STRAIN CAPACITY MODELS	67
7.1	CORRODED PIPE STRAIN CAPACITY	67
7.1.1	<i>Sensitivity Analysis</i>	70
7.1.2	<i>Bayesian Model for Corroded Pipe Strain Capacity</i>	74
7.2	PRESSURE INTEGRITY STRAIN CAPACITY	75
7.2.1	<i>Pressure Integrity Tensile Strain Capacity</i>	75
7.2.2	<i>Pressure Integrity Compressive Strain Capacity</i>	78
8	PIPELINE VULNERABILITY MODEL VALIDATION	83
8.1	CASE STUDY 1: PIPELINE RESPONSE TO DECADES OF SAN ANDREAS FAULT CREEP	83
8.2	CASE STUDY 2: PIPELINE RESPONSE TO RIDGECREST EARTHQUAKE FAULT DISPLACEMENT	87
9	SEISMIC VULNERABILITY OF GAS STORAGE FACILITIES	90
10	RISK MODEL AND RISK SOFTWARE	111
10.1	SOFTWARE ARCHITECTURE	111
10.2	SOFTWARE INPUTS	111
10.3	INPUTS FROM PIPELINE OPERATORS	113
10.3.1	<i>GPS Data:</i>	113
10.3.2	<i>Pipeline Data:</i>	114
10.3.3	<i>Soil Data:</i>	115
10.4	PRECOMPUTED SITE DATA	115
10.4.1	<i>Fault Displacement Data</i>	115
10.4.2	<i>Landslide & Liquefaction Data:</i>	116
10.5	HOW ARE THE INPUTS USED	116
10.6	SOFTWARE OUTPUTS	116
10.7	BAYESIAN NETWORK MODELS	117
10.8	GROUND MOTION SCENARIOS	123
10.9	DYNAMIC SEGMENTATION	136
11	END-USER GUIDE FOR USING RISK TOOLS	138
11.1	SOFTWARE LOGIN	139
11.2	SOFTWARE DASHBOARD	141
11.3	CREATING A NEW QUANTIFICATION	143
11.4	PIPELINE RISK ASSESSMENT RESULTS	146
11.5	STORAGE FACILITIES	147
12	ACRONYMS	152
13	REFERENCES	153
	APPENDIX A: PRESSURE INTEGRITY STRAIN CAPACITY FORMULATION	155

LIST OF FIGURES

Figure 1: Place of the Resistance Model into the Overall Scope.....	1
Figure 2: Size Distribution of California Natural Gas Pipelines	2
Figure 3: Variation of Scaling Factors Based Upon Internal Friction Angle	12
Figure 4: Variation of Scaling Factors Based Upon Cohesion	12
Figure 5: Approximate Soil Spring Fit	15
Figure 6: Configuration of the Elbow Element.....	17
Figure 7: Configuration of the Soil Springs.....	18
Figure 8: Force-displacement Curves of the Soil Springs	18
Figure 9: Representation of the Applied Fault Movement	19
Figure 10: Pipe Segment Deformation 60 Degree Case	20
Figure 11: Pipe Segment Deformation 90 Degree Case	20
Figure 12: Tensile (positive) and Compressive (negative) Strain as a Function of Pipe Displacement	21
Figure 13: Definition of Fault Displacement Components in Pipeline Analyses	22
Figure 14: Diagram of Fault Orientation Defined by Dip Direction, Strike, Dip and Rake Angles Using the Aki-Richards Rake Definition.....	23
Figure 15: Transforming Geological Definition to Pipeline Analysis Case Definition	24
Figure 16: Various θ_H Crossing Angles with Identical Horizontal Fault Displacement Components.....	25
Figure 17: Definition of Horizontal and Vertical Angles for Bayesian Model.....	26
Figure 18: Process for Computing Bayesian Model Angles.....	27
Figure 19: Representation of the Applied Landslide Movement.....	28
Figure 20: Pipe Segment Deformation - 30 Degree Case.....	29
Figure 21: Tensile and Compressive Strain as a Function of Pipe Displacement - 30 Degree Case	29
Figure 22: Pipe Segment Deformation - 60 Degree Case.....	30
Figure 23: Tensile and Compressive Strain as a Function of Pipe Displacement – 60 Degree Case	30
Figure 24: Fault Displacement Relative to the Pipeline for CASE 1	32
Figure 25: Fault Displacement Relative to the Pipeline for CASE 2	33
Figure 26: Tensile and Compressive Strain as a Function of Pipe Displacement for Steels with Various Yield Strengths – CASE 1.....	35
Figure 27: Tensile and Compressive Strain as a Function of Pipe Displacement for Steels with Various Yield Strengths – CASE 2.....	35
Figure 28: Tensile and Compressive Strain as a Function of Pipe Displacement for Pipelines with Various Pipe Diameters – CASE 1.....	36

Figure 29: Tensile and Compressive Strain as a Function of Pipe Displacement for Pipelines with Various Pipe Diameters – CASE 2.....	36
Figure 30: Tensile and Compressive Strain as a Function of Pipe Displacement for Pipelines with Various Pipe Wall Thickness – CASE 1.....	37
Figure 31: Tensile and Compressive Strain as a Function of Pipe Displacement for Pipelines with Various Pipe Wall Thickness – CASE 2.....	37
Figure 32: Tensile and Compressive Strain as a Function of Pipe Displacement for Pipelines with Various Pipe Pressures – CASE 1.....	38
Figure 33: Tensile and Compressive Strain as a Function of Pipe Displacement for Pipelines with Various Pipe Pressures – CASE 2.....	38
Figure 34: Tensile and Compressive Strain as a Function of Pipe Displacement for Pipelines with Various Pipe Depth of Cover – CASE 1.....	39
Figure 35: Tensile and Compressive Strain as a Function of Pipe Displacement for Pipelines with Various Pipe Depth of Cover – CASE 2.....	39
Figure 36: Tensile and Compressive Strain as a Function of Pipe Displacement for Pipelines with Various Soil Friction Angles – CASE 1.....	40
Figure 37: Tensile and Compressive Strain as a Function of Pipe Displacement for Pipelines with Various Soil Friction Angles – CASE 2.....	40
Figure 38: Tensile and Compressive Strain as a Function of Pipe Displacement for Pipelines with Various Soil Shear Strengths – CASE 1.....	41
Figure 39: Tensile and Compressive Strain as a Function of Pipe Displacement for Pipelines with Various Soil Shear Strengths – CASE 2.....	41
Figure 40: Tensile and Compressive Strain as a Function of Pipe Displacement for Pipelines with Various Soil Coefficients – CASE 1.....	42
Figure 41: Tensile and Compressive Strain as a Function of Pipe Displacement for Pipelines with Various Soil Coefficients – CASE 2.....	42
Figure 42: Tensile and Compressive Strain as a Function of Pipe Displacement for Pipelines with Various Soil Weights – CASE 1.....	43
Figure 43: Tensile and Compressive Strain as a Function of Pipe Displacement for Pipelines with Various Soil Weights – CASE 2.....	43
Figure 44: Illustration of Symmetric Response for Fault Crossing Evaluations.....	44
Figure 45: Tensile and Compressive Strain as a Function of Pipe Displacement for Pipelines with Horizontal Angles 0° - 180° – CASE 1.....	45
Figure 46: Tensile and Compressive Strain as a Function of Pipe Displacement for Pipelines with Horizontal Angles 180° - 360° – CASE 1.....	45
Figure 47: Tensile and Compressive Strain as a Function of Pipe Displacement for Pipelines with Horizontal Angles 0° - 180° – CASE 2.....	46
Figure 48: Tensile and Compressive Strain as a Function of Pipe Displacement for Pipelines with Horizontal Angles 180° - 360° – CASE 2.....	46

Figure 49: Tensile and Compressive Strain as a Function of Pipe Displacement for Pipelines with Various Vertical Angles 15° - 89° – CASE 1	47
Figure 50: Tensile and Compressive Strain as a Function of Pipe Displacement for Pipelines with Various Vertical Angles 15° - 89° – CASE 2	47
Figure 51: Fault Displacement Model (top Tensile and Compressive Strain Calculated Using SSS, bottom, Tensile and Compressive Strain Calculated Using SFA) ...	50
Figure 52: Illustration of Pipeline Response for Lateral Displacement Sensitivity Cases 1 and 2.....	52
Figure 53: Tensile and Compressive Strain as a Function of Pipe Displacement for Steels with Various Yield Strengths – CASE 1.....	53
Figure 54: Tensile and Compressive Strain as a Function of Pipe Displacement for Steels with Various Yield Strengths – CASE 2.....	53
Figure 55: Tensile and Compressive Strain as a Function of Pipe Displacement for Pipelines with Various Pipe Diameters – CASE 1.....	54
Figure 56: Tensile and Compressive Strain as a Function of Pipe Displacement for Pipelines with Various Pipe Diameters – CASE 2.....	54
Figure 57: Tensile and Compressive Strain as a Function of Pipe Displacement for Pipelines with Various Pipe Wall Thickness – CASE 1.....	55
Figure 58: Tensile and Compressive Strain as a Function of Pipe Displacement for Pipelines with Various Pipe Wall Thickness – CASE 2.....	55
Figure 59: Tensile and Compressive Strain as a Function of Pipe Displacement for Pipelines with Various Pipe Pressures – CASE 1.....	56
Figure 60: Tensile and Compressive Strain as a Function of Pipe Displacement for Pipelines with Various Pipe Pressures – CASE 2.....	56
Figure 61: Tensile and Compressive Strain as a Function of Pipe Displacement for Pipelines with Various Pipe Depth of Cover – CASE 1	57
Figure 62: Tensile and Compressive Strain as a Function of Pipe Displacement for Pipelines with Various Pipe Depth of Cover – CASE 2	57
Figure 63: Tensile and Compressive Strain as a Function of Pipe Displacement for Pipelines with Various Soil Friction Angles – CASE 1	58
Figure 64: Tensile and Compressive Strain as a Function of Pipe Displacement for Pipelines with Various Soil Friction Angles – CASE 2.....	58
Figure 65: Tensile and Compressive Strain as a Function of Pipe Displacement for Pipelines with Various Soil Shear Strengths – CASE 1	59
Figure 66: Tensile and Compressive Strain as a Function of Pipe Displacement for Pipelines with Various Soil Shear Strengths – CASE 2	59
Figure 67: Tensile and Compressive Strain as a Function of Pipe Displacement for Pipelines with Various Soil Coefficients – CASE 1	60
Figure 68: Tensile and Compressive Strain as a Function of Pipe Displacement for Pipelines with Various Soil Coefficients – CASE 2	60

Figure 69: Tensile and Compressive Strain as a Function of Pipe Displacement for Pipelines with Various Soil Weights – CASE 1	61
Figure 70: Tensile and Compressive Strain as a Function of Pipe Displacement for Pipelines with Various Soil Weights – CASE 2	61
Figure 71: Tensile and Compressive Strain as a Function of Pipe Displacement for Pipelines with Various Movement Direction Angles – CASE 2.....	62
Figure 72: Tensile and Compressive Strain as a Function of Pipe Displacement for Pipelines with Various Amount of Pipe Exposed – CASE 1	63
Figure 73: Tensile and Compressive Strain as a Function of Pipe Displacement for Pipelines with Various Amount of Pipe Exposed – CASE 2	63
Figure 74: Experienced Strain Model for Lateral Displacement – Tensile and Compressive Strain Calculated Using SSS (top) and SFA (bottom).....	66
Figure 75: Reference Tensile Strain Capacity	69
Figure 76: Reference Compressive Strain Capacity	69
Figure 77: Maximum Tensile and Compressive Strain as a Function of Pipe Yield Strength	70
Figure 78: Maximum Tensile and Compressive Strain as a Function of Pipe Diameter .	71
Figure 79: Maximum Tensile and Compressive Strain as a Function of Pipe Thickness	71
Figure 80: Maximum Tensile and Compressive Strain as a Function of Pipe Internal Pressure	72
Figure 81: Maximum Tensile and Compressive Strain as a Function of Corrosion Flaw Size	72
Figure 82: Maximum Tensile Strain as a Function of Corrosion Flaw Depth.....	73
Figure 83: Tensile and Compressive Strain Capacity Models for Corrosion Flaws.....	75
Figure 84: Comparison of Actual Versus Predicted Tensile Strain Capacity	76
Figure 85: Cumulative Probability Distribution of Actual-to-Predicted Tensile Strain Capacity.....	77
Figure 86: Approximation of Cumulative Probability Distribution with a Log-Normal Distribution.....	77
Figure 87: Example of Local Pipe Wall Buckling	79
Figure 88: Comparison of PRCI Recommended Pressure-Integrity Strain Limits with Test Data.....	80
Figure 89: Examples of Pressure Integrity Compressive Strain Capacity Fragility Curves	81
Figure 90: Tensile and Compressive Strain Capacity Models Without Corrosion.....	82
Figure 91 Orientation of the NPS 12 San Andreas Fault Zone Crossing	83
Figure 92 Fault Displacement Pattern Used for Site-Specific Assessment of NPS 12 Pipeline Response	84
Figure 93 Deformed Shape of Exposed NPS 12 Pipeline at the San Andreas Fault Crossing.....	85

Figure 94 PISRAM Estimates of Cumulative Probability of Exceeding Tensile and Compressive Strain Levels for the NPS 12 Pipeline San Andreas Fault Crossing	86
Figure 95 NPS 6 Pipeline M6.4 Ridgecrest Fault Crossing; Photograph of Exposed Pipeline at the Primary Fault Rupture Site (left) and Terrestrial Lidar Survey of the Pipeline Deformed Shape (right)	88
Figure 96 PISRAM Estimates of Cumulative Probability of Exceeding Tensile and Compressive Strain Levels for the NPS 6 Pipeline Ridgecrest Fault Crossing ..	89
Figure 97: Locations of California Natural Gas Storage Fields	90
Figure 98: Operational Diagram of a Gas Storage Field.....	92
Figure 99: McDonald Island Vessels	93
Figure 100: McDonald Electrical and Piping Components.....	93
Figure 101: Hazus® Slight Damage Fragilities for Refineries and Oil Pumping Plants .	96
Figure 102: Hazus® Moderate Damage Fragilities for Refineries and Oil Pumping Plants	96
Figure 103: Hazus® Extensive Damage Fragilities for Refineries and Oil Pumping Plants	97
Figure 104: Hazus® Complete Damage Fragilities for Refineries and Oil Pumping Plants	97
Figure 105: Recommended Slight Damage Fragilities for Gas Storage Facilities	98
Figure 106: Recommended Moderate Damage Fragilities for Gas Storage Facilities	98
Figure 107: Recommended Extensive Damage Fragilities for Gas Storage Facilities	99
Figure 108: Recommended Complete Damage Fragilities for Gas Storage Facilities	99
Figure 109: Estimated PGA Contours for the 1994 Northridge Earthquake	100
Figure 110: Post-earthquake reconnaissance of the Aliso Canyon storage field facility	101
Figure 111: Google Earth Image of Marathon Los Angeles Refinery Complex.....	106
Figure 112: Playa Del Rey Gas Storage Field Site.....	106
Figure 113: La Goleta Gas Storage Field Site	107
Figure 114: Los Medanos Gas Storage Field Site.....	107
Figure 115: Aliso Canyon Gas Storage Field Site	108
Figure 116: Comparison of Recommended Gas Storage Field Slight Damage State Fragility with Pumping Station and Refinery Fragilities.....	109
Figure 117: Comparison of Recommended Gas Storage Field Complete Damage State Fragility with Pumping Station and Refinery Fragilities.....	109
Figure 118: Recommended Fragility Relationship for Gas Storage Facilities	110
Figure 119: Software Architecture	113
Figure 120: GPS Data Input Example.....	114
Figure 121: Pipeline Data Input Example.....	115
Figure 122: Soil Data Input Example.....	115
Figure 123: POF Calculation Steps	116

Figure 124: Software Outputs.....	117
Figure 125: Fault Displacement BN.....	119
Figure 126: Landslide and Liquefaction BN.....	120
Figure 127: Pipe Capacity BN.....	121
Figure 128: POF BN	122
Figure 129 Quantification Process Flow Chart	138
Figure 130 Software Dashboard.....	139
Figure 131 Account Creation.....	140
Figure 132 Software Login After Account Creation	140
Figure 133 Option to Create a New Quantification or Load Previous Quantification Results.....	141
Figure 134 Load Previous Quantification Results Feature	141
Figure 135 The User Needs to Choose the Pipeline from the Dropdown Menu Showing the Saved Pipelines List	142
Figure 136 The User has the Option to Delete a Pipeline from the List.....	142
Figure 137 The User has to Enter the GPS Data of the Pipeline	143
Figure 138 The User has to Enter the Pipeline Data (Diameter, Thickness, and Depth of cover)	144
Figure 139 The User has to Enter the Soil Data	144
Figure 140 The Quantification Control tab.....	145
Figure 141 Thresholds for Color Coding of the POF of the Pipe Segments	145
Figure 142 Results Table	146
Figure 143 Color Coded Map Results	147
Figure 144 Aliso Canyon Results	147
Figure 145 Honor Rancho Results	148
Figure 146 Playa Del Rey Results	148
Figure 147 La Goleta Results	148
Figure 148 McDonald Island Results	149
Figure 149 Los Medanos Storage Facility Results	149
Figure 150 Pleasant Creek Results.....	149
Figure 151 Gill Ranch Results	150
Figure 152 Kirby Hills Results.....	150
Figure 153 Lodi Storage Results.....	150
Figure 154 Central Valley Gas Storage Results.....	151
Figure 155 Wild Goose Storage Results	151

LIST OF TABLES

Table 1: Mileage of California Natural Gas Pipelines by Size	3
Table 2: Minimum Depths of Cover in ASME B31.8	5
Table 3: Properties of Various California Geological Units	7
Table 4: California Geologic Units Categorized by Cohesion	8
Table 5: Soil Spring Values for 3 feet of Cover	9
Table 6: Soil Spring Values for 5 feet of Cover	10
Table 7: Soil Spring Values for 10 feet of Cover	11
Table 8: Approximate Soil Spring Parameters for California Based upon Depth of Cover	14
Table 9: Recommended Soil Spring Parameters for California Based upon Depth of Cover.....	16
Table 10: Data Used for Sensitivity Analysis for Fault Displacement.....	31
Table 11: Variable Values Examined in the Sensitivity Analyses for Fault Displacement	34
Table 12: Relative Importance of Input Parameters for the Gas Pipeline Strain Experience Model	48
Table 13: Model Discretization using Sensitivity Analysis for Fault Displacement	49
Table 14: Data Used for Sensitivity Analysis	51
Table 15: Relative Importance of Input Parameters for the Gas Pipeline Strain Experience Model for Lateral Displacement.....	64
Table 16: Model Discretization using Sensitivity Analysis for Lateral Displacement	65
Table 17: Summary of Key Parameters for TSC and CSC Models.....	68
Table 18: Data Used for Sensitivity Analysis	70
Table 19: Relative Importance of Input Parameters for the Gas Pipeline Maximum Allowable Strain Model	74
Table 20: Maximum Allowable Strain Model Discretization using Sensitivity Analysis	74
Table 21: Assumed Girth Weld Flaw Length Probability	78
Table 22: Hazus® Fragility Definitions for Refineries and Oil Pumping Plants	94
Table 23: Hazus® Facility Loss Ratios	95
Table 24: Median Damage State Estimates for PGA of 0.85g	101
Table 25: Comparison of Fragilities for Water and Oil Pumping Plants	102
Table 26: Comparison of Hazus® Fragilities for Small Refineries and Water Treatment Plants	103
Table 27: Comparison of Hazus® Fragilities for Large Refineries and Large Water Treatment Plants	103

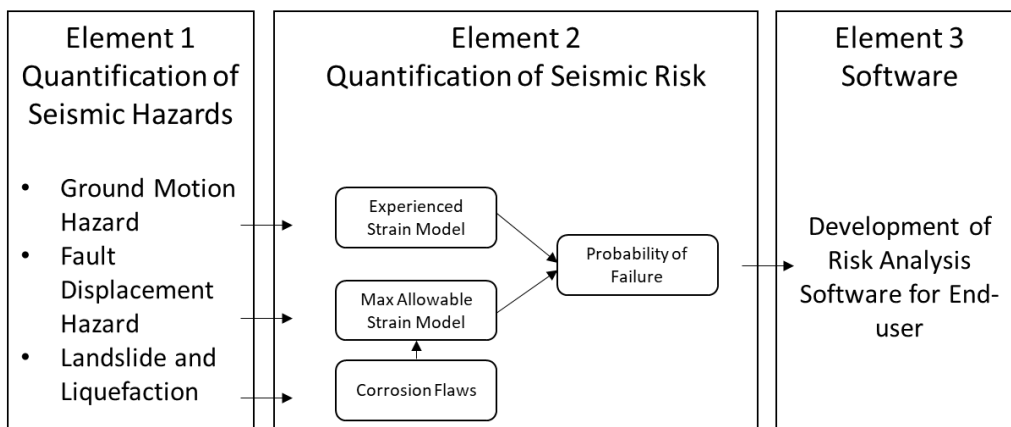
Table 28: Median PGA Capacity for Anchored Water Treatment Plant Subcomponents	104
Table 29: Median PGA Capacity for Anchored Refinery Subcomponents.....	105
Table 30: Recommended Gas Storage Field Fragility Parameters	110
Table 31 Ground Motion Scenarios	124
Table 32 The Units Required in the Inputs Fields	144

1 Introduction

The structural integrity of pipelines under seismic loading depends on the fracture resistance of the pipeline materials. The fracture resistance depends on a variety of material and environmental conditions. The material conditions include metallurgical factors and any pre-existing defects. The environmental factors include corrosion and environmentally assisted cracking. The environmental effects on materials result in a fracture resistance. The overall project PIR 18-02 can be sub-divided into three large “elements” (Figure 1). Element 1 is on the Quantification of Seismic Hazards, including earthquake ground motion, fault displacement, landslides and liquefaction. The resistance model is part of the second element of project: Quantification of Seismic Risk. This second element provides a model for the third element: Development of Risk Analysis Software for End-Users. The second element relates levels of seismic-induced hazards to failure probability of engineered components and includes time dependent degradation mechanisms to provide a full risk picture.

As shown in Figure 1, this report presents elements 2 and 3, the development of the Resistance Model and Risk Model, as well as the development of risk analysis software for end-users. Chapters 2 to 7 explain the development of the Resistance Model. First, a finite element analysis (FEA) of stresses using geohazard characteristics (such as displacement amplitude, direction of displacement) and pipeline characteristics (such as pipe diameter, thickness) are used to create a resistance model. Second, fracture resistance analysis using a well-established fracture model is used to evaluate the maximum strain the pipeline can survive. Finally, these two models are combined to predict a probability of failure. Then, the interaction (mainly through wall thinning) between geohazards and other hazards (such as corrosion) will be incorporated. Moreover, validation of the pipeline vulnerability model is explained in Chapter 8. Chapter 9 explains seismic vulnerability of gas storage facilities. The risk model software and end-user guide of risk tools are explained in the last two chapters. Chapter 10 provides an overall description of the free, open source, software platform for Natural Gas Infrastructure risk assessment and proactive risk management. Chapter 11 provides step by step guide and examples on how to run various analyses and use different risk management features of the software.

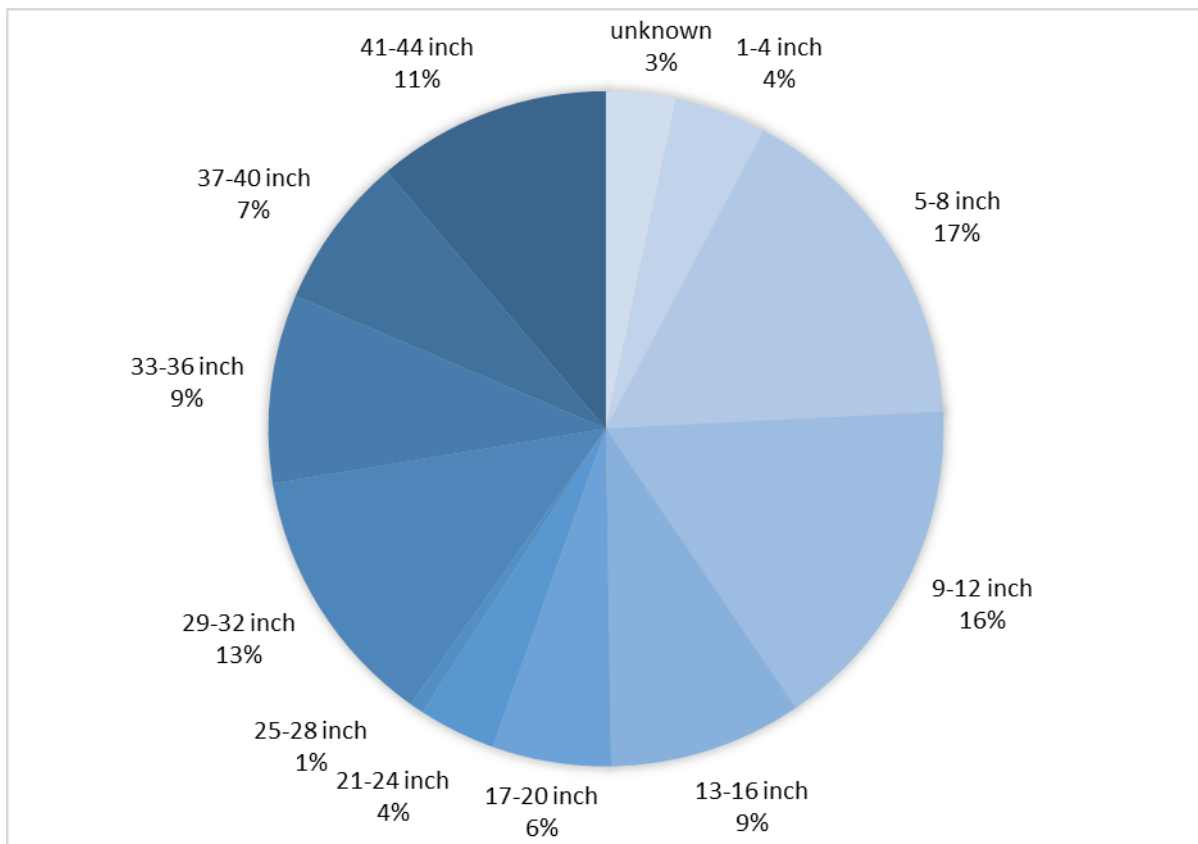
Figure 1: Place of the Resistance Model into the Overall Scope



2 Pipeline Properties Relevant to California Gas Transmission Pipelines

The natural gas transmission pipeline system in California includes a wide range of pipe sizes from NPS 4 to NPS 42¹. The distribution of sizes based upon information provided by the CEC is illustrated in Figure 2: Size Distribution of California Natural Gas Pipelines. Table 1 provides an alternate means to examine the distribution of gas pipeline sizes in California.

Figure 2: Size Distribution of California Natural Gas Pipelines



¹ NPS is an abbreviation for Nominal Pipe Size and provides a consistent reference for pipe sizes. Pipe sizes less than NPS 14 have outside diameters that are some fraction of an inch larger than the NPS size. For example, an NPS 10 pipe has an outside diameter of 10.75 inches.

Table 1: Mileage of California Natural Gas Pipelines by Size

Size Category	Size Range	Mileage	Percentage
Small	Less than NPS 8	2,559	20
Intermediate	NPS 10 to NPS 16	2,388	18
Large	NPS 18 to NPS 30	2,997	23
Very Large	NPS 32 to NPS 42	3,677	28

Pipeline wall thickness is a function of pipe diameter, operating pressure, pipe steel yield strength, and class location, as shown by the equation below.

$$t = \frac{PD}{2F\sigma_y}$$

Where:

- P = operating pressure
- D = pipe outer diameter
- F = class factor (0.5 to 0.72)
- σ_y = pipe steel yield stress

In addition, there are specified permissible minimum wall thickness limits in line-pipe standard API 5L. These permissible minimum wall thicknesses range from 0.156 inches for NPS 4 pipe to 0.250 inches for NPS 42 pipe. The operating pressures for transmission pipelines in the SoCalGas/SDG&E system range from 100 psi to 1,032 psi². This range is assumed to cover the range of operating pressures for other gas transmission pipelines in California as well as pipelines that may be constructed in the future.

The largest wall thickness is associated with the largest pipe diameter and pressure and the lowest pipe yield strength and location factor. Assuming 1,032 psi as the maximum operating pressure in California, the maximum pipe wall thickness is estimated to be 1.238 inches using a location factor of 0.5 and Grade B steel.

² Response to third data request from Shell Energy North as part of the 2009 Biennial Cost Allocation Proceeding (A.08-02-001), <https://www.socalgas.com/regulatory/documents/a-08-02-001/Shell-03.doc>, [last accessed May 10, 2022].

3 Characterizing Pipe-Soil Interaction for Finite Element Analysis

Soil surrounding a buried pipeline provides both the means by which ground displacement transfers load to the pipeline and a means by which the ground can resist the loads imposed by ground displacement. The most direct example of this is a straight pipeline exposed to ground displacement over a limited length in a direction purely parallel to the axis of the pipeline. The axial load transferred from the ground to the pipeline within the zone of ground displacement is resisted by axial soil restraint on either side of the portion of pipeline exposed to ground displacement. For simplicity, the soil loads transferred to the pipeline will be referred to as “soil restraint”.

For a particular pipeline size, the level of soil restraint varies with the following parameters:

- Depth of soil cover
- Effective soil weight
- Soil particle size distribution
- Smoothness of the pipe coating (for axial soil restraint)

The soil restraint is modelled using non-linear springs that are assumed to act independently in three orthogonal directions oriented in the axial, horizontal, and vertical directions. Tests to investigate oblique soil restraint the vertical and horizontal plane do not provide conclusive evidence supporting or refuting this assumption. Small-scale tests and numerical analysis methods seem to refute the assumption of independent action (Daiyan et al., 2010, Hsu and Hung, 2001, 2006). Large-scale tests examining horizontal oblique ground displacement tend to support the assumption (Honegger et al, 2011). Since the majority of ground displacement hazards for natural gas pipelines in California can be characterized as primarily horizontal ground displacement, adopting the assumption of independent orthogonal soil springs is considered appropriate.

3.1 Depth of Soil Cover

For economic reasons, the depth of cover over pipelines is always minimized to the extent possible. The minimum depth of cover for gas pipelines is specified in standard ASME B31.8 and is provided below for reference.

Table 2: Minimum Depths of Cover in ASME B31.8

Location	Cover, in		
	Normal Excavation	Rock Excavation (requires blasting)	
		Pipe Size	
		NPS 20 and Smaller	Larger Than NPS 20
Class 1	24	12	18
Class 2	30	18	18
Classes 3 and 4	30	24	24
Public Road Drainage Ditch	36	24	24
Railroad Crossings	36	24	24

Examples of situations where a greater depth of cover is required include agricultural areas subject to deep plowing, locations where excessive surface loads are possible, to pass below existing buried infrastructure, and most trenchless installations. We have assumed depths of cover up to 10 feet. Greater depths of cover have not been considered as this is a rare situation that is inherently highly vulnerable to damage from permanent ground displacement.

3.2 Soil Weight

The effective soil weight is most influenced by whether the pipeline is above or below the water table. Given the generally shallow depths of cover over pipelines, it is assumed the typical installation is above the water table. With this assumption, the range in the effective soil weight is assumed to be 90 pcf to 120 pcf.

3.3 Soil Particle Size Distribution and Soil Strength

The particle size distribution in soil can have considerable variation. Soils consisting primarily of coarse-grained particles (mean diameter greater than 0.074 mm) are generally considered “sand” with the strength represented by an internal friction angle. Finer particles, silts and clays are generally considered “clay” with the strength represented by an undrained shear strength.

The most common test to assess soil strength is a direct shear test. Soil samples are sheared at controlled rate of displacement under different levels of vertical load that represents the vertical stress in the field. The tests should be run at moisture contents representing actual field conditions (not saturated) and are therefore appropriate for all soil types in applications for pipeline evaluations. For pipeline applications, the vertical stress of interest is low compared to what would be relevant for typical foundation design. For example, the vertical stress for an NPS 24 pipeline with 3 feet of cover is roughly 400 psf while the design for spread footing for a structure would be interested in the shear strength at a vertical stress of 2,000 psf or greater.

The small sample size of standard direct shear tests (2.5 inches in diameter for circular shear boxes or 2.5 inches on a side for square shear boxes) and the low confining vertical stress of interests,

amplifies the variability in results that can arise from lack of uniformity in the prepared soil sample. Plots of the maximum shear strength of the soil sample versus the vertical stress are used to define the internal friction angle or shear strength. In practice, some judgment is generally used to interpret the results of the direct shear tests such that strength is characterized solely by an internal friction angle (sandy soils) and a single shear strength (clay soils). The internal friction angle for sand soils typically ranges from 30° to 50° and clay soils with undrained shear strengths of 300 psf to 1,000 psf.

For clay soils, the soil restraint is derived from shear failure within the clay at the clay-to-coating interface and is thus equal to the soil shear strength acting around the circumference of the pipeline.

3.4 Axial Restraint Interface Friction Factor

Axial soil restraint in sand soil is derived from the stress normal to the surface of the pipeline and the friction that can develop between the soil and the pipe surface. The interface friction angle that defines the sliding friction can approach the internal friction angle of the soil for very rough coatings or coatings that are soft enough to allow sand particles to become partially embedded. Smooth and hard coatings can have interface friction angles that approach 60% of the internal friction angle of the soil.

3.5 Characterizing Generic Soil Strength for California

The most common approach to characterizing soil strength for pipe-soil interaction analysis is to define either an internal friction angle (granular soils that exhibit drained response) or a cohesive shear strength (fine-grained soil that exhibit undrained response). This is the approach taken in developing the Bayesian model. Where this distinction cannot be made, both internal friction angle and shear strength are used to define pipeline soil loading.

The Bayesian model used to estimate pipeline response to ground displacement can accommodate situations where there is no information on soil strength by assuming any of the soil strength parameters used to define the model are possible. As an alternative, representative soil properties for different surficial geological units in California, defined as part of the characterization of landslide hazards, were used to define a set of soil strength parameters representative of the entire state of California.

Soil information for various geological units in northern and southern California are listed in Table 3. To examine how the soil load on a pipeline varies among the different soil units, the soils data were segregated into four groups according to the value of cohesion as shown in Table 4. Soil spring values were computed based upon the cohesion and internal friction angle for depths of cover of 3 feet, 5 feet and 10 feet. The results are shown in Table 5 through Table 7. As the goal was to try to represent the soil properties by a single internal friction angle or cohesion value, scale factors were defined as the ratio of the spring force including internal friction angle and cohesion to the spring values with only internal friction angle or cohesion. The trends of these ratios are shown in Figure 3 and Figure 4. The trends in scaling ratios for scaling by internal friction angle are much better behaved than the scaling according to cohesion. The axial and horizontal soil

spring scaling factors using internal friction angle are relatively constant for depths of cover of 5 and 10 feet. This observation led to a decision to assign an internal friction angle scaling factor based upon depth of cover.

Table 3: Properties of Various California Geological Units

Geologic Unit ID	Geologic Description	Cohesion (psf)	friction angle (°)
3	Southern California crystalline	359	36.9
5	Southern California Kss	424	33.4
8	Southern California Qal3	207	32.2
10	Southern California Qoa	232	32
12	Southern California QT	359	31.4
14	Southern California Tsh	443	30.2
15	Southern California Tss	374	32.8
16	Southern California Tv	503	30.5
20	Northern California crystalline	547	32
21	Northern California KJf	577	32
22	Northern California Kss	579	31
25	Northern California Qal3	437	24.3
27	Northern California Qoa	564	26.8
29	Northern California QT	606	28.5
30	Northern California sp	564	28
31	Northern California Tsh	606	26.8
32	Northern California Tss	627	28.3
33	Northern California Tv	401	33

Table 4: California Geologic Units Categorized by Cohesion

Geologic Unit ID	Geologic Description	Cohesion (psf)	Internal Friction Angle (°)
8	Southern California Qal3	207	32.2
10	Southern California Qoa	232	32
12	Southern California QT	359	31.4
3	Southern California crystalline	359	36.9
15	Southern California Tss	374	32.8
33	Northern California Tv	401	33
5	Southern California Kss	424	33.4
25	Northern California Qal3	437	24.3
14	Southern California Tsh	443	30.2
16	Southern California Tv	503	30.5
20	Northern California crystalline	547	32
27	Northern California Qoa	564	26.8
30	Northern California sp	564	28
21	Northern California KJf	577	32
22	Northern California Kss	579	31
29	Northern California QT	606	28.5
31	Northern California Tsh	606	26.8
32	Northern California Tss	627	28.3

Table 5: Soil Spring Values for 3 feet of Cover

Geologic Unit ID	Maximum Soil Spring Value (kip/ft)			
	Axial	Horizontal	Bearing	Uplift
8	2.0	8.7	32.4	2.7
10	2.0	9.0	31.9	2.9
12	2.5	10.4	31.0	3.9
3	2.6	11.2	60.5	4.1
15	2.6	10.6	36.5	4.1
33	2.7	10.9	37.6	4.3
5	2.8	11.2	39.7	4.5
25	2.6	11.3	16.5	4.3
14	2.7	11.4	28.1	4.5
16	2.9	12.1	29.6	5.0
20	3.0	12.5	35.1	5.4
27	2.9	12.7	21.6	5.4
30	2.9	12.7	24.0	5.4
21	3.0	12.9	35.4	5.7
22	3.0	12.9	32.0	5.6
29	2.9	13.2	25.5	5.8
31	2.9	13.2	22.1	5.7
32	2.9	13.4	25.2	5.9
Mean	2.7	11.7	31.4	4.7
Standard Deviation	0.30	1.40	9.56	0.97

Table 6: Soil Spring Values for 5 feet of Cover

Geologic Unit ID	Maximum Soil Spring Value (kip/ft)			
	Axial	Horizontal	Bearing	Uplift
8	2.4	14.0	44.2	4.9
10	2.4	14.3	43.5	5.2
12	2.9	16.2	41.9	6.6
3	3.1	17.7	81.3	7.1
15	3.0	16.4	49.2	6.9
33	3.1	16.8	50.6	7.3
5	3.2	17.1	53.3	7.6
25	2.9	17.3	21.8	7.0
14	3.1	17.4	37.6	7.5
16	3.3	18.3	39.5	8.3
20	3.4	18.9	46.7	8.9
27	3.2	19.1	28.3	8.7
30	3.2	19.1	31.5	8.8
21	3.4	19.3	47.0	9.3
22	3.4	19.3	42.3	9.2
29	3.3	19.7	33.4	9.3
31	3.2	19.7	28.7	9.2
32	3.3	20.0	33.0	9.6
Mean	3.1	17.8	41.9	7.9
Standard Deviation	0.29	1.81	13.09	1.42

Table 7: Soil Spring Values for 10 feet of Cover

Geologic Unit ID	Maximum Soil Spring Value (kip/ft)			
	Axial	Horizontal	Bearing	Uplift
8	2.57	5.78	15.44	3.43
10	2.34	5.20	14.37	3.15
12	1.69	4.06	10.86	2.36
3	1.87	4.63	20.98	2.65
15	1.69	3.97	12.45	2.37
33	1.62	3.81	12.26	2.29
5	1.57	3.69	12.44	2.24
25	1.31	3.62	4.88	1.83
14	1.45	3.59	8.51	2.05
16	1.37	3.33	8.17	1.94
20	1.39	3.16	9.14	1.91
27	1.28	3.11	5.32	1.72
30	1.30	3.11	5.95	1.76
21	1.39	3.07	8.85	1.87
22	1.37	3.06	7.93	1.83
29	1.30	2.98	5.99	1.72
31	1.27	2.98	5.11	1.67
32	1.30	2.91	5.76	1.69
Mean	4.0	31.6	68.2	15.1
Standard Deviation	0.30	1.47	21.93	1.77

Figure 3: Variation of Scaling Factors Based Upon Internal Friction Angle

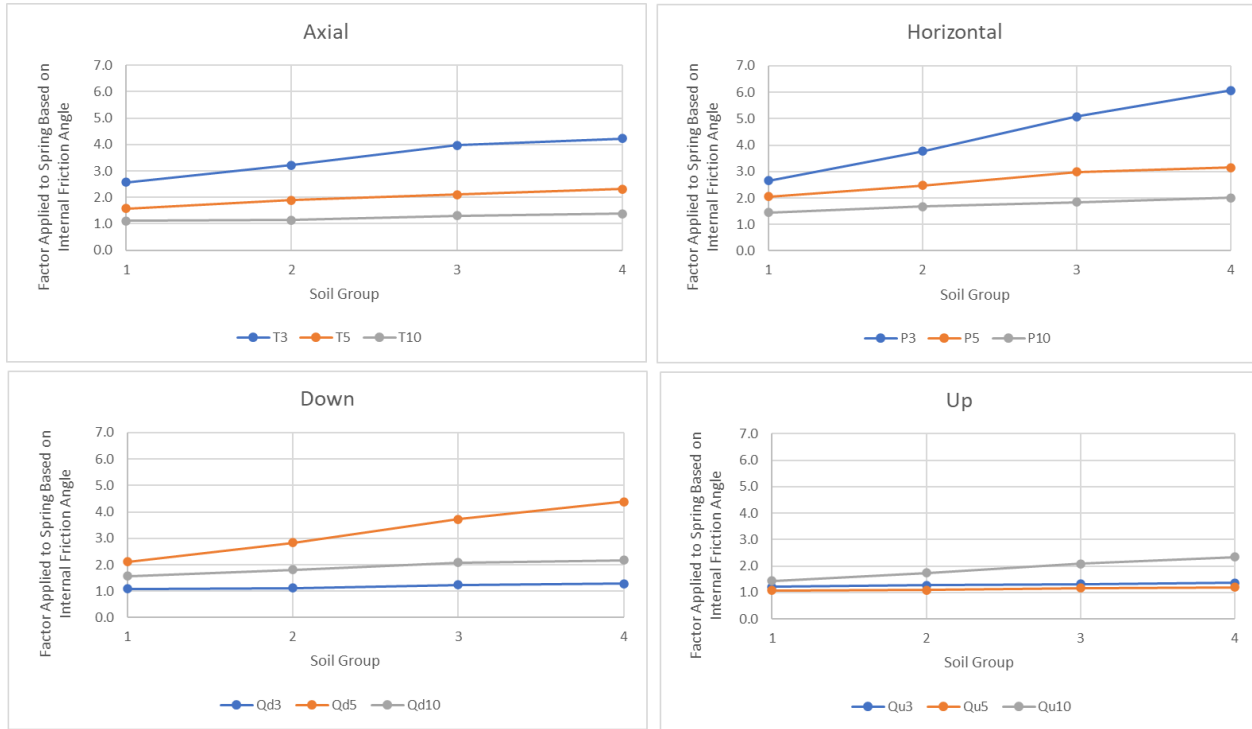
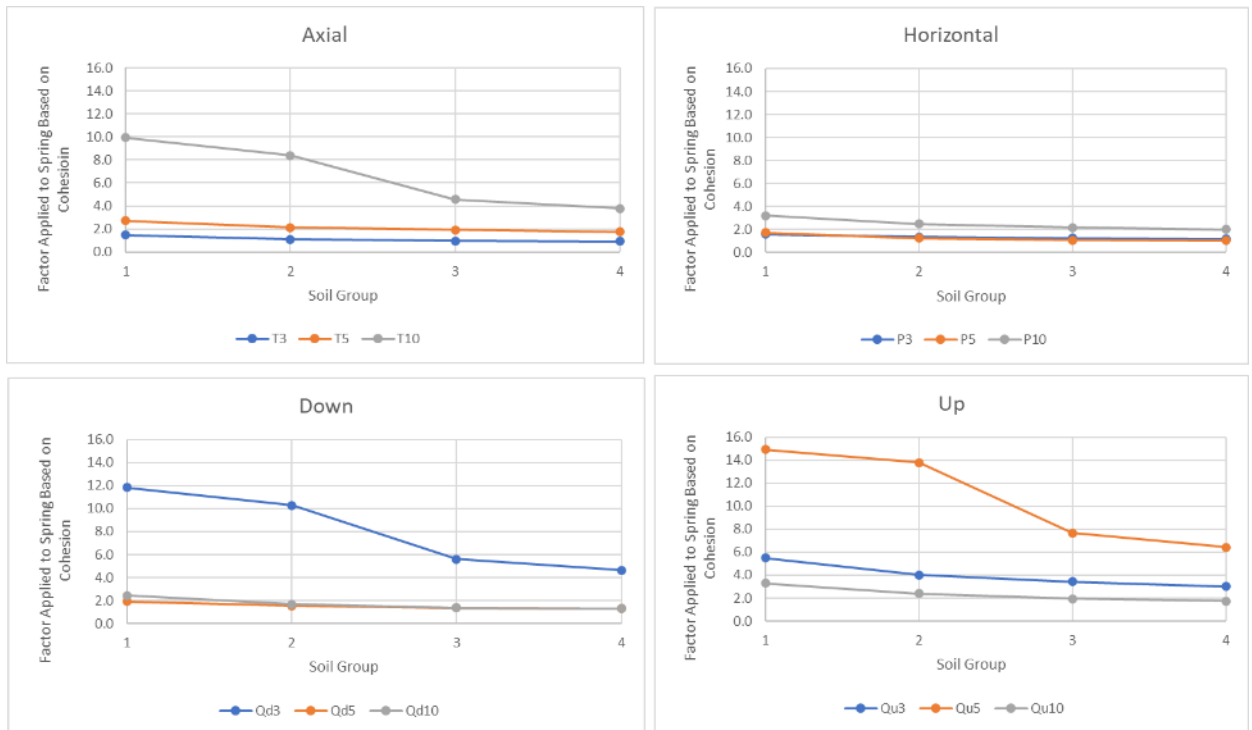


Figure 4: Variation of Scaling Factors Based Upon Cohesion



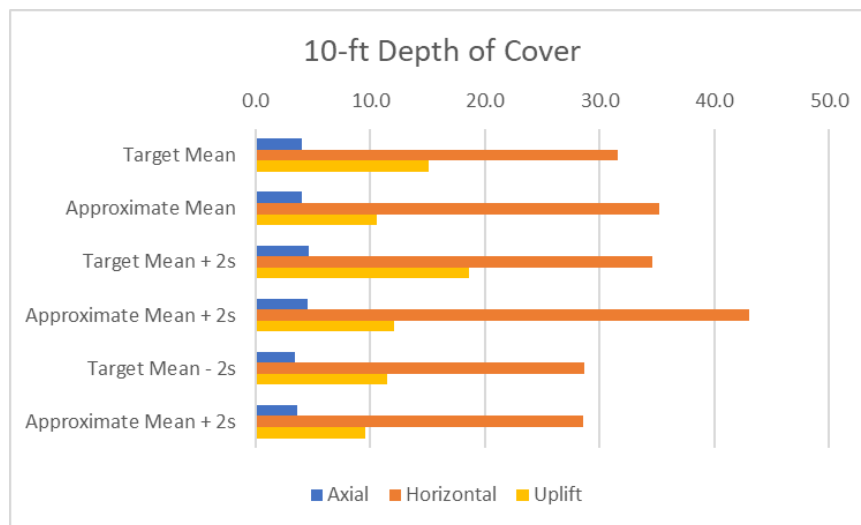
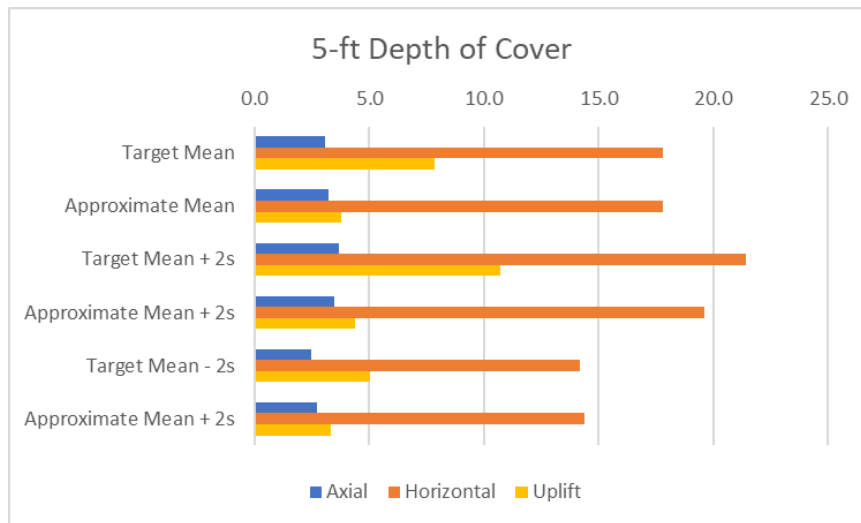
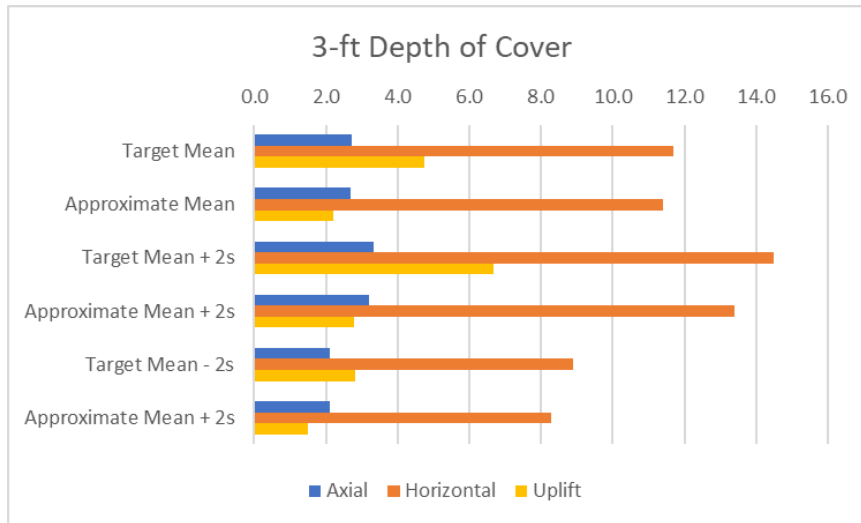
This was accomplished by setting target soil spring values as the average of the calculated values for each depth of cover and then iterating on assumed internal friction angles and horizontal pressure coefficient, K_0 to obtain a reasonable fit to the axial and horizontal soil spring values. The interface friction factor was assumed to be 0.7 and the soil unit weight was assumed to be 120 pcf. The pipeline diameter was assumed to be 24 inches for the calculation. This is the same pipe diameter used to assess pipeline response sensitivity as discussed in Section 5.1.

Pipeline response will be most impacted by changes in axial and lateral soil restraint as the uplift resistance for typical pipeline burial depth is much less than the bearing resistance. This results in relative vertical displacement forcing the pipeline to be pulled up out of the ground. Once a fit to the average soil spring values was determined, the friction angle was varied to capture plus or minus two standard deviations in soil spring values computed with internal friction angle and cohesion.

Table 8: Approximate Soil Spring Parameters for California Based upon Depth of Cover

Depth of Cover (feet)	Target	Maximum Soil Spring Value (kip/ft)			
		Axial	Horizontal	Bearing	Uplift
3	Mean	2.7	11.7	31.4	4.7
	$K_o = 1.5, f = 50^\circ$	2.7	11.4	1022	2.2
	Mean + 2s	3.3	14.5	50.5	6.7
	$K_o = 1.5, f = 50^\circ$	2.7	11.4	1022	2.2
	Mean - 2s	2.1	8.9	12.2	2.8
	$K_o = 1.5, f = 42^\circ$	2.1	8.3	121	1.5
5	Mean	3.1	17.8	41.9	7.9
	$K_o = 1.2, f = 46^\circ$	3.2	17.8	308	3.8
	Mean + 2s	3.7	21.4	68.1	10.7
	$K_o = 1.2, f = 50^\circ$	3.5	19.6	624	4.4
	Mean - 2s	2.5	14.2	15.7	5.0
	$K_o = 1.2, f = 41^\circ$	2.7	14.4	139	3.3
10	Mean	4.0	31.6	68.2	15.1
	$K_o = 0.8, f = 40^\circ$	4	35.2	197	10.6
	Mean + 2s	4.6	34.6	112	18.6
	$K_o = 0.8, f = 44^\circ$	4.5	43	361	12.1
	Mean - 2s	3.4	28.7	24.3	11.5
	$K_o = 10.8, f = 37^\circ$	3.6	28.6	130	9.6

Figure 5: Approximate Soil Spring Fit



For the case of 3 feet of soil cover, the internal friction angles necessary to get a reasonable match between axial and horizontal soil restraint are outside of the bounds of actual soils and outside the limit of 50° used for generating data for the Bayesian model. Therefore, 50° becomes an upper limit in Table 8 and Figure 5.

The final recommended soil factors for the state are summarized in Table 9.

Table 9: Recommended Soil Spring Parameters for California Based upon Depth of Cover

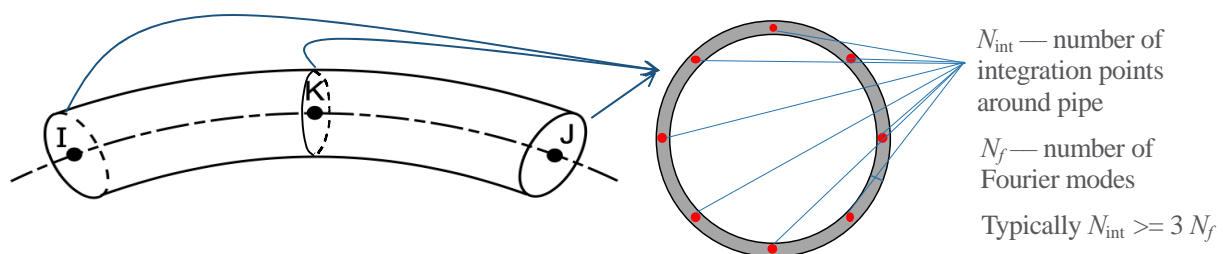
Depth of Cover (feet)	Condition	Interface Friction Factor (ϕ)	Horizontal Pressure Coefficient (K_o)	Internal Friction Angle
0 to 4	Mean	0.7	1.5	50°
	Mean + 2 σ	0.7	1.5	50°
	Mean - 2 σ	0.7	1.5	42°
4 to 7.5	Mean	0.7	1.2	46°
	Mean + 2 σ	0.7	1.2	50°
	Mean - 2 σ	0.7	1.2	41°
Greater than 7.5	Mean	0.7	1.25	40°
	Mean + 2 σ	0.7	1.25	44°
	Mean - 2 σ	0.7	1.25	37°

4 Finite Element Analysis Procedure

The experienced strain model will be built via 3D high-fidelity finite element analysis using Ansys Mechanical, which is a powerful commercial FEA software specialized in structural analysis. “Elbow” elements and bi-linear soil springs will be adopted to simulate the nonlinear structural (i.e., pipe) and soil behavior, respectively.

The elbow element (referred to ELBOW290 in Ansys), as shown in Figure 6, is a three-node “beam” element embedded with multiple integration points along the circumferential line of the cross-section. Distinct from regular beam elements, this elbow element allows general section deformation, including radial expansion, ovalization, and warping, which is hence a perfect candidate for curved pipes or straight pipes in large-deformation analysis.

Figure 6: Configuration of the Elbow Element



As for soil springs, in this project, we applied them in four directions, namely, axial, transverse horizontal, transverse uplift and transverse downward. Figure 7 shows the representation of the discrete soil springs, and Figure 8 presents the bi-linear force-displacement curves of the soil springs in all four directions. The formulations used to define the maximum soil spring forces and were based upon approaches described in PRCI seismic guidelines (PRCI, 2017).

Figure 7: Configuration of the Soil Springs

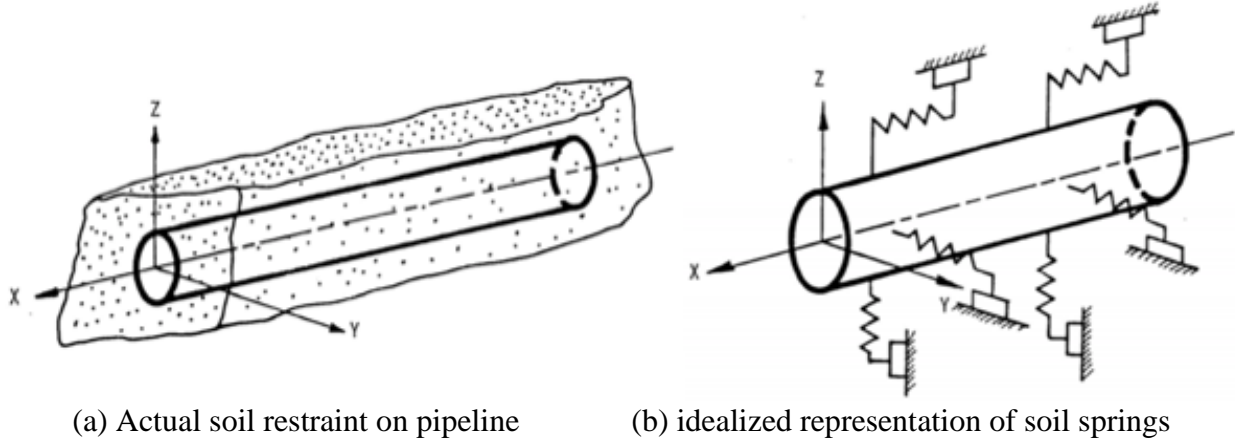
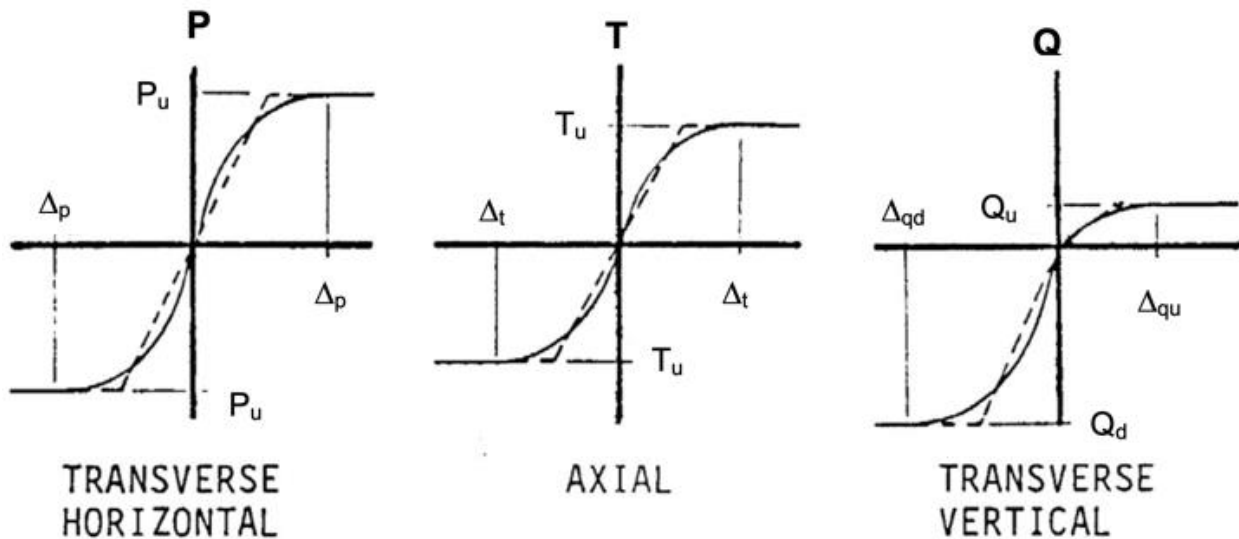


Figure 8: Force-displacement Curves of the Soil Springs



Our assessment of the seismic response of natural gas transmission pipelines is limited to seismic hazards that result in permanent ground displacement from surface fault displacement and earthquake triggered landslides and lateral spread displacement (simply referred to as lateral displacement). The modeling approach used for determining pipeline response to these seismic hazards is essentially the same. The primary difference is in the definition of the ground displacement hazard along the pipeline model. Surface faulting is modelled as an abrupt shearing displacement at one location. Lateral displacement is defined by a zone of displacement centrally located within the pipeline model.

We consider seismic ground shaking as a triggering force for landslides and liquefaction. This is justified considering the good performance of natural gas transmission pipelines, that are constructed of steel with butt-welded joints, in past earthquakes in California and around the world.

4.1 Generic Modeling Approach for Surface Faulting

The approach to modelling pipeline response to surface fault displacement is illustrated in Figure 9 for the case of pure right-lateral strike-slip fault displacement. Actual fault analysis cases incorporated at complete range of horizontal and vertical components of displacement.

Every pipe node is connected with three soil independent springs representing soil restraint in the axial, vertical, and perpendicular horizontal directions relative to the pipeline axis. Then, as shown in Figure 9, The bases of the soil springs are displaced according to the direction of fault displacement. The fault displacement analyses assumed an abrupt offset with displacement occurring only on one side of the fault. Loads are transferred to the pipeline through the soil springs and result in displacement of the pipeline as illustrated in **Figure 10** and **Figure 11**, which display an example of the deformed pipe segment and two cross-sections in which maximum compressive and tensile strains are located. **Figure 12** shows a plot of tensile (positive) and compressive (negative) strain as a function of pipe displacement.

Figure 9: Representation of the Applied Fault Movement

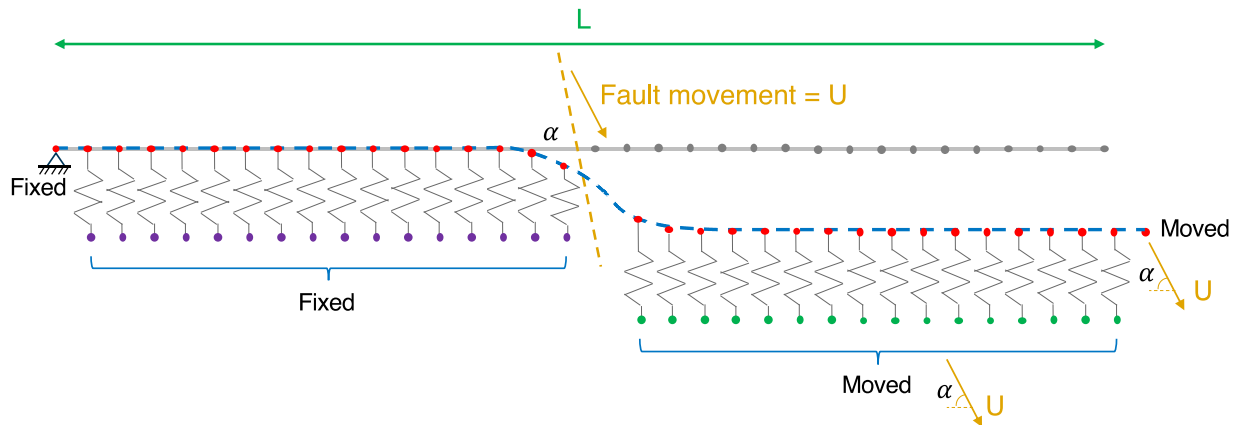


Figure 10: Pipe Segment Deformation 60 Degree Case

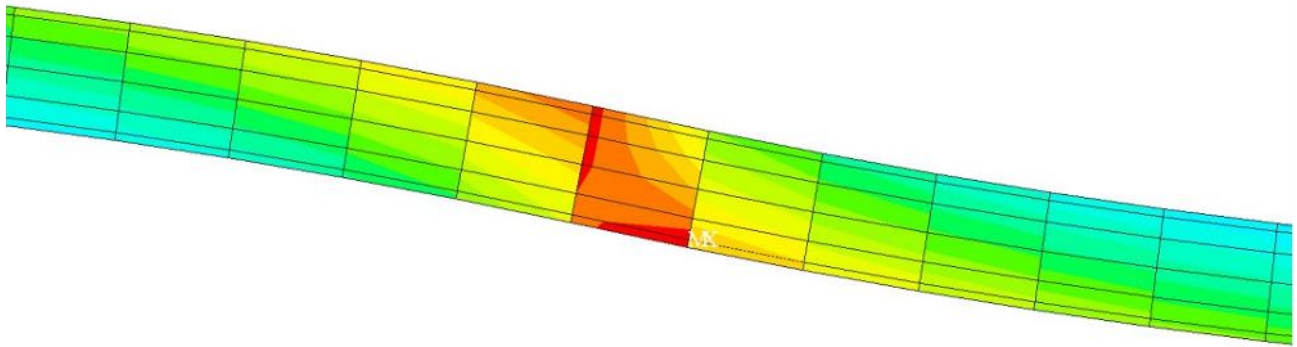
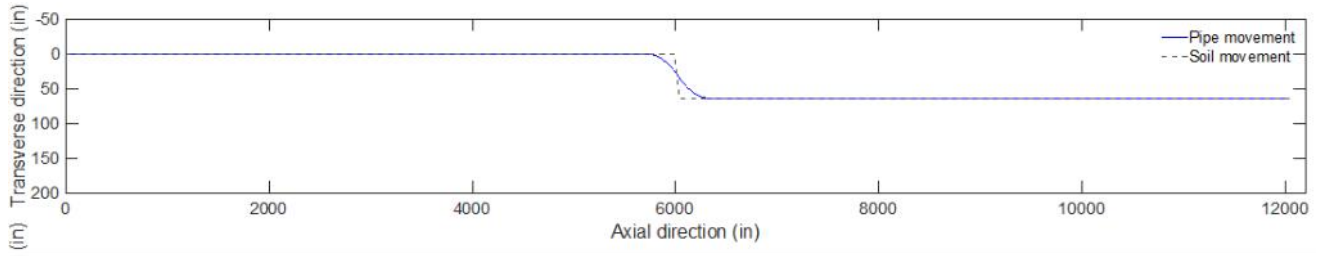


Figure 11: Pipe Segment Deformation 90 Degree Case

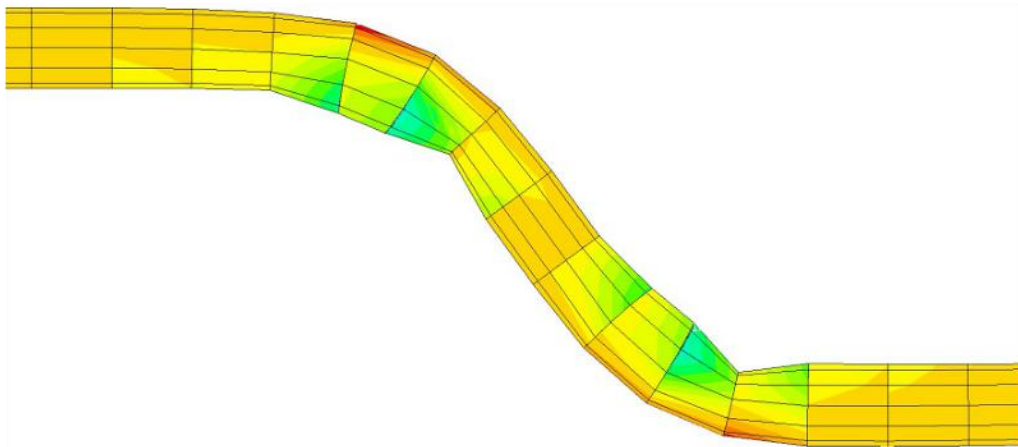
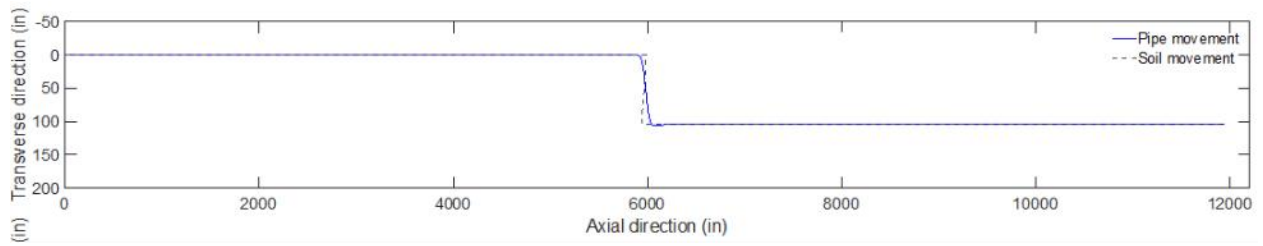
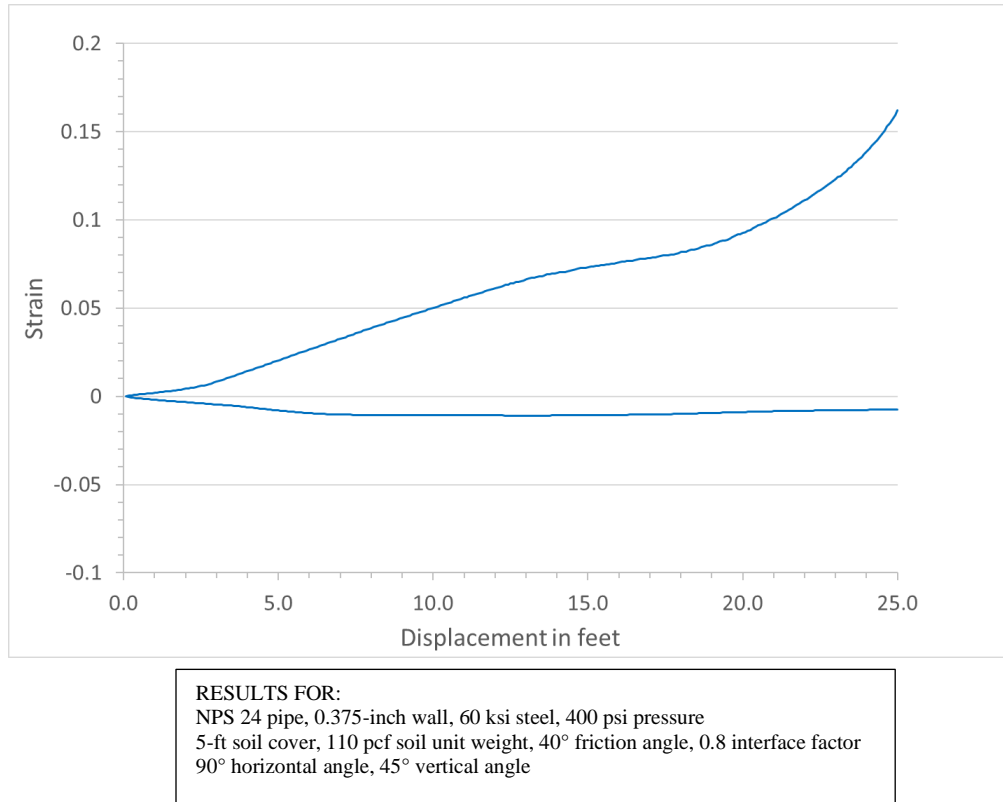


Figure 12: Tensile (positive) and Compressive (negative) Strain as a Function of Pipe Displacement



As noted previously, fault displacements are modelled in three dimensions. A displacement vector can be defined the three-dimensional space by a displacement magnitude, the angle between the displacement vector and a horizontal plane, and an angle between a vertical plane and the projection of the displacement vector on the horizontal plane. The concept is adopted in defining the components of fault displacement applied to the pipeline in the analyses as follows:

1. The amount of total displacement
2. The angle between the vector of total displacement and a point below a horizontal plane
3. The counterclockwise angle between the pipeline and a projection of the displacement vector on a horizontal plane

These three parameters are illustrated in Figure 13 and described below.

- R is the total displacement.
- θ_v is the generic vertical angle, which is the angle between the vector of total displacement and the vertical upward direction.
- θ_H is the generic horizontal angle, which is the counterclockwise angle between the pipeline and a projection of the displacement vector on a horizontal plane.

The definition of ground displacement typically described by geologists defines the displacement of the hanging wall of a fault (i.e., foot wall is stationary). The direction of displacement is defined

by three angles, the direction of fault dip, dip angle, and rake angle. For computation purposes, it is more convenient to use the fault strike angle which is simply 90° less than the direction of fault dip. With this convention, the following notation applies:

- ϕ is the fault strike measured clockwise from north to the fault plane with an angle of 0° to 360° .
- δ is the fault dip angle.
- λ is the fault rake angle measured on the fault plane from the horizontal. This is defined as a range from 0° to 360° counterclockwise from a parallel to the strike on the dip plane as illustrated in Figure 14. With this definition, 0° is pure left-lateral strike-slip displacement, 90° is pure reverse-slip, 180° is pure right-lateral strike slip, and 270° is pure normal slip.

Translating the geological parameters to displacements relative to the pipeline requires specifying the angle, φ , at which the pipeline crosses the fault strike. The angle φ is measured clockwise from north and varies from 0° to 360° .

It is noted that the rake angle definition provided by the fault definition team defines the rake angle as varying from 0° to 180° and 0° to -180° . To be consistent with the definition of λ in Figure 14, 360° needs to be added to negative rake angles.

The development of relationships to translate the geological definitions of fault displacement to the applicable pipeline analysis configuration used in developing the Bayesian model is illustrated in Figure 15.

Figure 13: Definition of Fault Displacement Components in Pipeline Analyses

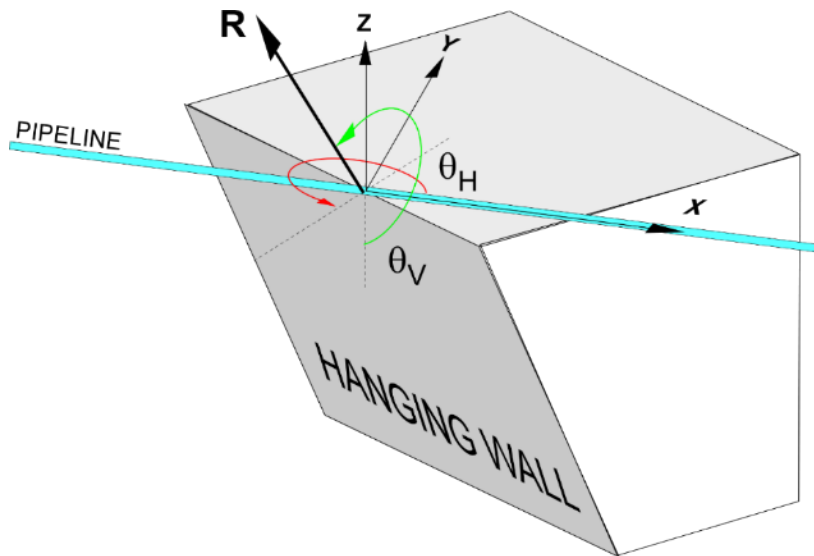


Figure 14: Diagram of Fault Orientation Defined by Dip Direction, Strike, Dip and Rake Angles Using the Aki-Richards Rake Definition

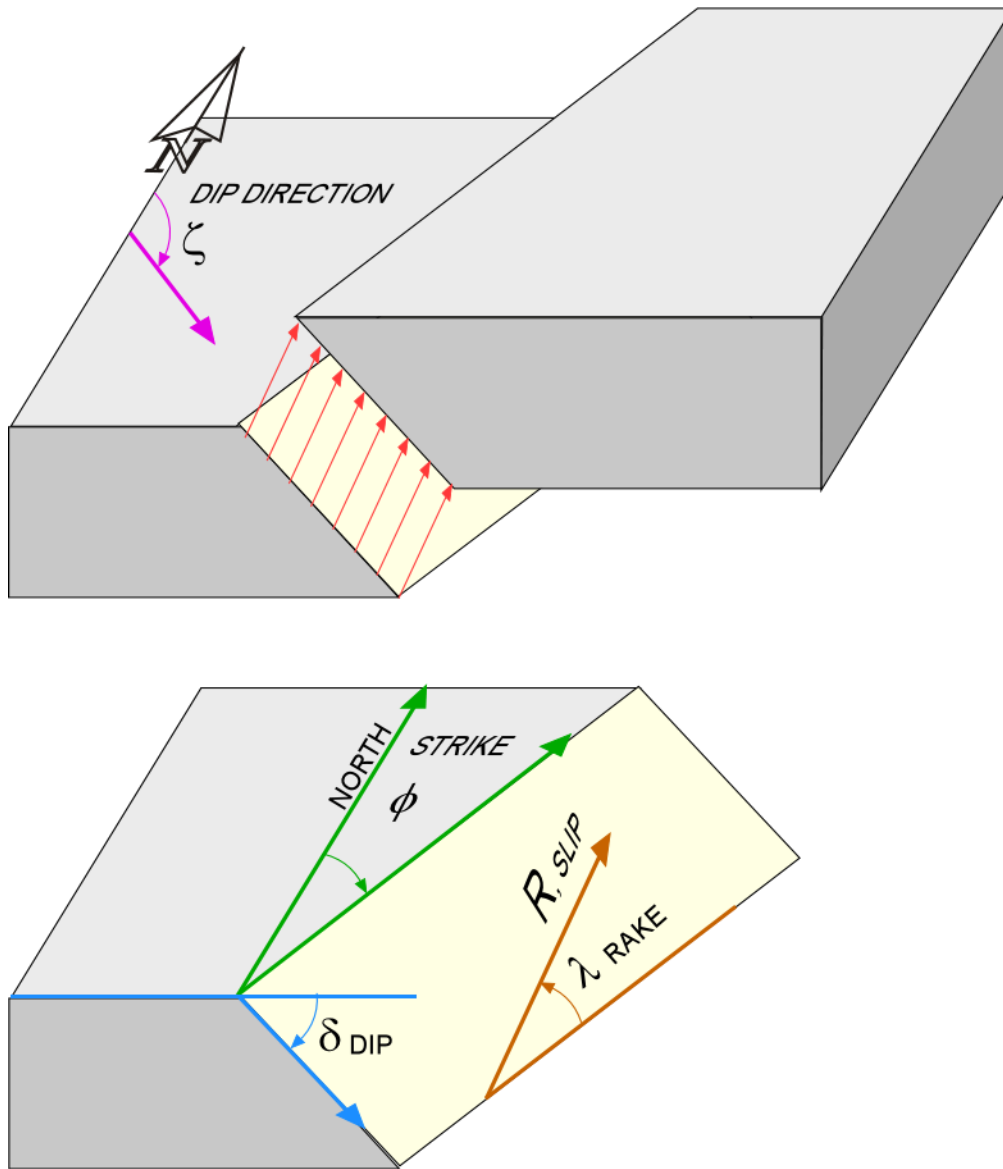
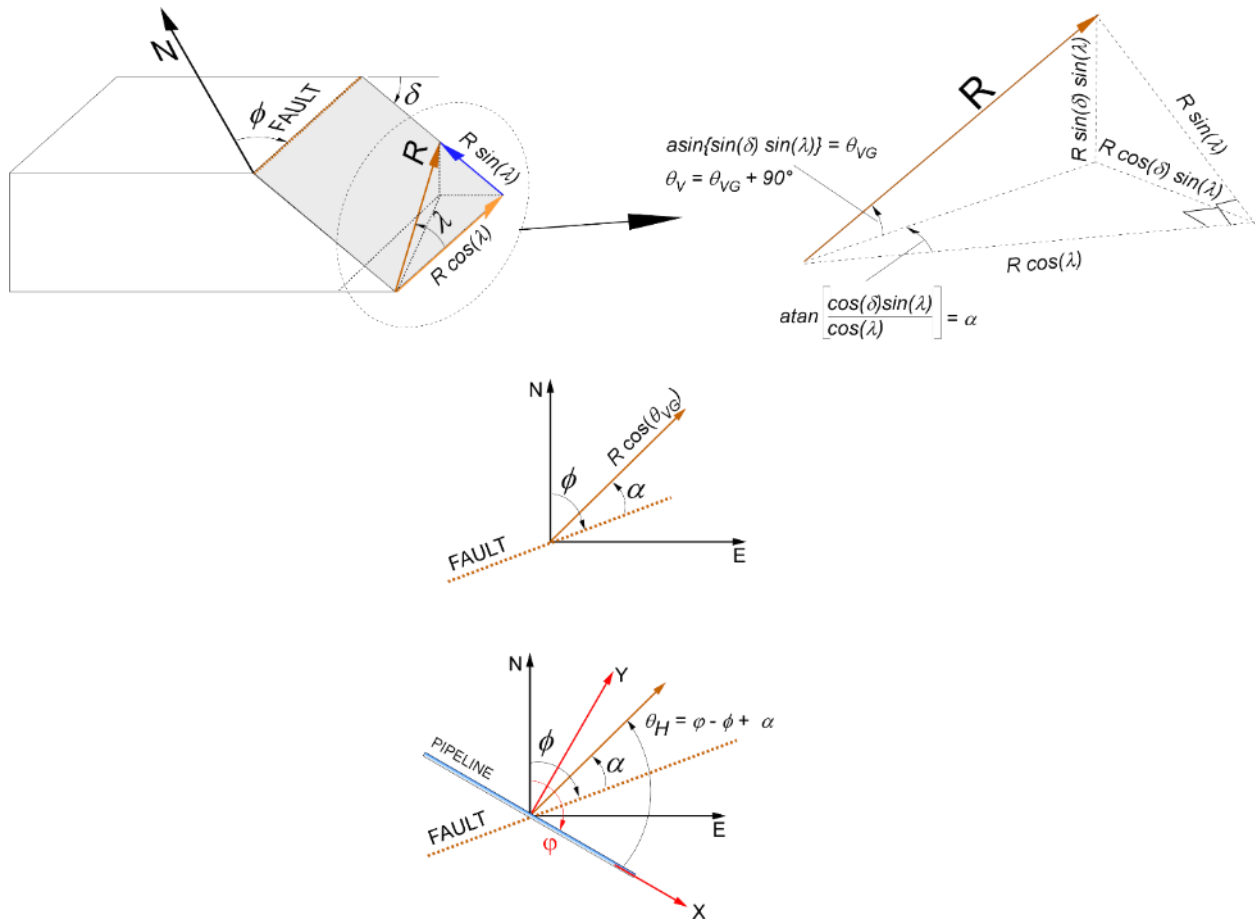
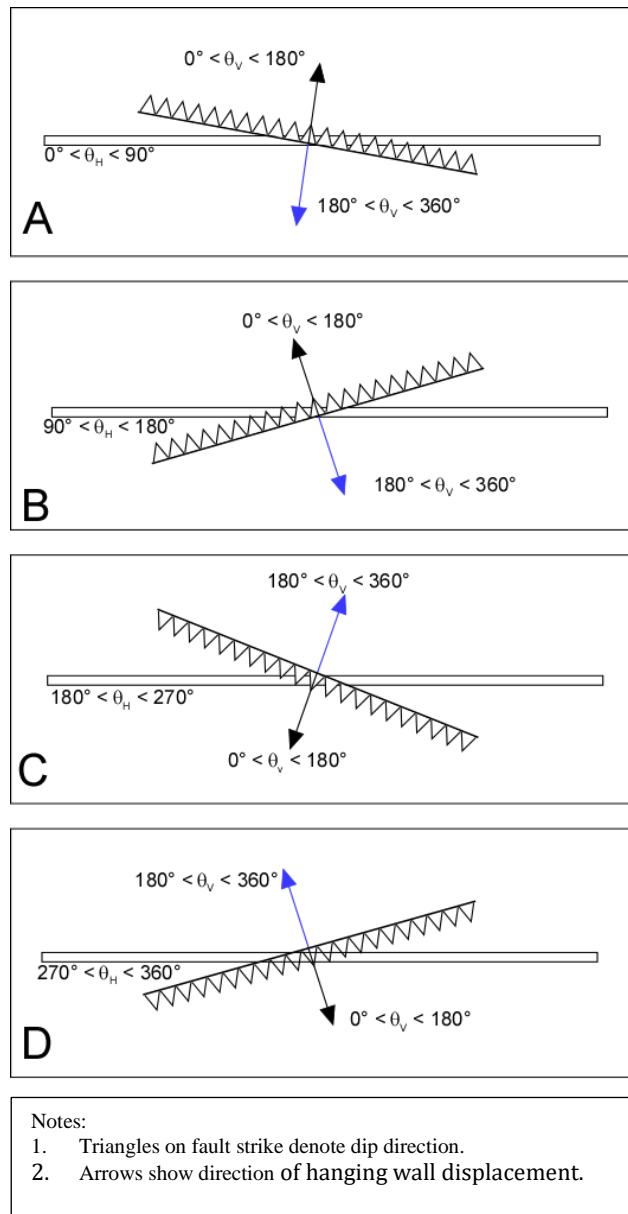


Figure 15: Transforming Geological Definition to Pipeline Analysis Case Definition



Defining displacement with a minimum number of parameters substantially reduces the number of analysis cases necessary for building the Bayesian network model. The number of parameters was minimized by taking advantage of symmetry in pipeline response as θ_V and θ_H vary from 0° to 360° . Figure 16 shows an example of how the relative horizontal components of fault displacement applied to a pipeline (θ_V equal to 90°) is the same provided θ_H results in the same acute angle between the pipeline and direction of horizontal displacement. For simplicity, the direction of fault displacement in Figure 16 is assumed to be parallel to the fault dip.

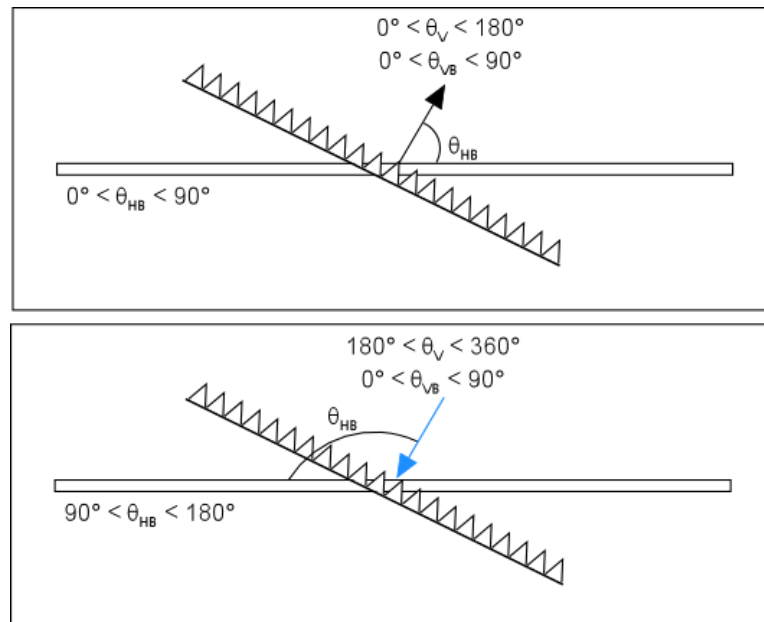
Figure 16: Various θ_H Crossing Angles with Identical Horizontal Fault Displacement Components



Note that the magnitude of the horizontal fault displacement components relative to the pipeline can be defined by a range of 0° to 90° . However, an additional parameter is necessary to determine where the fault displacement imposes axial tension or compression in the pipeline.

Three Bayesian model parameters were used to define the pipeline fragility cases, horizontal angle, vertical angle, and amount of displacement. The vertical angle definition was limited to 0° to 90° and the horizontal angle definition was 0° to 180° . As noted above, the magnitude of the horizontal components of fault displacement only requires specifying an angle from 0° to 90° . For cases where fault displacement has a pipe-parallel component imposing tension, this convention was adopted, and the horizontal angle range was set to 0° to 90° . If the pipe-parallel component imposes compression, the horizontal angle for the Bayesian model was defined as 180° minus the corresponding horizontal angle. This is illustrated in Figure 17 where the Bayesian model horizontal and vertical angles are noted as θ_{HB} and θ_{VB} and the direction of displacement is assumed to be parallel to the fault dip.

Figure 17: Definition of Horizontal and Vertical Angles for Bayesian Model



As noted in the previous discussion, determination of the appropriate horizontal and vertical angles to select from the Bayesian model requires geological input on fault geometry (strike, dip, and rake angles) and information on the pipeline alignment. This process is laid out in Figure 18.

Figure 18: Process for Computing Bayesian Model Angles

Geology Information (Figure 14)

Dip direction angle, ζ , defined as 0° to 360°

Dip angle, δ , defined as 0° to 90°

Rake angle, λ , defined as 0° to 180° and 0° to -180°

Pipeline Information (Figure 15)

Pipe azimuth, ϕ , defined as 0° to 360° from measured clockwise from north

Generic Angle Conversion (Figure 15)

Strike angle, ϕ , defined as ζ minus 90°

Alternate rake angle, ψ , defined as λ if λ is positive and $360^\circ + \lambda$ if λ is negative

Generic vertical angle, θ_v , defined as $\theta_v = \text{asin}[\sin(\delta)\sin(\psi)] + 90^\circ$

Generic horizontal angle, θ_H , defined as $\theta_H = \phi - \phi + \alpha$ where α is as follows:

$$\text{for } 0^\circ \leq \psi < 90^\circ \quad \alpha = \text{atan}[\cos(\delta)\tan(\psi)]$$

$$\text{for } \psi = 90^\circ \quad \alpha = 90^\circ$$

$$\text{for } \psi = 270^\circ \quad \alpha = 270^\circ$$

$$\text{for } 90^\circ < \psi < 270^\circ \quad \alpha = \text{atan}[\cos(\delta)\tan(\psi)] + 180^\circ$$

$$\text{for } 270^\circ < \psi \leq 360^\circ \quad \alpha = \text{atan}[\cos(\delta)\tan(\psi)] + 360^\circ$$

Bayesian Model Angle Conversion (Figure 16)

Vertical Angle, θ_{VB} , defined as

$$\theta_{VB} = 90^\circ - \theta_v \text{ if } 0^\circ \leq \theta_v \leq 90^\circ$$

$$\theta_{VB} = \theta_v - 90^\circ \text{ if } 90^\circ < \theta_v \leq 180^\circ$$

$$\theta_{VB} = 270^\circ - \theta_v \text{ if } 180^\circ < \theta_v \leq 270^\circ$$

$$\theta_{VB} = \theta_v - 270^\circ \text{ if } 270^\circ < \theta_v \leq 360^\circ$$

Horizontal Angle, θ_{HB} , defined in terms of a base angle, θ_{BA} , defined as

$$\theta_{BA} = \theta_H \text{ if } 0^\circ \leq \theta_H \leq 90^\circ$$

$$\theta_{BA} = 180^\circ - \theta_H \text{ if } 90^\circ < \theta_H \leq 180^\circ$$

$$\theta_{BA} = \theta_H - 180^\circ \text{ if } 180^\circ < \theta_H \leq 270^\circ$$

$$\theta_{BA} = 360^\circ - \theta_H \text{ if } 270^\circ < \theta_H \leq 360^\circ$$

The horizontal Angle, θ_{HB} , is dependent upon generic vertical angle, θ_v .

$$\theta_{HB} = \theta_{BA} \text{ if } 0 < \theta_v \leq 180^\circ$$

$$\theta_{HB} = 180^\circ - \theta_{BA} \text{ if } 180^\circ < \theta_v \leq 360^\circ$$

4.2 Generic Modelling Approach for Lateral Displacement

The only differences in the modelling approach for lateral displacement compared to fault displacement is in the definition of the ground displacement hazard. The lateral displacement is assumed to be in the same horizontal plane as the pipeline so there is no relative vertical ground displacement. However, the length of pipeline exposed to ground displacement is an important variable. As illustrated in Figure 19, displacement is applied over a specified length, H , in a direction, α , measured counterclockwise with respect to the pipeline axis with values varying from 0° to 90° .

Figure 20 through Figure 23 illustrate the variation in the development of longitudinal strain for two hypothetical cases with a 30° and 60° direction of displacement. The results are quite similar owing to the fact that the only real difference is the amount of bending imposed by ground displacement is larger for the 60° case. This leads to a slightly higher maximum tensile strain and the development of the maximum compressive strain at a displacement approximately two-thirds of that for the 30° case.

Figure 19: Representation of the Applied Landslide Movement

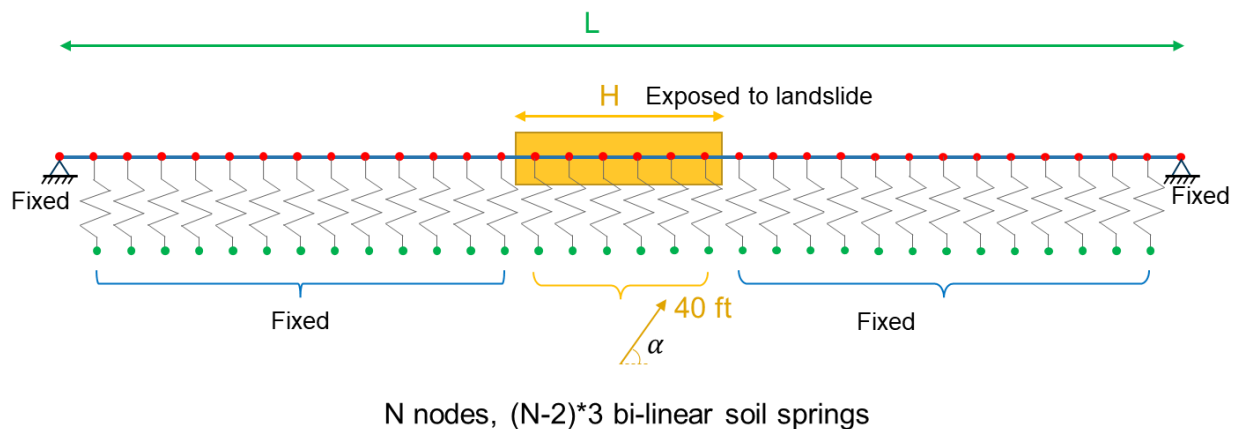


Figure 20: Pipe Segment Deformation - 30 Degree Case

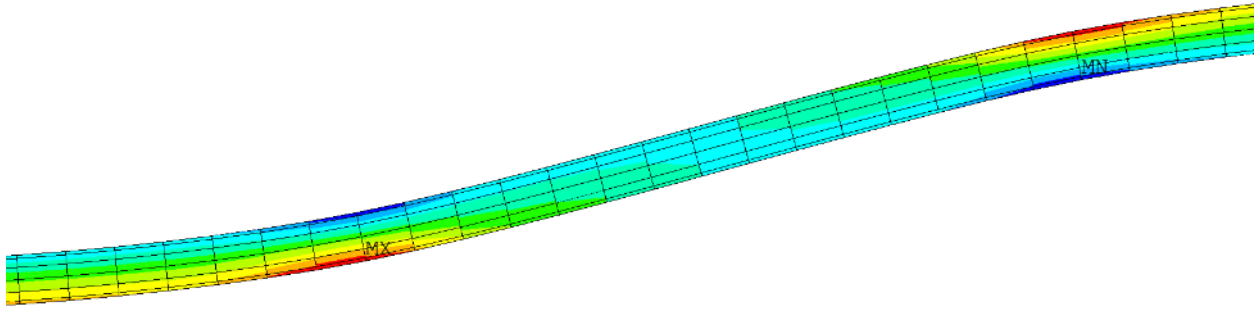


Figure 21: Tensile and Compressive Strain as a Function of Pipe Displacement - 30 Degree Case

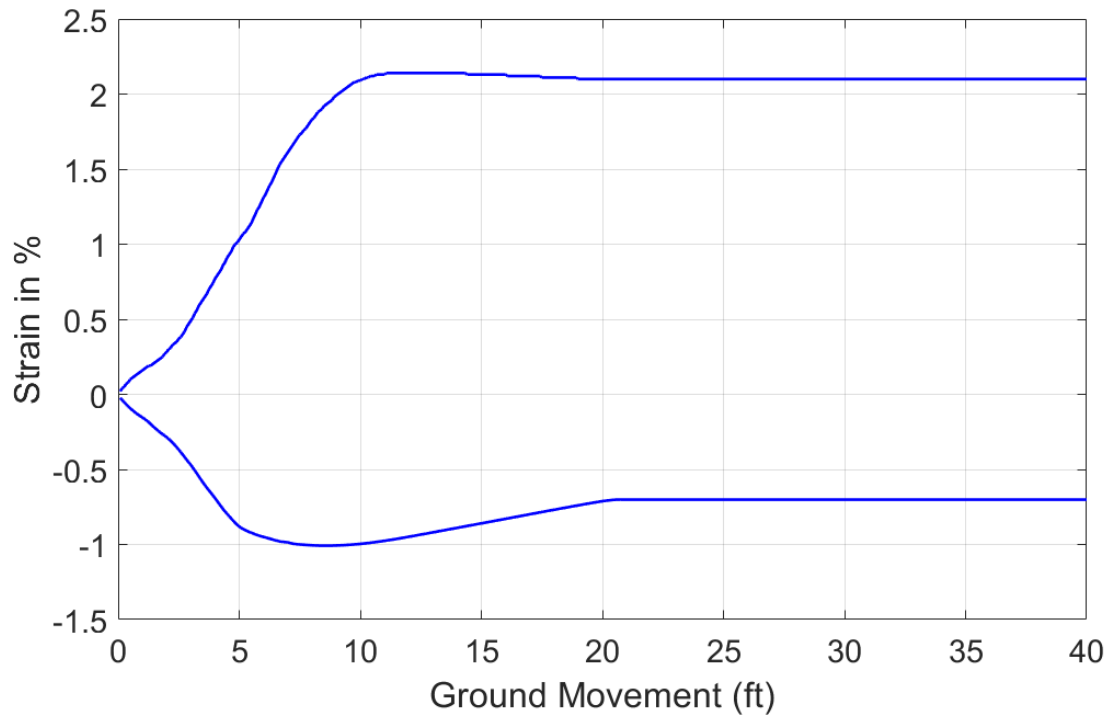


Figure 22: Pipe Segment Deformation - 60 Degree Case

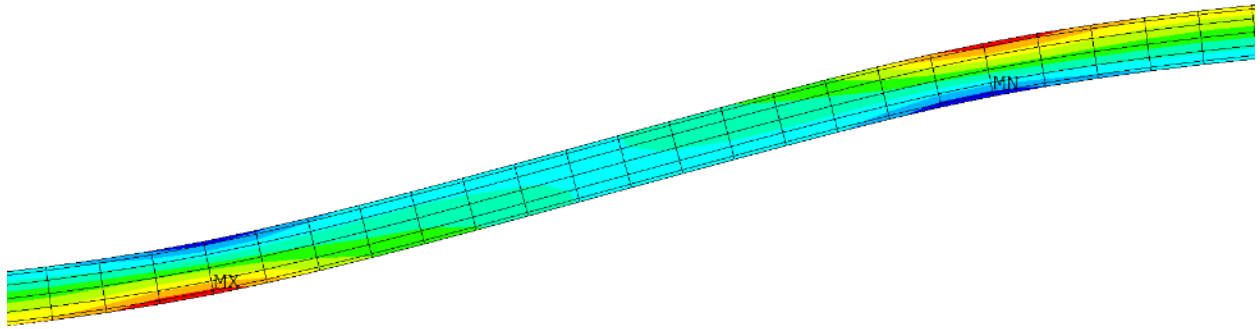
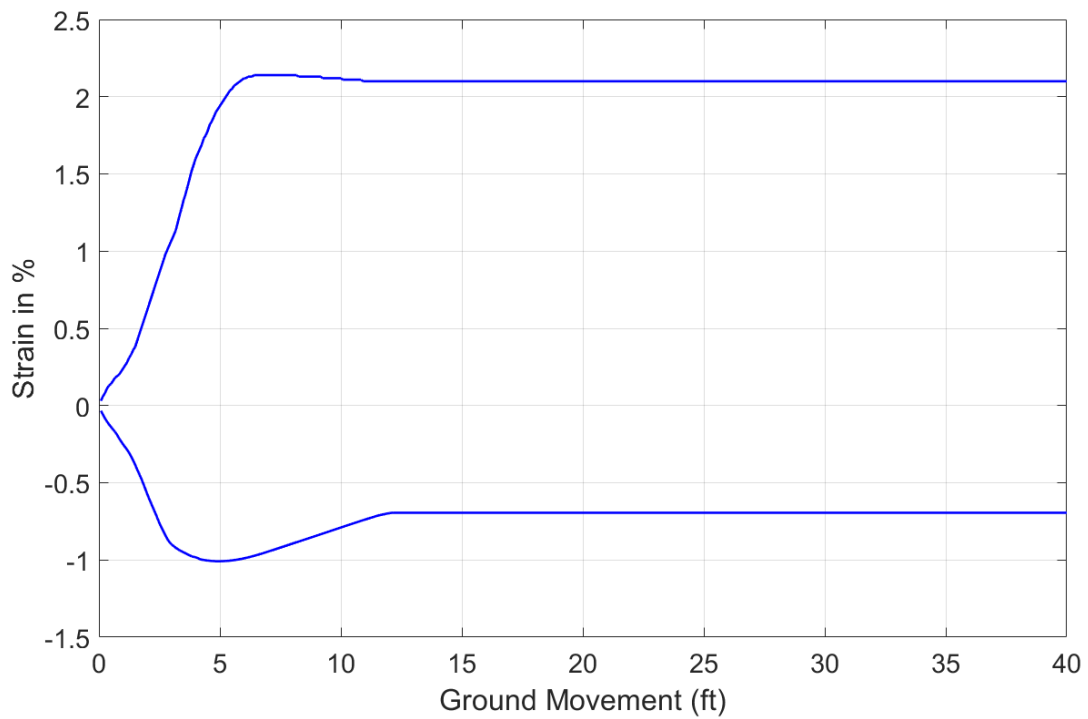


Figure 23: Tensile and Compressive Strain as a Function of Pipe Displacement – 60 Degree Case



5 Experienced Strain Model for Fault Displacement

5.1 Sensitivity Analysis for Fault Displacement

The objective of the sensitivity analysis is to optimize the number of simulations required to build the strain model for fault displacement. The process is explained in the literature (Ayello, 2014). The model has 10 inputs, if we perform 10 simulations for each input this would lead to 10^{10} simulations. So many FEAs are obviously too large to perform. The sensitivity analysis was done using two base case scenarios as defined in the Table 10. These base cases are used to determine which inputs have the most impact of the strain experienced by the pipeline and therefore help us focus our numerical study in the most useful domains. It should be noted that the fault angles in Table 10, Figure 24 and Figure 25 are generic horizontal angles θ_H and vertical angles θ_v defined in Figure 13.

Table 10: Data Used for Sensitivity Analysis for Fault Displacement

	BASE CASE 1	BASE CASE 2
Steel type	X60	X60
Pipe diameter	24 inch	24 inch
Pipe thickness	0.375 inch	0.375 inch
Pipe internal pressure	400 psi	400 psi
Soil Cover Depth	5 feet	5 feet
Soil Friction Angle	40°	40°
Soil Shear Strength	0 psf	0 psf
Soil Coefficient	0.375 and 0.8	0.375 and 0.8
Soil Unit Weight	110 pcf	110 pcf
Fault Angles	90° horizontal angle 45° vertical angle	210° horizontal angle 60° vertical angle

The fault displacements relative to the pipeline for the two cases are illustrated in Figure 24 and Figure 25. The need for two sets of base cases arises because of the large difference in pipeline response between cases where the component of ground displacement parallel to the pipeline

induces tension compared to cases where the axial component of displacement induces compression. Under axial tension, the bending strength of the pipeline is increased as a result of catenary tension (geometric nonlinearity). For a perpendicular strike-slip fault crossing, where there is not an axial component of ground displacement, tension still develops because of the change in length required to accommodate lateral offset of the pipeline. Conversely, axial compression can eliminate the change in length required by the pipeline. For typical tensile and compressive strain limits, the displacement capacity for a pipeline subjected to axial tension can be an order of magnitude greater than a pipeline subjected to axial compression.

Each variable for the two base cases was varied to examine the impact of that variable on the development of tensile and compressive strain as a function of applied fault displacement. The amount of fault displacement applied in each case was 40 feet with strain results extracted at every inch of displacement.

Figure 24: Fault Displacement Relative to the Pipeline for CASE 1

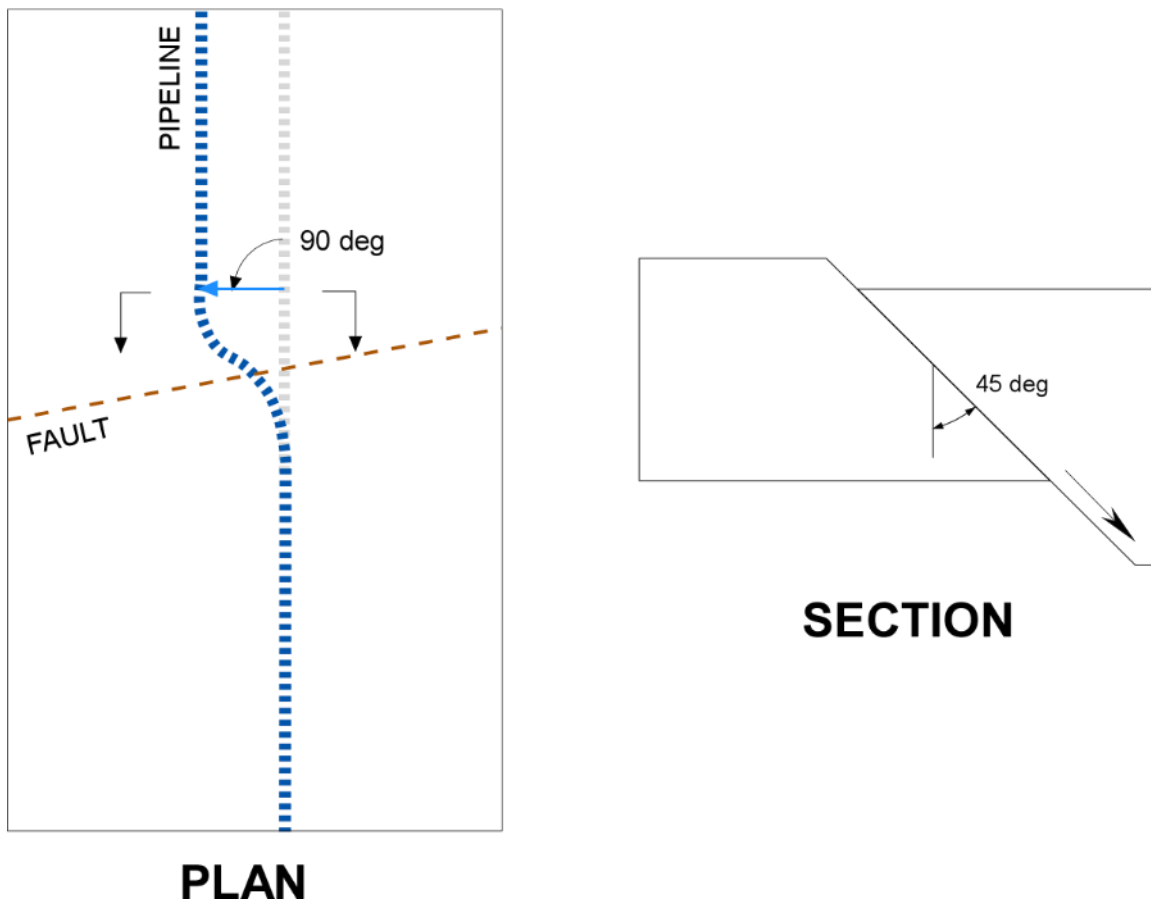
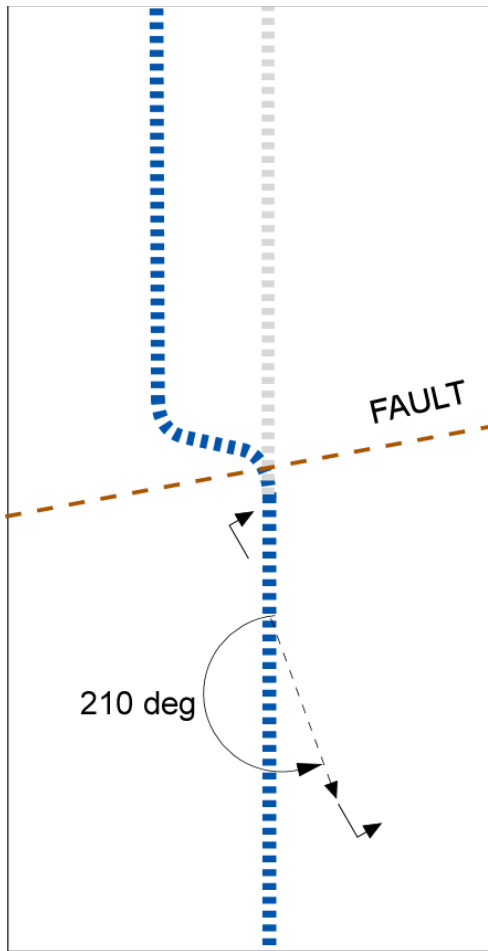
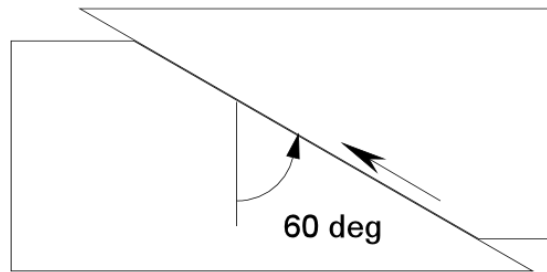


Figure 25: Fault Displacement Relative to the Pipeline for CASE 2



PLAN



SECTION

The variation in variables applied in the sensitivity analyses is summarized in Table 11. The remainder of this section discusses the trends in analysis results with variation of each variable.

Table 11: Variable Values Examined in the Sensitivity Analyses for Fault Displacement

Variable	Variable Values Examined in the Sensitivity Analyses
Steel type	Grade B, X42, X52, X60, X65, X70
Pipe diameter (inches)	8, 12, 16, 20, 24, 28, 32, 36, 40, and 42
Pipe thickness (inches)	0.188, 0.250, 0.375, 0.500, 0.562, 0.688, 0.750, 0.850, 0.989, and 1.219
Pipe internal pressure (psi)	0, 100, 200, 300, 400, 500, 600, 700, 800, 900, and 1,000
Soil Cover Depth (feet)	1, 2, 3, 4, 5, 6, 7, 8, 9, and 10
Soil Friction Angle	30°, 35°, 40°, 45°, and 50°
Soil Shear Strength (psf)	100, 200, 300, 400, 500, 600, 700, 800, 900, and 1,000
Soil Coefficient	0.6, 0.7, 0.8, and 1.0
Soil Unit Weight (pcf)	90, 100, 110, 120
Generic Horizontal Angle	0° to 360° in 10° increments
Generic Vertical Angle	15°, 30°, 45°, 60°, 75° and 90°

5.1.1 Pipeline Response Sensitivity to Steel Type

Changes in pipeline response with changes in the pipe steel grade are illustrated in Figure 26 and Figure 27. Both cases show limited impact from steel type on the strain experienced by the pipe. This result was expected, there is only a factor of two in yield strength between the two extremes tested (Grade B and X70). CASE 1 shows no significant effect in tension (all simulations would fail between 7 to 10 ft ground motion displacement) and CASE 2 shows no significant effect in compression (all simulations would fail between 2 to 3 ft ground motion displacement).

Figure 26: Tensile and Compressive Strain as a Function of Pipe Displacement for Steels with Various Yield Strengths – CASE 1

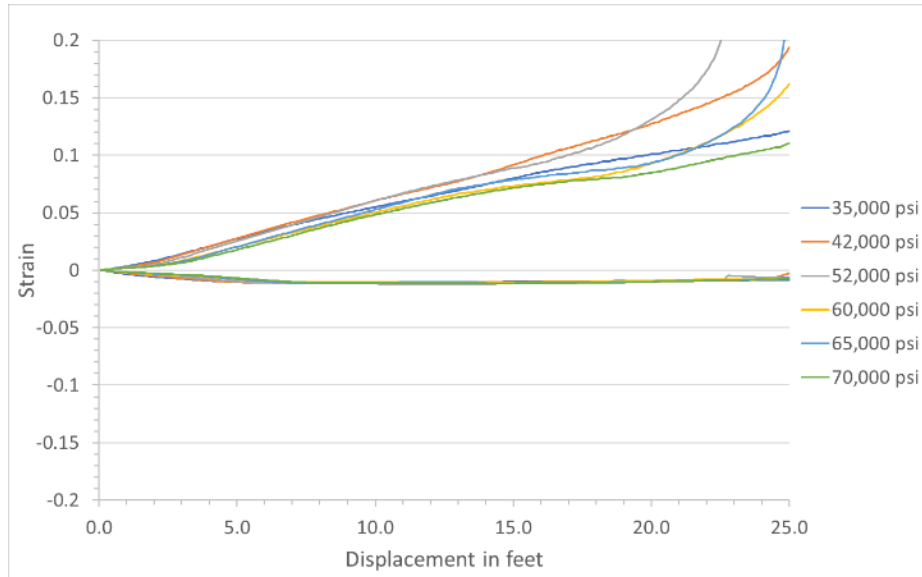
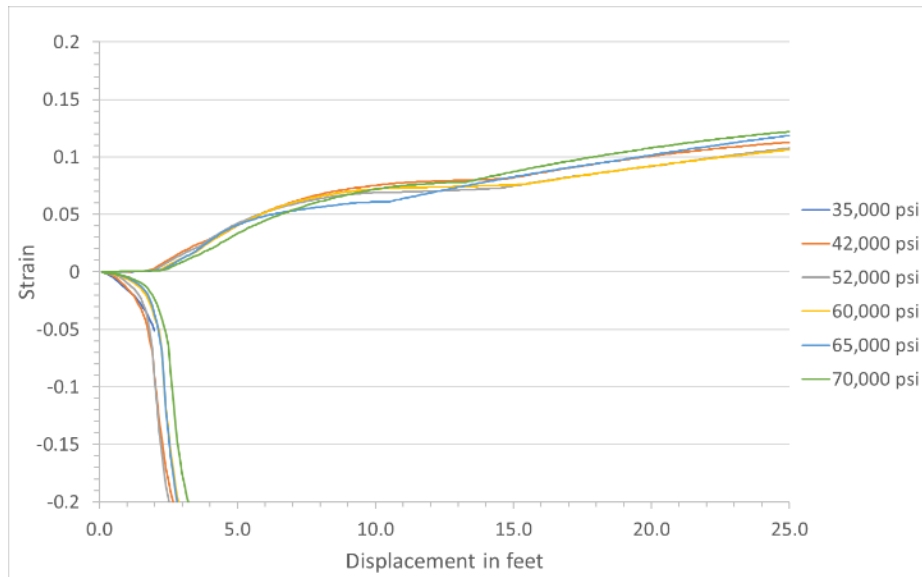


Figure 27: Tensile and Compressive Strain as a Function of Pipe Displacement for Steels with Various Yield Strengths – CASE 2



5.1.2 Pipeline Response Sensitivity to Pipe Diameter

Changes in pipeline response with changes in the pipe diameter are illustrated in Figure 28 and Figure 29. First, it should be noted that the smaller pipe diameter (8 inch) simulation ended prematurely, this is due to high increases in tensile strain with incremental changes in displacement that led to numerical instability in the analysis. Next, we observe great changes in tensile stress for the smaller pipe diameter while for the larger pipe diameter the amount of stress change is limited.

Figure 28: Tensile and Compressive Strain as a Function of Pipe Displacement for Pipelines with Various Pipe Diameters – CASE 1

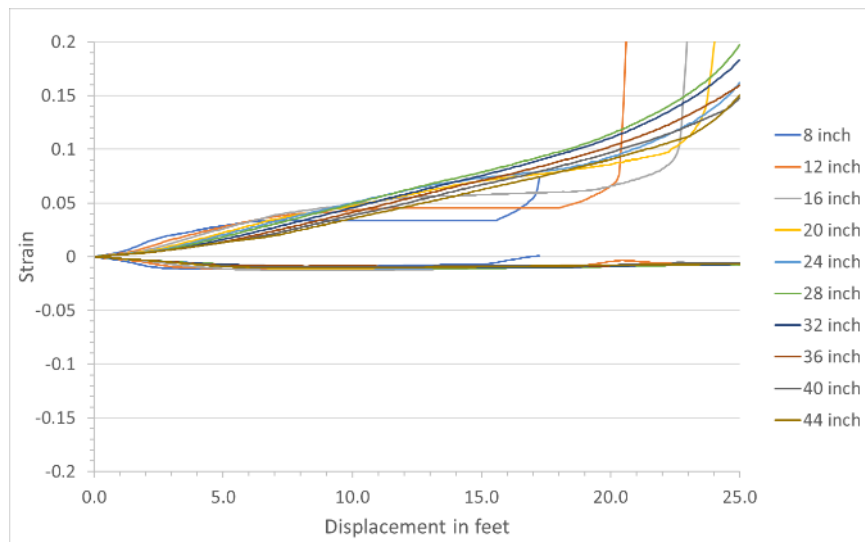
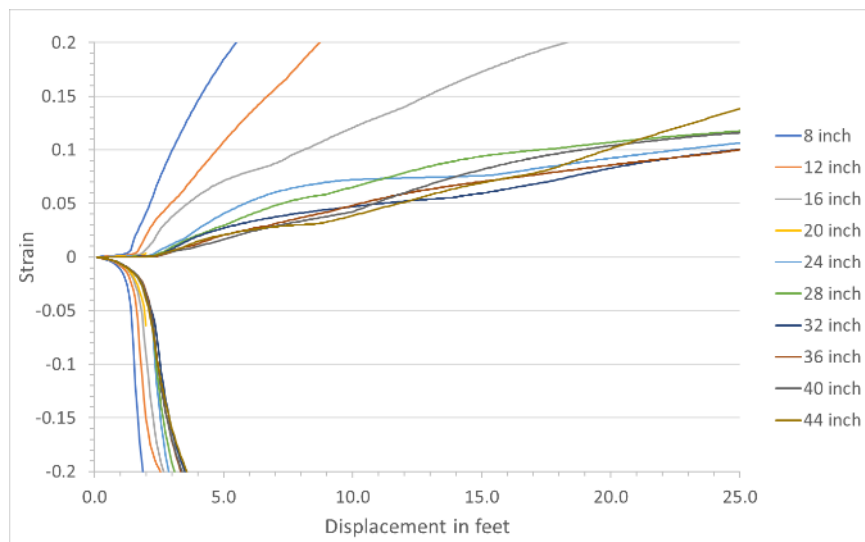


Figure 29: Tensile and Compressive Strain as a Function of Pipe Displacement for Pipelines with Various Pipe Diameters – CASE 2



5.1.3 Pipeline Response Sensitivity to Pipe Wall Thickness

Changes in pipeline response with changes in the pipe wall thickness are illustrated in Figure 30 and Figure 31. Pipe wall thickness has impacts both on tensile strain and compressive strain. Wall thickness was expected to have the greatest impact. We observe the most change in strain for the low wall thickness in tension for CASE 1 and compression for CASE 2.

Figure 30: Tensile and Compressive Strain as a Function of Pipe Displacement for Pipelines with Various Pipe Wall Thickness – CASE 1

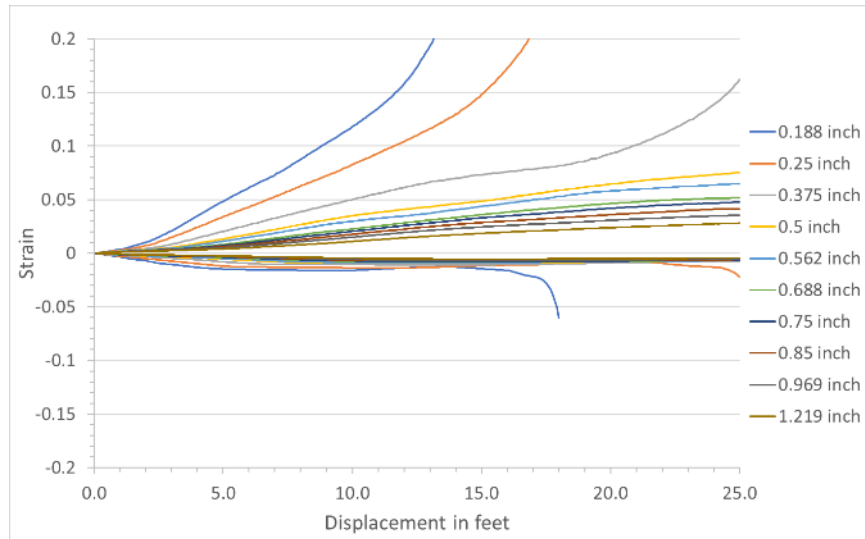
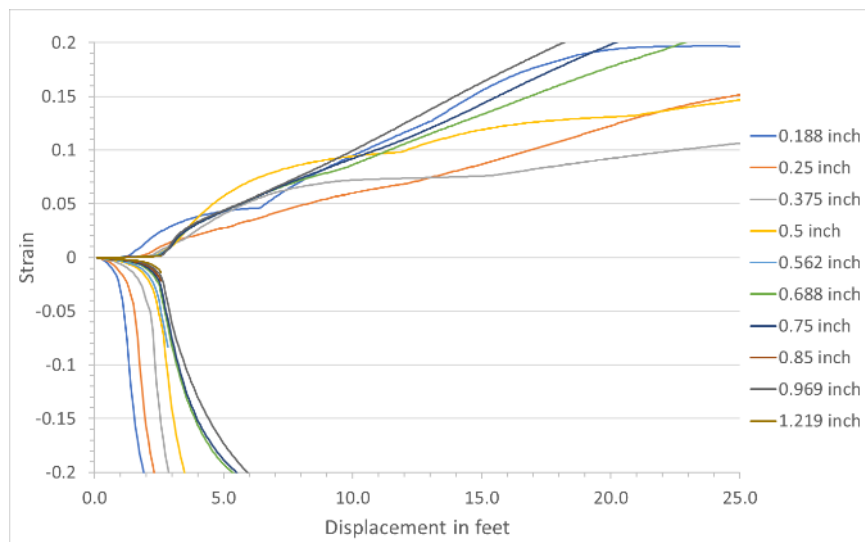


Figure 31: Tensile and Compressive Strain as a Function of Pipe Displacement for Pipelines with Various Pipe Wall Thickness – CASE 2



5.1.4 Pipeline Response Sensitivity to Internal Pressure

Changes in pipeline response with changes in internal pressure are illustrated in Figure 32 and Figure 33. Internal pressure has virtually no effect on the amount of stress experienced, as the forces applied by the ground motion on the pipe are much stronger. Both cases show the same effect. This will allow us to simplify the model and reduce the number of simulations required to create the model.

Figure 32: Tensile and Compressive Strain as a Function of Pipe Displacement for Pipelines with Various Pipe Pressures – CASE 1

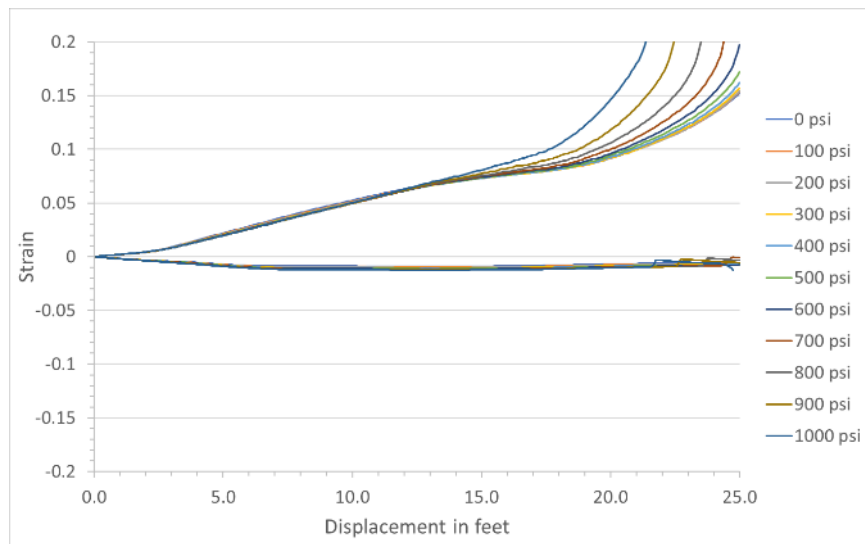
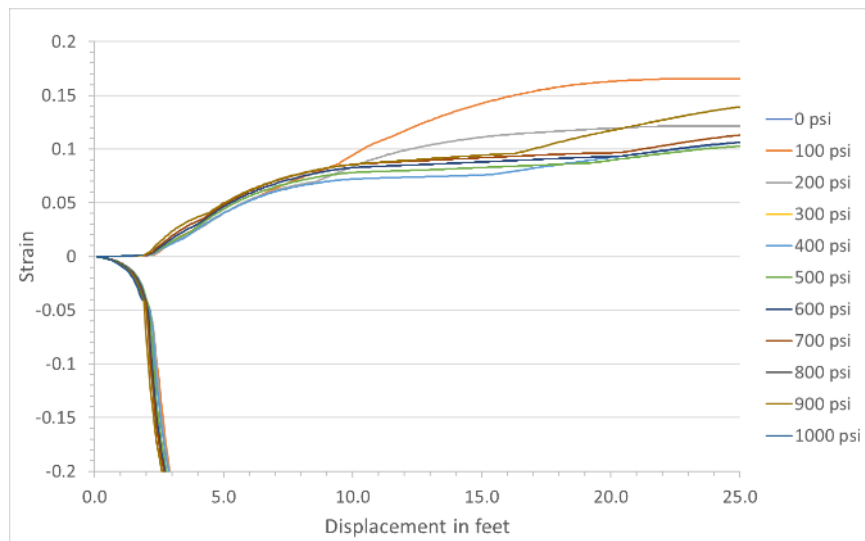


Figure 33: Tensile and Compressive Strain as a Function of Pipe Displacement for Pipelines with Various Pipe Pressures – CASE 2



5.1.5 Pipeline Response Sensitivity to Pipeline Depth of Soil Cover

Changes in pipeline response with changes in the depth of soil cover are illustrated in Figure 34 and Figure 35. The amount of soil above the pipeline (i.e., depth of cover) has a great impact on the amount of strain calculated. However, comparison between CASE 1 and CASE 2 shows that in tension the effect is very large (variation in ground motion required for failure goes from 4 to 25 ft), while in compression the effect is not as significant (ground motion required for failure goes from 3 to 4 ft).

Figure 34: Tensile and Compressive Strain as a Function of Pipe Displacement for Pipelines with Various Pipe Depth of Cover – CASE 1

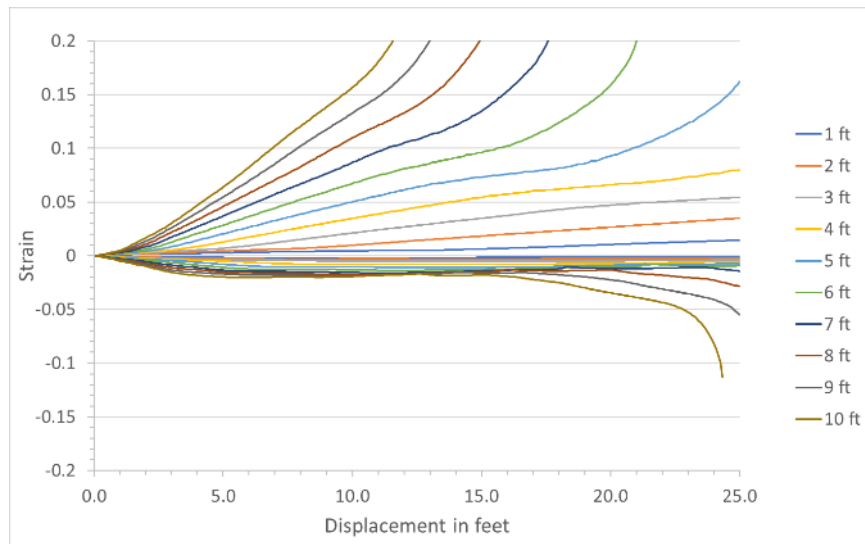
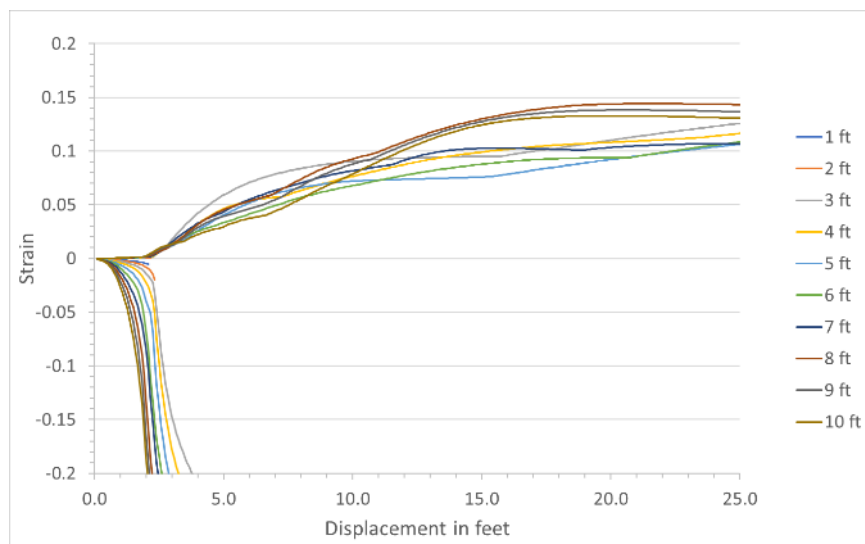


Figure 35: Tensile and Compressive Strain as a Function of Pipe Displacement for Pipelines with Various Pipe Depth of Cover – CASE 2



5.1.6 Pipeline Response Sensitivity to Levels of Soil Restraint

There are two ways to assess soil restraints on the pipe using soil friction angle (SFA) and soil shear strength (SSS). Changes in pipeline response with changes in SFA are illustrated in Figure 36 and Figure 37. Changes in pipeline response with changes in SSS are illustrated in Figure 38 and Figure 39. Although SFA and SSS have a great impact on the amount of soil restraint and therefore the strain experienced by the pipe, the variability of soil restraint is limited making the impact for SFA and SSS on pipe strain limited also.

Figure 36: Tensile and Compressive Strain as a Function of Pipe Displacement for Pipelines with Various Soil Friction Angles – CASE 1

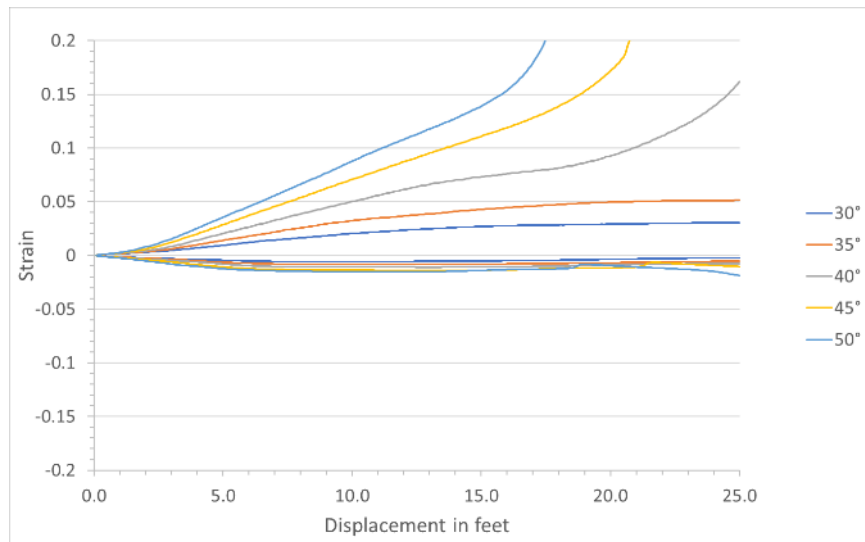


Figure 37: Tensile and Compressive Strain as a Function of Pipe Displacement for Pipelines with Various Soil Friction Angles – CASE 2

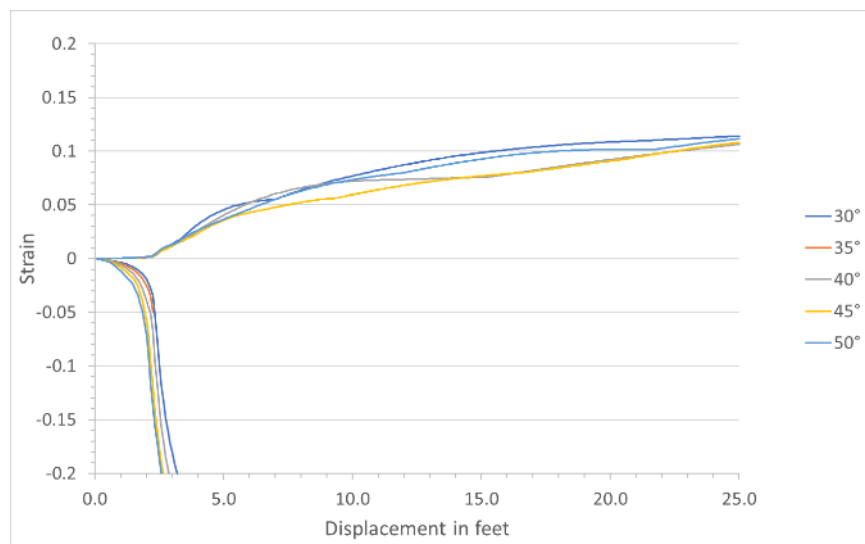


Figure 38: Tensile and Compressive Strain as a Function of Pipe Displacement for Pipelines with Various Soil Shear Strengths – CASE 1

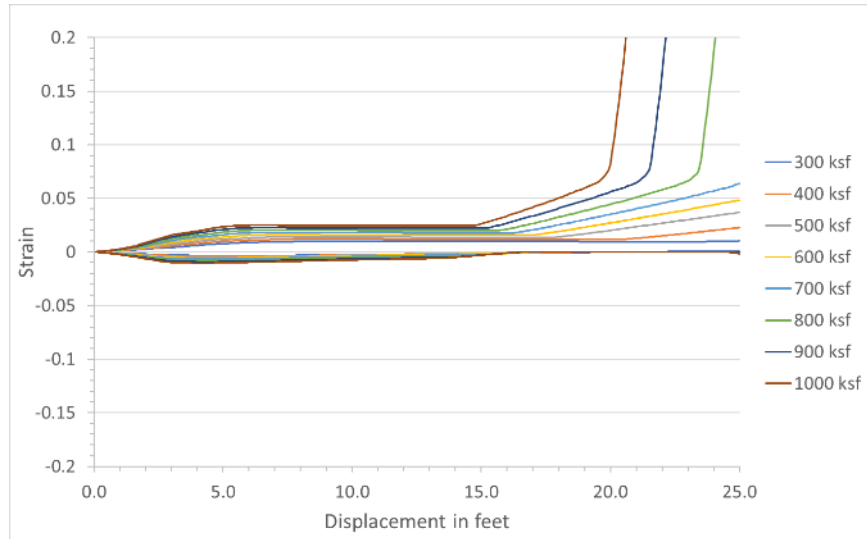
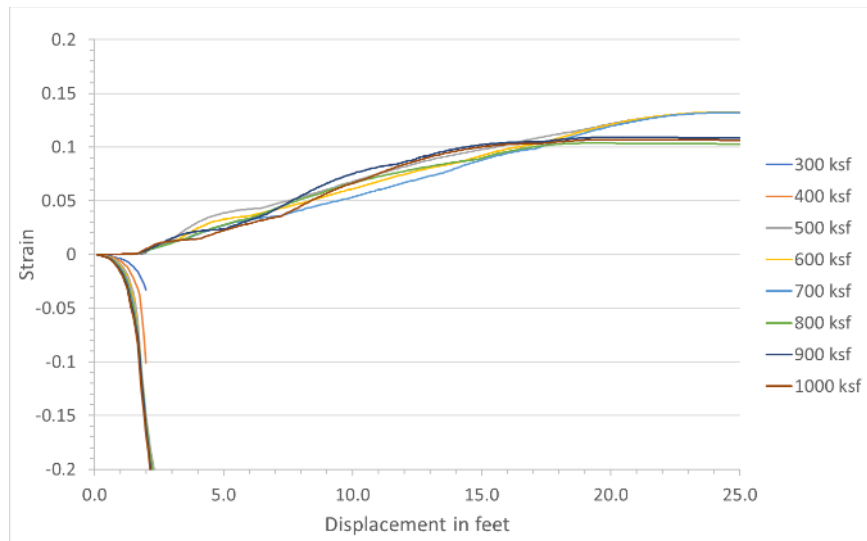


Figure 39: Tensile and Compressive Strain as a Function of Pipe Displacement for Pipelines with Various Soil Shear Strengths – CASE 2



5.1.7 Pipeline Response Sensitivity to Soil Coefficient

Changes in pipeline response with changes in the soil coefficient used to determine axial soil restraint for soils with strength defined by SFA are illustrated in Figure 40 and Figure 41. A value of 1.0 applies for very rough pipeline surfaces that might be represented by a coarse concrete coating. For a hard smooth pipeline coating, such as epoxy coating, the effective friction angle could be as low as 0.60 of the soil internal friction angle. The sensitivity of pipeline response to the soil coefficient is greatest for cases where the pipeline response is primarily axial since the soil coefficient only modifies the axial soil restraint.

Figure 40: Tensile and Compressive Strain as a Function of Pipe Displacement for Pipelines with Various Soil Coefficients – CASE 1

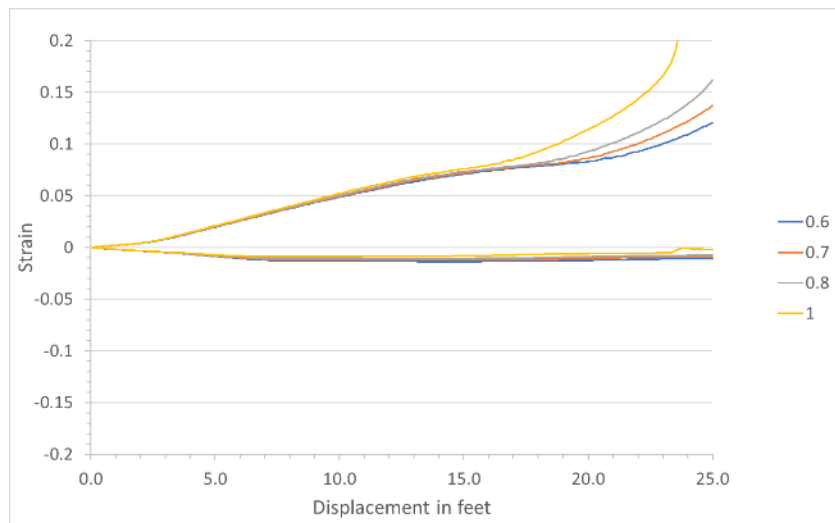
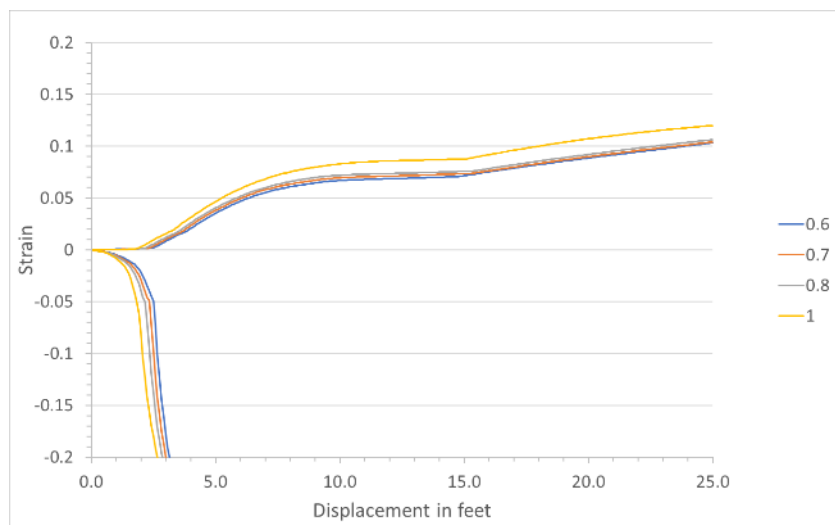


Figure 41: Tensile and Compressive Strain as a Function of Pipe Displacement for Pipelines with Various Soil Coefficients – CASE 2



5.1.8 Pipeline Response Sensitivity to Soil Unit Weight

Changes in pipeline response with changes in the unit weight of soil cover are illustrated in Figure 42 and Figure 43. Soil weight shows limited effect on strain experienced by the pipe both in tension (CASE 1) and in compression (CASE 2).

Figure 42: Tensile and Compressive Strain as a Function of Pipe Displacement for Pipelines with Various Soil Weights – CASE 1

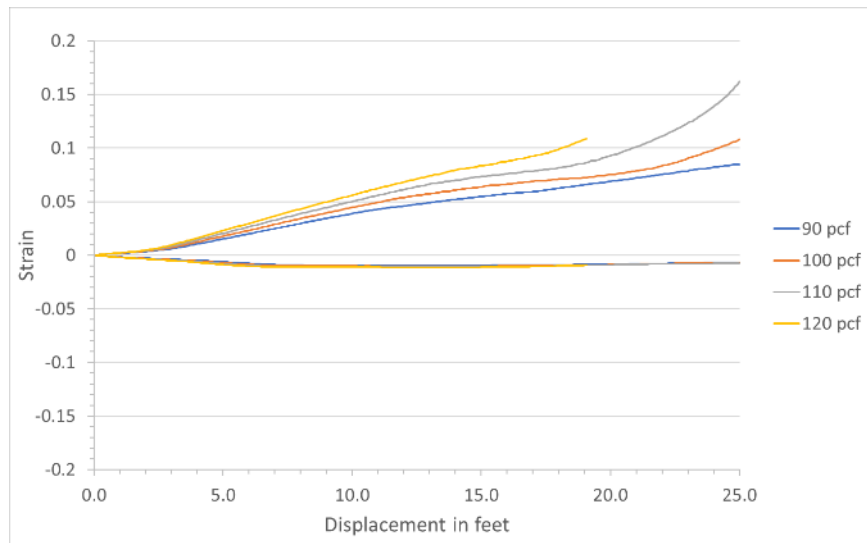
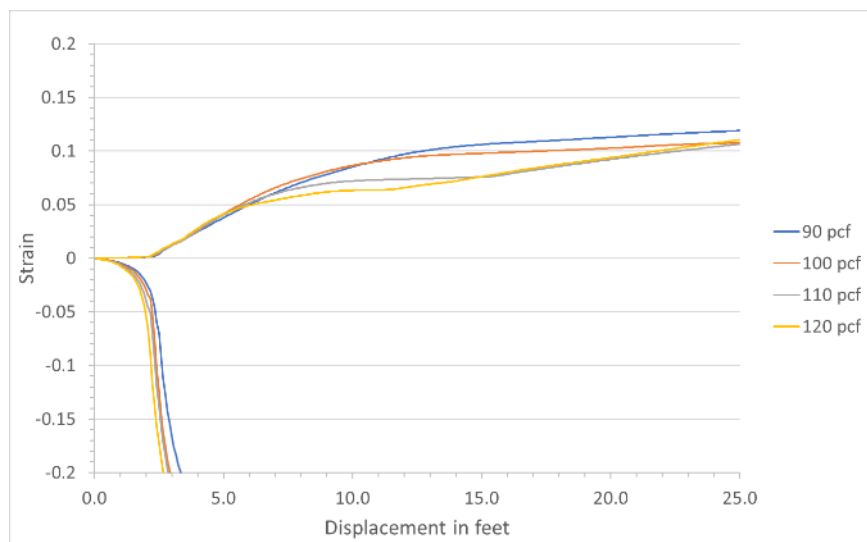


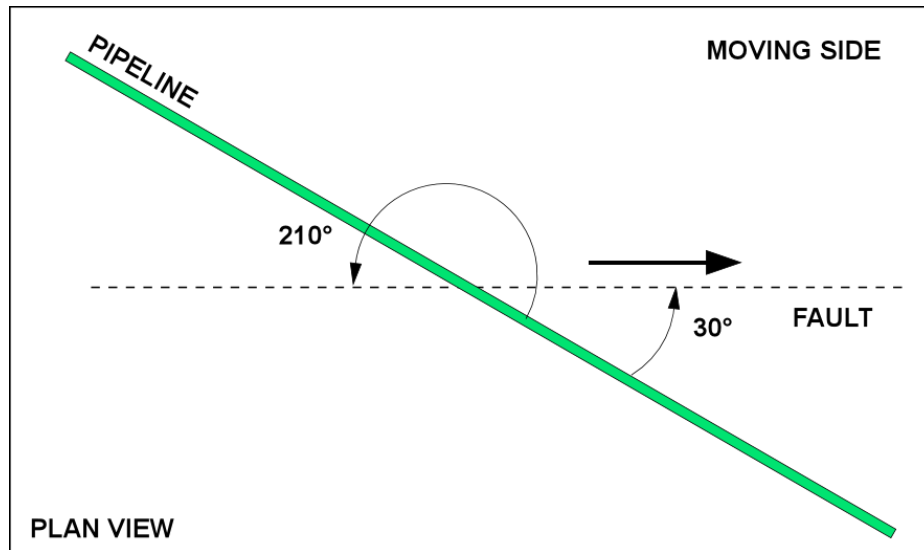
Figure 43: Tensile and Compressive Strain as a Function of Pipe Displacement for Pipelines with Various Soil Weights – CASE 2



5.1.9 Pipeline Response Sensitivity to Fault Displacement Direction

Pipeline response is strongly impacted by the direction of ground displacement relative to the axis of the pipeline. For fault crossings, the full range of pipeline response is covered by examining horizontal angles (see Figure 13) between 0° and 180° because of symmetry. As an example, consider purely horizontal, right-lateral, strike-slip displacement. A pipeline crossing such a fault at a horizontal angle of 30° relative to the fault strike is the same as a pipeline crossing the fault at a horizontal angle of 210° (see Figure 44).

Figure 44: Illustration of Symmetric Response for Fault Crossing Evaluations



This is confirmed by the plots of strain versus displacement for horizontal angles of 0° to 180° and 180° to 360° in Figure 45 and Figure 46 for CASE 1 and also Figure 47 and Figure 48 for CASE 2 that show virtually identical results.

Similarly, symmetry allows the full range of vertical angles to be represented by analyses for vertical angles between 0° and 90° . The variation in strain versus fault displacement for a horizontal angle of 90° and 210° and vertical angles between 15° and 90° for CASE 1 and CASE 2 are illustrated in Figure 49 and Figure 50, respectively.

Figure 45: Tensile and Compressive Strain as a Function of Pipe Displacement for Pipelines with Horizontal Angles 0° - 180° – CASE 1

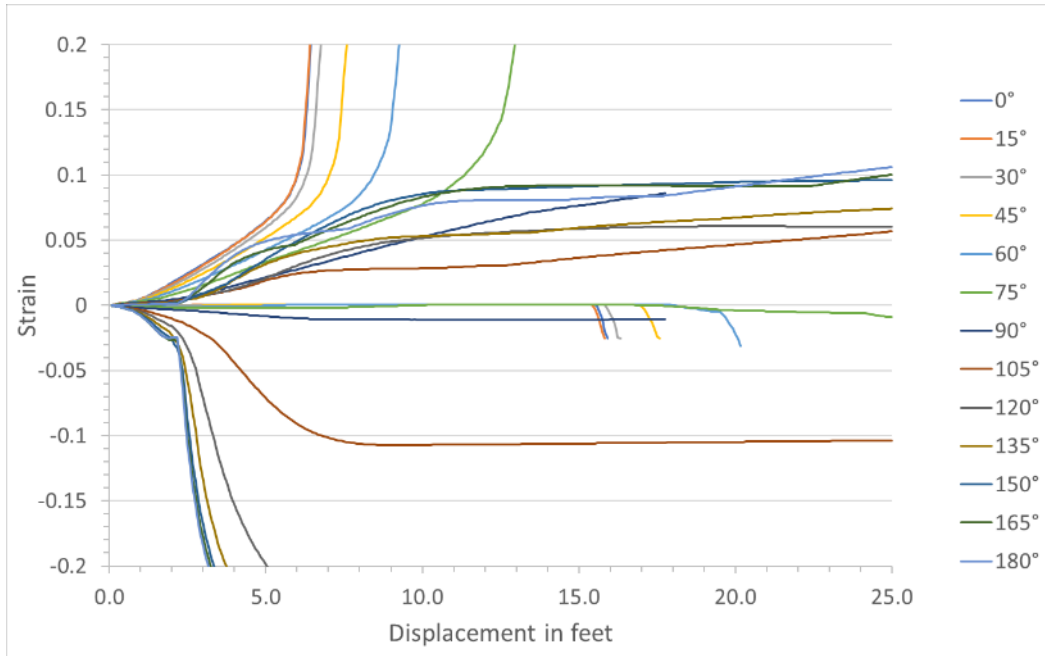


Figure 46: Tensile and Compressive Strain as a Function of Pipe Displacement for Pipelines with Horizontal Angles 180° - 360° – CASE 1

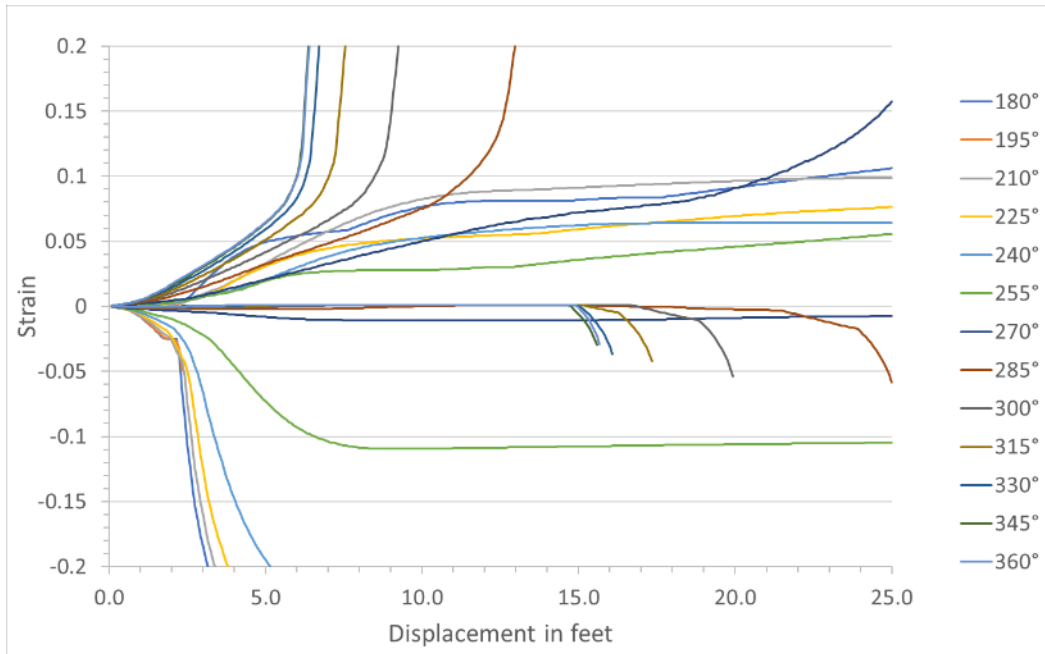


Figure 47: Tensile and Compressive Strain as a Function of Pipe Displacement for Pipelines with Horizontal Angles 0° - 180° – CASE 2

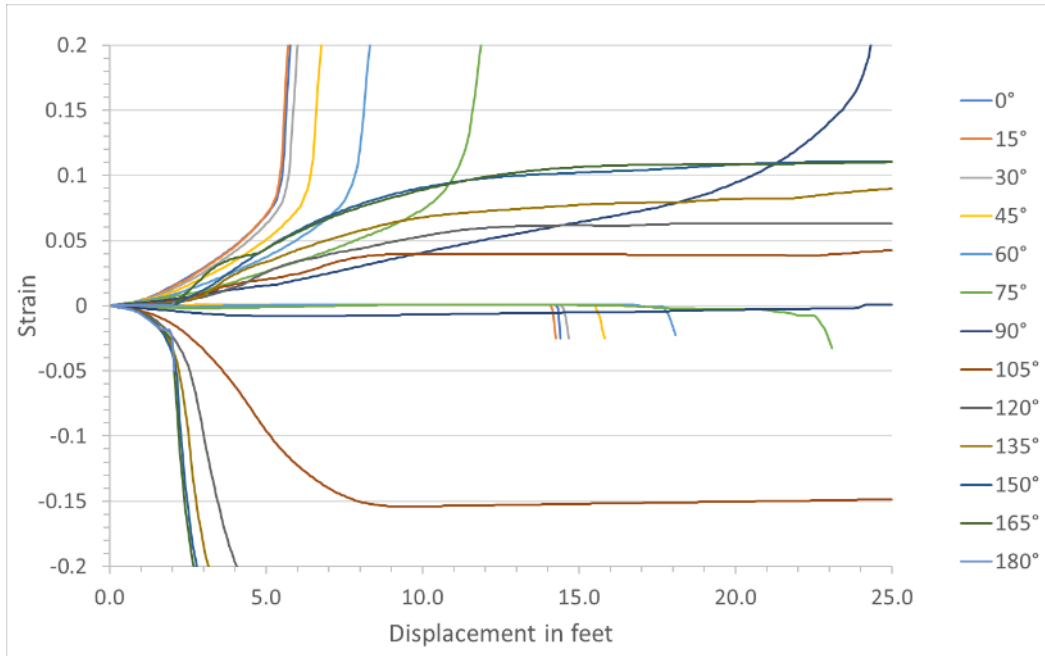


Figure 48: Tensile and Compressive Strain as a Function of Pipe Displacement for Pipelines with Horizontal Angles 180° - 360° – CASE 2

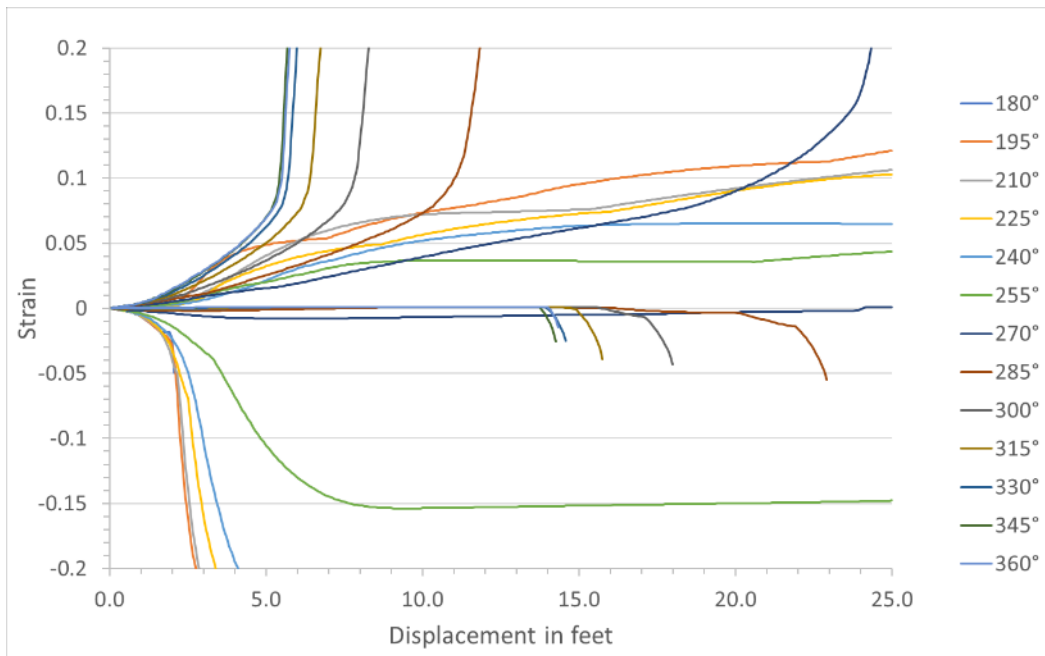


Figure 49: Tensile and Compressive Strain as a Function of Pipe Displacement for Pipelines with Various Vertical Angles 15° - 89° – CASE 1

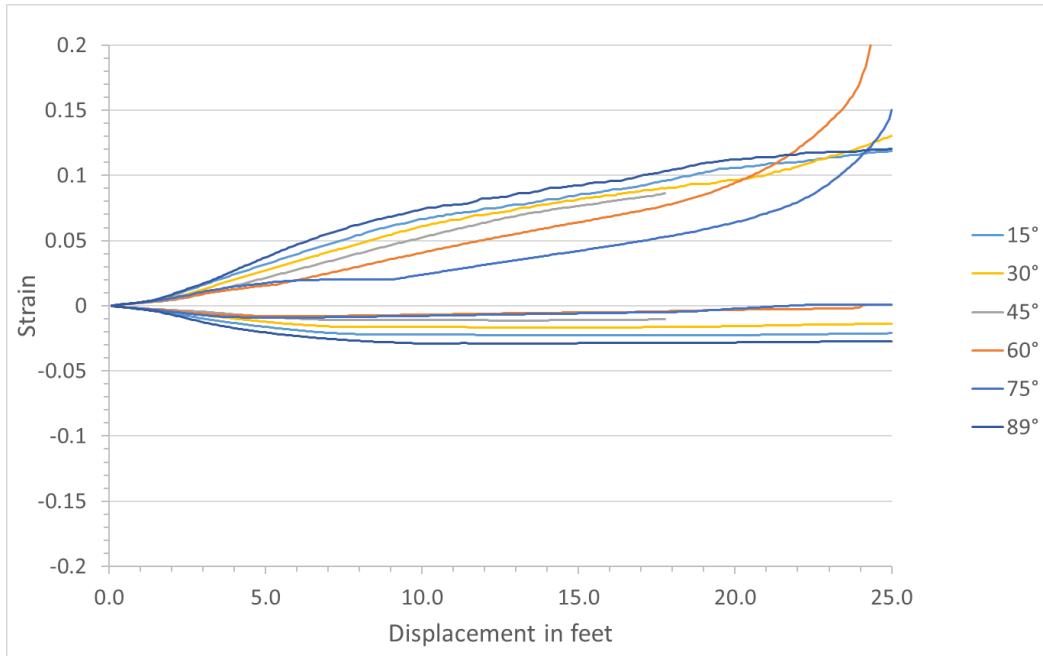
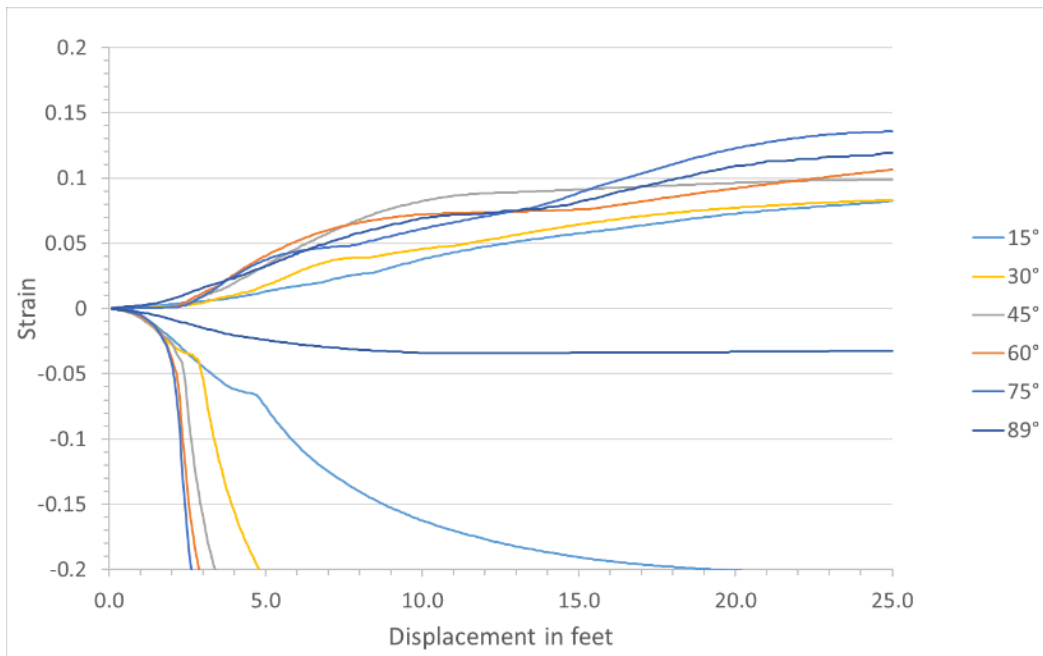


Figure 50: Tensile and Compressive Strain as a Function of Pipe Displacement for Pipelines with Various Vertical Angles 15° - 89° – CASE 2



5.2 Gas Pipeline Strain Experienced Bayesian Model for Fault Displacement

5.2.1 Fault Crossing Model Inputs for Fault Displacement

Table 12 shows the results of the fault crossing sensitivity analyses. To create an objective measure, we computed the amount of pipe displacement required to reach 2.5% strain. Inputs showing the greatest variation in displacement are the inputs that are considered to have the most impact on pipe strain. As shown in the previous section (sensitivity analysis) fault angle, pipe thickness and pipe depth of cover have the most impact on pipe strain, not accounting for the fault displacement (i.e., the main cause of pipe failure). On the other end of the spectrum, pipe pressure and soil coefficient have virtually no effects on the pipe strain.

Table 12: Relative Importance of Input Parameters for the Gas Pipeline Strain Experience Model

	Tensile Strain		Compressive Strain	
	Variation in displacement	Relative importance	Variation in displacement	Relative importance
Pipe Yield Strength	1.58 ft	0.02	0.67 ft	0.02
Pipe Diameter	4.58 ft	0.07	0.67 ft	0.02
Pipe Thickness	17.92 ft	0.26	1.75 ft	0.05
Pipe Pressure	0.83 ft	0.01	0.17 ft	0.00
Depth of Cover	16.42 ft	0.24	6.42 ft	0.19
Soil Friction Angle	9.17 ft	0.13	0.58 ft	0.02
Soil Shear Strength	6.67 ft	0.10	0.67 ft	0.02
Soil Coefficient	0.27 ft	0.00	0.40 ft	0.01
Soil Unit Weight	1.75 ft	0.03	0.33 ft	0.01
Horizontal Fault Angle	4.42 ft	0.06	22.42 ft	0.65
Vertical Fault Angle	6.17 ft	0.09	0.33 ft	0.01

Using the results of the sensitivity analysis, we ranked each input from the most important to least important. The most important input (fault displacement) was given 6 states, while the least

important inputs are given only one state (as shown in Table 13). It should be noted that the states are not even. For example, the range of the pipe thickness first state is 0.1 inch (0.1 to 0.2 inch) while the last state is 0.6 inch (6 times more, 0.6 to 1.2 inch). The states have been organized to create an even change in pipe strain from state to state. The horizontal fault angle from 0° to 180° and vertical fault angle from 0° to 90° are defined in Bayesian model convention as shown in Table 13 to eliminate symmetry.

Table 13: Model Discretization using Sensitivity Analysis for Fault Displacement

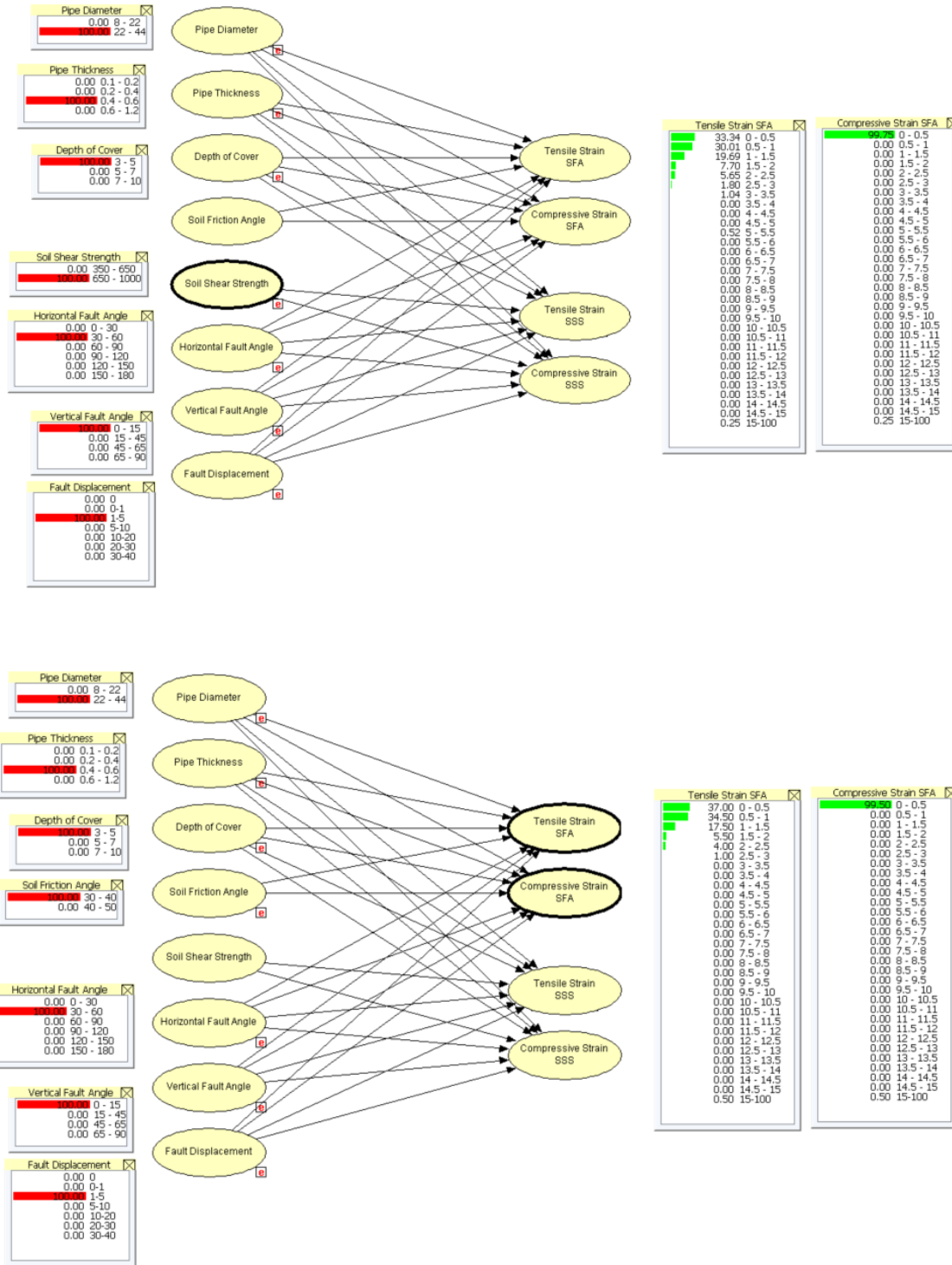
Input	Ranking	Bayesian Network Model States	Unit
Pipe Yield Strength	10	[42000,70000]	psi
Pipe Diameter	8	[8.625,22] [22,44]	in
Pipe Thickness	3	[0.1,0.2] [0.2,0.4] [0.4,0.6] [0.6,1.2]	in
Pipe Pressure	11	[0,1000]	psi
Depth of Cover	4	[3,5] [5,7] [7,10]	ft
Soil Friction Angle	5	[30,40] [40,50]	deg
Soil Shear Strength	6	[300,650] [650,1000]	psf
Soil Coefficient	12	0.8	-
Soil Unit Weight	9	[90,120]	pcf
Horizontal Fault angle	2	[0,30] [30,60] [60,90] [90,120] [120,150] [150,180]	deg
Vertical Fault angle	7	[0, 15] [15,45] [45,65] [65,90]	deg
Fault displacement	1	1, 5, 10, 20, 30, 40	ft

5.2.2 Gas Pipeline Strain Experienced Bayesian Model for Fault Displacement

For every combination of inputs shown in the Table 13, we performed 150 FEA simulations (alike to a Monte Carlo approach). We generated 158,400 simulations for SFA and 158,400 simulations for SSS. In total we performed over 240 thousand simulations. Cases corresponding to a hoop stress greater than 72% of the pipe yield strength were not performed. Collaboration with experts from ANSYS Inc. and Texas Advanced Computing Center (TACC) was necessary to run the simulations. The simulations generated 5PB of data. At this stage of the process our main objective is to compress the data until it becomes useful to the user. This is done by combining all results into four conditional probability tables (CPTs) for SFA and SSS and for tensile and compressive

strain. The four CPTs are used to create a Bayesian network (BN) model. The model is depicted in Figure 51.

Figure 51: Fault Displacement Model (top Tensile and Compressive Strain Calculated Using SSS, bottom, Tensile and Compressive Strain Calculated Using SFA)



6 Experienced Strain Model for Landslides and Liquefaction

6.1 Sensitivity Analysis for Lateral Displacement

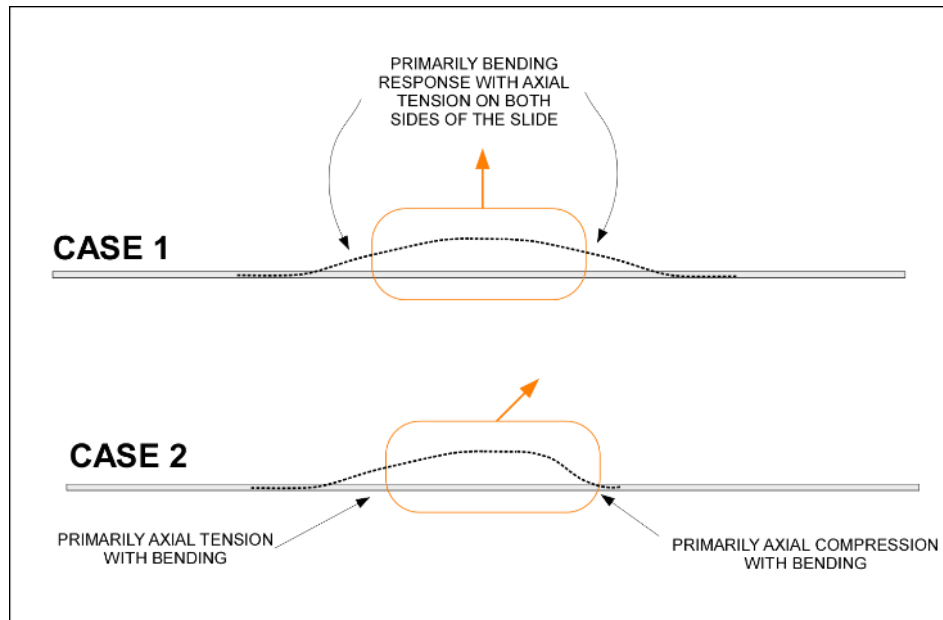
The type of modeling and analysis for landslides and liquefaction are similar, as the pipeline would be subjected to lateral displacement. Section 4.2 explains the difference between modeling approach for lateral displacement compared to fault displacement. As explained in Chapter 5, before running all the FEA required to create the Bayesian model conditional probability table (CPT) a sensitivity analysis is performed to optimize the number of FEAs. The objective of the sensitivity analysis is not to be perfect but to be a guide for the next step of the process. Two cases were selected as shown in Table 14.

Table 14: Data Used for Sensitivity Analysis

	BASE CASE 1	BASE CASE 2
Steel type	X60	X60
Pipe diameter	24 inch	24 inch
Pipe thickness	0.375 inch	0.375 inch
Pipe internal pressure	400 psi	400 psi
Soil Cover Depth	5 feet	5 feet
Soil Friction Angle	40 degrees	40 degrees
Soil Shear Strength	0 psf	0 psf
Soil Coefficient	0.375 and 0.8	0.375 and 0.8
Soil Unit Weight	110 pcf	110 pcf
Movement direction	90 degree crossing	45 degree crossing

Similar to the sensitivity cases for fault crossings, two separate cases are considered for the landslide/liquefaction sensitivity analyses that represent a situation with bending and axial tension and a condition where there is bending and axial compression. Covering these two conditions is necessary because the pipeline displacement capacity differs significantly from cases dominated by tension versus compression. This is illustrated in Figure 52.

Figure 52: Illustration of Pipeline Response for Lateral Displacement Sensitivity Cases 1 and 2



6.1.1 Pipeline Response Sensitivity to Steel Type

The steel type chosen for the sensitivity analysis varied from 35 ksi to 70 ksi with the specific selections the same as for the fault displacement calculations in the previous section (i.e., B, X42, X52, X60, X65, X70). Although important, the grade of steel has a limited effect on the computed strain, as shown in Figure 53 and Figure 54. Strains begin to rapidly increase after a displacement of 20 to 25 ft for CASE 1 and 19 to 25 ft for CASE 2.

Figure 53: Tensile and Compressive Strain as a Function of Pipe Displacement for Steels with Various Yield Strengths – CASE 1

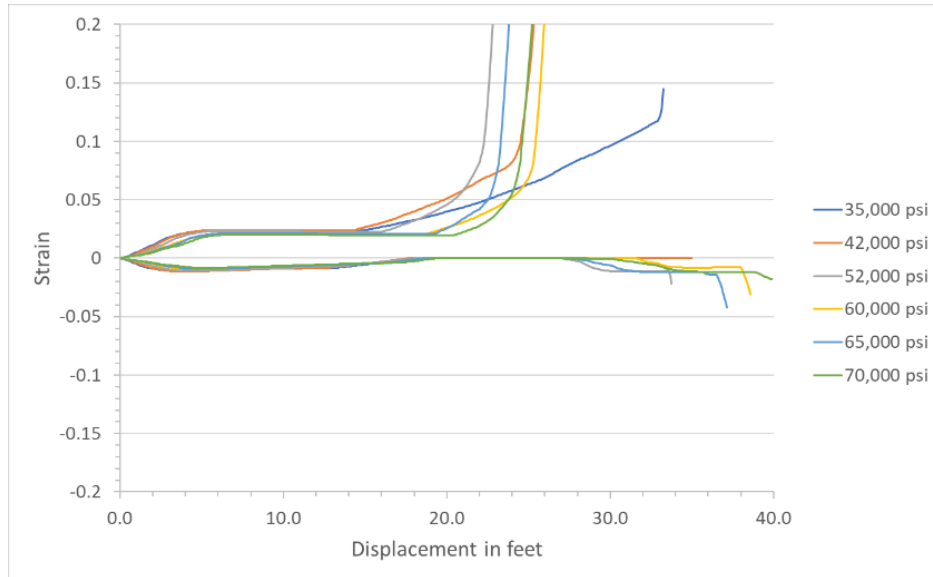
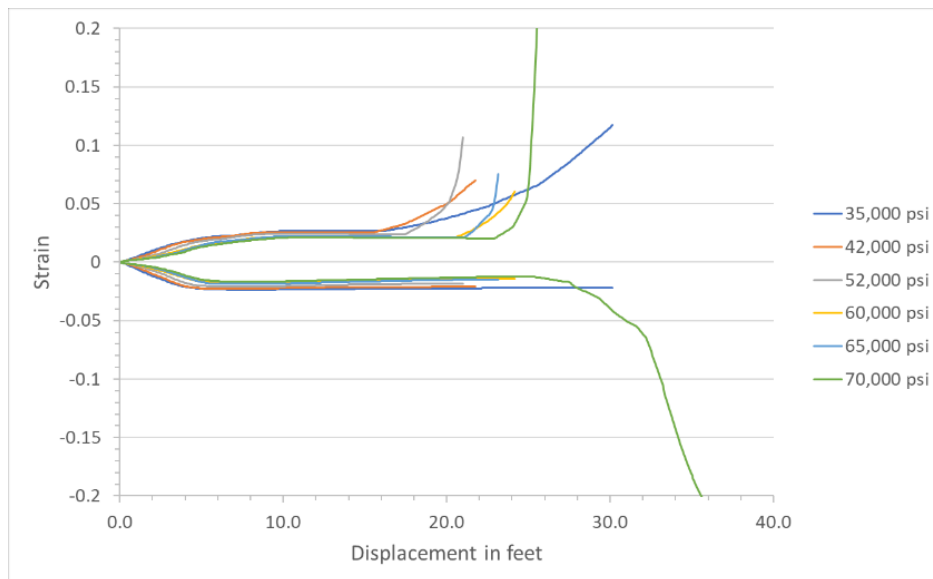


Figure 54: Tensile and Compressive Strain as a Function of Pipe Displacement for Steels with Various Yield Strengths – CASE 2



6.1.2 Pipeline Response Sensitivity to Pipe Diameter

Pipe diameter has a limited effect on the computed strain as shown in Figure 55 and Figure 56. As with the ground fault displacement cases in the previous chapter, the strongest effect occurs for the smaller pipe diameter.

Figure 55: Tensile and Compressive Strain as a Function of Pipe Displacement for Pipelines with Various Pipe Diameters – CASE 1

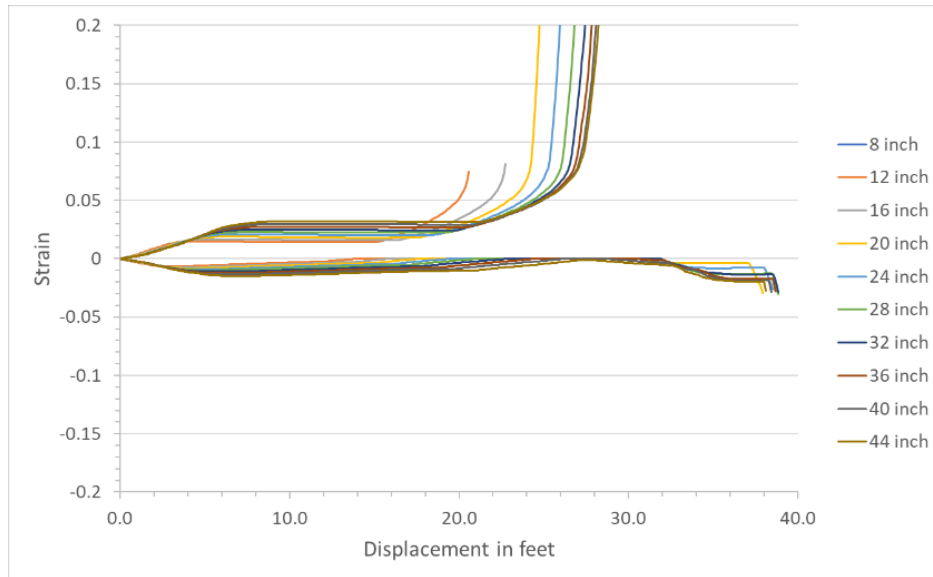
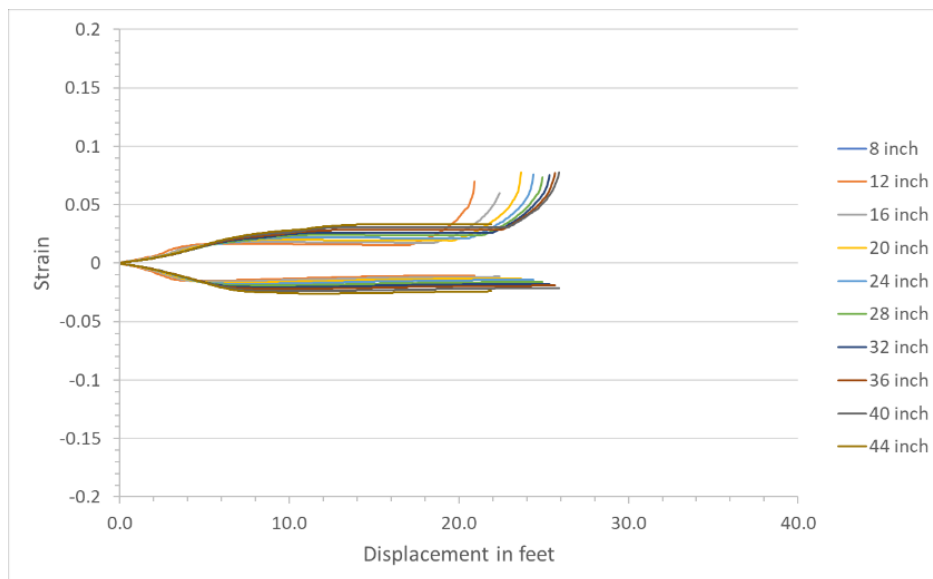


Figure 56: Tensile and Compressive Strain as a Function of Pipe Displacement for Pipelines with Various Pipe Diameters – CASE 2



6.1.3 Pipeline Response Sensitivity to Pipe Wall Thickness

As with the fault displacement simulations, wall thickness has a strong impact on compute pipe strain, both in tension and compression. The trends are illustrated in Figure 57 and Figure 58. The sensitivity to changes in wall thickness is greatest when the pipe wall thickness is small (less than 0.5 inch).

Figure 57: Tensile and Compressive Strain as a Function of Pipe Displacement for Pipelines with Various Pipe Wall Thickness – CASE 1

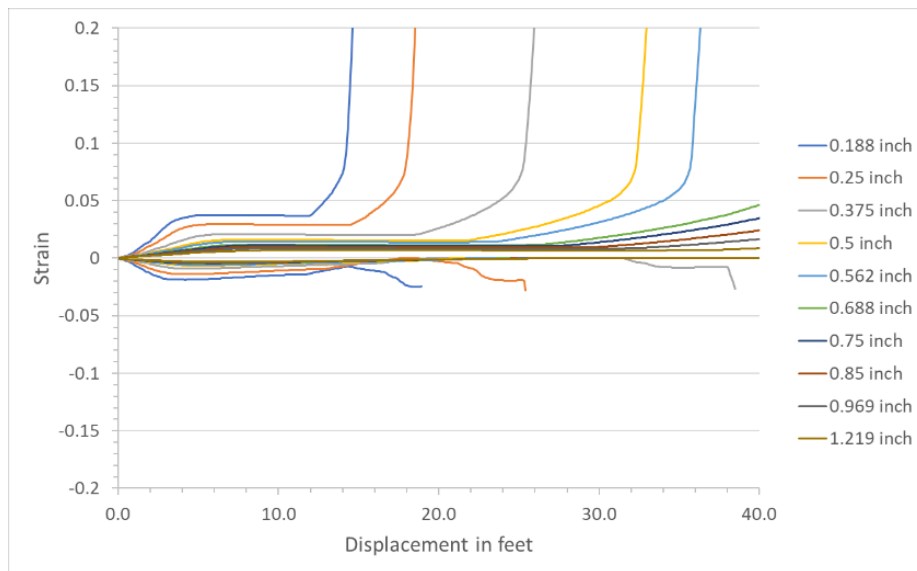
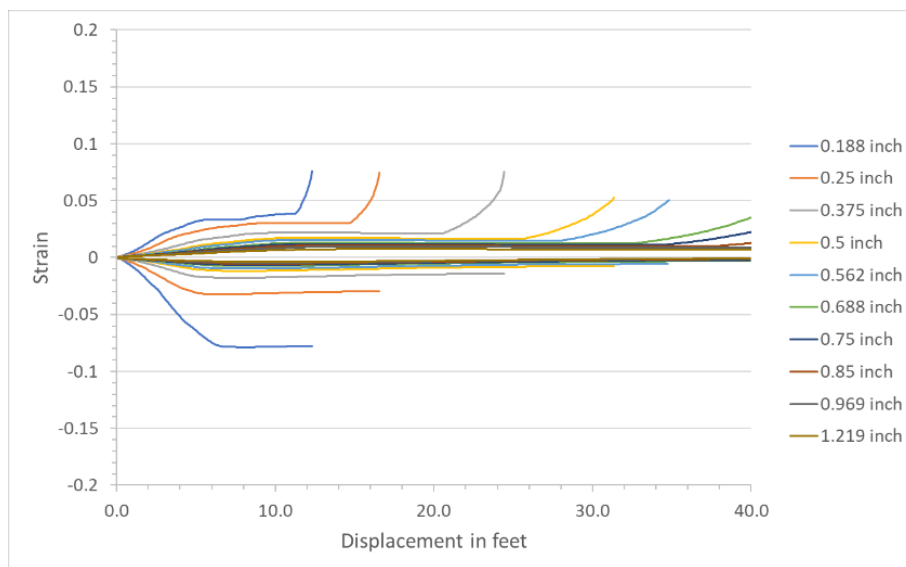


Figure 58: Tensile and Compressive Strain as a Function of Pipe Displacement for Pipelines with Various Pipe Wall Thickness – CASE 2



6.1.4 Pipeline Response Sensitivity to Internal Pressure

As seen in Figure 59 and Figure 60, internal pressure has a limited effect on strain experienced by the pipe. This was expected as the forces applied by the ground on the pipe are much stronger than the forces applied to the pipe by the internal pressure.

Figure 59: Tensile and Compressive Strain as a Function of Pipe Displacement for Pipelines with Various Pipe Pressures – CASE 1

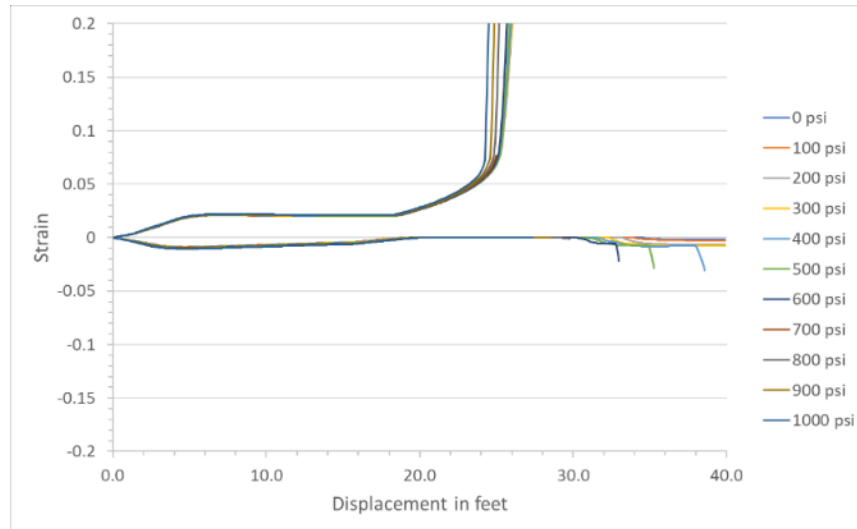
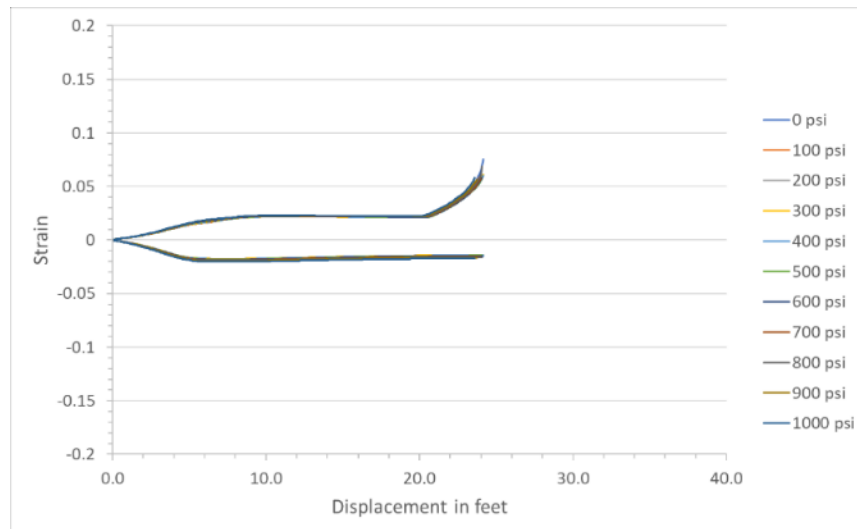


Figure 60: Tensile and Compressive Strain as a Function of Pipe Displacement for Pipelines with Various Pipe Pressures – CASE 2



6.1.5 Pipeline Response Sensitivity to Depth of Soil Cover

The depth of soil cover has a relatively large effect on the strain experienced by the pipe. As in the fault displacement simulations, strains are reduced when the depth of cover is shallow (less 4 feet). For example, in CASE 1 the pipeline may survive 40 ft displacement if the depth of over is less than 2 feet. 3 ft depth of cover would lead to a failure in tension at 39 ft displacement and 4 ft depth of cover would lead to a failure in tension at 31 ft displacement. A similar observation can be made using CASE 2.

Figure 61: Tensile and Compressive Strain as a Function of Pipe Displacement for Pipelines with Various Pipe Depth of Cover – CASE 1

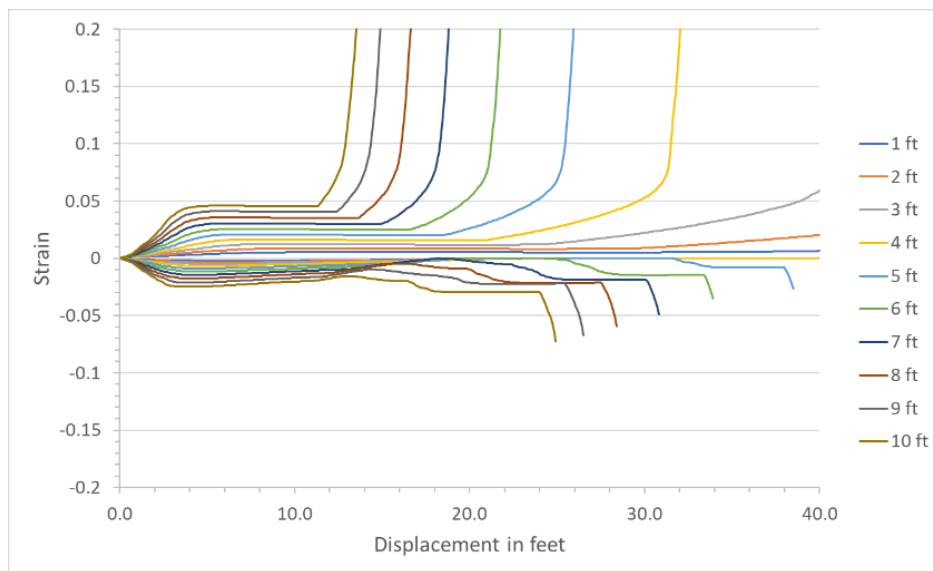
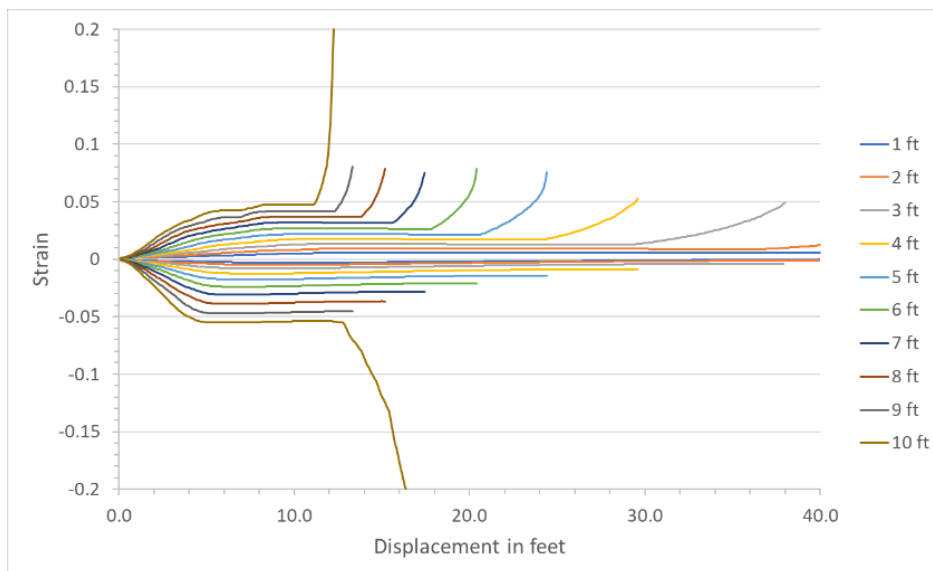


Figure 62: Tensile and Compressive Strain as a Function of Pipe Displacement for Pipelines with Various Pipe Depth of Cover – CASE 2



6.1.6 Pipeline Response Sensitivity to Levels of Soil Restraint

Changes in pipeline response with changes in SFA are illustrated in Figure 63 and Figure 64. Changes in pipeline response with changes in SSS are illustrated in Figure 65 and Figure 66. Although SFA and SSS have a great impact on the amount of soil restraint and therefore the strain experienced by the pipe, the variability of soil restraint is limited, making the impact for SFA and SSS on pipe strain limited also.

Figure 63: Tensile and Compressive Strain as a Function of Pipe Displacement for Pipelines with Various Soil Friction Angles – CASE 1

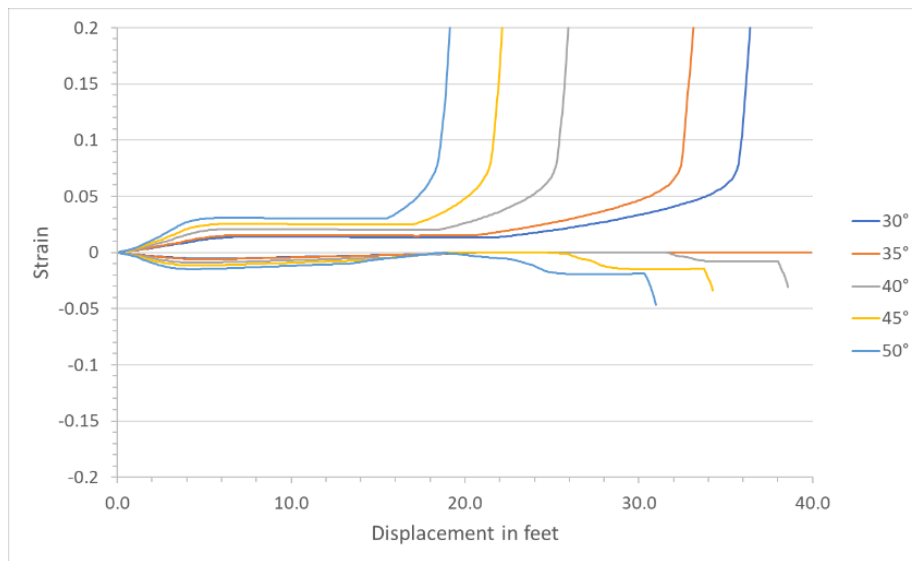


Figure 64: Tensile and Compressive Strain as a Function of Pipe Displacement for Pipelines with Various Soil Friction Angles – CASE 2

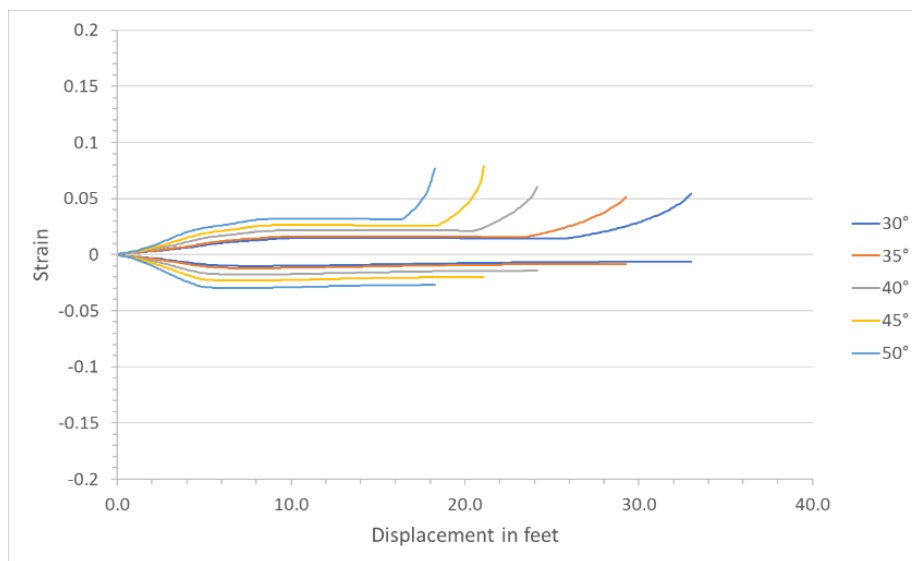


Figure 65: Tensile and Compressive Strain as a Function of Pipe Displacement for Pipelines with Various Soil Shear Strengths – CASE 1

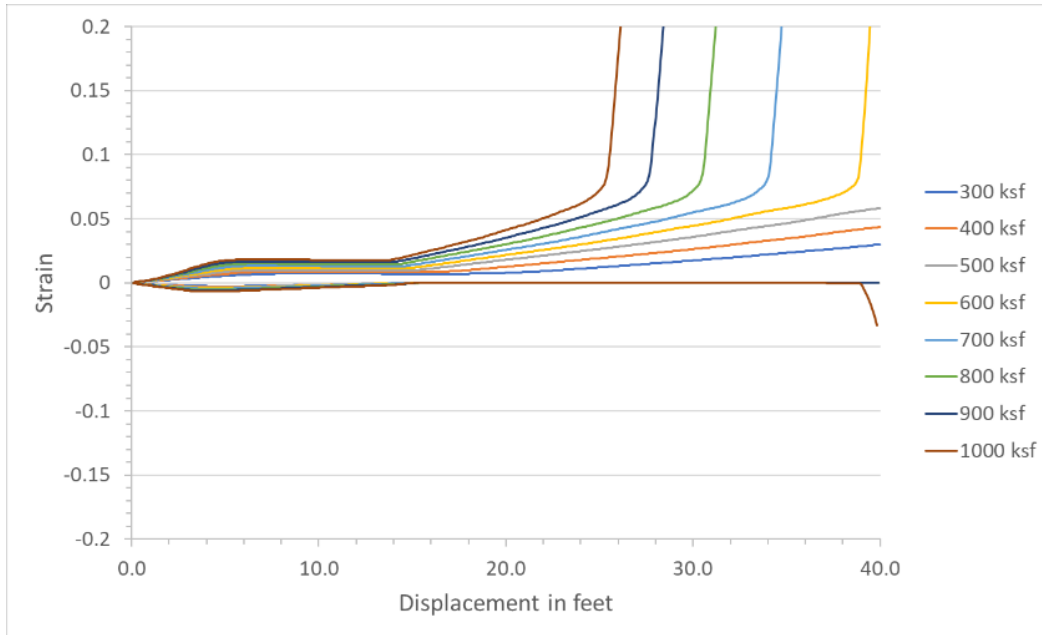
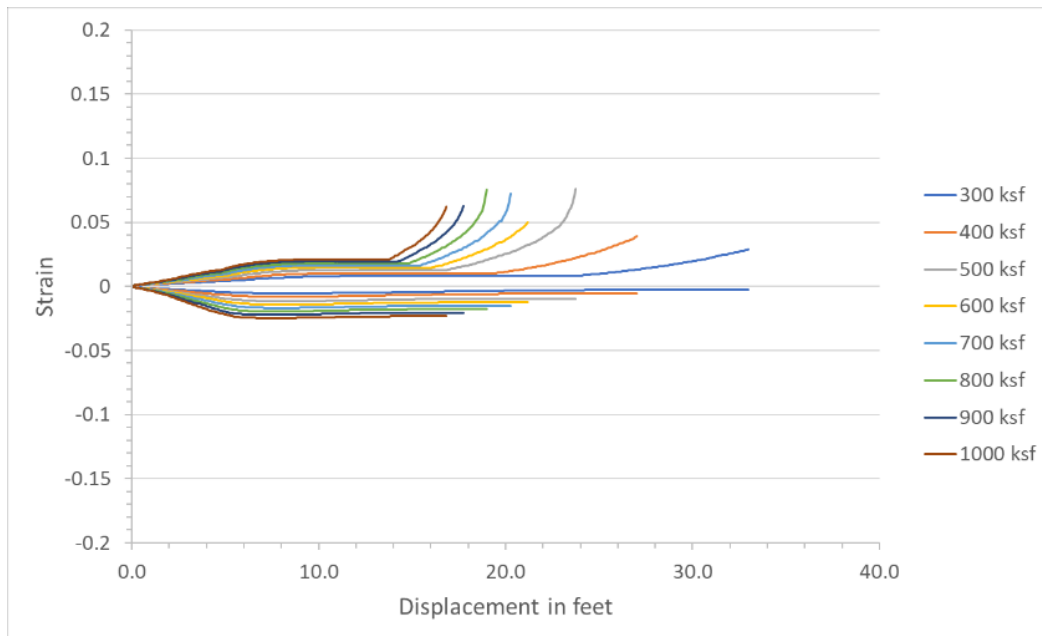


Figure 66: Tensile and Compressive Strain as a Function of Pipe Displacement for Pipelines with Various Soil Shear Strengths – CASE 2



6.1.7 Pipeline Response Sensitivity to Soil Coefficient

As with the fault crossing sensitivity analyses, the soil coefficient has small effect on the strain experienced by the pipe, as seen in Figure 67 and Figure 68.

Figure 67: Tensile and Compressive Strain as a Function of Pipe Displacement for Pipelines with Various Soil Coefficients – CASE 1

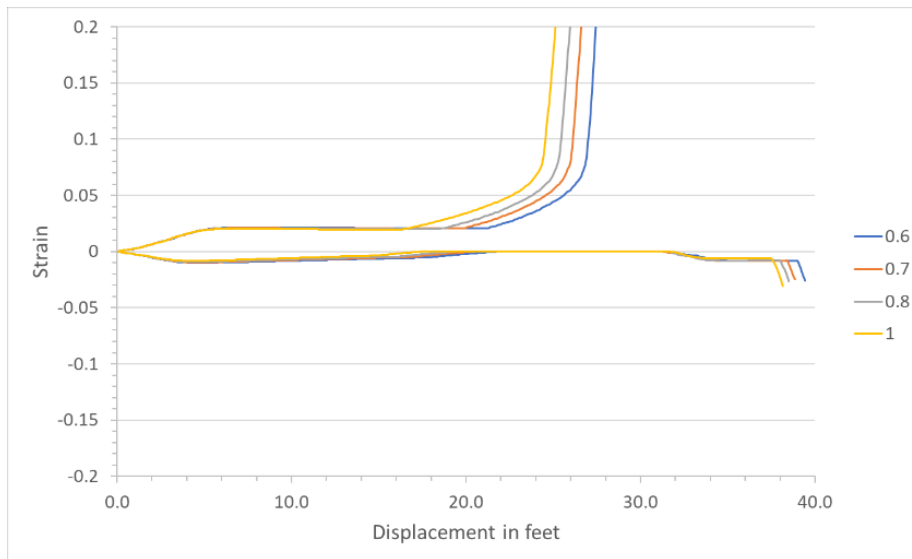
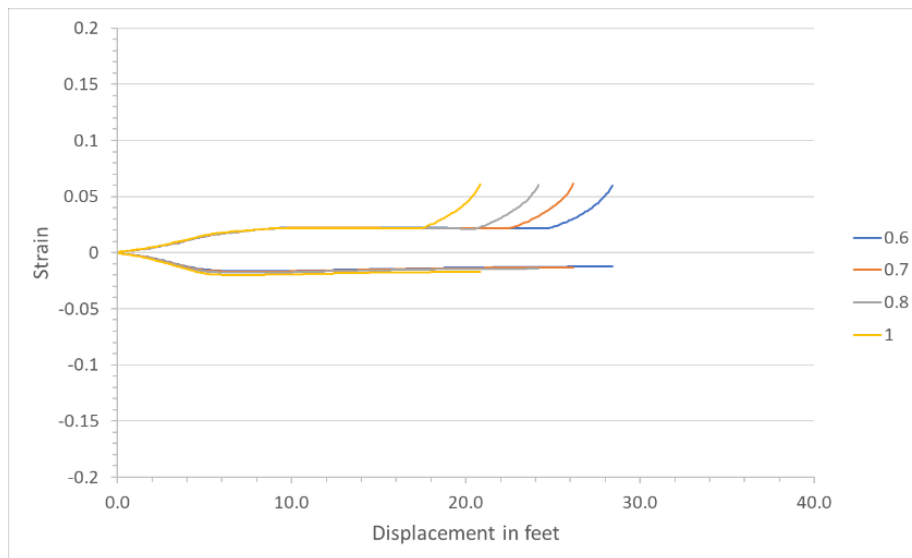


Figure 68: Tensile and Compressive Strain as a Function of Pipe Displacement for Pipelines with Various Soil Coefficients – CASE 2



6.1.8 Pipeline Response Sensitivity Soil Unit Weight

The change in soil unit weight has a limited effect on the strain experienced by the pipe, similar to the fault crossing cases, as seen in Figure 69 and Figure 70.

Figure 69: Tensile and Compressive Strain as a Function of Pipe Displacement for Pipelines with Various Soil Weights – CASE 1

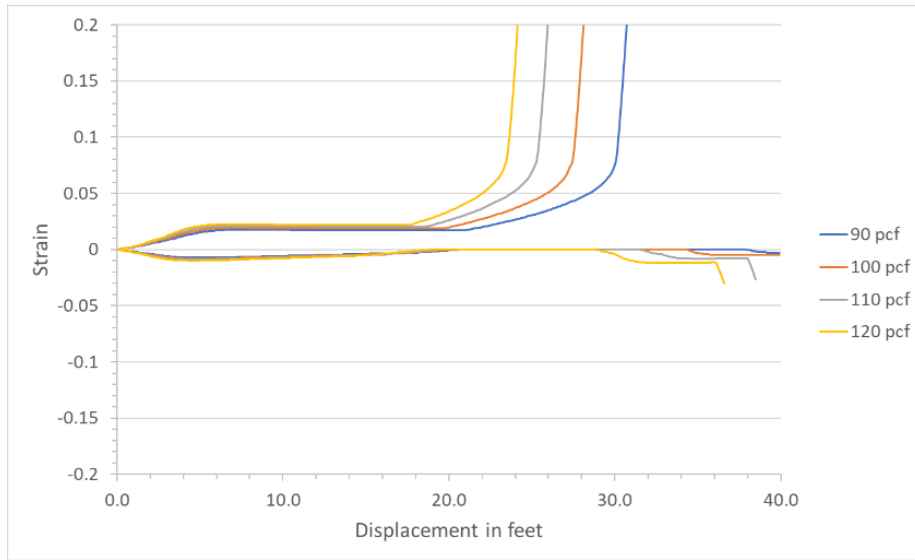
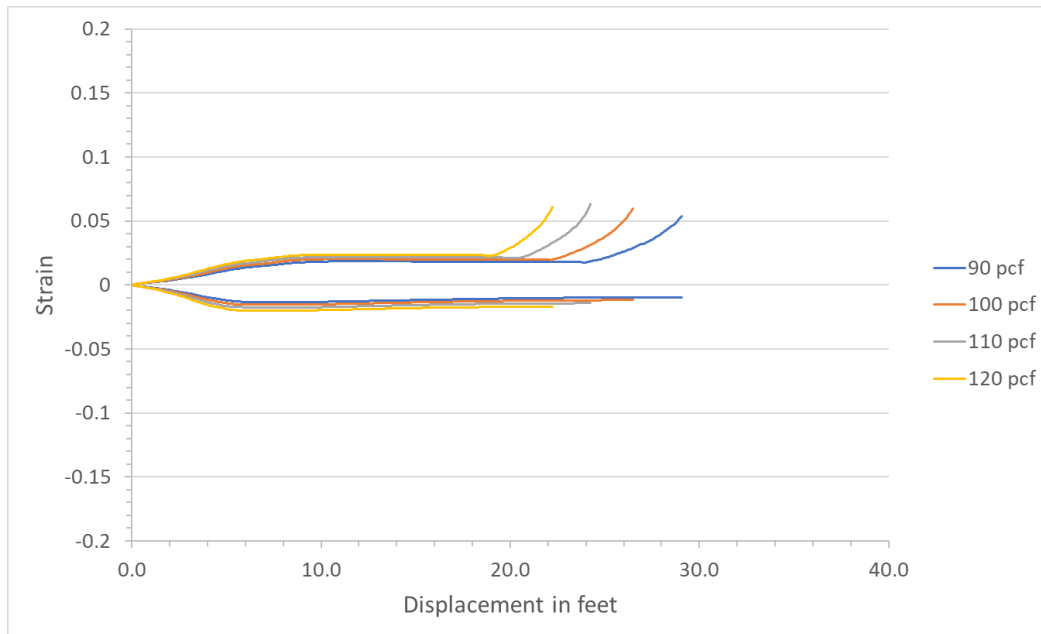


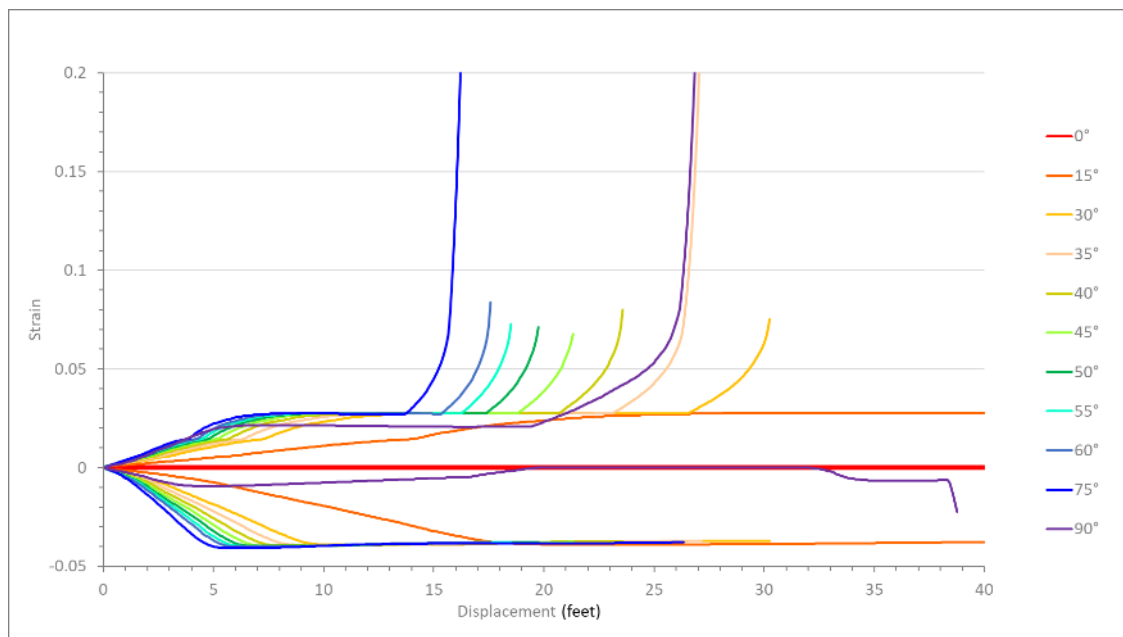
Figure 70: Tensile and Compressive Strain as a Function of Pipe Displacement for Pipelines with Various Soil Weights – CASE 2



6.1.9 Pipe Soil Interactions – Movement Direction Angle

The direction of movement has a significant impact on the strains that the pipeline experiences. This is seen in Figure 71 by the reduction in the displacement at which the pipeline strains start to rapidly increase. The computed strains for direction angles of 0° is constant at a very small value because the 200-ft length of pipeline loaded by ground displacement cannot generate appreciable axial load in the pipeline. The same limit on axial load leads to the strains for a direction angle of 15° are relatively constant after approximately 20 ft of ground displacement. Beyond this, the only loading on the pipeline is from the lateral component of ground displacement which is approximately 26% of the total displacement (i.e., a lateral offset of around 5 ft for the remaining 20 ft of displacement applied in the analyses). The displacement at which strains begin to rapidly increase steadily decreases with increasing direction angle, except for the 90° case. For loading directions other than 90° , the pipeline response at the boundary of the zone of ground displacement is tension with bending at one side and compression with bending on the other. This prevents the development of catenary tension over the length of displaced soil, which reduces the effective bending strength. For a 90° displacement direction, catenary tension is in effect which greatly increases the pipeline bending capacity and the ability to carry the lateral soil load.

Figure 71: Tensile and Compressive Strain as a Function of Pipe Displacement for Pipelines with Various Movement Direction Angles – CASE 2



6.1.10 Pipeline Sensitivity to the Length of Pipe Exposed to Displacement

The amount of pipe exposed to ground displacement is an important factor impacting the level of strain experienced by a pipeline. The results of varying the length of pipeline exposed to

displacement for CASE 1 and CASE 2 are shown in Figure 72 and Figure 73. The sensitivity of the pipeline response in CASE 1 is not as apparent as for CASE 2 because with a 90° direction angle, the pipeline can withstand unlimited displacement for a small exposure length since it can carry the maximum soil load that can develop. For very long exposed lengths, the pipeline response is largely controlled by bending at the margins of the displacement zone and the only differences is in the change in bending strength from catenary effects. For CASE 2, the response for small exposed lengths is similar to CASE 1. At larger exposed lengths, the compressive loading at one end of the zone of displacement reduces the effective bending strength of the pipeline. As a result, high compressive strains dominate the response for exposure lengths greater than 500 ft.

Figure 72: Tensile and Compressive Strain as a Function of Pipe Displacement for Pipelines with Various Amount of Pipe Exposed – CASE 1

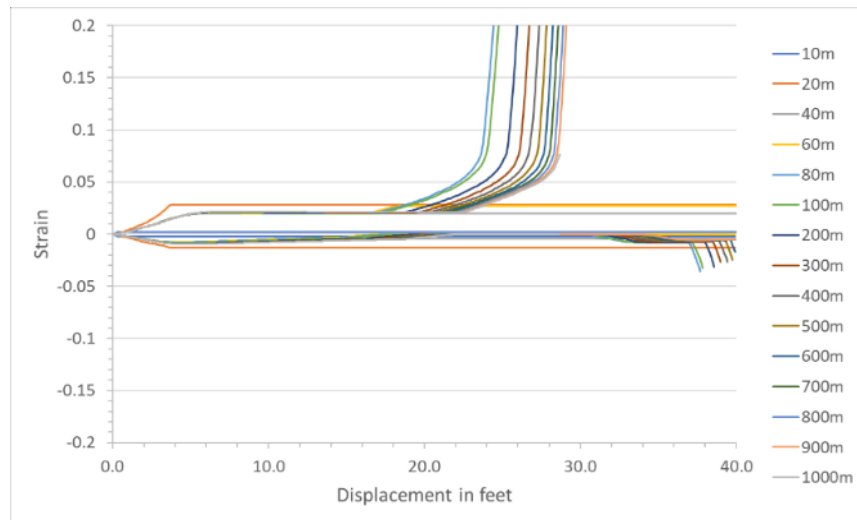
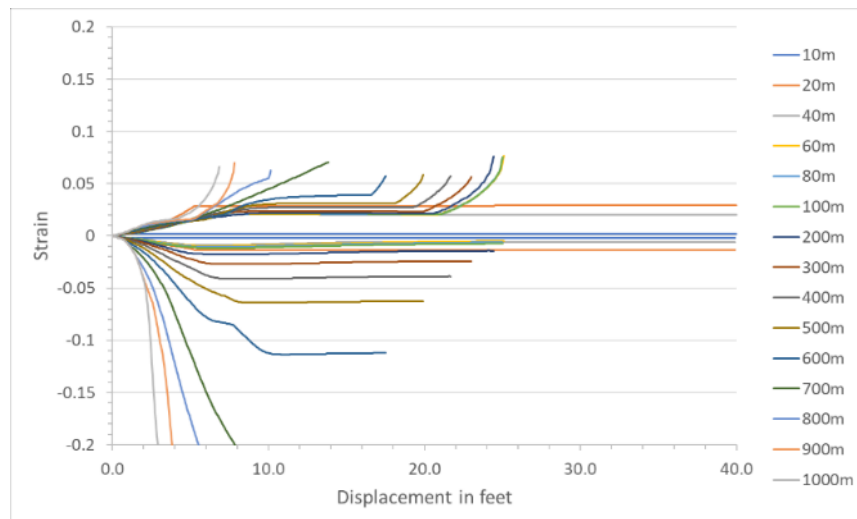


Figure 73: Tensile and Compressive Strain as a Function of Pipe Displacement for Pipelines with Various Amount of Pipe Exposed – CASE 2



6.2 Gas Pipeline Strain Experienced Bayesian Model for Landslide & Liquefaction

6.2.1 Gas Pipeline Strain Experienced Bayesian Model Inputs for Lateral Displacement

Table 15 lists the results of the sensitivity analysis. To create an objective measure, we computed the amount of pipe displacement required to reach 3% tensile strain. Inputs showing the greatest variation in displacement are the inputs that have the most impact on pipe strain. As with the fault displacement model, the pipe thickness has a strong effect on pipeline strain. It was found the ground movement direction angle compared to the pipe has a strong effect also, the effect is stronger than the effect of both horizontal and vertical angles for fault displacement. Depth of cover, soil properties (i.e., SFA, SSS) and amount of pipe exposed have also been found to have a significant effect on pipe strain. On the other end of the spectrum, pipe pressure, pipe yield strength and soil unit weight have virtually no effects on the pipe strain.

Table 15: Relative Importance of Input Parameters for the Gas Pipeline Strain Experience Model for Lateral Displacement

	Tensile Strain	
	Variation in displacement	Relative importance
Pipe Yield Strength	7.33 ft	0.03
Pipe Diameter	14 ft	0.06
Pipe Thickness	35.08 ft	0.16
Pipe Pressure	0.5 ft	0.00
Depth of Cover	31.83 ft	0.15
Soil Friction Angle	23.83 ft	0.11
Soil Shear Strength	22.75 ft	0.11
Soil Coefficient	7.5 ft	0.03
Soil Unit Weight	6.58 ft	0.03
Movement Direction Angle	50 ft	0.23
Amount of Pipe Exposed	16.83 ft	0.08

The same process as in Section 5 is followed to create lateral displacement model inputs. Using the results of the sensitivity analysis, inputs were ranked from the most important to least important. The most important inputs (ground movement direction angle and amount of displacement) were given six states, while the least important inputs are given only one state (as shown in Table 16). The number and range of the states for the various inputs are selected to capture the sensitivity in pipeline response while maintaining a manageable number of computations needed.

Table 16: Model Discretization using Sensitivity Analysis for Lateral Displacement

Input	Ranking	Bayesian Network Model States	Unit
Pipe Yield Strength	9	[35000,70000]	psi
Pipe Diameter	10	[8,22] [22,44]	in
Pipe Thickness	2	[0.1,0.2] [0.2,0.4] [0.4,0.6] [0.6,1.2]	in
Pipe Pressure	11	[0,1000]	psi
Depth of Cover	3	[3,5] [5,7] [7,10]	ft
Soil Friction Angle	6	[30,40] [40,50]	deg
Soil Shear Strength	6	[300,650] [650,1000]	psf
Soil Coefficient	7	0.8	-
Soil Unit Weight	8	[90,120]	pcf
Movement Direction Angle	5	[0,15] [15,30] [30,45] [45,60] [60,75] [75,90]	deg
Amount of Pipe Exposed	4	[10,50] [50,100] [100,200] [200,500]	m
Amount of Displacement	1	[0,1] [1,5] [5,10] [10,20] [20,30] [30,40]	ft

6.2.2 Gas Pipeline Strain Experienced Bayesian Model for Lateral Displacement

For every combination of inputs shown in Table 16, we performed 150 FEA simulations (alike to a Monte Carlo approach). There are 2,304 combinations therefore we generated 172,800 simulations for SFA and 172,800 simulations for SSS. In total we performed over 310 thousand simulations. Cases corresponding to a hoop stress greater than 72% of the pipe yield strength were not performed. Collaboration with experts from ANSYS Inc. and Texas Advanced Computing

Center (TACC) was necessary to run the simulations. The simulations generated 5PB of data. At this stage of the process our main objective is to compress the data until it becomes useful to the user. This is done by combining all results into four conditional probability tables (CPTs) for SFA and SSS and for tensile and compressive strain. The four CPTs are used to create a Bayesian network (BN) model. The model is depicted in Figure 74.

Figure 74: Experienced Strain Model for Lateral Displacement – Tensile and Compressive Strain Calculated Using SSS (top) and SFA (bottom)



7 Pipeline Strain Capacity Models

Pipeline response to external forces of ground movement hazards is gauged by comparing the estimates of longitudinal tensile and compressive strains caused by ground movement to the tensile and compressive strain capacity for a specific set of conditions related to pipeline wall thickness, presence of flaws related to weld defects or corrosion, internal pipeline pressure, etc. The strain capacity chosen to compare with strain demand is also a function of the level of pipeline performance that is being evaluated. Pipelines may experience strains beyond yield and continue to function safely. Pipeline construction inevitably requires cold bending of the pipeline to accommodate topographic variability. In current practice, the plastic strains developed during cold bending are neglected in determining the safe operating pressure for gas pipelines. The acceptability of strains developed during field bending is related to maintaining a uniform pipeline cross section with no evidence of local pipe wall wrinkling or coating damage. The strain capacity limits meeting performance objectives similar to those for field bends are referred to by a variety of terms such as “operational” or “continued safe operation”. The response of pipelines exceeding these strain limits is typically characterized by ovaling of the pipe cross section that could impede the passage of internal measurement devices and local pipe wall wrinkling that could damage pipeline coatings.

Evaluating the potential for pipeline rupture needs to be based upon levels of strain associated with a significant chance of causing pipeline rupture. These strain capacity limits are referred to in such terms as “pressure integrity”, “loss of content” and “rupture”. For the purposes of this report, we will refer to the two performance limits: “continued operation” and “pressure integrity”. Continued operation tensile and compressive strain capacities are based upon the severity of corrosion defects in the pipe body. Pressure integrity tensile and compressive strain capacities are based upon comparing predictive tensile strain capacity formulations with test results and full-scale tests of pipeline specimens under compression and bending.

Continued operation strain capacity limits for corrosion defects are based upon formulations of tensile and compressive strain capacity associated with corrosion defects developed using a combination of experimental and FEA simulations (Zhou et al., 2018). Tensile pressure integrity strain limits are based upon comparisons of tests and predictive formulations. Compressive pressure integrity strain capacity limits are based upon examining trends in the maximum local compressive strains obtained in full-scale testing.

Pressure integrity tensile strain capacity formulations are taken from a PRCI report on strain-based design. Pressure integrity compressive strain capacity is based upon full scale tests performed at the University of Alberta and CFER.

7.1 Corroded Pipe Strain Capacity

Our formulation for continued operation strain capacity is based upon recent work focused on formulation of tensile strain capacity (TSC) and compressive strain capacity (CSC) models for

corrosion defects that used a combination of experimental studies and FEA simulations (Zhou et al., 2018). These TSC and CSC models utilize four key parameters shown to affect strain capacity of a pipeline. The key parameter categories include pipe geometry, pipe material properties, corrosion anomaly dimensions and internal pressure. Pipe geometry is defined by the nominal outside diameter (D) and wall thickness (t). The pipe material property utilized is the ratio of yield strength to the tensile strength (R_{YT}). A corrosion anomaly is defined by the longitudinal length (L_C), circumferential length (W_C) and depth (d_C). Internal pressure is incorporated by way of pressure factor (f_p). Pressure factor is the ratio of the hoop stress ($p_i D/2t$) to the pipe yield strength (σ_y) and is calculated using the following relationship:

$$f_p = \frac{p_i D}{2t\sigma_y}$$

Table 17 list the key parameter categories utilized by the TSC and CSC corrosion models along with the specific parameter definitions.

Table 17: Summary of Key Parameters for TSC and CSC Models

Category	Definition of Parameters	Non-dimensional Symbol
Pipe Geometry	Diameter to wall thickness ratio	D/t
Pipe Material Properties	Yield to tensile strength ratio	R_{YT}
Corrosion Anomaly Geometry	Longitudinal Length of Corrosion Anomaly	$L_c \sqrt{Dt}$
	Circumferential Length of Corrosion Anomaly	$W_c \sqrt{Dt}$
	Depth of Corrosion Anomaly	$d_c \sqrt{Dt}$
Internal Pressure	Pressure Factor	f_p

Procedurally both the TSC model and CSC models used in this work follow similar paths. Each parameter listed in Table 17 is quantified. With the required parameters known the reference TSC and CSC are calculated from the TSC and CSC curves that were derived from experimental work and FEA simulations. Figure 75 and Figure 76 show the reference TSC and reference CSC curve set, respectively.

The reference TSC and reference CSC are then modified as needed using expressions below to produce the TSC and CSC.

$$TSC = \begin{cases} \gamma_t \varepsilon_{t,corr}^{ref} & R_{YT} \leq 0.83 \\ \gamma_t \varepsilon_{t,corr}^{ref} (-7.14R_{YT} + 6.92) & R_{YT} > 0.83 \end{cases}$$

$$CSC = \gamma_c \varepsilon_{c,corr}^{ref} F_{DP}$$

$$F_{DP} = 539.3 \cdot (2.87 - 2.13R_{YT}) \left(\frac{D}{t}\right)^{-1.6}$$

Where γ_t and γ_c are safety factors with recommended values of less than or equal to 0.6 and 0.8, respectively.

Figure 75: Reference Tensile Strain Capacity

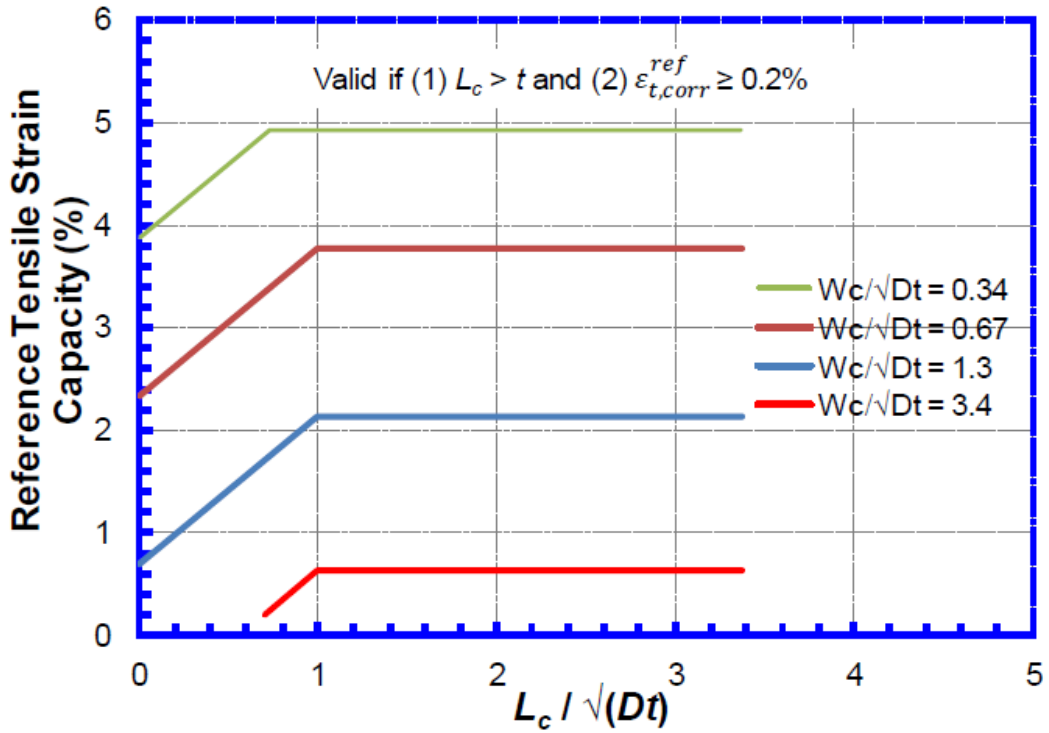
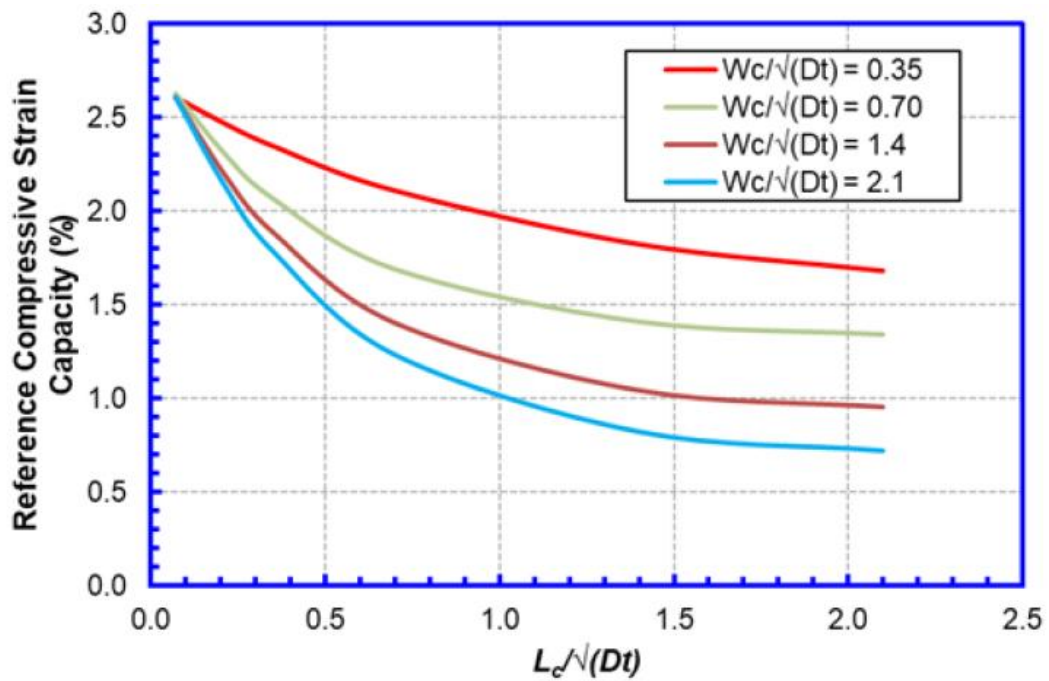


Figure 76: Reference Compressive Strain Capacity



7.1.1 Sensitivity Analysis

A sensitivity analysis is performed on two selected cases as shown in Table 18.

Table 18: Data Used for Sensitivity Analysis

	BASE CASE 1	BASE CASE 2
Steel type	X52	X70
Pipe diameter	12 inch	40 inch
Pipe thickness	0.25 inch	0.575 inch
Pipe internal pressure	400 psi	400 psi
Corrosion Flaw size	4 X 4 inch	4 X 4 inch
Corrosion Flaw Depth	0.187 inch	0.187 inch

The sensitivity results are shown in Figure 77 through Figure 82.

Figure 77: Maximum Tensile and Compressive Strain as a Function of Pipe Yield Strength

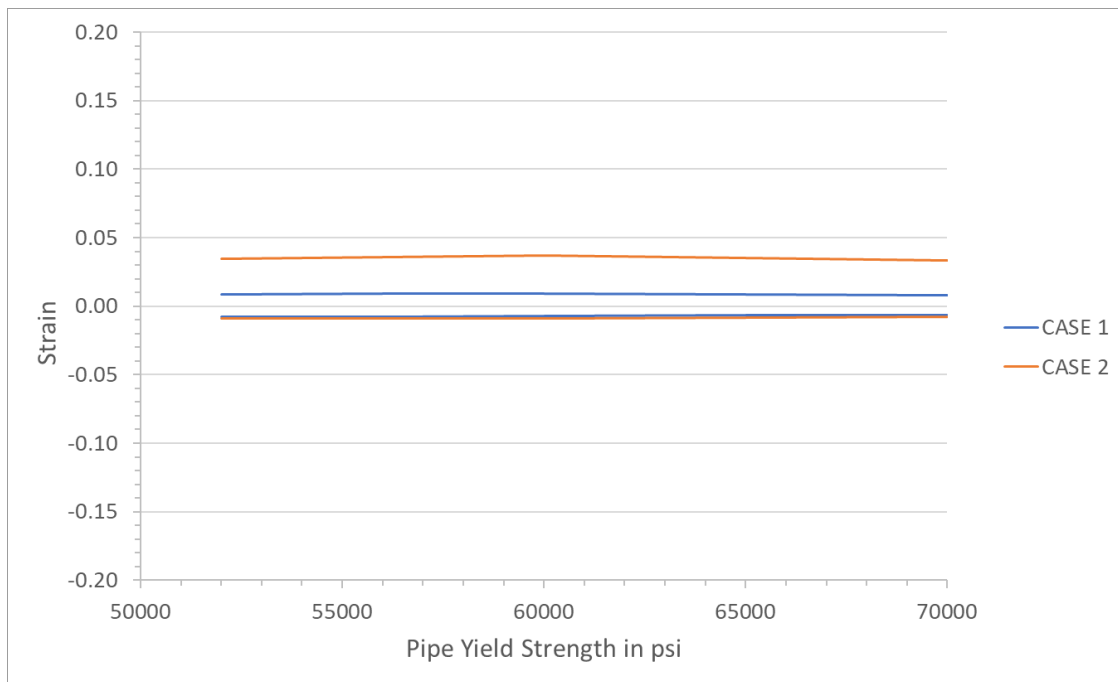


Figure 78: Maximum Tensile and Compressive Strain as a Function of Pipe Diameter

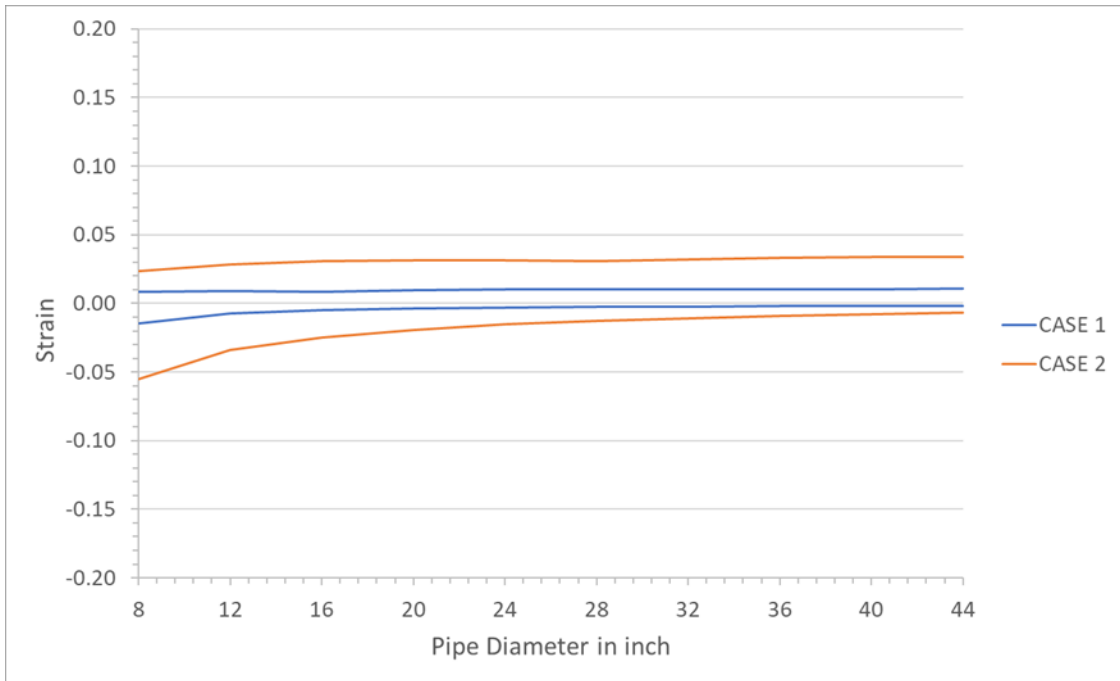


Figure 79: Maximum Tensile and Compressive Strain as a Function of Pipe Thickness

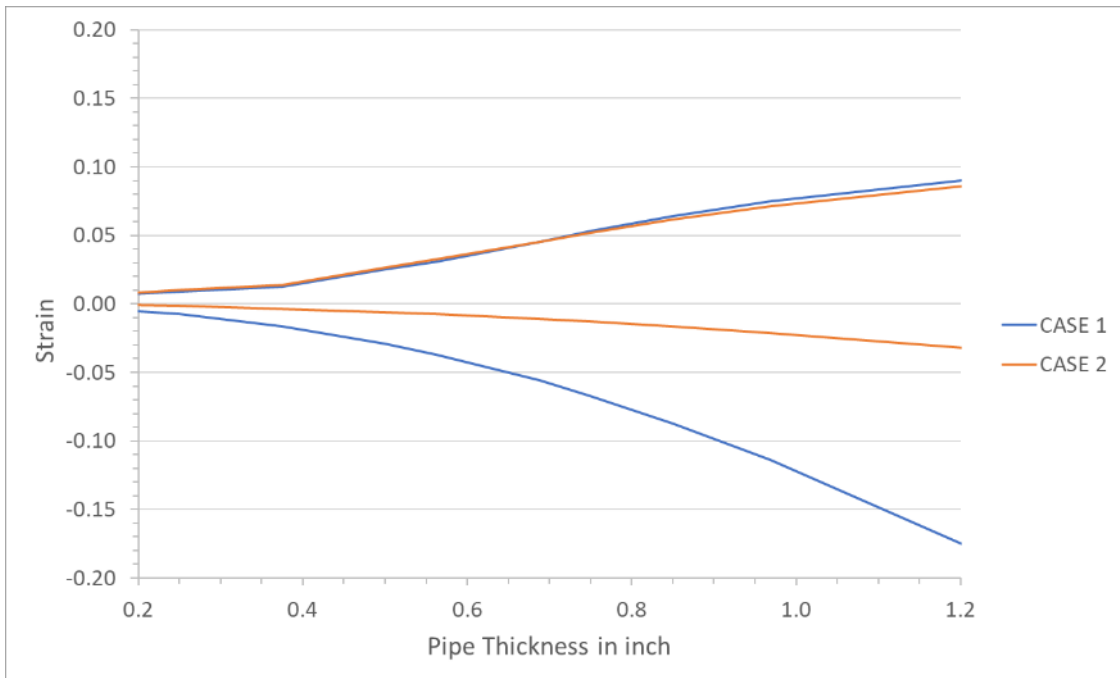


Figure 80: Maximum Tensile and Compressive Strain as a Function of Pipe Internal Pressure

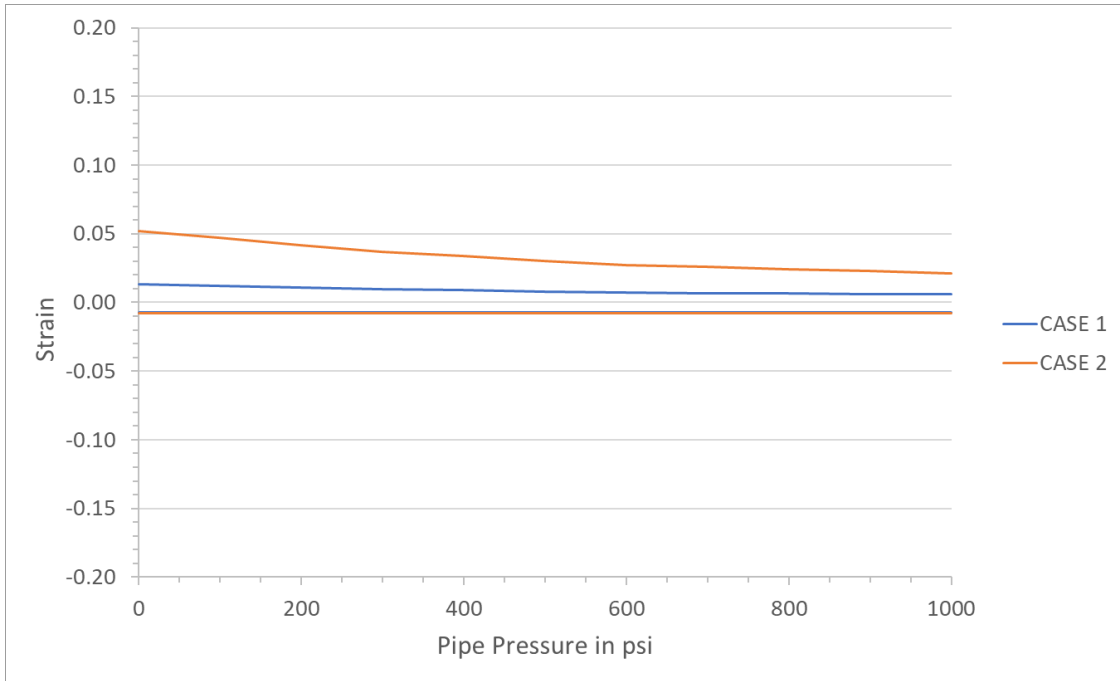


Figure 81: Maximum Tensile and Compressive Strain as a Function of Corrosion Flaw Size

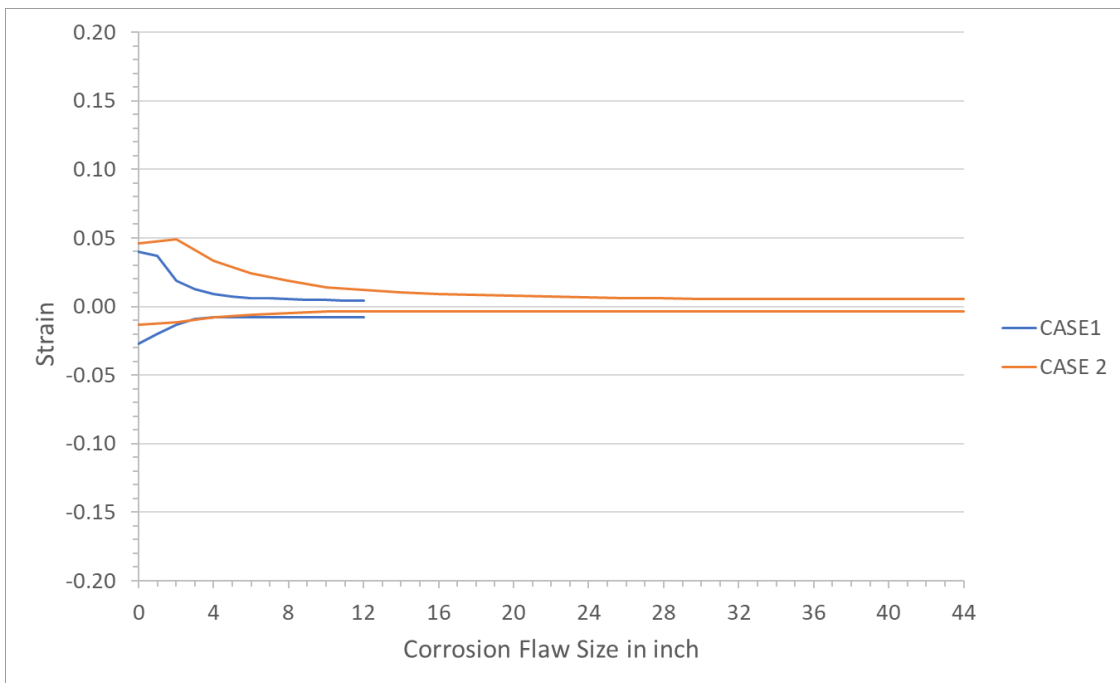
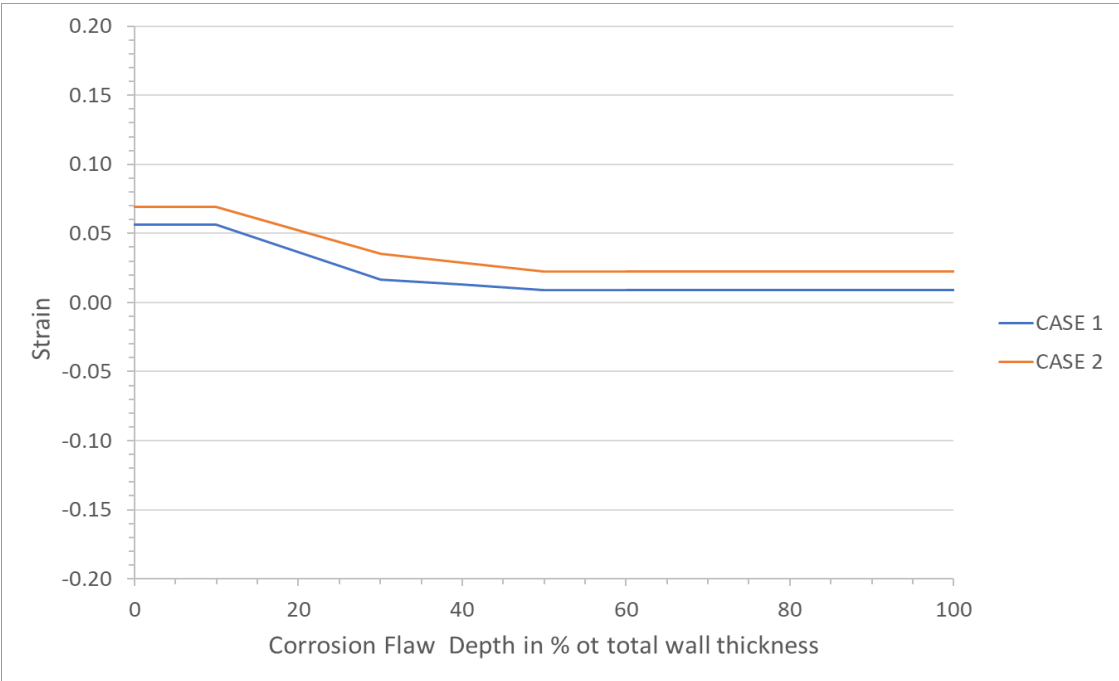


Figure 82: Maximum Tensile Strain as a Function of Corrosion Flaw Depth



7.1.2 Bayesian Model for Corroded Pipe Strain Capacity

The relative importance of input parameters from the sensitivity analyses is shown in Table 19. Based upon the relative importance, the bins of variable variations were defined as shown in Table 20.

Table 19: Relative Importance of Input Parameters for the Gas Pipeline Maximum Allowable Strain Model

	Tensile Strain		Compressive Strain	
	Strain variation in percent	Relative importance	Strain variation in percent	Relative importance
Pipe Yield Strength	0.34	0.02	0.11	0.01
Pipe Diameter	1.04	0.05	1.96	0.18
Pipe Thickness	8.45	0.38	7.40	0.68
Pipe Pressure	3.06	0.14	0.33	0.03
Corrosion Flaw Size	4.39	0.20	1.09	0.10
Corrosion Flaw depth	4.74	0.22		

According to the relative importance ranking, the BN model States are shown in the table below.

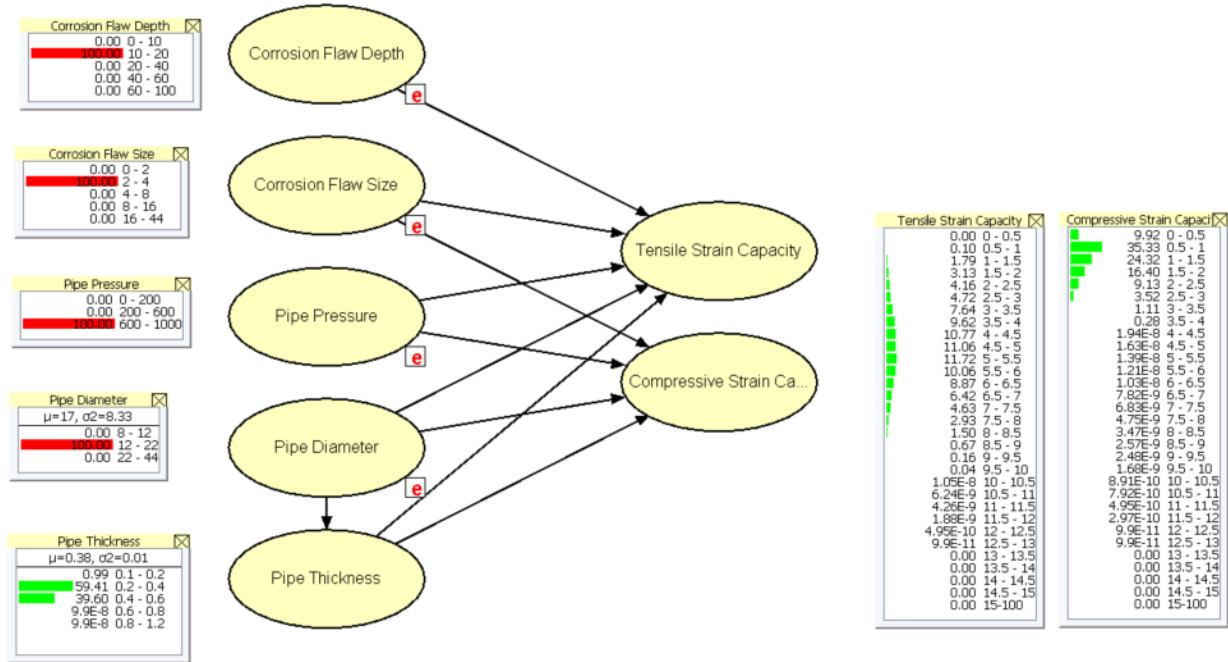
Table 20: Maximum Allowable Strain Model Discretization using Sensitivity Analysis

Input	Ranking	Bayesian Network Model States	Unit
Pipe Yield Strength	6	[52000,70000]	psi
Pipe Diameter	5	[8.625,12] [12,22] [22,44]	in
Pipe Thickness	1	[0.1,0.2] [0.2,0.4] [0.4,0.6] [0.6,0.8] [0.8,1.2]	in
Pipe Pressure	4	[0,200] [200,600] [600,1000]	psi
Corrosion Flaw Size	2	[0,2] [2,4] [4,8] [8,16] [16,44]	inch
Corrosion Flaw depth	3	[0,10] [10,20] [20,40] [40,60] [60,100]	% of total wall thickness

Since the corrosion flaw depth does not affect the compressive strain capacity, the CPT for the compressive strain capacity has only 225 columns while the CPT for the tensile strain capacity has 1125 columns. Consequently, we performed 225000 simulations for tensile strain model and 45000 simulations for compressive strain model (i.e., 200 simulations for each column). The model is represented in Figure 83

Figure 83.

Figure 83: Tensile and Compressive Strain Capacity Models for Corrosion Flaws



7.2 Pressure Integrity Strain Capacity

Pressure integrity strain capacity is based on information available from reports that compare tensile strain capacity models with full-scale test data (Wang, 2011) and compressive strains measured at the end of full-scale tests that exercised the pipe specimens far beyond the continued operation strain levels (Mohareb et al., 1994, Dorey et al., 2001, Yoosef Ghodsi et al., 1994, Zimmerman et al., 1995).

7.2.1 Pressure Integrity Tensile Strain Capacity

Efforts to determine the ultimate tensile strain capacity of steel pipelines have existed for several decades. Within the last 10 to 15 years, the Pipeline Research Council International, Inc. (PRCI) and energy pipeline corporations have focused such efforts with a focus on understanding the influence of welding flaws, welding procedures, and material properties of pipe and weld metal on tensile strain capacity. PRCI project ABD-1 resulted in a set of expressions to predict the ultimate tensile strain capacity for two types of welding processes and various definitions of weld toughness. The project also included comparisons between the predictive equations and full-scale tests. The ABD-1 strain capacity equations are provided in Appendix A. A comparison of the predicted to actual tensile strain capacity for toughness measure by Charpy V-notch (CVN) testing is shown in Figure 84. A cumulative probability distribution of the ratio of the predicted to actual tensile strain results is shown in Figure 85.

The cumulative probability distribution based upon the test data can be represented by a lognormal standard deviation with a median value of 1.2 and a lognormal standard deviation of 0.52, as shown in Figure 86.

The tensile strain capacity based upon correcting the strain capacity formulations is dependent upon a specific sized flaw being present in the girth weld. Based upon recommendation on past projects incorporating probabilistic pipe failure estimates, the likelihood for flaws of a specific length (the height for all flaws is assumed to be 1.8 mm) is defined in

Table 21.

Other assumptions used to define pressure integrity strain capacity for the Bayesian model are listed below:

- Girth weld high-low 0.0 mm
- Steel ratio of yield to tensile strength 0.87
- Weld strength overmatch 1.1
- Apparent CTOD 0.98 mm
- Pressure factor 0.72
- Ultimate strain capacity 0.08 (8%)

Figure 84: Comparison of Actual Versus Predicted Tensile Strain Capacity

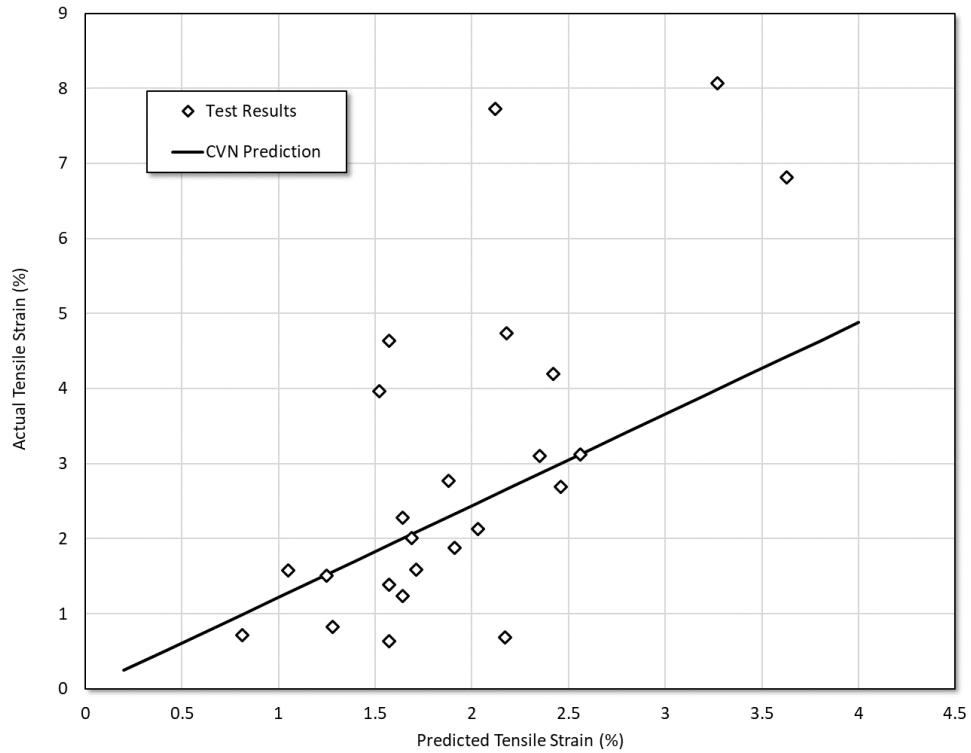


Figure 85: Cumulative Probability Distribution of Actual-to-Predicted Tensile Strain Capacity

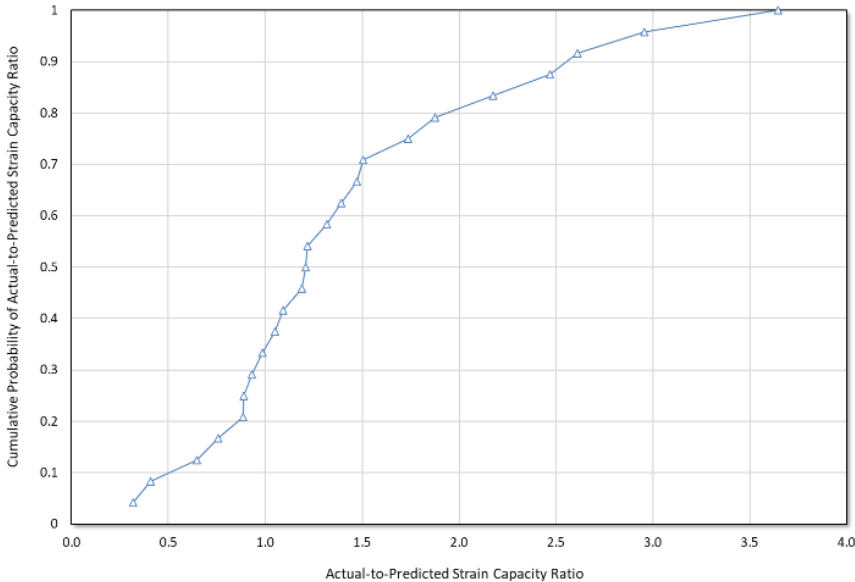


Figure 86: Approximation of Cumulative Probability Distribution with a Log-Normal Distribution

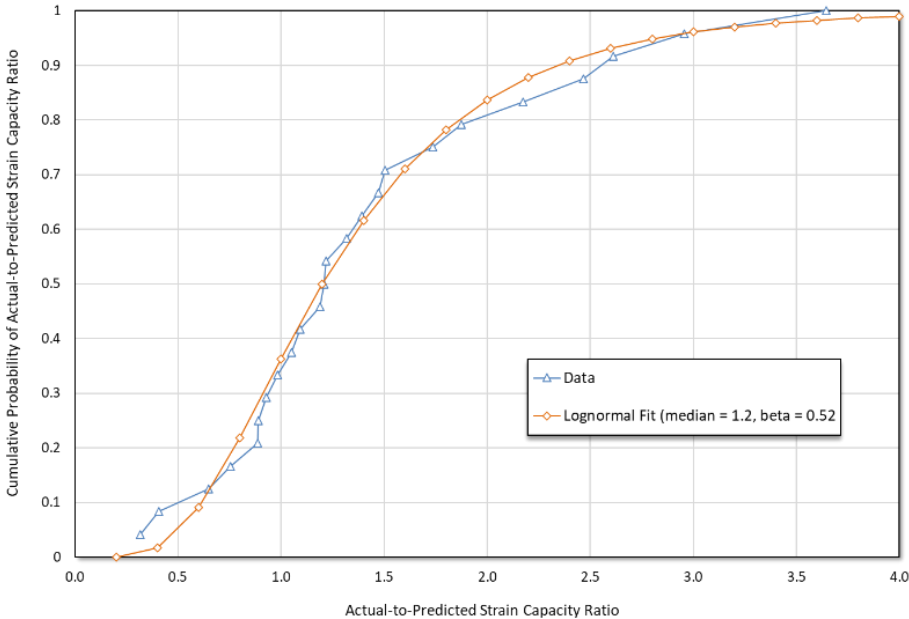


Table 21: Assumed Girth Weld Flaw Length Probability

Flaw Length (mm)	Probability (%)
0	92.1
4	4.0
44	2.0
84	1.0
124	0.5
164	0.3
204	0.1

7.2.2 Pressure Integrity Compressive Strain Capacity

The failure of pipelines loaded in compression through direct axial loading or a combination of loads producing axial and bending deformations typically initiates with local pipe wall buckling as illustrated in Figure 87. Once buckling initiates, the load-bearing capacity of the pipeline drops and can lead to the formation of a plastic hinge if the loads are maintained. This response phenomenon has resulted in nearly all past investigations into compressive strain capacity focusing on strains associated with the loss of strength through pipe wall buckling or excessive ovalization of the pipe cross section.

Pipelines can withstand deformations well beyond those associated with the loss of load-bearing capacity. This is recognized in PRCI guidelines for designing pipelines for ground deformations related to earthquakes, landslides, and subsidence by assigning a much higher compressive strain capacity for displacement-controlled loading conditions where pressure integrity is the primary performance objective (PRCI, 2009, 2017). The PRCI guidelines recommend setting the ultimate compressive strain capacity as 1.76 times the ratio of the pipe wall thickness to the pipe outside diameter. This recommendation is based upon a relationship developed by Mohareb et al. (1994) for predicting the longitudinal bending strain associated with 8% ovalization of the pipe cross section. The PRCI recommendation is still conservative compared to what has been achieved in testing.

Figure 87: Example of Local Pipe Wall Buckling



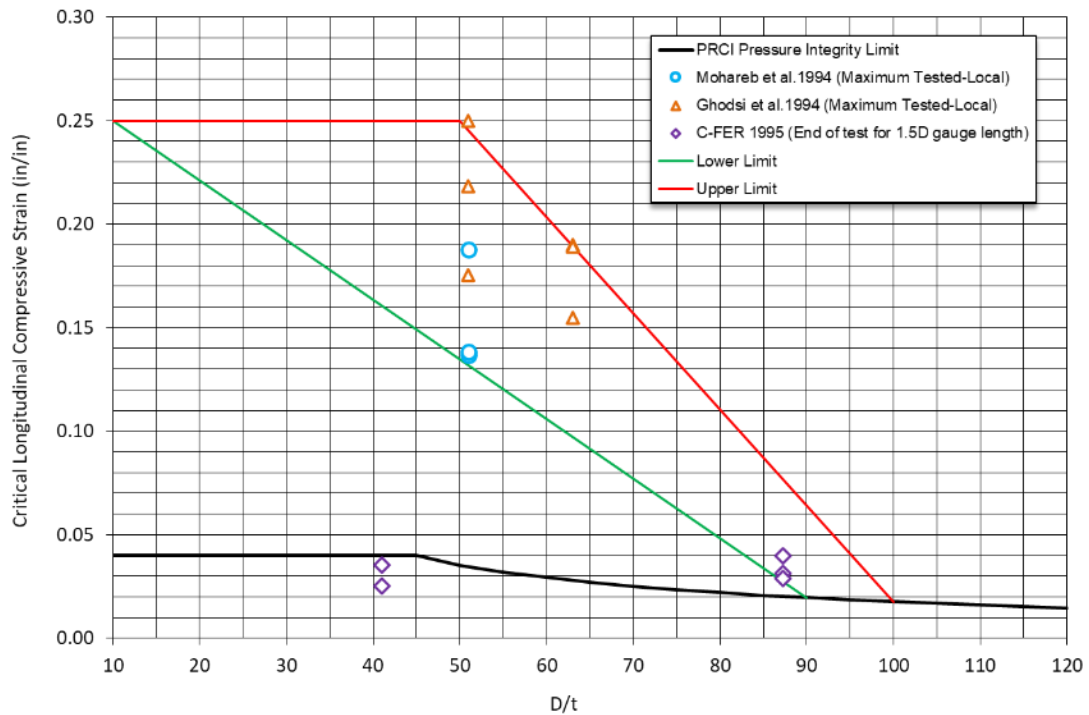
Tests performed at the University of Alberta in the mid-1990s are unique in that the tests exercised the pipe specimens well beyond the onset of pipe wall wrinkling or the point at which the maximum load capacity of the pipeline was achieved. The PRCI recommended compressive strain capacity for pressure integrity are compared with test data in Figure 88. Also shown in Figure 88 are lines that bound the trends in the test data.

The probability that the pressure integrity compressive strain capacity is exceeded is based upon the assumption of a triangular probability distribution defined by a minimum value, A, a maximum value, B, and a peak value, C. The cumulative probability function for a triangular distribution is defined as follows:

$$CDF = \begin{cases} 0 & \text{for } x \leq A \\ \frac{(x - A)^2}{(B - A)(C - A)} & \text{for } A \leq x \leq C \\ 1 - \frac{(B - x)^2}{(B - A)(B - C)} & \text{for } C < x < B \\ 1 & \text{for } B \leq x \end{cases}$$

1. The maximum value, A, is defined by the upper limit in Figure 88.
2. The minimum value, B, is defined as the PRCI limit.
3. The peak value, C, is the lower limit in Figure 88 for D/t ratios less than or equal to 90 and the average of the PRCI limit and the upper limit in Figure 88 for D/t Values Greater than 90.

Figure 88: Comparison of PRCI Recommended Pressure-Integrity Strain Limits with Test Data



This approach is applicable to D/t values less than 100 as there is no supporting test data. With the above approach, the fragility curves for pressure integrity compressive strain capacity can be defined as shown in Figure 89.

The Bayesian model for determining tensile and compressive strain capacity is shown in Figure 90.

Figure 89: Examples of Pressure Integrity Compressive Strain Capacity Fragility Curves

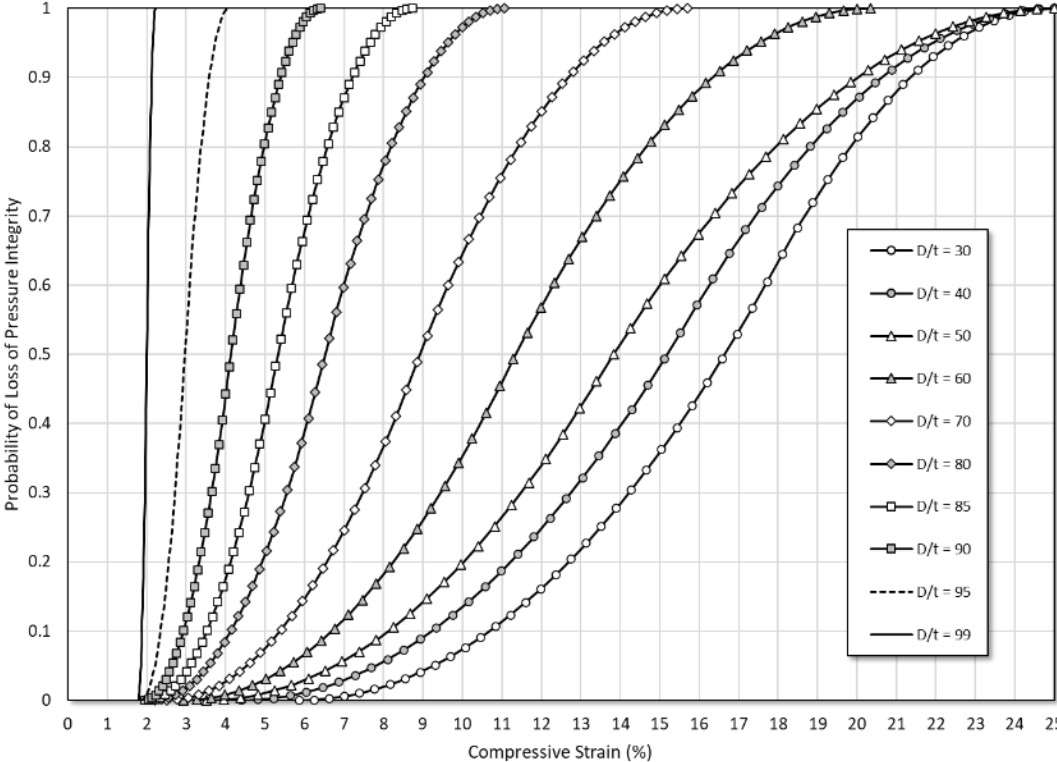
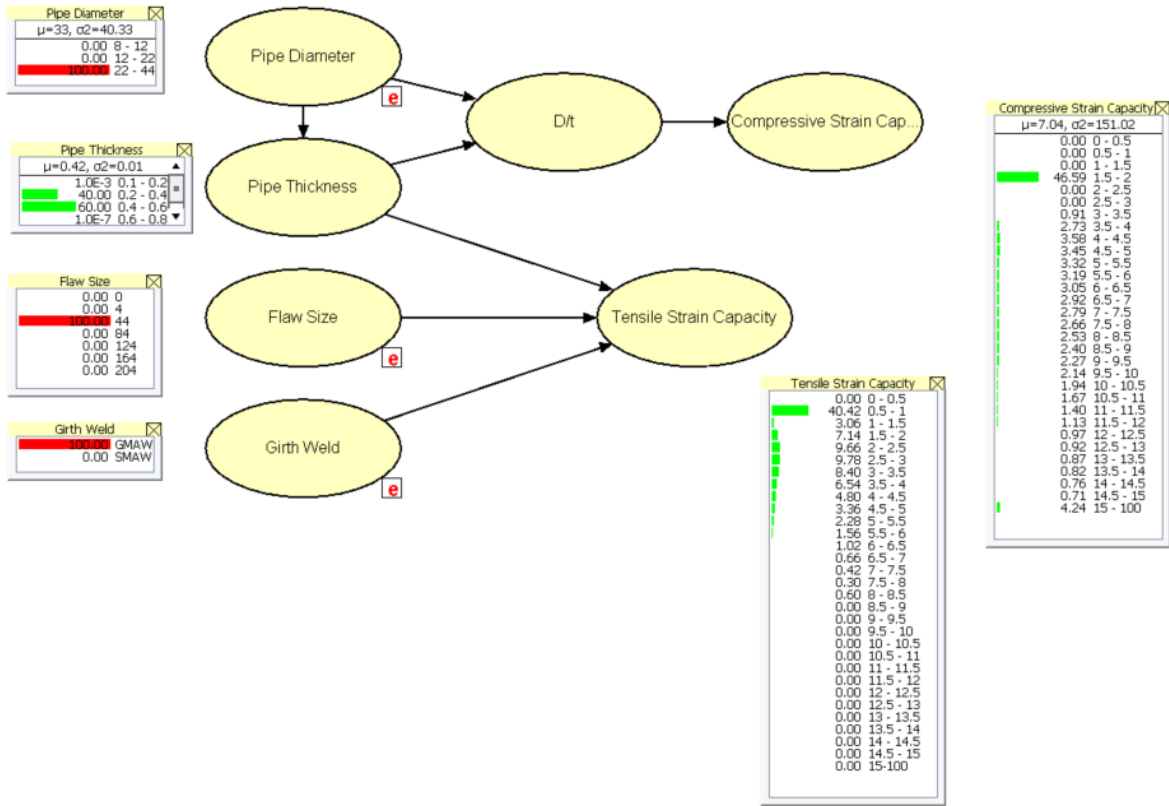


Figure 90: Tensile and Compressive Strain Capacity Models Without Corrosion



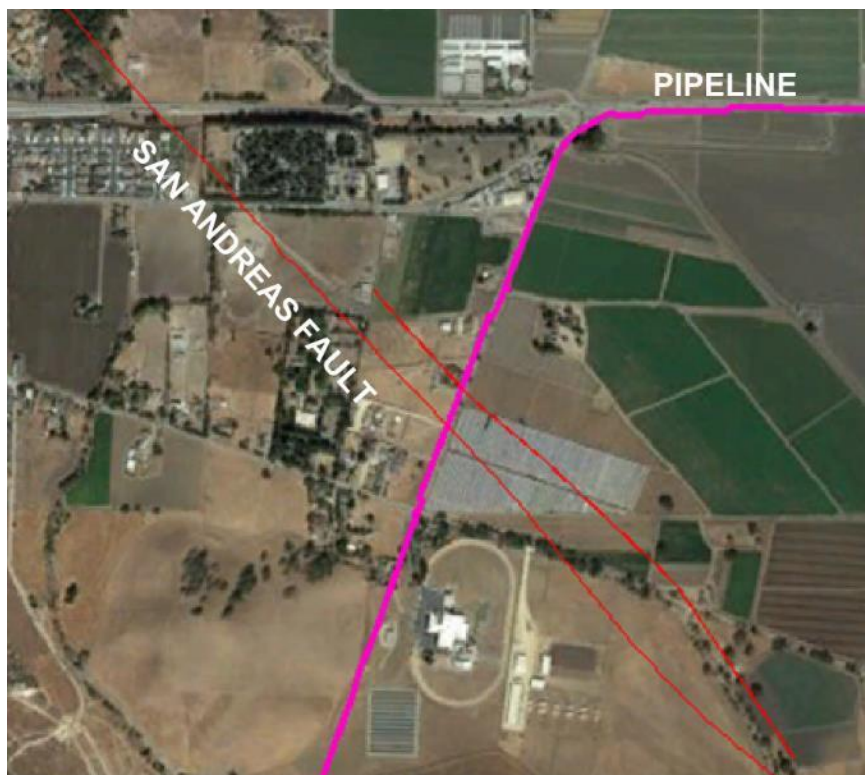
8 Pipeline Vulnerability Model Validation

The accuracy of pipeline fragility model is measured by comparison with two case studies in which the deformed pipeline shape caused by ground displacement is well defined by close interval survey or terrestrial lidar.

8.1 Case Study 1: Pipeline Response to Decades of San Andreas Fault Creep

An NPS 12 pipeline crossing the San Andreas fault has been subject to creep since construction in 1933. The creep at this location is estimated to be 13.4 ± 4 mm/year based upon USGS creep meter measurements adjacent to the pipeline fault crossing location. This correlates to a total fault creep displacement of 1.1 ± 0.32 m (43 ± 13 inches). The orientation of the pipeline at the fault crossing is shown in Figure 91.

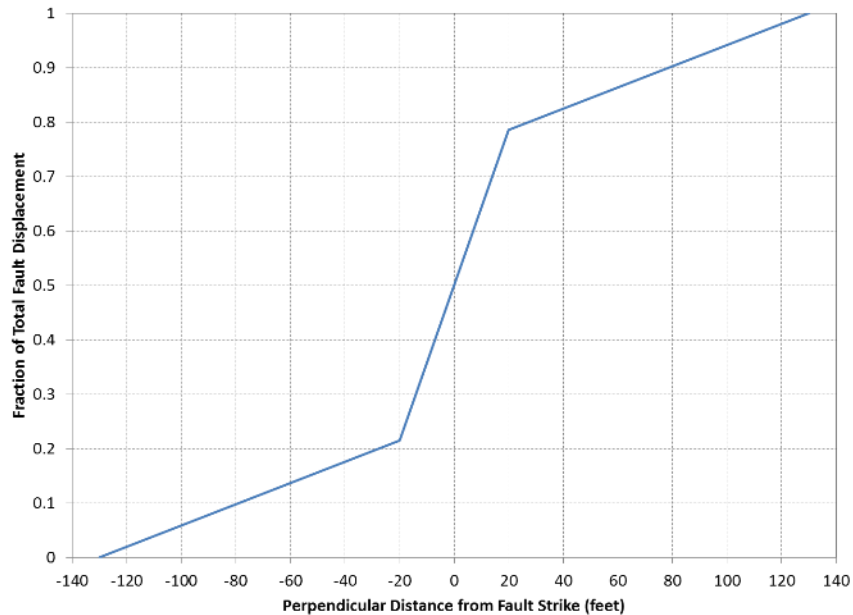
Figure 91 Orientation of the NPS 12 San Andreas Fault Zone Crossing



The San Andreas fault is a right-lateral strike-slip fault that crosses the NPS 12 pipeline. Two fault splays, separated by 320 feet, were identified in a geological study of the crossing location. One trace has exhibited rupture in the past while the other trace is experiencing active creeping. The

geologists provided a fault displacement pattern based upon their estimate of the width of the main and secondary fault zones as shown in Figure 92.

Figure 92 Fault Displacement Pattern Used for Site-Specific Assessment of NPS 12 Pipeline Response



A site-specific pipeline response analysis was performed using the parameters listed below.

Pipe Diameter:	12.75 inches
Pipe Wall Thickness:	0.250 inches
Steel Yield Strength:	33,000 psi
Pipe Internal Pressure:	350 psi
Pipe Coating Factor:	0.9
Depth of Cover	40 in
Soil Unit Weight:	103 pcf
Soil Internal Friction Angle:	41°
Pipe Direction:	25°
Fault Displacement:	3.6 ft
Fault Strike Angle:	145°
Fault Dip Angle:	85°

The site-specific pipeline analysis for the above parameters confirmed that the pipeline response is governed by direct axial compression with a longitudinal compressive strain of -1.4% to -1.8% at the estimated creep displacement of 3.6 feet. Tensile strains were found to be negligible. Acceptable compressive strain for continued operation of the pipeline was taken to be the level of compressive strain associated with local pipe wall wrinkling, which was estimated to be

between -1.08% and -1.43%. This range is related to uncertainty regarding the steel stress-strain curve characteristics of the pipeline installed in 1933.

Given the likelihood that fault creep had resulted in strains exceeding the level considered acceptable for continued operation, a portion of the pipeline crossing the San Andreas fault zone was replaced despite the fact that the probability of pipeline failure for the D/t ratio of 51 for Line 103 was considered essentially zero for longitudinal compressive strains less than 3.5%.

A prior analytical evaluation had concluded that there was significant damage from creep displacement. To resolve the discrepancy between the two analytical evaluations, the pipeline was exposed at the fault crossing to observe the pipeline condition (Figure 93). The pipeline exposure confirmed that the fault crept and resulted in a gradual bending deformation of the pipeline without any local pipe wall wrinkling.

Figure 93 Deformed Shape of Exposed NPS 12 Pipeline at the San Andreas Fault Crossing



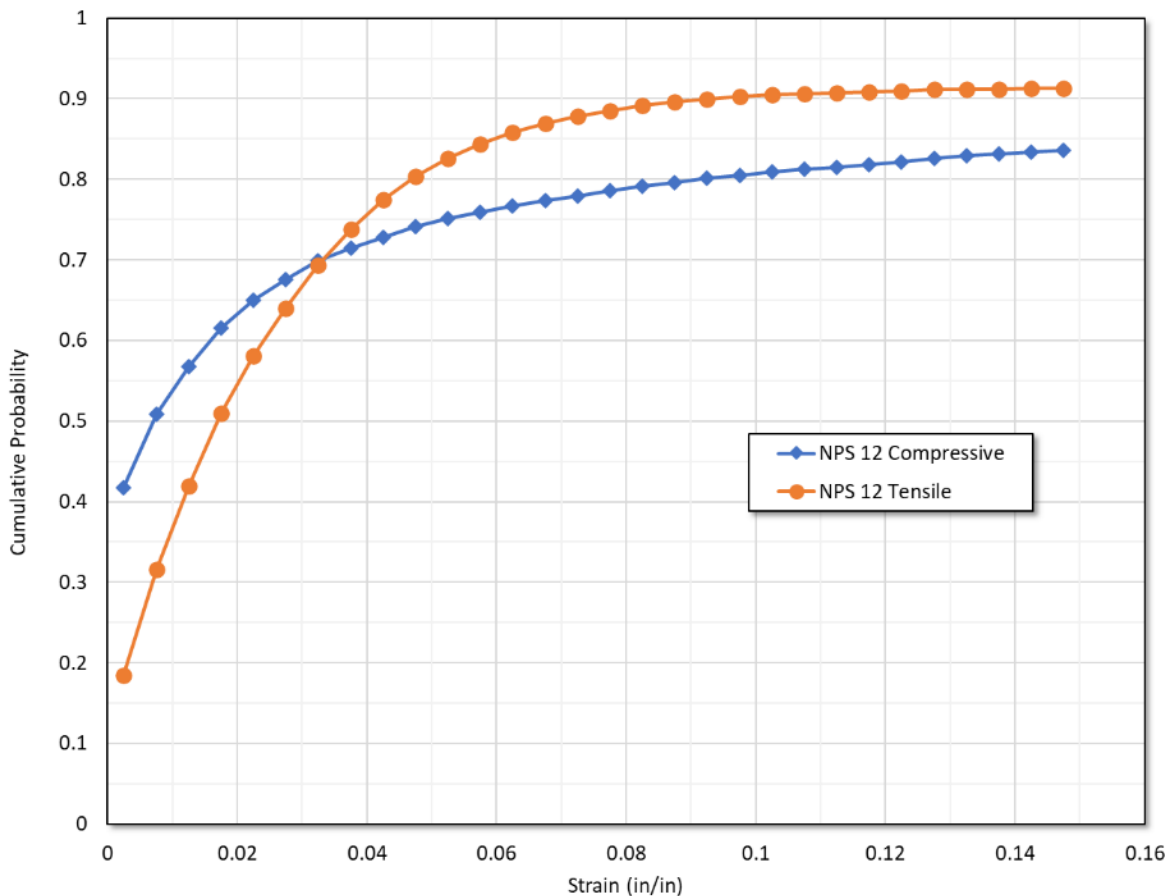
The fault and pipeline parameters for the NPS 12 pipeline were used as input to the risk software (PISRAM: Pipeline Infrastructure Seismic Risk Assessment and Management Software) for comparison with the site-specific evaluation. The results from the PISRAM are illustrated in shown in Figure 94 as plots of the cumulative probability distribution for maximum longitudinal tensile and compressive strain. The probability of compressive strains exceeding -1.43% is nearly

60%. However, there is more than a 70% probability that the compressive and tensile strains exceed $\pm 4\%$, a level often adopted as indicative of a high likelihood for pipeline rupture.

There is a significant difference between the tensile strain estimates from the PISRAM and the site-specific evaluation, which found negligible tensile strain from fault displacement.

The results from the PISRAM are consistent with the site-specific evaluation in highlighting a concern for the seismic integrity of the pipeline. However, future refinement of the PISRAM should focus on understanding the high probability of large tensile strains. Possible factors could be related to the difference in steel properties (33 ksi yield for the site-specific evaluation versus 42 ksi for the PISRAM) or differences in the length of pipeline modelled (approximately 540 feet between the fault and end of the model versus more than 5,000 feet for the PISRAM)

Figure 94 PISRAM Estimates of Cumulative Probability of Exceeding Tensile and Compressive Strain Levels for the NPS 12 Pipeline San Andreas Fault Crossing



8.2 Case Study 2: Pipeline Response to Ridgecrest Earthquake Fault Displacement

An NPS 6 pipeline was subjected to fault displacement in the M6.4 July 4th, 2019 Ridgecrest earthquake. Initial analyses, performed within 48 hours of the fault rupture based upon initial field observations, indicated the range of pipeline fault crossing angles and soil strength characteristics could lead to pipeline deformations could be sufficient to raise concerns regarding continued safe operation. A decision was made to take steps to replace a portion of the pipeline impacted by fault displacement. An NPS 10 pipeline was subjected to fault rupture in the M7.1 July 5th earthquake in the same area. Again, the range of potential fault crossing angles and soil properties was judged to possibly result in an unsafe, long term, operating condition and replacement actions were initiated.

The overall replacement efforts incorporated detailed measurements of the deformed shape of the pipelines using terrestrial lidar and trenching investigations to record details of the faulting features. Photographs of the primary fault crossings for the NPS 6 pipeline and the deformed shape of the pipeline is shown in Figure 95.

Parameters used in the analyses of pipeline response at line the NPS 6 pipeline fault crossing location to assess the potential for pipeline damage are provided below:

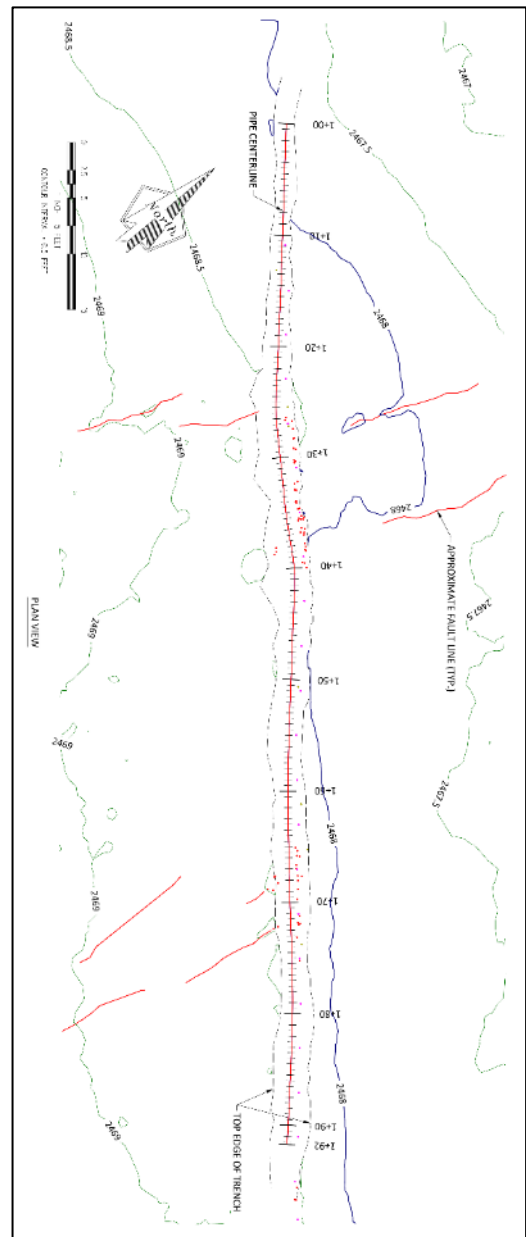
Parameter	NPS 6 Pipeline
Pipe Diameter:	6.625 inches
Pipe Wall Thickness:	0.188 inches
Steel Yield Strength:	42,000 psi
Pipe Internal Pressure:	700 psi
Pipe Coating Factor:	1.0
Depth of Cover:	2.5 ft
Soil Unit Weight:	115 pcf
Soil Internal Friction Angle:	35° and 45°
Fault Displacement:	3 ft
Fault Dip Angle:	90°
Fault Rake Angle:	0°
Fault Crossing Angle:	80° causing compression and 90°

The above fault displacement and fault crossing angles were based upon initial field observations. These values were used to assess whether or not emergency measures were necessary. Based upon the analysis of pipeline response, it was estimated the tensile and compressive strains could range from less than $\pm 1\%$ for the 90° crossing angle to a tensile strain of nearly 3% and a compressive strain of 4% to 5% for the 80° crossing angle. Based upon these results, it was decided to expedite replacement of the deformed section of pipeline.

The above parameters were used as input to the PISRAM as a validation on the post-earthquake assessment. Given the range in soil internal friction angle, this parameter was treated as

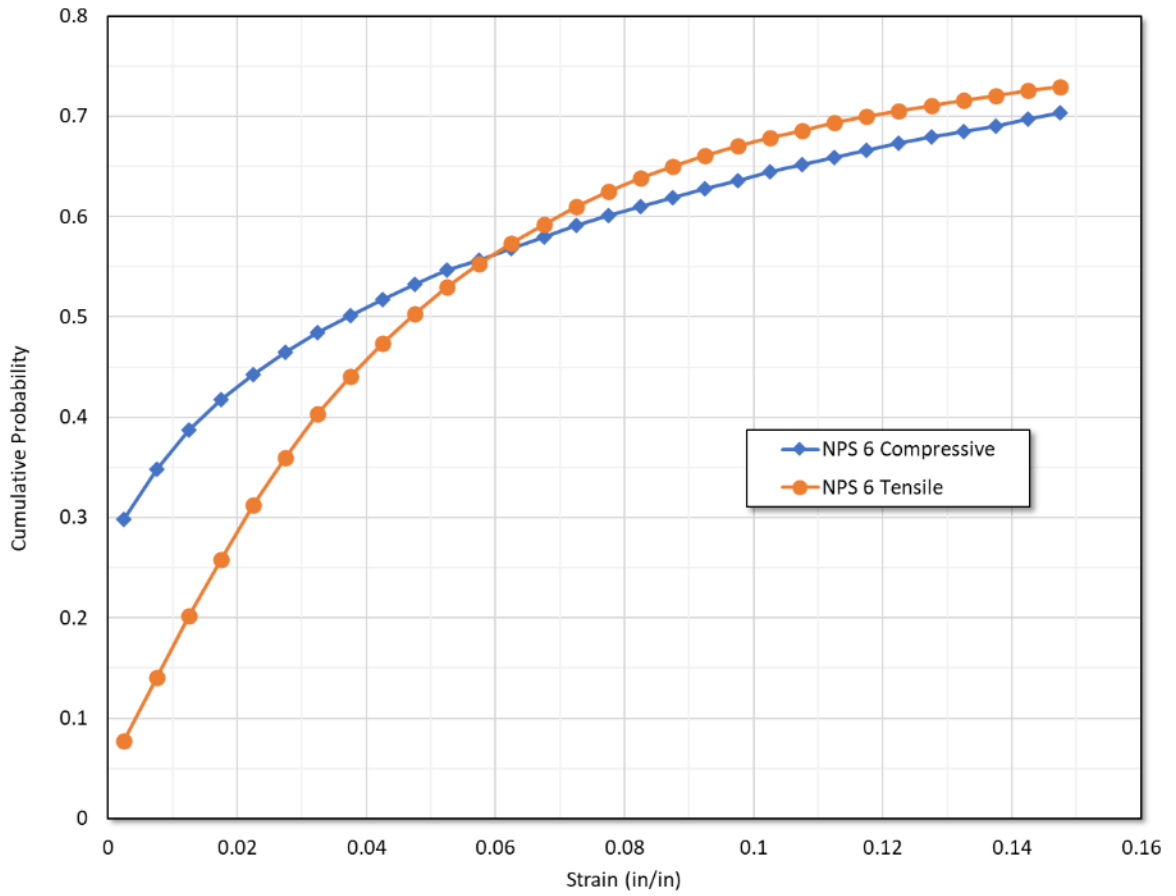
“unknown”. The results from the PISRAM are illustrated in shown in Figure 96 as plots of the cumulative probability distribution for maximum longitudinal tensile and compressive strain. From Figure 96, the PISRAM results in an estimate of a 50% chance that the tensile and compressive strain for the NPS 6 line exceed $\pm 4\%$. This result generally matches the findings from the site specific assessment in the days following the Ridgecrest earthquake.

Figure 95 NPS 6 Pipeline M6.4 Ridgecrest Fault Crossing; Photograph of Exposed Pipeline at the Primary Fault Rupture Site (left) and Terrestrial Lidar Survey of the Pipeline Deformed Shape (right)



Source: PG&E/Infracore, 2019

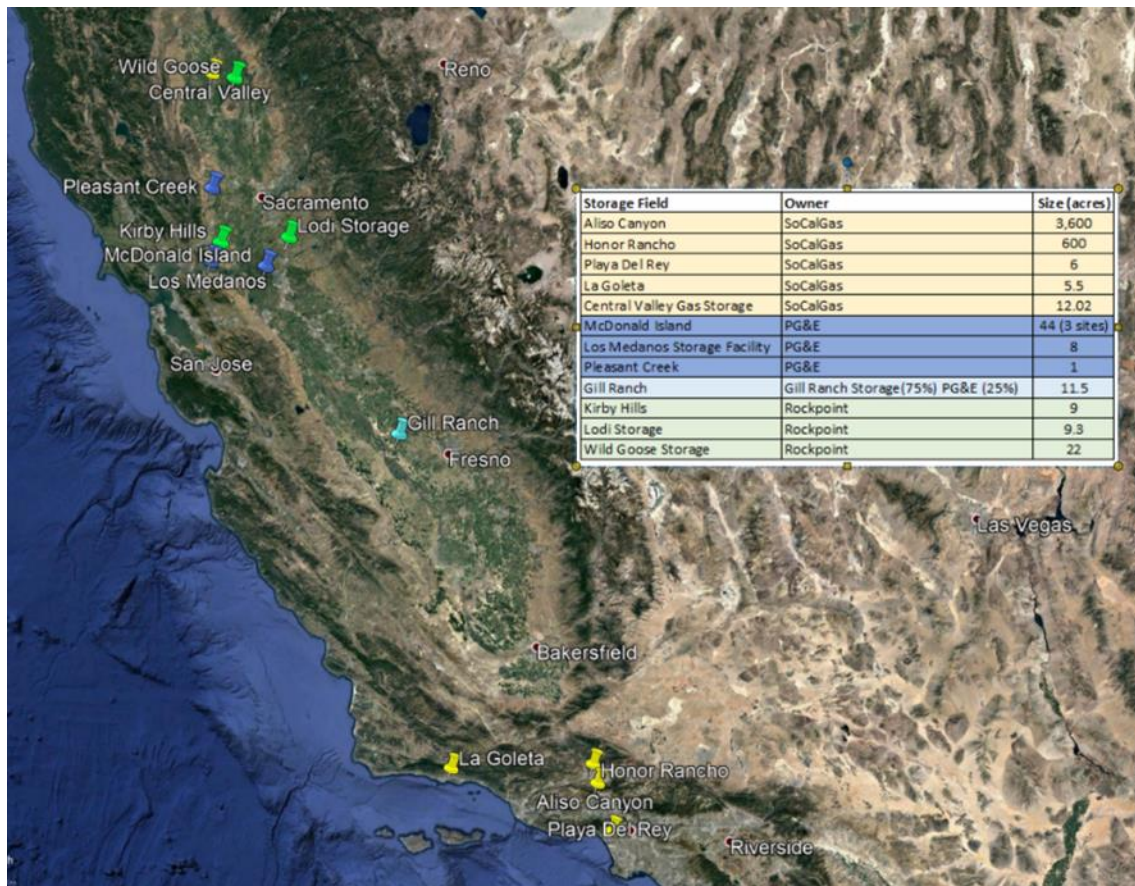
Figure 96 PISRAM Estimates of Cumulative Probability of Exceeding Tensile and Compressive Strain Levels for the NPS 6 Pipeline Ridgecrest Fault Crossing



9 Seismic Vulnerability of Gas Storage Facilities

There are twelve operating natural gas storage fields in California as shown in Figure 97. SoCalGas operates four storage fields between Goleta, Burbank, and Playa Del Rey and fifth field west of Gridley. PG&E owns and operates three storage fields near Bay Point, Winters, and west of Stockton. In addition, PG&E has a minority share in a storage field near Mendota. The remaining three storage fields in California are operated by Rockpoint and are located near Gridley, southeast of Fairfield, and North of Lodi. The four gas storage fields in southern California owned by SoCalGas were originally oil production fields. The remaining eight gas storage fields were originally gas producing fields.

Figure 97: Locations of California Natural Gas Storage Fields



Source: Google Maps ©2021 with data from DGHC

The size of the various storage fields in Figure 97 is based upon a review of the extent of mechanical support infrastructure at each site. Gas injection requires compressors to raise the gas pressure to the storage pressure (e.g., 7-8 MPa pipeline pressure to 20 MPa storage pressure) and

equipment to cool the compressed gas, such as fin-fan coolers. Gas extraction requires controlling the cooling of the stored gas as it decompresses and cleaning and drying the gas for delivery to the gas transmission system. A simplistic flow diagram for gas storage field operation is shown in Figure 98. The generally types of equipment used at underground gas storage facilities are also common to petrochemical refinery operations and largely consist of piping, cylindrical pressure vessels, compressors, coolers, electrical control equipment, and offices, and control rooms. The wells for injection or withdrawal of gas can be located within the fenced perimeter of the facility or at remote well locations.

Each gas storage field facility is unique as a result of differences in the original product extraction (gas or oil), the development of wells within the field, the age of the facility, storage capacity, and the maximum desired extraction rate. The existence of potential seismic vulnerabilities within a facility is largely dependent upon the seismic design requirements at the time of construction and the attention given to routine inspections to identify and correct seismic deficiencies.

Under ideal conditions, groups of engineers would be assigned to visit each of the storage fields and obtain information on the number and types of key equipment components and gauge the level of seismically resistant installations with respect to equipment anchorage and potential for seismic interaction from dynamic displacement. Given the political climate surrounding gas storage fields, and utilization of natural gas in general, this was not possible. We were fortunate to arrange a 1-day visit to the McDonald Island storage field, the largest facility operated by PG&E with two gas processing stations. While only a cursory observation was possible, the site visit was useful in gaining an understanding of the basic operational components common to all gas storage fields.

Without any detailed information, we have taken the approach to leverage generic fragility formulations within Hazus® as the basis for the seismic fragility of the aboveground assets at natural gas storage fields. The level of detail required to evaluate damage functions for buildings using the Hazus® methodology includes the level of seismic shaking hazard, the seismic force resisting system (e.g., steel frame, wood frame), and the age of construction, and the degree to which building requirements represent relatively modern seismic design codes (i.e., post 1994 Uniform Building Code). This level of detail is generally not available for structures found in gas storage fields. Also, the majority of components at gas storage field facilities are non-building structure and electrical and mechanical equipment.

The approach adopted for estimating the likelihood of seismic damage to gas storage field facilities adopts the methodology in Hazus® that considers four damage states: slight, moderate, extensive, and complete damage. Other than pipelines, which are directly addressed by another part of the CEC research project, we focus on the Hazus® fragility formulations for oil and natural gas systems. Key Hazus® components (other than pipelines) of oil systems are refineries, pumping plants, and storage tanks. Similarly, the key non-pipeline Hazus® components for natural gas systems are compressor stations. Pumping plants and compressor stations are treated in the same way as pumping stations for water or wastewater systems.

While gas storage fields require a compressor to raise the gas pressure to a level for injection, they also share some features with refineries. Removing water from natural gas relies upon three methods: Joule-Thomson expansion, solid desiccant dehydration, and liquid desiccant dehydration. Joule-Thomson expansion relies upon rapid cooling of the gas by reducing gas

pressure to cause the water to form ice crystals that can be removed. Solid desiccant dehydration relies upon repeated passes through absorbents such as silica or activated carbon. Liquid desiccant dehydration passes gas through a tri-ethylene glycol using a contactor tower where the tri-ethylene glycol extracts the water vapor from the gas (see Figure 98). Site photos in Figure 99 and Figure 100 provide a general picture of the types of mechanical components at the McDonald Island storage field. Note that the McDonald Island facility is unique in that all equipment is located on elevated platforms as a protection measure against flooding.

Figure 98: Operational Diagram of a Gas Storage Field

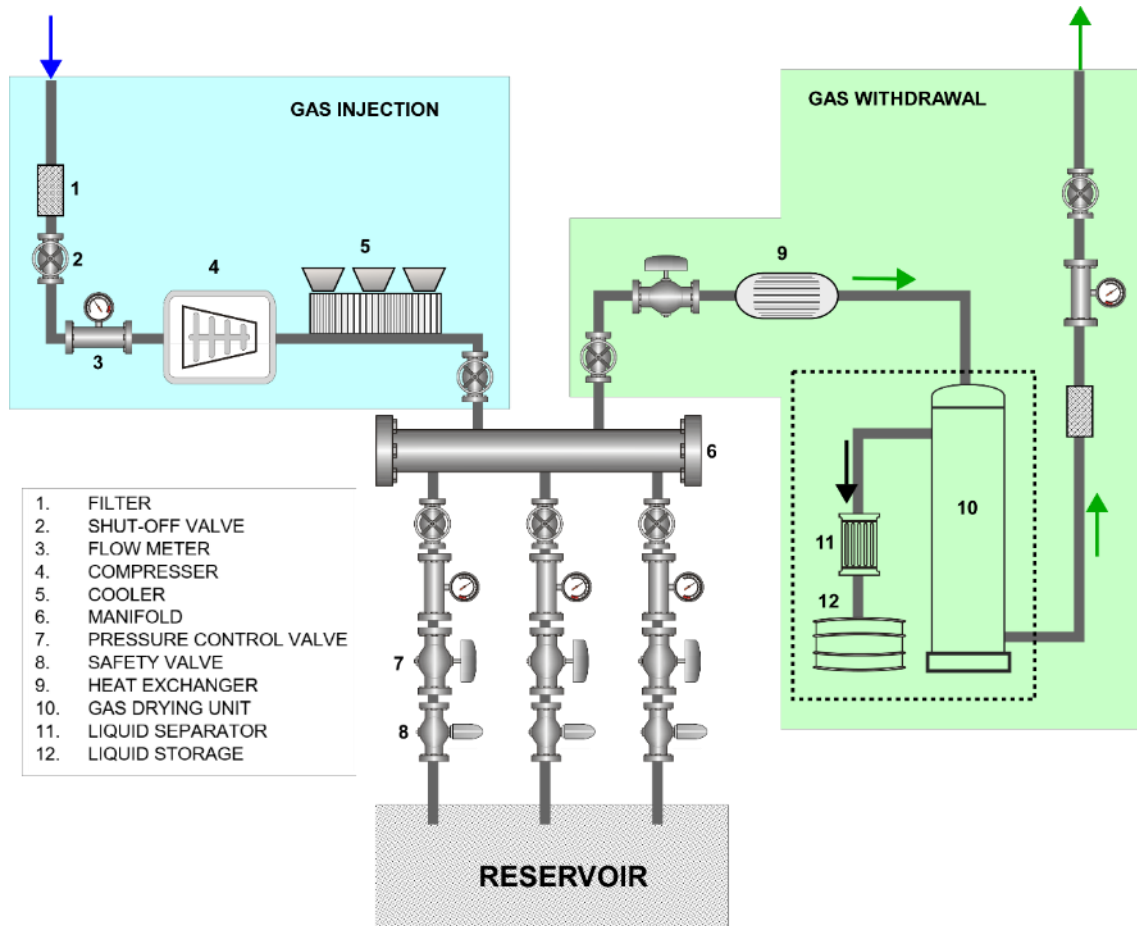


Figure 99: McDonald Island Vessels



Figure 100: McDonald Electrical and Piping Components



Initial efforts examined using aspects of the Hazus® fragility functions for refineries and oil pumping plants to represent the seismic performance of the above-ground components of natural gas storage fields. The fragility functions for refineries are segregated into “small” (refining capacity less than 100,000 barrels per day) and “medium to large” (refining capacity greater than 100,000 barrels per day). In addition, the refinery fragility functions vary based upon whether the refinery components are anchored or unanchored.

Damage functions for facilities are defined in terms of peak ground acceleration. The Hazus® damage functions for refineries and oil pumping plants are defined as lognormal distributions with median and lognormal standard deviation values provided in Table 22.

In Hazus® applications, anchored equipment refers to equipment installed with engineered restraints or flexibility to meet specific seismic criteria. Nominal anchorage in accordance with manufacturer’s recommendations, such as restraint of vibrating mechanical equipment, is not considered to be “anchored” to meet seismic criteria.

Table 22: Hazus® Fragility Definitions for Refineries and Oil Pumping Plants

Facility	Damage State	Median PGA	s
Small Refinery Unanchored	Slight	0.13	0.50
	Moderate	0.27	0.50
	Extensive	0.43	0.60
	Complete	0.68	0.55
Small Refinery Anchored	Slight	0.29	0.50
	Moderate	0.52	0.50
	Extensive	0.64	0.60
	Complete	0.86	0.55
Medium/Large Refinery Unanchored	Slight	0.17	0.40
	Moderate	0.32	0.45
	Extensive	0.68	0.50
	Complete	1.04	0.45
Medium/Large Refinery Anchored	Slight	0.38	0.45
	Moderate	0.60	0.45
	Extensive	0.98	0.50
	Complete	1.26	0.45
Oil Pumping Plant Unanchored	Slight	0.12	0.60
	Moderate	0.24	0.60
	Extensive	0.77	0.65
	Complete	1.50	0.80
Oil Pumping Plant Anchored	Slight	0.15	0.75
	Moderate	0.34	0.65
	Extensive	0.77	0.65
	Complete	1.50	0.80

Source: Hazus® technical manual

Plots of the probability of exceeding a specified level of damage versus PGA are provided in Figure 101 through Figure 104. Based upon guidance in the Hazus® technical manual for relating the level of damage associated with each damage state for refineries, the recommended fraction of facility value lost is as summarized in Table 23.

It should be recognized that there is no basis for the Hazus® fragility parameters or loss ratios provided in the Hazus® technical manual. Based upon the references listed and personal experiences of the investigators on the Hazus® project, it is likely that most of the fragility and

loss ratio values are largely judgement-based. With this perspective, the reliance upon generic facility fragility relationships, and the variability in gas storage field facilities, the estimates of damage should account for considerable uncertainty. The range of uncertainty is assumed to be bounded by the variation in fragility functions for anchored or unanchored facilities. For example, the average moderate damage function for anchored facilities is assumed to vary between the damage functions for small and moderate/large refineries. The average damage functions and ranges are plotted in Figure 105 through Figure 108. An exception to this is for the complete damage state where there is not a fragility function that represents a lower bound for the anchored condition. The lower-bound fragility function for complete damage for an anchored facility assumption was assumed to be 75% of the median value.

Table 23: Hazus® Facility Loss Ratios

Damage State	Loss Ratio
Slight	0.10
Moderate	0.25
Extensive	0.60
Complete	0.90

Source: Hazus® technical manual, Table 11-17

The following approach has been incorporated into the gas storage field vulnerability assessment:

1. Define separate fragility functions for unanchored and anchored facilities that are defined by the average median and average lognormal standard deviation for oil pumping plants and refineries.
2. Facilities that began operations prior to 1980 are considered to be “unanchored” unless there is evidence that a review of the facility to identify and rectify potential seismic deficiencies has been performed since 1980. This is based upon assuming anything installed after 1980 would have been designed to meet the seismic requirements of the 1976 Uniform Building Code.
3. The uncertainty in the probability of damage is assumed to be a simple triangular distribution between the extremes plotted in Figure 105 through Figure 108.

With this approach, a gas storage facility that is classified as unanchored and subject to a PGA of 0.7 g would have a median probability of complete damage of 28% with a range of 19% to 52%. The probability of complete damage with a 90% confidence of not being exceeded is 47%.

Figure 101: Hazus® Slight Damage Fragilities for Refineries and Oil Pumping Plants

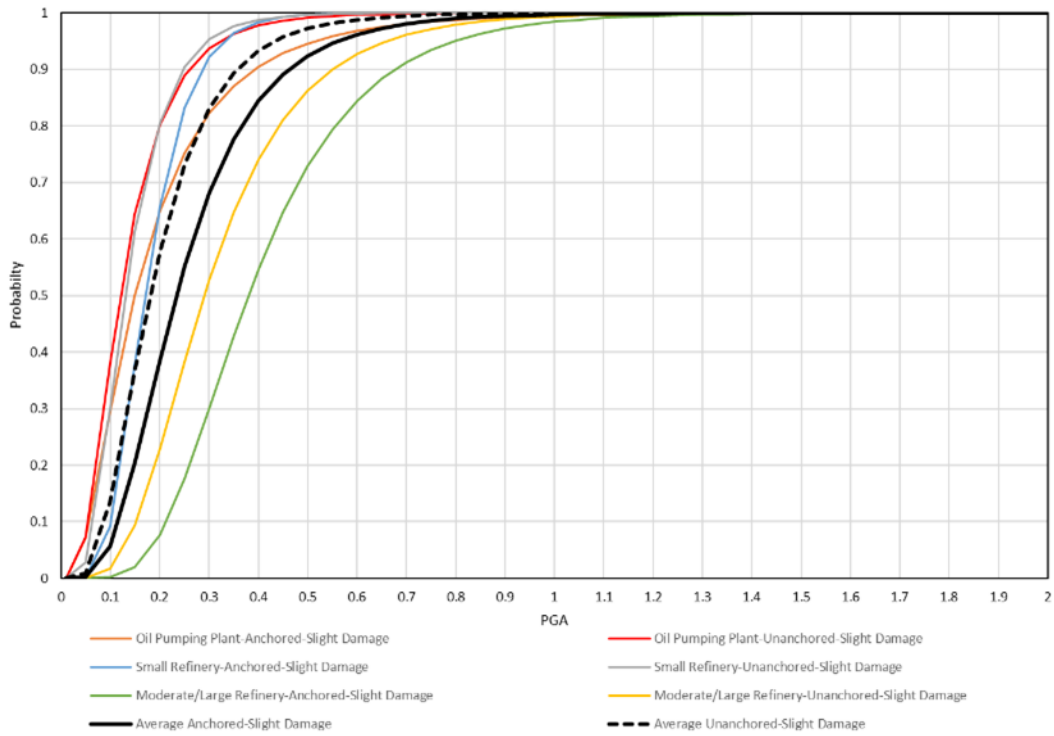


Figure 102: Hazus® Moderate Damage Fragilities for Refineries and Oil Pumping Plants

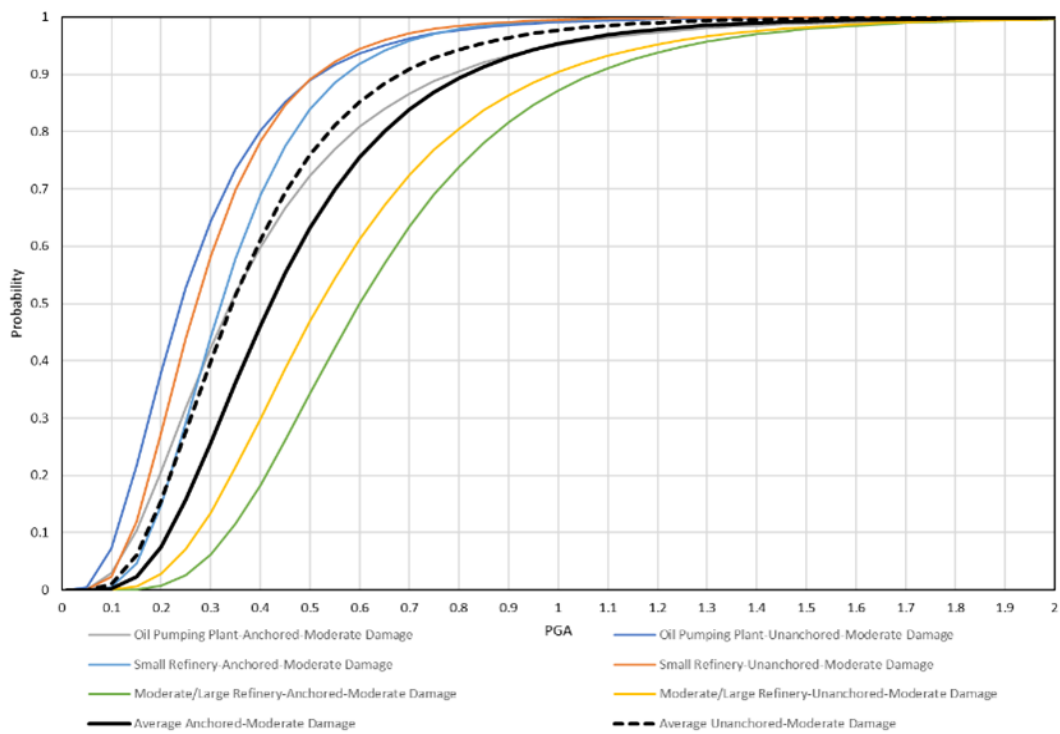


Figure 103: Hazus® Extensive Damage Fragilities for Refineries and Oil Pumping Plants

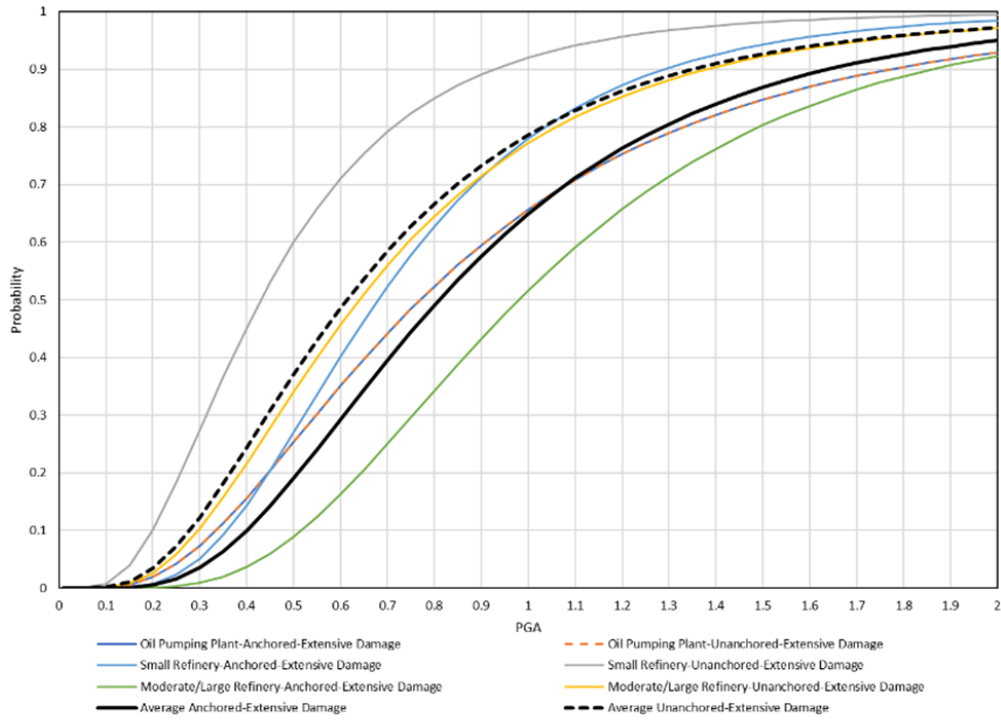


Figure 104: Hazus® Complete Damage Fragilities for Refineries and Oil Pumping Plants

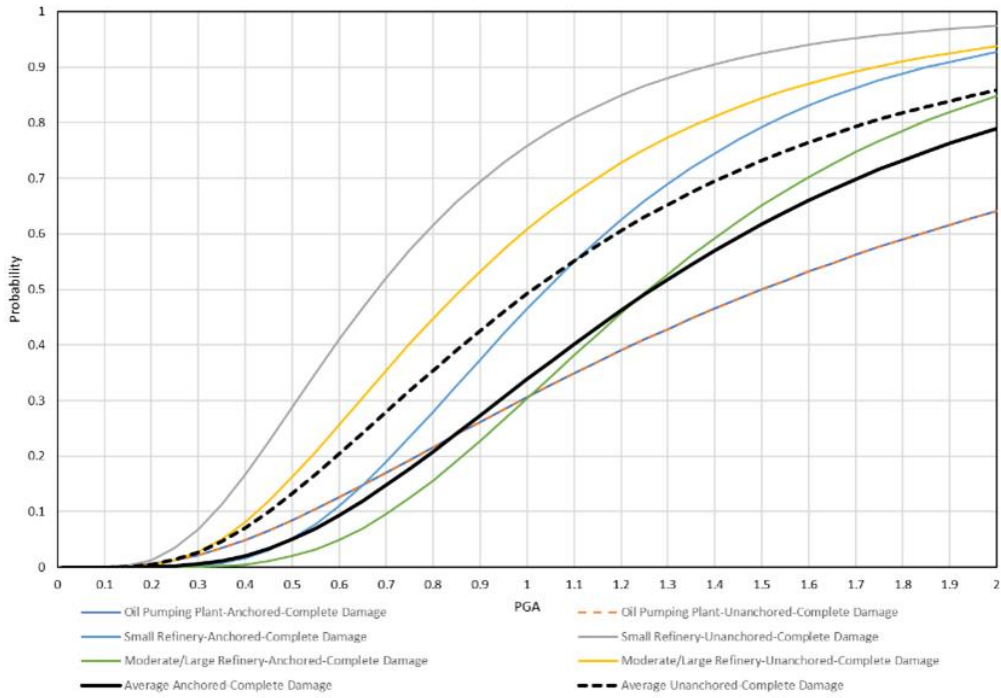


Figure 105: Recommended Slight Damage Fragilities for Gas Storage Facilities

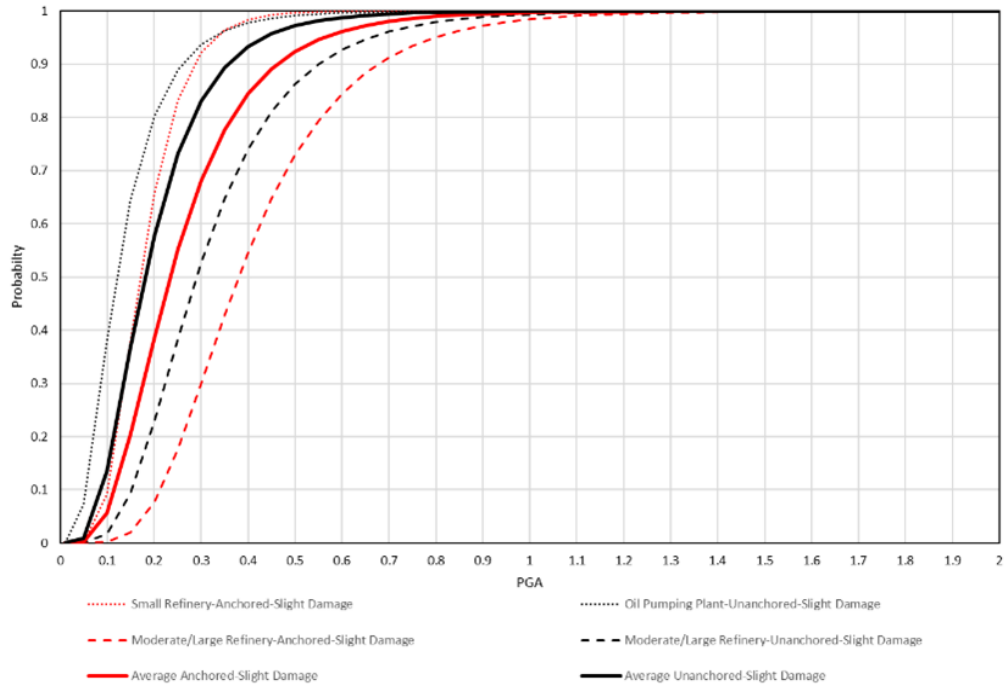


Figure 106: Recommended Moderate Damage Fragilities for Gas Storage Facilities

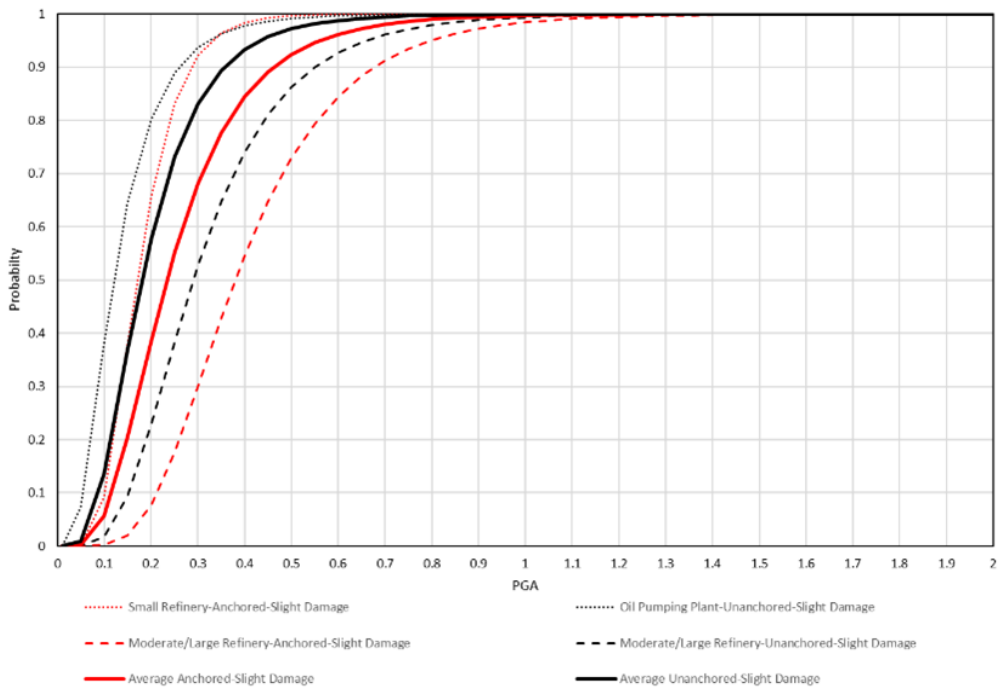


Figure 107: Recommended Extensive Damage Fragilities for Gas Storage Facilities

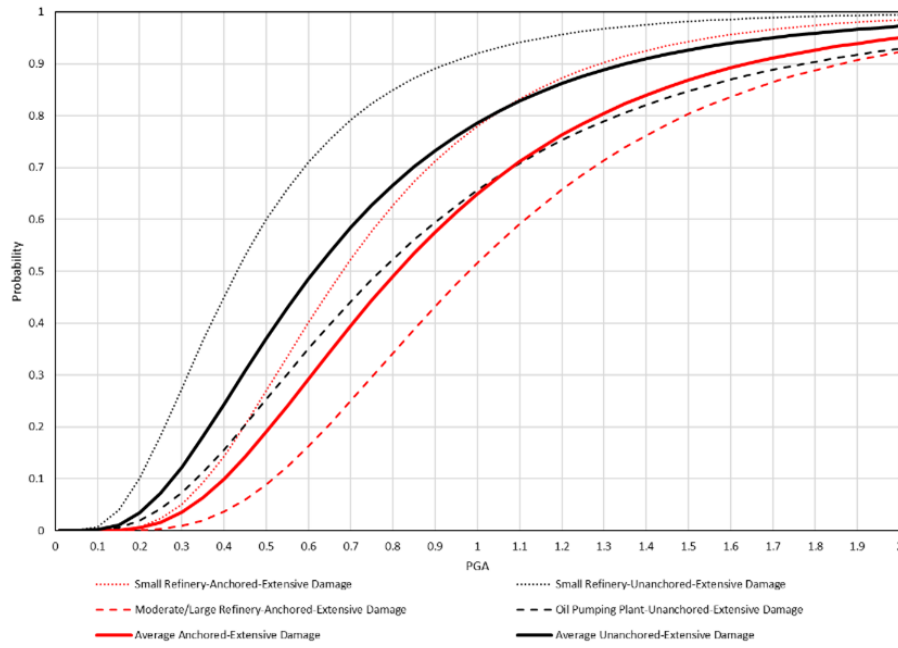
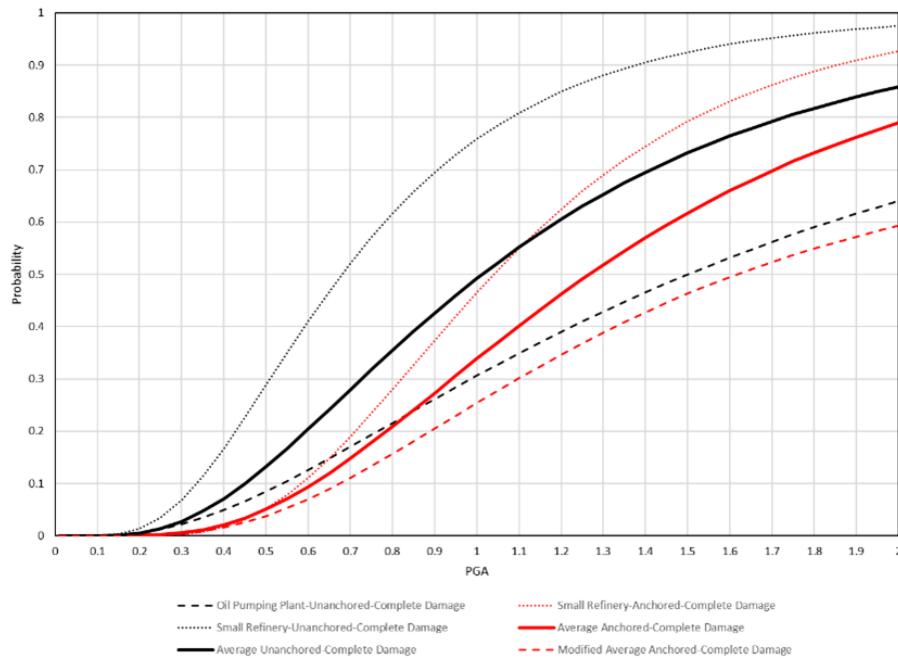
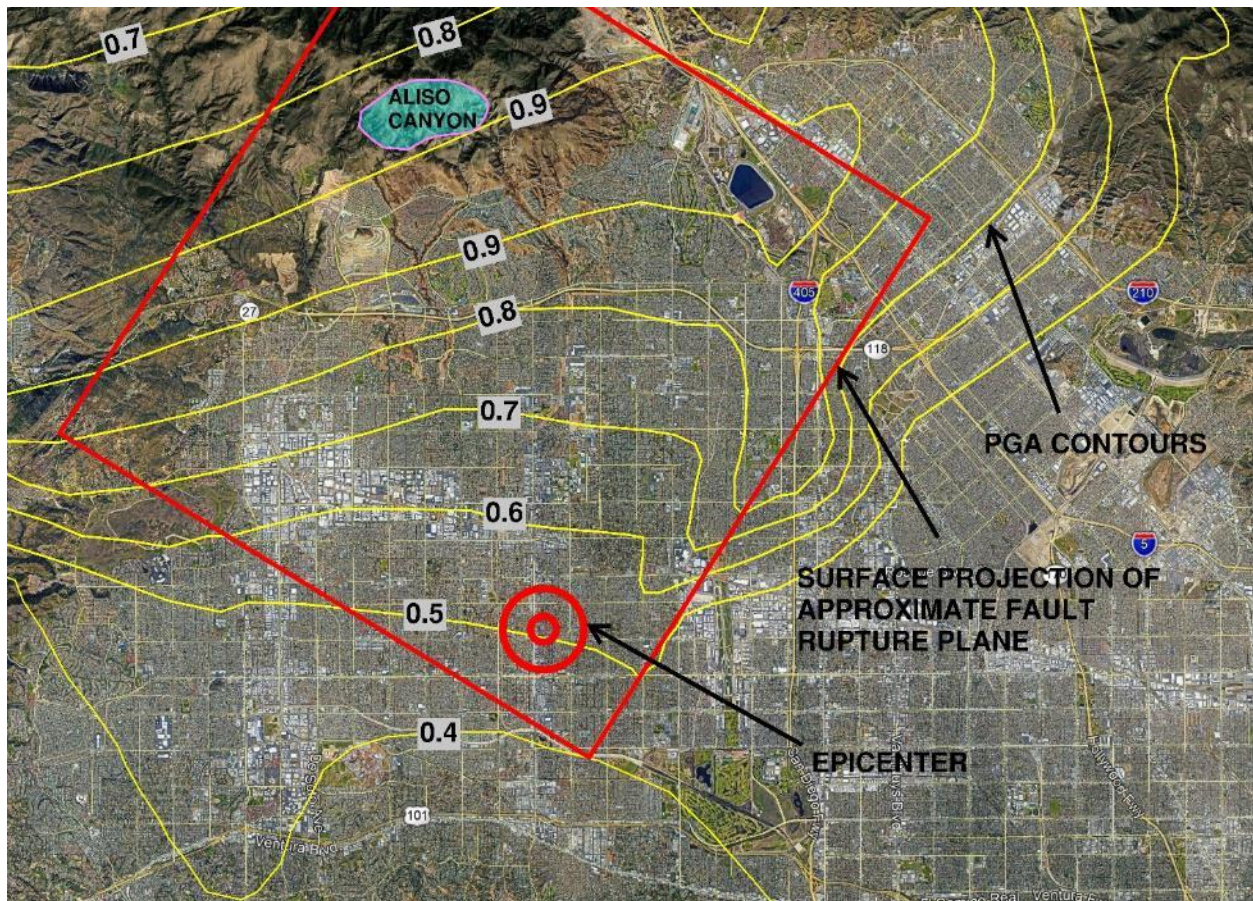


Figure 108: Recommended Complete Damage Fragilities for Gas Storage Facilities



The only gas storage field in California that has experienced strong ground shaking is the Aliso Canyon field that covers approximately 3,600 acres with 35 miles of access roads. The Aliso Canyon field is located approximately 12 km north of the epicenter of the 1994 Northridge earthquake. The ground motions and projected fault rupture plane for the Northridge earthquake are shown in Figure 109 which is adapted from Chang et al. (1995).

Figure 109: Estimated PGA Contours for the 1994 Northridge Earthquake



Source: Google Maps ©2021, Chang et al., 1995, DGHC

Peak ground acceleration at the Aliso Canyon facility is estimated to have ranged from 0.8 g to 0.9 g. It is believed that most of the conversion from oil field operations to gas storage occurred in the mid-1970s and that SoCalGas did undertake a systematic review of the seismic vulnerability of the facility prior to the Northridge earthquake. For this reason, the facility is characterized as “anchored” for the purposes of comparing the response to the predicted damage.

Post-earthquake reconnaissance of the Aliso Canyon storage field facility revealed the following types of damage:

1. Damage to injection and withdrawal piping and pipe supports, primarily from slope failures and to rock falls, see Figure 110 (a) and (b).
2. Damage to a fin-fan cooling unit.

contrast with the expected damage from the adapted Hazus® fragility relationships. Based upon this single benchmark the initial approach of simply using a mean and range of Hazus® fragility values was considered inadequate.

There is no background on the basis for the Hazus® fragility relationships in the Technical Manual. However, some insight into what drives the oil system fragility relationships can be gained by examining how component fragilities influence the overall facility fragility.

The fragilities for large water and oil pumping plants are virtually identical (see Table 25). This is somewhat counterintuitive considering the much higher operating pressures and resulting potential dynamic loading scenarios from flow instabilities.

A comparison of the Hazus® fragility relationships for refineries with those for water or wastewater treatment plants are provided in Table 26 and Table 27. For anchored small facilities, the median PGA values at the four damage states for refineries are generally greater than for water treatment plants. The exception is the complete damage state that has nearly the same PGA value. This trend does not continue for the unanchored small facilities in which the PGA is similar for the slight and moderate damage states but the refinery PGA values are lower than water treatment plants for the extensive and complete damage states.

Table 25: Comparison of Fragilities for Water and Oil Pumping Plants

Damage State	Pumping Plant PGA (Dispersion)			
	Anchored		Unanchored	
	Large Water	Oil	Large Water	Oil
Slight	0.15 (0.75)	0.15 (0.75)	0.13 (0.60)	0.12 (0.60)
Moderate	0.36 (0.65)	0.34 (0.65)	0.28 (0.50)	0.24 (0.50)
Extensive	0.77 (0.65)	0.77 (0.65)	0.77 (0.65)	0.77 (0.65)
Complete	1.50 (0.80)	1.50 (0.80)	1.50 (0.80)	1.50 (0.80)

Source: Hazus® - MH 2.1 Technical Manual

Table 26: Comparison of Hazus® Fragilities for Small Refineries and Water Treatment Plants

Damage State	PGA (Dispersion)			
	Anchored		Unanchored	
	Refinery	Water Treatment	Refinery	Water Treatment
Slight	0.29 (0.55)	0.25 (0.50)	0.13 (0.45)	0.16 (0.40)
Moderate	0.52 (0.50)	0.38 (0.50)	0.27 (0.50)	0.27 (0.40)
Extensive	0.64 (0.60)	0.53 (0.60)	0.43 (0.60)	0.53 (0.60)
Complete	0.86 (0.55)	0.83 (0.60)	0.68 (0.55)	0.83 (0.60)

Source: Hazus® - MH 2.1 Technical Manual

Table 27: Comparison of Hazus® Fragilities for Large Refineries and Large Water Treatment Plants

Damage State	PGA (Dispersion)			
	Anchored		Unanchored	
	Refinery	Water Treatment	Refinery	Water Treatment
Slight	0.38 (0.45)	0.44 (0.40)	0.17 (0.40)	0.22 (0.40)
Moderate	0.60 (0.45)	0.58 (0.40)	0.32(0.45)	0.35 (0.40)
Extensive	0.98 (0.50)	0.87 (0.45)	0.68(0.50)	0.87 (0.45)
Complete	1.26 (0.45)	1.57 (0.45)	1.04 (0.45)	1.57 (0.45)

Source: Hazus® - MH 2.1 Technical Manual

For large refineries and water treatment plants, the PGA values for the slight and moderate damage states are similar for refineries and water treatment plants. For the extensive and complete damage states, the median PGAs for refineries are less than water treatment plants.

Based upon these trends, the development of the Hazus fragilities seem to be based upon a calculation that leads to refineries being more vulnerable to extensive and complete damage than water treatment plants. This does not seem logical given that refineries operate at significantly higher pressures and temperature ranges that typically require more robust installations (more supports, heftier supports, heavier pipe and vessel wall thicknesses, etc.) compared to water treatment plants.

The subcomponent fragility relationships in Appendix B of the Hazus Technical Manual for water treatment plants and refineries were reviewed to see what reasons might lead to refineries being considered more vulnerable than water treatment plants (see the summary of median PGA capacities in Table 28 and Table 29 for anchored facilities). There are two differences in the types

of subcomponents listed in Appendix B related to the determination of fragility for the two types of facilities. Unique subcomponents for water treatment plants are listed as chlorination equipment, sediment flocculation systems, chemical tanks, and the filter gallery. The unique subcomponents of refineries are listed as tanks and “stacks”, which actually refers to the tall vessels where fractionating occurs. All other subcomponents have the same median PGA capacity for the same damage state. The only other difference is the inclusion of a moderate damage median PGA for elevated piping in water treatment plants but not for refineries.

The computation of facility fragilities in Hazus® only considers component fragilities that have a defined median PGA value for a particular damage state. If only a complete damage state median PGA is provided, that component is the only one considered in the calculation of the complete facility damage state. This was verified through independent calculation of facility fragility using the component fragilities in Appendix B of the Hazus® technical manual.

The fragility for pumping plants and refineries are strongly influenced by the component fragilities for buildings and tanks, respectively. For a large refinery, tanks are a major subcomponent as illustrated in the Google Earth image of the Marathon Los Angeles Refinery in Figure 111. Aboveground storage tanks are a minor component for gas storage field operations, especially for storage fields that were originally gas producing fields (see Figure 112 through Figure 115). Oil producing fields are more likely to have storage tanks to manage ongoing oil seepage or if there are ongoing levels of oil extraction. However, these are ancillary to the operation of the storage field. On the other hand, there are buildings that house equipment and offices at gas storage field locations that are considered similar to buildings at pumping plants and compressor stations.

Table 28: Median PGA Capacity for Anchored Water Treatment Plant Subcomponents

Subcomponent	Damage State	Median PGA
Electric Power (Backup)	Slight	0.80
	Moderate	1.00
Loss of Commercial Power	Slight	0.15
	Moderate	0.30
Electric Equipment	Moderate	1.00
Elevated Piping	Extensive	0.53
	Complete	1.00
Chlorination Equipment	Slight	0.65
	Moderate	1.00
Chemical Tanks	Slight	0.40
	Moderate	0.65
Sediment Flocculation	Slight	0.36
	Moderate	0.60
Filter Gallery	Complete	2.00

Source: Hazus® - MH 2.1 Technical Manual

Table 29: Median PGA Capacity for Anchored Refinery Subcomponents

Subcomponent	Damage State	Median PGA
Electric Power (Backup)	Slight	0.80
	Moderate	1.00
Loss of Commercial Power	Slight	0.15
	Moderate	0.30
Electrical & Mechanical Equipment	Moderate	1.00
Elevated Piping	Complete	1.00
Tanks	Slight	0.30
	Moderate	0.70
	Extensive	1.25
	Complete	1.60
Stacks	Extensive	0.75

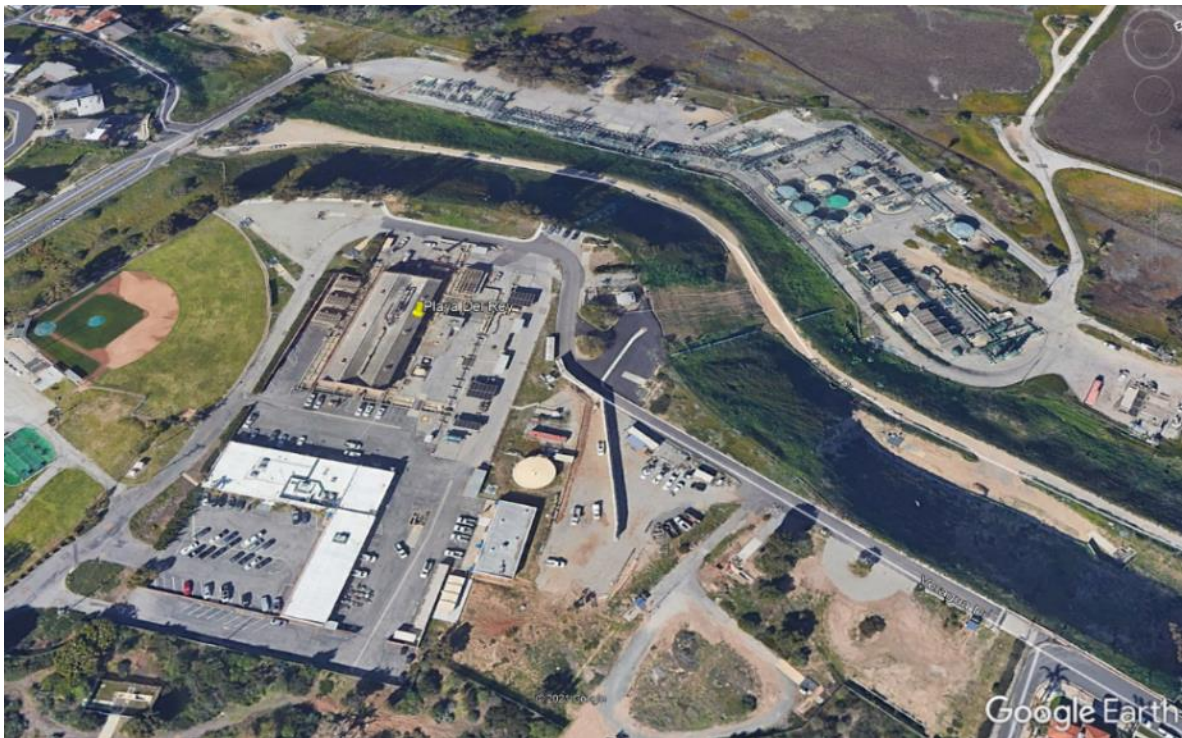
Source: Hazus® - MH 2.1 Technical Manual

Figure 111: Google Earth Image of Marathon Los Angeles Refinery Complex



Source: Google Maps ©2021

Figure 112: Playa Del Rey Gas Storage Field Site



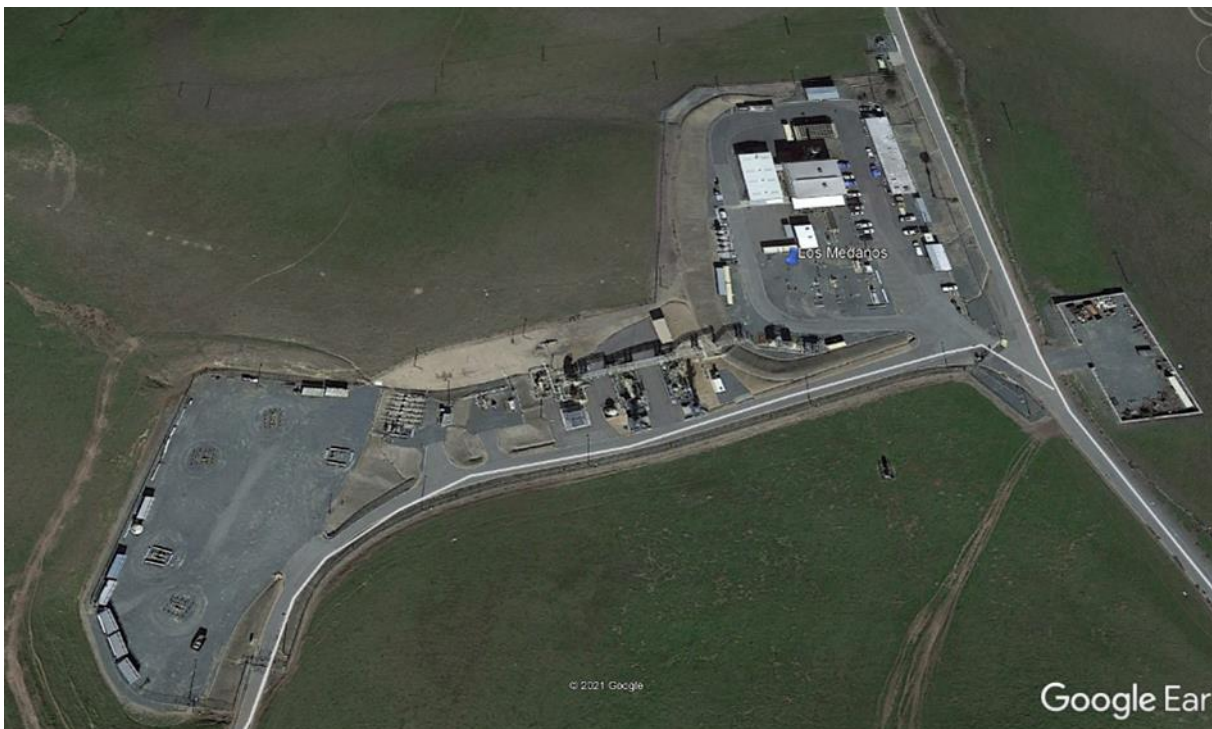
Source: Google Maps ©2021

Figure 113: La Goleta Gas Storage Field Site



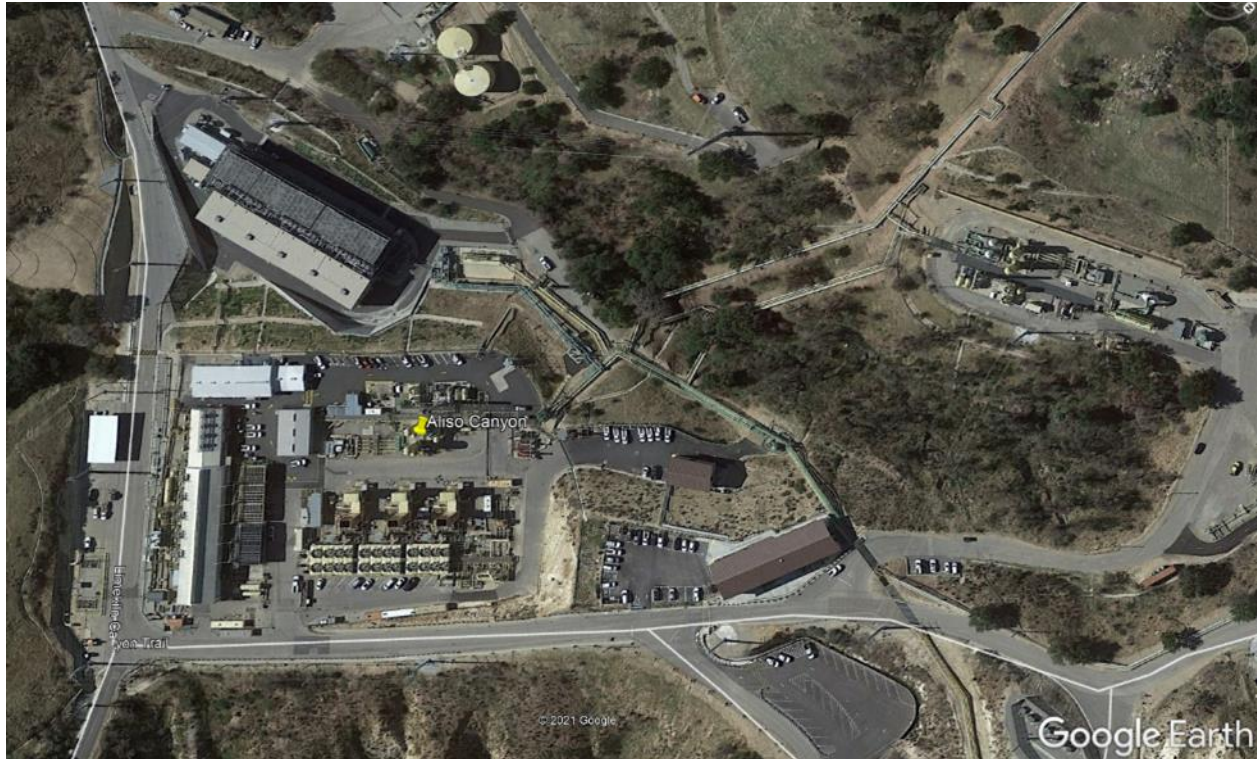
Source: Google Maps ©2021

Figure 114: Los Medanos Gas Storage Field Site



Source: Google Maps ©2021

Figure 115: Aliso Canyon Gas Storage Field Site



Source: Google Maps ©2021

The first approach to address the reliance on tanks in the refinery fragility calculation was to simply remove the tank component fragility from the calculation. This change greatly increases the median PGA for slight damage from about 0.3 g to about 0.8 g. The increase for the other three damage states is more moderate, from 0.12 g to 0.20 g. The increase in the median PGA from excluding the tank component for the slight damage state exceeded the corresponding median PGA for the moderate damage state, which is not logical. Further, the reduction in the probability of complete damage for the 0.85 g experienced in the Northridge earthquake from 50% to 40% was still considered too high.

As noted before, gas storage field facilities share common components with refineries and compressor stations. The median Hazus® pumping plant PGA for slight damage is much greater than the refinery slight damage value when tanks are excluded. Conversely, the median pumping plant PGA for complete damage is less than the refinery slight damage value when tanks are excluded. Given this, the recommended fragility relationships for gas storage fields were taken to be the average fragility for pumping plants and refineries without considering tanks. A comparison of the components of the resulting fragility for slight and complete damage are provided in Figure 116 and Figure 117. The resulting recommend gas storage field fragility curves are shown for anchored conditions are shown in Figure 118. The median PGA and dispersion for the curves in Figure 118 are provided in Table 30.

Figure 116: Comparison of Recommended Gas Storage Field Slight Damage State Fragility with Pumping Station and Refinery Fragilities

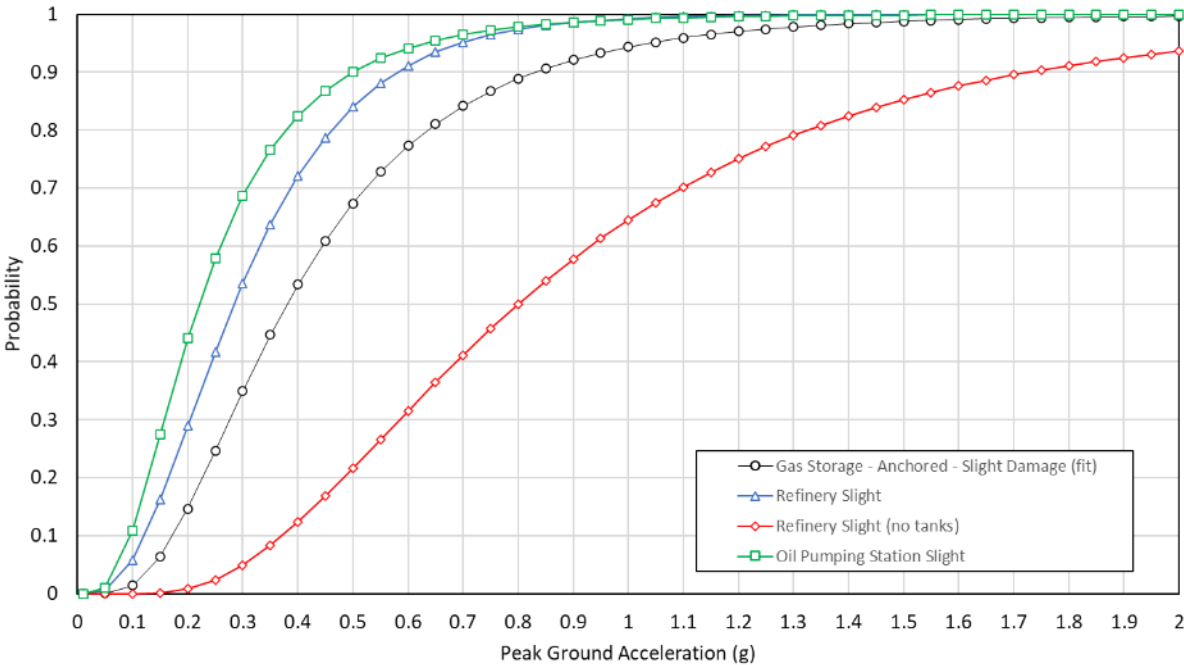


Figure 117: Comparison of Recommended Gas Storage Field Complete Damage State Fragility with Pumping Station and Refinery Fragilities

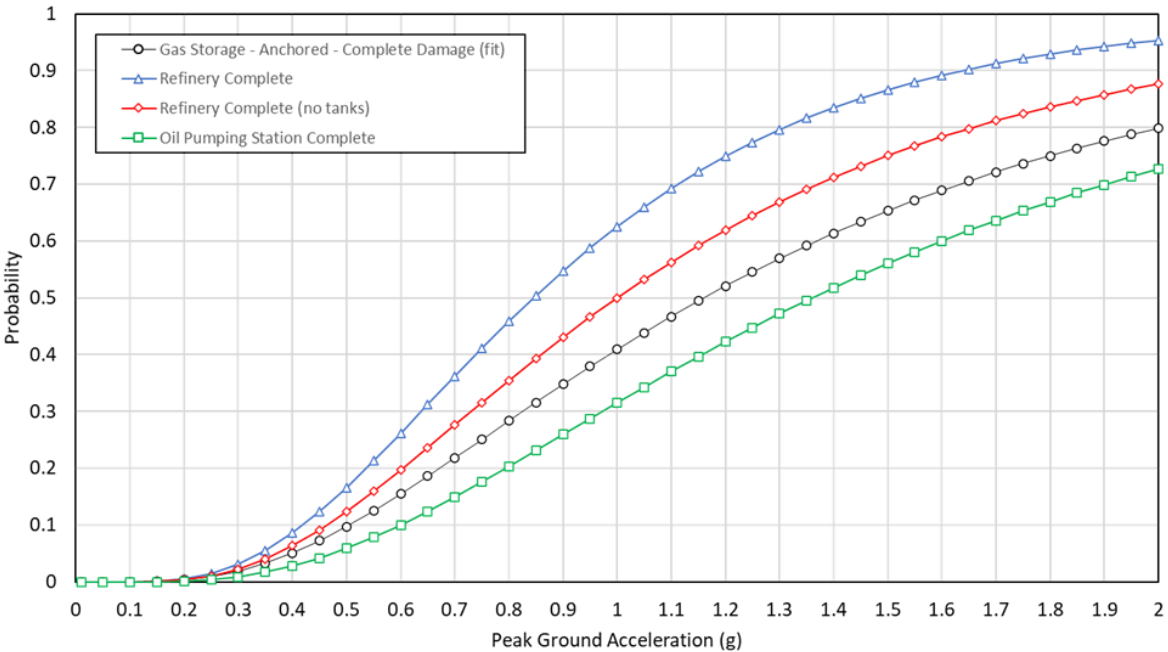


Figure 118: Recommended Fragility Relationship for Gas Storage Facilities

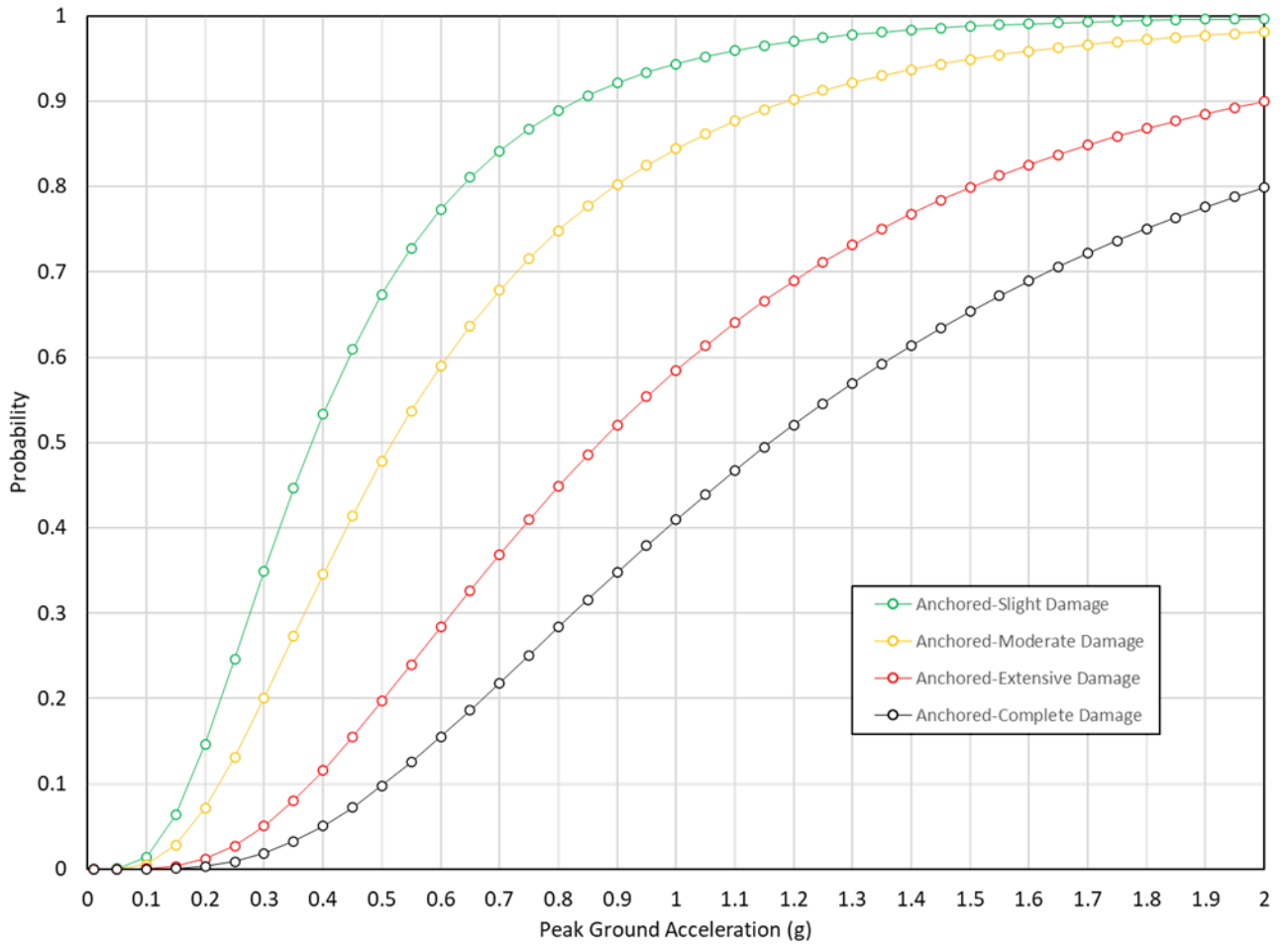


Table 30: Recommended Gas Storage Field Fragility Parameters

Damage State	PGA (Dispersion)	
	Anchored	Unanchored
Slight	0.38 (0.61)	0.13 (0.65)
Moderate	0.52 (0.65)	0.27 (0.65)
Extensive	0.87 (0.65)	0.43 (0.65)
Complete	1.16 (0.65)	0.68 (0.65)

10 Risk Model and Risk Software

This chapter provides an overall description of the free, open source, software platform for Natural Gas Infrastructure risk assessment and proactive risk management. The operational concept of the software platform enables users to (1) conduct risk assessment at different levels of complexity and sophistication, depending on the needs and objectives of the analysis; and (2) use the platform as decision support system for gas infrastructure proactive risk management, including tracking and use of leading risk indicators, and (3) if desired, develop or upload new models and databases.

10.1 Software Architecture

Figure 119 shows the overall software architecture that explains how the pipe data is collected and used by the hazard models and risk models. The software displays the pipeline risk results as an output of all the models that will be explained in the coming sections of this chapter.

10.2 Software Inputs

The software inputs are hazards data that are already compiled into a large database in Element 1 and pipeline/soil data that is requested from Operator (end-user).

All data is (1) aligned along the pipeline for the correct location and (2) converted into probability distributions. Consequently, if some data is missing (e.g., pipe thickness), the software will still run, although the results uncertainty will be increased.

CEC PIR18-002
 Element 3
 Software Architecture

User Specifies Pipeline Name

Step 1 Get Preliminary Data

The main objective of this block is to get the data that will be required to interface with element 1 and 2 of the project

Pipeline Data	
Pipe Yield Strength	Not used
Pipeline GPS Location	Array of GPS coordinates
Pipe Diameter	Number from 8 inch to 44 inch
Pipe Thickness	Number from 0.1 to 1.2 inch
Pipe Pressure	Number from 0 to 1000 psi
Depth of Cover	Number from 3 to 10 feet

Soil Data	
Soil Type	Clay or Sand
Soil Friction Angle	Number from 30 to 50 degrees
Soil Shear Strength	Number from 300 to 1000 psf
Soil Coefficient	Not used
Soil Unit Weight	Number from 90 to 120 pcf

Pipe Data Management

Shape file for pipeline location in California

California soil Information

Pipeline Location

Module 1 Hazards

Step 2 Get Element 1 Data

The main objective of this block is to get the data that was already calculated in Element 1 of the project

Fault Displacement	
Horizontal Fault angle	
Vertical Fault angle	
Fault displacement	Distribution in ft [0,1] [1,5] [5,10] [10,20] [20,30] [30,40]

Landslide & Liquefaction Displacement	
Movement Direction	Azimuth distribution
Amount of Pipe exposed	
Fault displacement	Amount to displacement

Element 1 Fault Displacement Data

Element 1 Landslide & Liquefaction Data

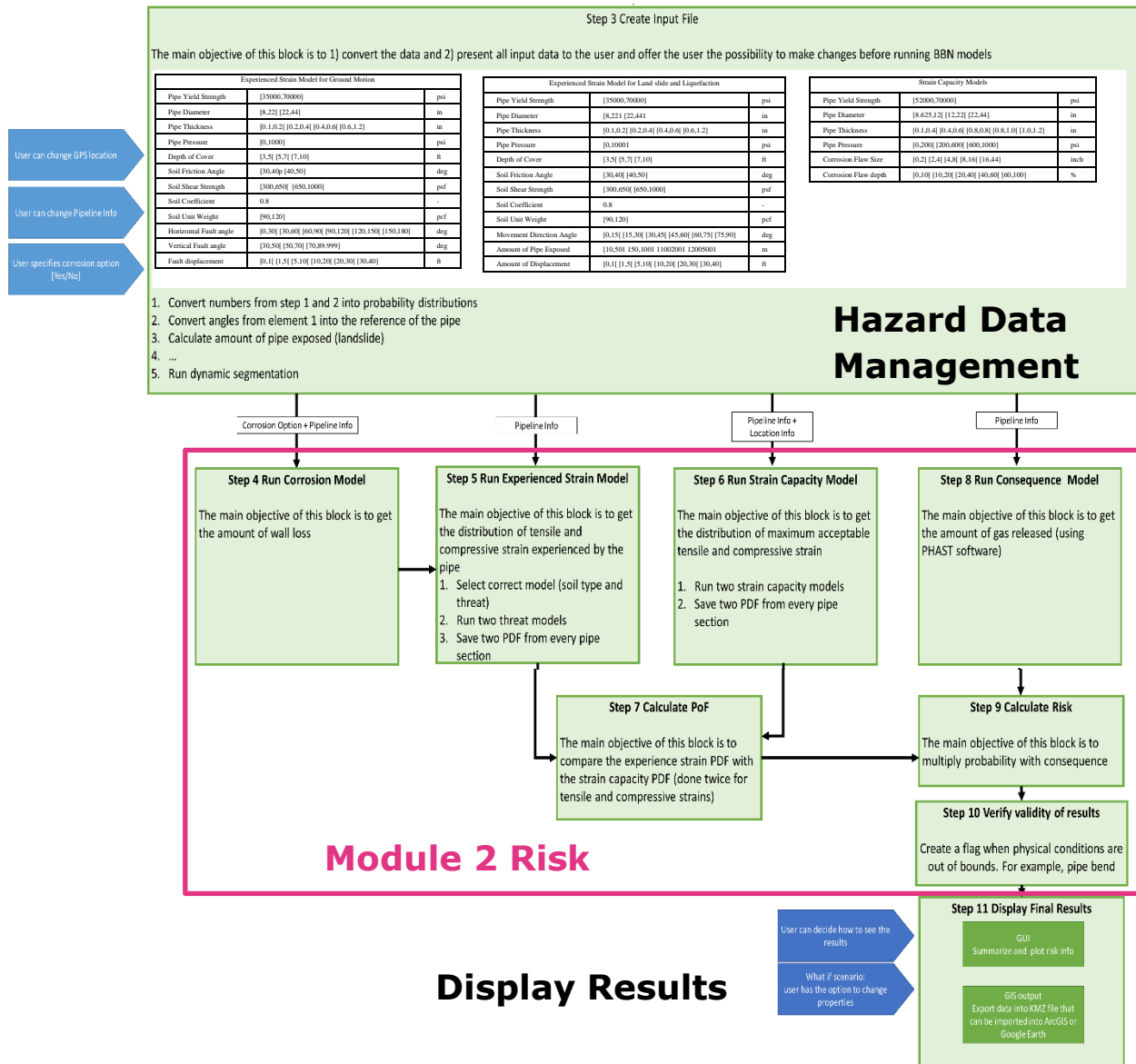


Figure 119: Software Architecture

10.3 Inputs from Pipeline Operators

10.3.1 GPS Data:

The GPS data inputs are the physical location of the pipeline. The inputs formats are the latitude and longitude pairs of the location of the pipeline (see Figure 120). The first coordinates of the

pipeline should be the starting point of the pipeline, followed by the coordinates of the location where the pipeline pass by, and end with the ending point of the pipeline.

Figure 120: GPS Data Input Example

	A	B
1	Latitude	Longitude
2	36.86390276	-121.4301665
3	36.86088549	-121.4303094
4	36.85783555	-121.4304808
5	36.85777381	-121.4297724
6	36.85614395	-121.4298096
7	36.85594559	-121.429985
8	36.85576248	-121.430191
9	36.85441208	-121.4302444
10	36.85245132	-121.430275
11	36.85263061	-121.4296188
12	36.85211182	-121.4292603
13	36.85151948	-121.4305122
14	36.85041791	-121.4326235
15	36.85005951	-121.4334259
16	36.84993362	-121.4339294
17	36.85013962	-121.4340286
18	36.85011569	-121.437336
19	36.85011291	-121.4378128
20	36.85020447	-121.4378204
21	36.85021536	-121.4382991

10.3.2 Pipeline Data:

The pipeline data consists of three data: pipe diameter, pipe thickness, and depth of cover. The pipeline diameter has a unit of inch, the pipe thickness also has a unit of inch, and the depth of cover has a unit of feet. Whenever there is a change in pipe diameter, pipe thickness, or depth of cover along the pipeline, the new data must be provided by the operator using the distance (in meters) and location information. For example, if the pipe thickness from the starting point to the first 500 meters of the pipeline is 42 inches, then in the input table, from 0 meter to 500 meters, the user should put 42 inches in the input table as shown in Figure 121.

Figure 121: Pipeline Data Input Example

1	Pipe Diameter (in)			Pipe Thickness (in)			Pipe Depth of Cover (ft)		
2	From (m)	To (m)	Value	From (m)	To (m)	Value	From (m)	To (m)	Value
3	0	500	42	0	500	0.25	0	500	2.5
4	500	1000	38	500	1000	0.2	500	20000	8
5	1000	2000	28	1000	20000	0.35			
6	2000	3000	30						
7	3000	8000	35						
8	8000	20000	30						

10.3.3 Soil Data:

Soil Data has three parts as shown in Figure 122: Soil type, soil shear strength, and soil friction angle. There are two soil types: clay and sand. If the soil type of a pipeline segment is unknown, the user can put “Unknown” in the table. If the soil type is sand, the user should fill in the soil friction angle data, and if the soil type is clay, the user should fill in the soil shear strength table. The input format for soil data is the same as the pipeline data, and the user needs to put the new data and location information whenever there is a change in the soil data on the pipeline.

Figure 122: Soil Data Input Example

1	Soil Type			Soil Shear Strength (psf) [Used for Clay]			Soil Friction Angle (deg) [Used for Sand]			
2	From (m)	To (m)	Value	From (m)	To (m)	Value	From (m)	To (m)	Value	
3	0	10000	Sand		10000	20000	520	0	1000	5
4	10000	20000	Clay					1000	2000	10
5								2000	4000	5
6								4000	8000	10
7								8000	10000	10

10.4 Precomputed Site Data

10.4.1 Fault Displacement Data

The fault displacement data has three parts: fault displacement probabilities, horizontal fault angle, and vertical fault angle. The horizontal fault angle and vertical fault angle are measured in degrees. These three data describe the fault displacement information across the entire California and are stored in the software based on the location. When the user puts in the location of the pipeline, the software will pick the fault displacement data near the pipeline for computation.

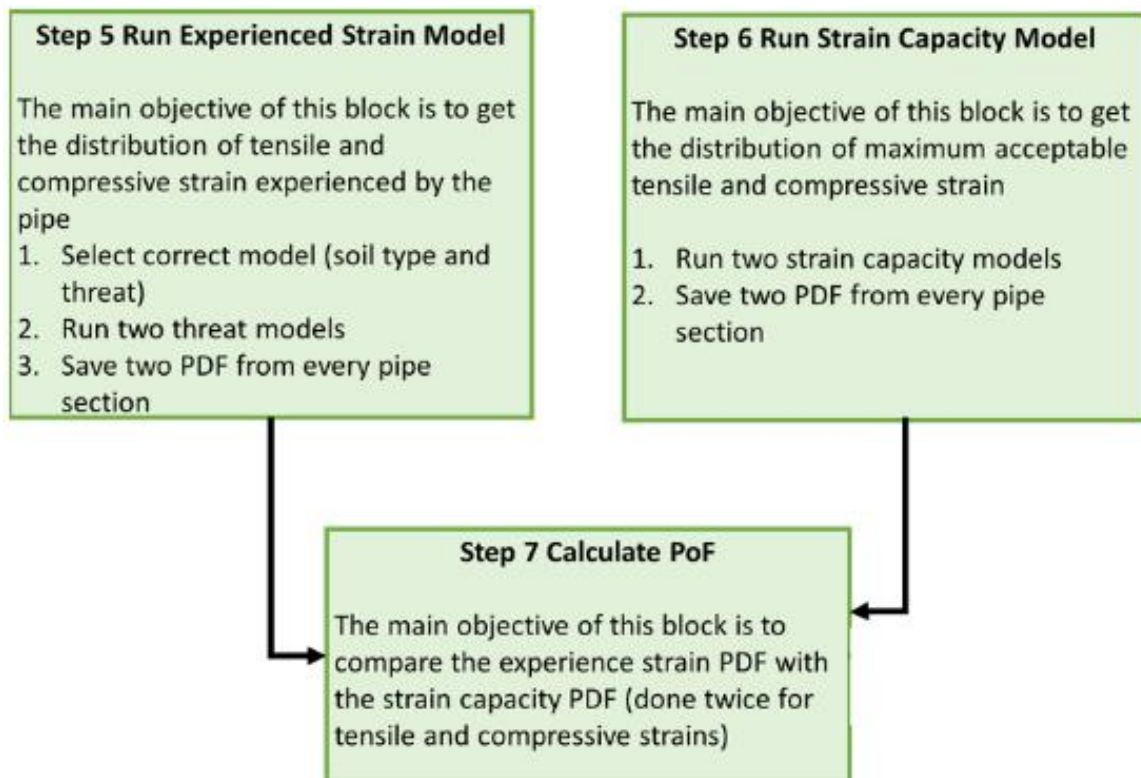
10.4.2 Landslide & Liquefaction Data:

Both the landslide data and liquefaction data have three parts: amount of displacement probabilities, amount of pipe exposed, and movement direction angle. These three datasets describe the landslide and liquefaction information across the entire California and are categorized into 25 scenarios, which are explained in part 6. These datasets are stored in the software based on the location. When the user puts in the location of the pipeline, the software will pick the landslide and liquefaction near the pipeline for computation.

10.5 How are the Inputs Used

The inputs described above are used by both the Experienced Strain Model and the Strain Capacity Model to get the distribution of tensile and compressive strain experienced by the pipe as well as the distribution of maximum acceptable strains as shown in Figure 123. Then both models are used to calculate the probability of failure (POF).

Figure 123: POF Calculation Steps

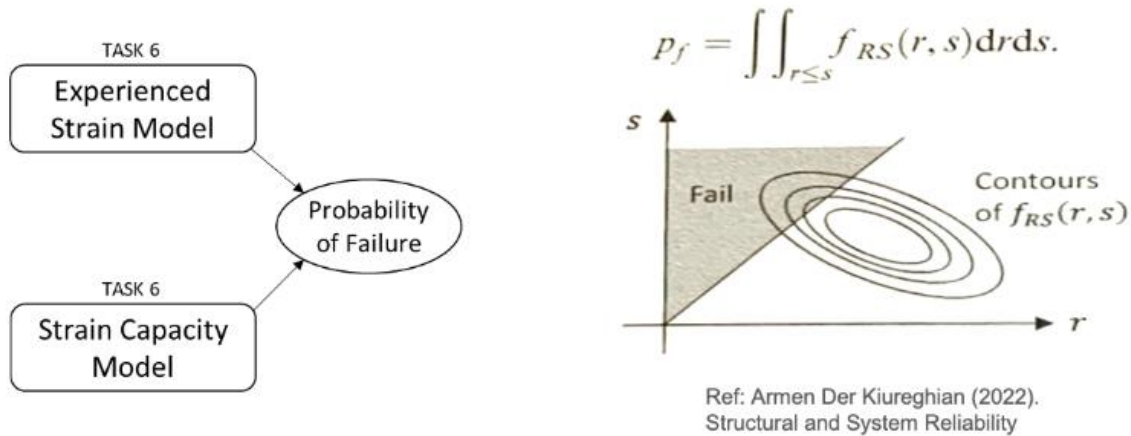


10.6 Software Outputs

For each segment of the pipeline, the software will output three major results: strain experienced probability distribution, strain capacity probability distribution, and probability of pipe failure.

Also, more detailed information, such as the pipeline and soil data, the hazard data, and other useful information about each segment of the pipeline will also be generated. Besides, the software will also generate a color-coded map of the entire pipeline, and mark each segment with red, yellow, or green color to reflect different probability of failure. These colors are reflected based on the end user desired thresholds.

Figure 124: Software Outputs



Regarding the probability of failure, the computational concept was described by Der Kiureghian, (2022). Assuming R and S take on only non-negative values, Figure 124 shows the failure domain in the outcome space of the two random variables together with the illustrative contour plots of the joint PDF. The failure probability is the integral of the joint PDF over the failure domain.

10.7 Bayesian Network Models

There are four Bayesian networks used in the software: fault displacement Bayesian network, landslide and liquefaction Bayesian network, capacity Bayesian network, and probability of failure Bayesian network.

The fault displacement Bayesian network (Figure 125) takes in the pipe diameter, pipe thickness, depth of cover, soil friction angle, and soil shear strength. These data come from the user input. And the fault displacement Bayesian network also takes in the horizontal fault angle, vertical fault angle, and fault displacement data from the pre-computed data from the software. The experienced strain for fault displacement model will output the experienced strain for tension and compression models, and both tension and compression models will have an experienced strain for sand and clay soil type, in total of four output strains.

The landslide and liquefaction Bayesian network (Figure 126) takes in the same pipeline and soil data from the user input, and it uses the movement direction angle, amount of pipe exposed, and

amount of displacement from the stored landslide and liquefaction data as inputs. It also has four output strains, where both the tension model and compression model have two strain results: for sand and clay soil types.

The capacity Bayesian network (Figure 127) takes in the corrosion flaw size, corrosion flaw depth, pipe pressure, pipe diameter, pipe thickness, flaw size, grith weld. All these data come from the user input. And it will output a tension strain and compression strain.

For the probability of failure Bayesian network (**Error! Reference source not found.**), it will take the tension experienced strain from the fault displacement Bayesian network output or landslide and liquefaction Bayesian network output, and the capacity tension strain to compute the probability of failure for tension. Similarly, it will take the compression experienced strain and compression capacity strain and compute the probability of failure for compression.

Figure 125: Fault Displacement BN

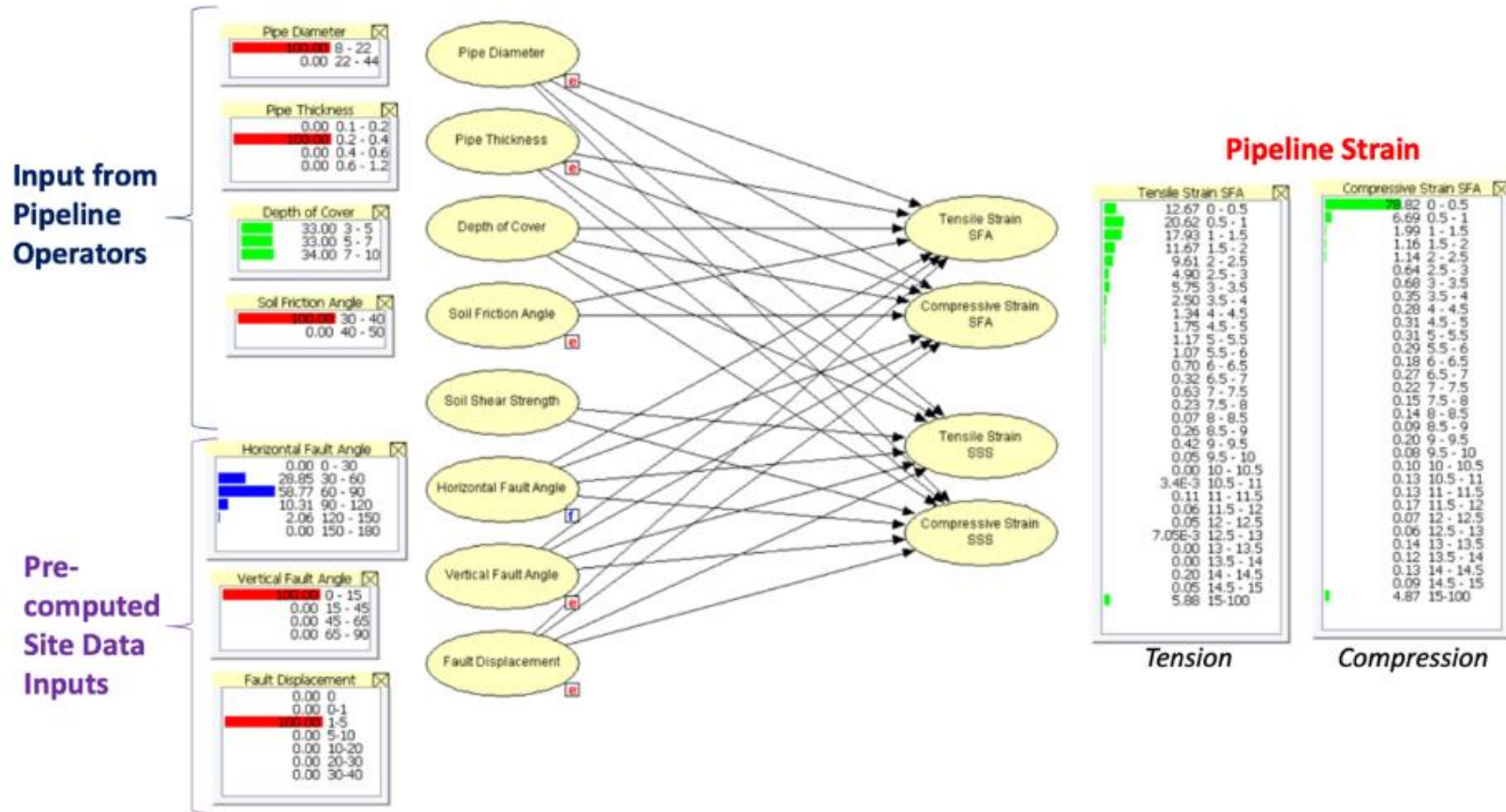


Figure 126: Landslide and Liquefaction BN

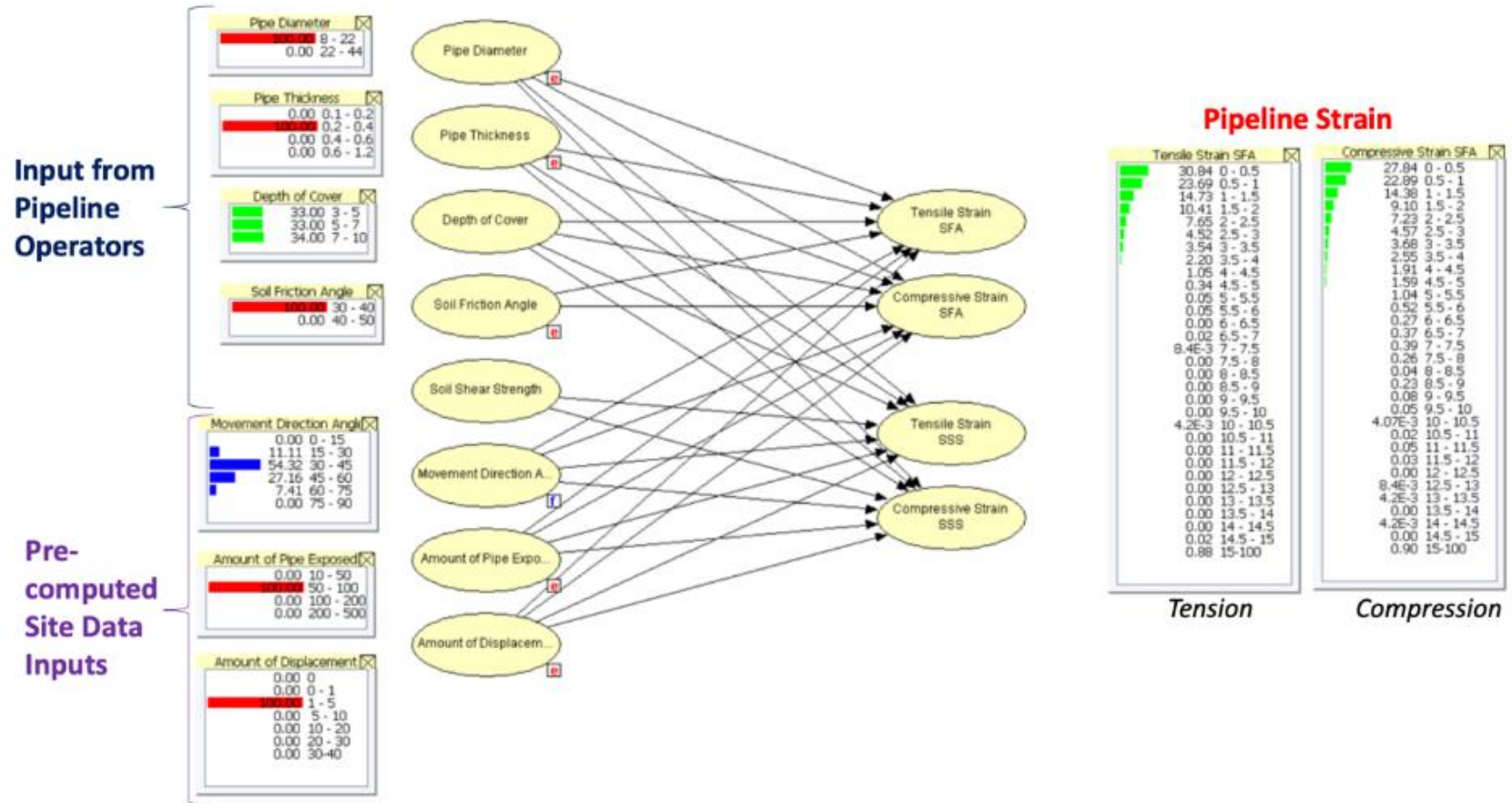


Figure 127: Pipe Capacity BN

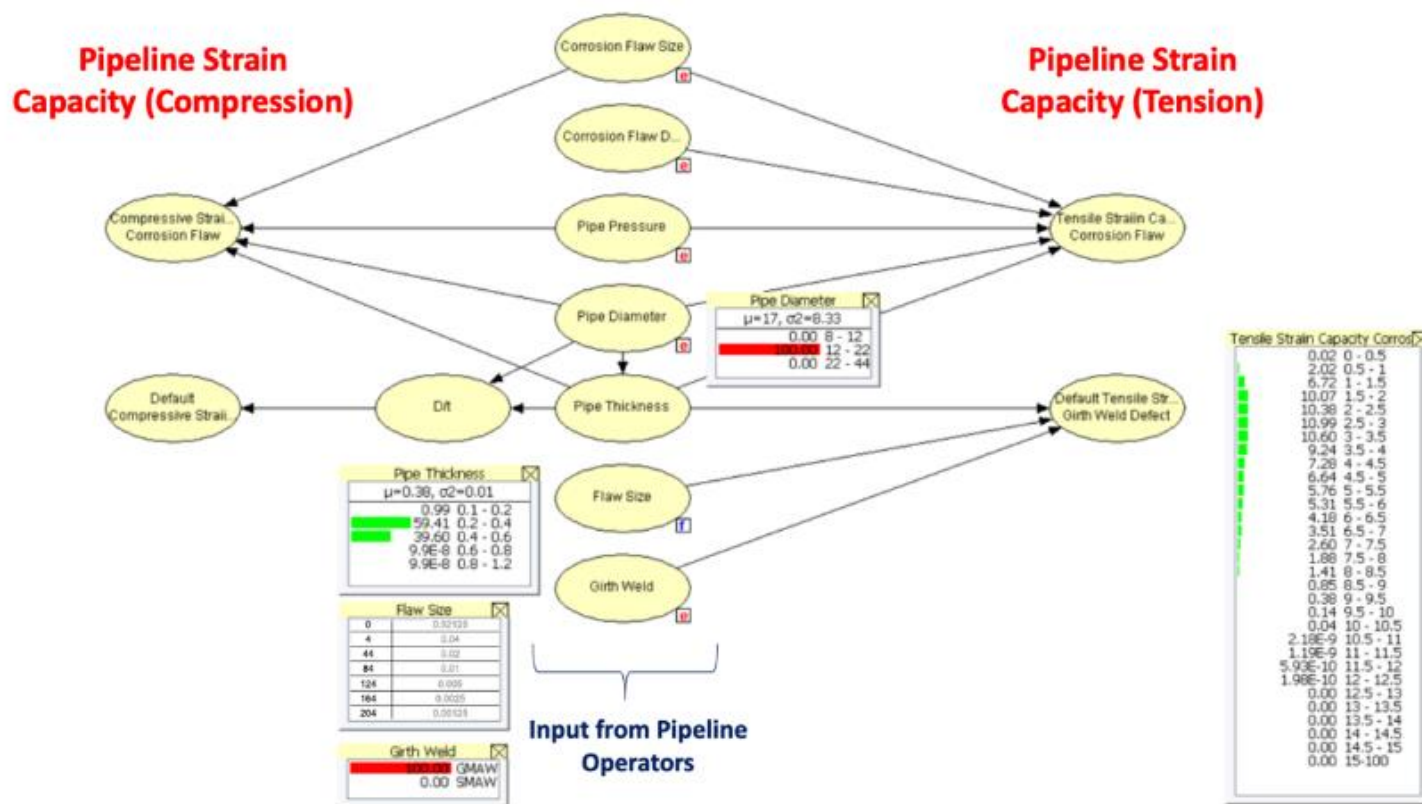
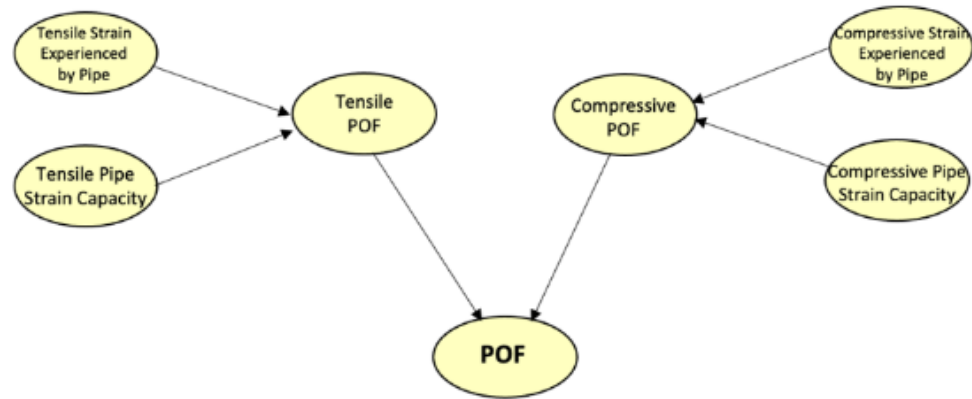
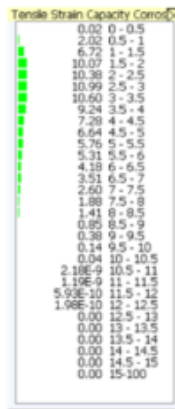
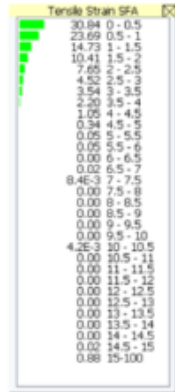


Figure 128: POF BN



10.8 Ground Motion Scenarios

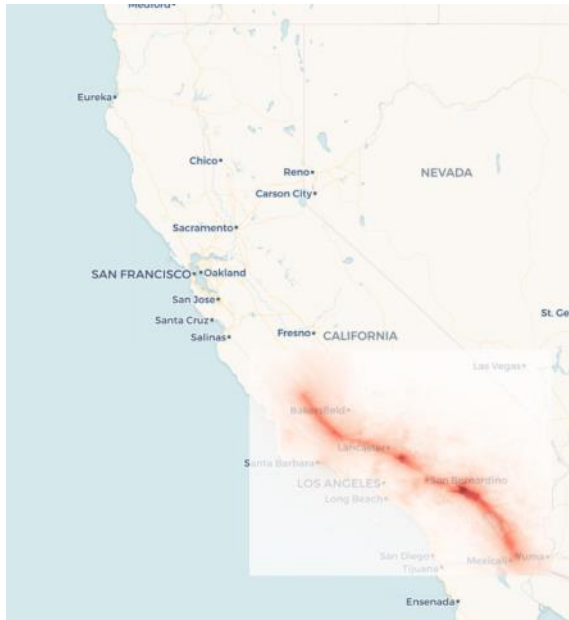
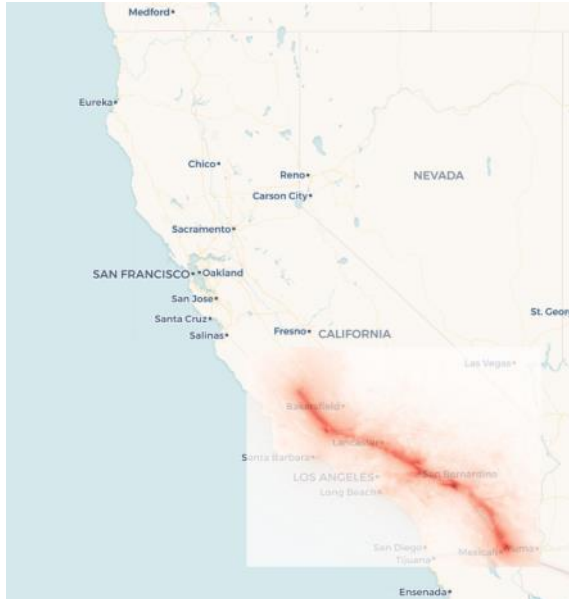
Table 31 shows the different ground motion scenarios, their respective maps, and descriptions. PGA stands for Peak Ground Acceleration (g) and PGV stands for Peak Ground Velocity (cm/s).

The basis for the methodology and procedures for developing spatially correlated hazard-consistent ground motions for seismic hazard risk analysis have three major steps: 1) conduct conventional point-based PSHA to obtain hazard curves and disaggregation as input (as described in the Sections above); 2) select hazard-consistent scenario earthquake events; and 3) generate spatially correlated ground motion realizations for each selected scenario event and select a manageable subset of hazard-consistent ground motion realizations.

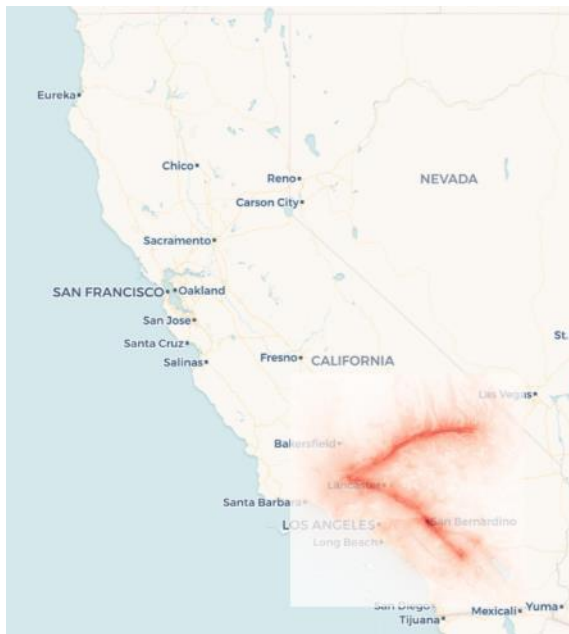
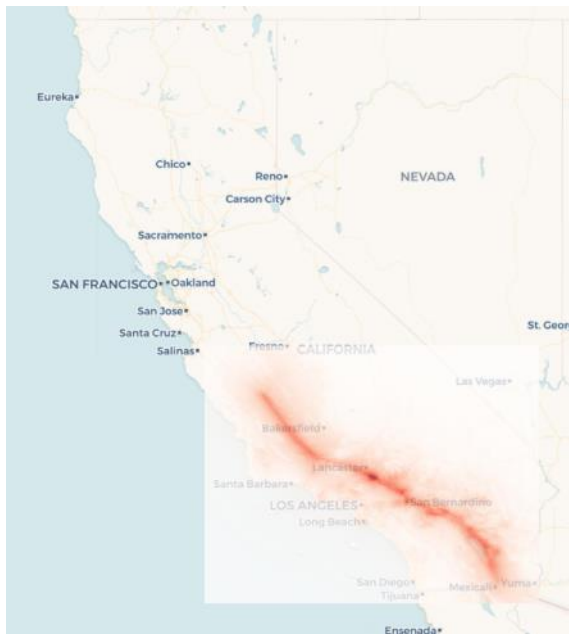
The aim of the scenario event selection is a manageable event subset that, in aggregate, approximately matches the hazard for single or multiple ground motion intensity measures across the spatially distributed system while preserving contributions of different magnitudes and distances to the PSHA. A flexible and efficient regression-based method that meets these requirements using point-based PSHA results as inputs is presented. The ground motion selection methodology is formulated similarly, but instead of selecting a subset of events among many candidate events, it selects realizations of ground motion from all selected events among many such possible realizations.

The procedure was applied to derive correlated hazard-consistent ground motion realizations from scenarios events for application to risk analyses for California natural gas pipeline infrastructure. 1,220 gridded sites were selected that are within 1 km of gas pipelines as the target hazard sites. The regression-based method was applied to select 599 hazard-consistent scenario events to preserve the hazard curves for Peak Ground Acceleration (PGA) and Peak Ground Velocity (PGV) from return periods of 200 years to 2,475 years and their magnitude distributions from disaggregation at the 1,220 target sites. The regression-based method was applied a second time to select 25 hazard-consistent correlated ground motion distributions for both PGA and PGV from scenario events. Lastly, co-Kriging was implemented to interpolate the selected correlated maps to a 100 m square resolution. (Wang et al, 2023).



Table 31 Ground Motion Scenarios

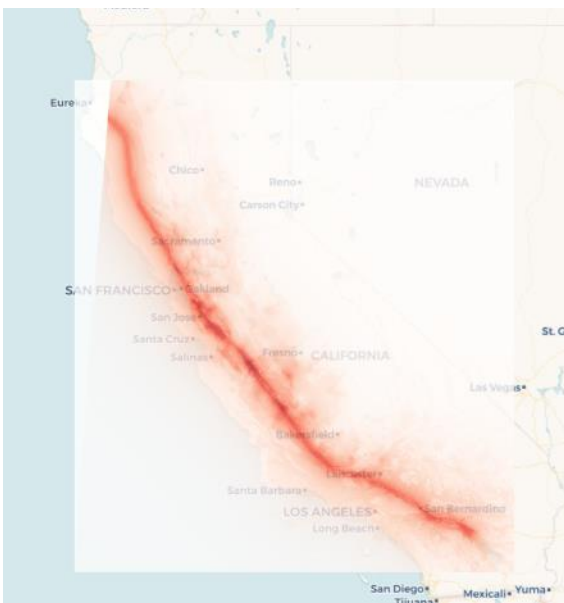
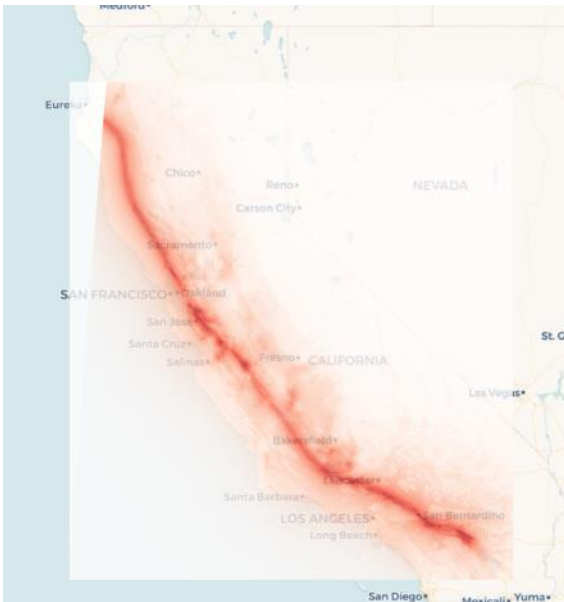
Scenario Number	Scenario Map	Scenario Description
1		<p>The paired PGA and PGV maps are generated by a multi-fault rupture event with a magnitude = 8.02. The annual occurrence rate of the ground motion scenario is 0.000239689. The maximum PGA and PGV on the maps are 3.15 g and 481.17 cm/s, respectively.</p>
2		<p>The paired PGA and PGV maps are generated by a multi-fault rupture event with a magnitude = 8.02. The annual occurrence rate of the ground motion scenario is 0.000603635. The maximum PGA and PGV on the maps are 1.62 g and 238.09 cm/s, respectively.</p>


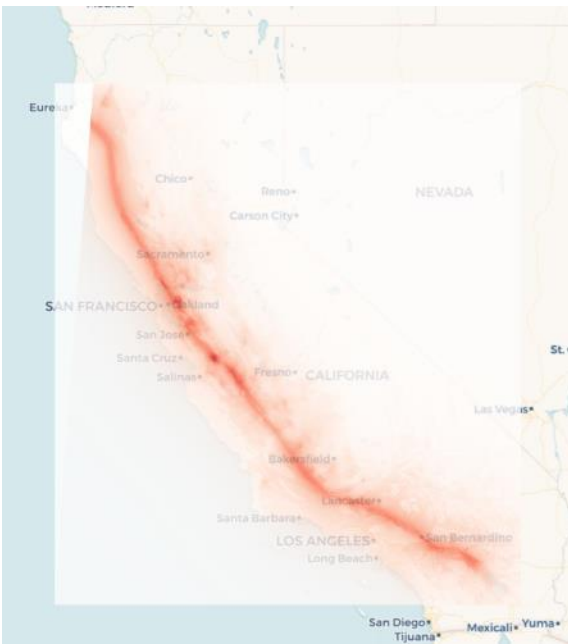
<p>3</p>		<p>The paired PGA and PGV maps are generated by a multi-fault rupture event with a magnitude = 8.02. The annual occurrence rate of the ground motion scenario is 0.000168888. The maximum PGA and PGV on the maps are 2.67 g and 433.05 cm/s, respectively.</p>
<p>4</p>		<p>The paired PGA and PGV maps are generated by a multi-fault rupture event with a magnitude = 8.01. The annual occurrence rate of the ground motion scenario is 0.000629249. The maximum PGA and PGV on the maps are 1.90 g and 407.90 cm/s, respectively.</p>

5		<p>The paired PGA and PGV maps are generated by a multi-fault rupture event with a magnitude = 8.02. The annual occurrence rate of the ground motion scenario is 0.000547440. The maximum PGA and PGV on the maps are 2.45 g and 249.13 cm/s, respectively.</p>
6		<p>The paired PGA and PGV maps are generated by a multi-fault rupture event with a magnitude = 8.02. The annual occurrence rate of the ground motion scenario is 0.000378089. The maximum PGA and PGV on the maps are 1.89 g and 348.36 cm/s, respectively.</p>



7		<p>The paired PGA and PGV maps are generated by a multi-fault rupture event with a magnitude = 8.00. The annual occurrence rate of the ground motion scenario is 0.000508390. The maximum PGA and PGV on the maps are 2.21 g and 309.65 cm/s, respectively.</p>
8		<p>The paired PGA and PGV maps are generated by a multi-fault rupture event with a magnitude = 8.50. The annual occurrence rate of the ground motion scenario is 0.000160122. The maximum PGA and PGV on the maps are 1.19 g and 249.04 cm/s, respectively.</p>

<p>9</p>		<p>The paired PGA and PGV maps are generated by a multi-fault rupture event with a magnitude = 8.50. The annual occurrence rate of the ground motion scenario is 0.000176656. The maximum PGA and PGV on the maps are 1.19 g and 323.58 cm/s, respectively.</p>
<p>10</p>		<p>The paired PGA and PGV maps are generated by a multi-fault rupture event with a magnitude = 8.50. The annual occurrence rate of the ground motion scenario is 0.000096526. The maximum PGA and PGV on the maps are 1.10 g and 347.36 cm/s, respectively.</p>

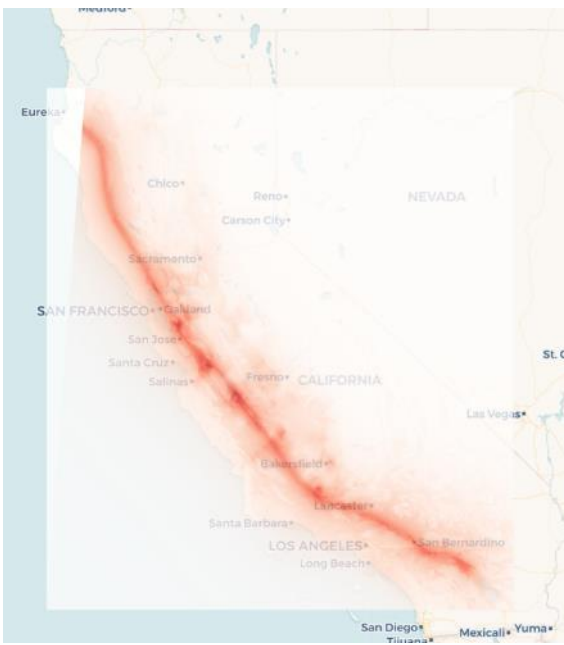

<p>11</p>		<p>The paired PGA and PGV maps are generated by a multi-fault rupture event with a magnitude = 8.50. The annual occurrence rate of the ground motion scenario is 0.000062931. The maximum PGA and PGV on the maps are 1.23 g and 251.52 cm/s, respectively.</p>
<p>12</p>		<p>The paired PGA and PGV maps are generated by a multi-fault rupture event with a magnitude = 8.50. The annual occurrence rate of the ground motion scenario is 0.000175257. The maximum PGA and PGV on the maps are 0.95 g and 207.40 cm/s, respectively.</p>

<p>13</p>		<p>The paired PGA and PGV maps are generated by a multi-fault rupture event with a magnitude = 8.50. The annual occurrence rate of the ground motion scenario is 0.000227218. The maximum PGA and PGV on the maps are 1.37 g and 388.91 cm/s, respectively.</p>
<p>14</p>		<p>The paired PGA and PGV maps are generated by a multi-fault rupture event with a magnitude = 8.50. The annual occurrence rate of the ground motion scenario is 0.000365825. The maximum PGA and PGV on the maps are 1.36 g and 315.00 cm/s, respectively.</p>

<p>15</p>		<p>The paired PGA and PGV maps are generated by a multi-fault rupture event with a magnitude = 8.50. The annual occurrence rate of the ground motion scenario is 0.000075634. The maximum PGA and PGV on the maps are 1.49 g and 443.20 cm/s, respectively.</p>
<p>16</p>		<p>The paired PGA and PGV maps are generated by a multi-fault rupture event with a magnitude = 8.50. The annual occurrence rate of the ground motion scenario is 0.000205857. The maximum PGA and PGV on the maps are 1.54 g and 235.89 cm/s, respectively.</p>

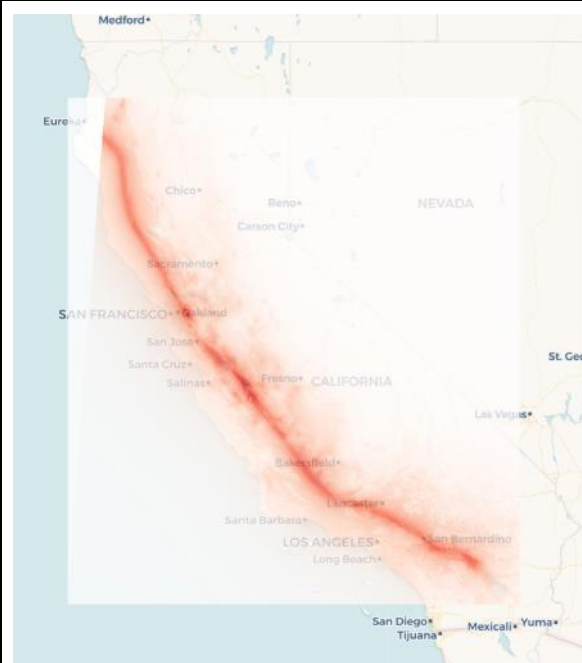
<p>17</p>		<p>The paired PGA and PGV maps are generated by a multi-fault rupture event with a magnitude = 8.50. The annual occurrence rate of the ground motion scenario is 0.000179798. The maximum PGA and PGV on the maps are 1.55 g and 314.20 cm/s, respectively.</p>
<p>18</p>		<p>The paired PGA and PGV maps are generated by a multi-fault rupture event with a magnitude = 8.50. The annual occurrence rate of the ground motion scenario is 0.000080414. The maximum PGA and PGV on the maps are 1.10 g and 355.42 cm/s, respectively.</p>

<p>19</p>		<p>The paired PGA and PGV maps are generated by a multi-fault rupture event with a magnitude = 8.50. The annual occurrence rate of the ground motion scenario is 0.000095709. The maximum PGA and PGV on the maps are 1.36 g and 254.18 cm/s, respectively.</p>
<p>20</p>		<p>The paired PGA and PGV maps are generated by a multi-fault rupture event with a magnitude = 8.50. The annual occurrence rate of the ground motion scenario is 0.000176437. The maximum PGA and PGV on the maps are 1.11 g and 281.89 cm/s, respectively.</p>

<p>21</p>		<p>The paired PGA and PGV maps are generated by a multi-fault rupture event with a magnitude = 8.50. The annual occurrence rate of the ground motion scenario is 0.000041338. The maximum PGA and PGV on the maps are 1.22 g and 306.22 cm/s, respectively.</p>
<p>22</p>		<p>The paired PGA and PGV maps are generated by a multi-fault rupture event with a magnitude = 8.50. The annual occurrence rate of the ground motion scenario is 0.000212124. The maximum PGA and PGV on the maps are 1.14 g and 241.00 cm/s, respectively.</p>

<p>23</p>		<p>The paired PGA and PGV maps are generated by a multi-fault rupture event with a magnitude = 8.50. The annual occurrence rate of the ground motion scenario is 0.000181260. The maximum PGA and PGV on the maps are 1.19 g and 236.17 cm/s, respectively.</p>
<p>24</p>		<p>The paired PGA and PGV maps are generated by a multi-fault rupture event with a magnitude = 8.50. The annual occurrence rate of the ground motion scenario is 0.000200312. The maximum PGA and PGV on the maps are 1.25 g and 281.65 cm/s, respectively.</p>

25



The paired PGA and PGV maps are generated by a multi-fault rupture event with a magnitude = 8.50. The annual occurrence rate of the ground motion scenario is 0.000305482. The maximum PGA and PGV on the maps are 1.19 g and 288.36 cm/s, respectively.

10.9 Dynamic Segmentation

Dynamic segmentation is a critical part in the quantification, where the entire pipeline is divided into smaller, manageable segments. This segmentation process enables a more focused and precise analysis of potential hazards, including fault displacement, landslides, and liquefaction. Each hazard type has a specific proximity threshold: 50 meters for fault displacement and liquefaction, and 10 meters for landslides. This approach allows for a more accurate assessment of the pipeline's probability of failure.

Once the pipeline is segmented, the software evaluates the proximity of each segment to hazard data points. These data points provide essential information about potential risks associated with each hazard type. When a segment falls within the specified distance threshold to a hazard data point, the software incorporates that hazard data into the risk assessment process.

For fault displacement and liquefaction hazards, a threshold of 50 meters is used. If a pipeline segment is within this distance of a hazard data point for either of these hazards, the software takes the hazard data into account to quantify the probability of failure. Similarly, for landslide hazards with a 10-meter threshold, if a segment is within this range of a hazard data point, the software factors in this information to assess the risk.

Also, for the user inputs of pipeline data and soil data, if there's a change in the value of the data, the software will also take the new data into the calculations of probability of failure.

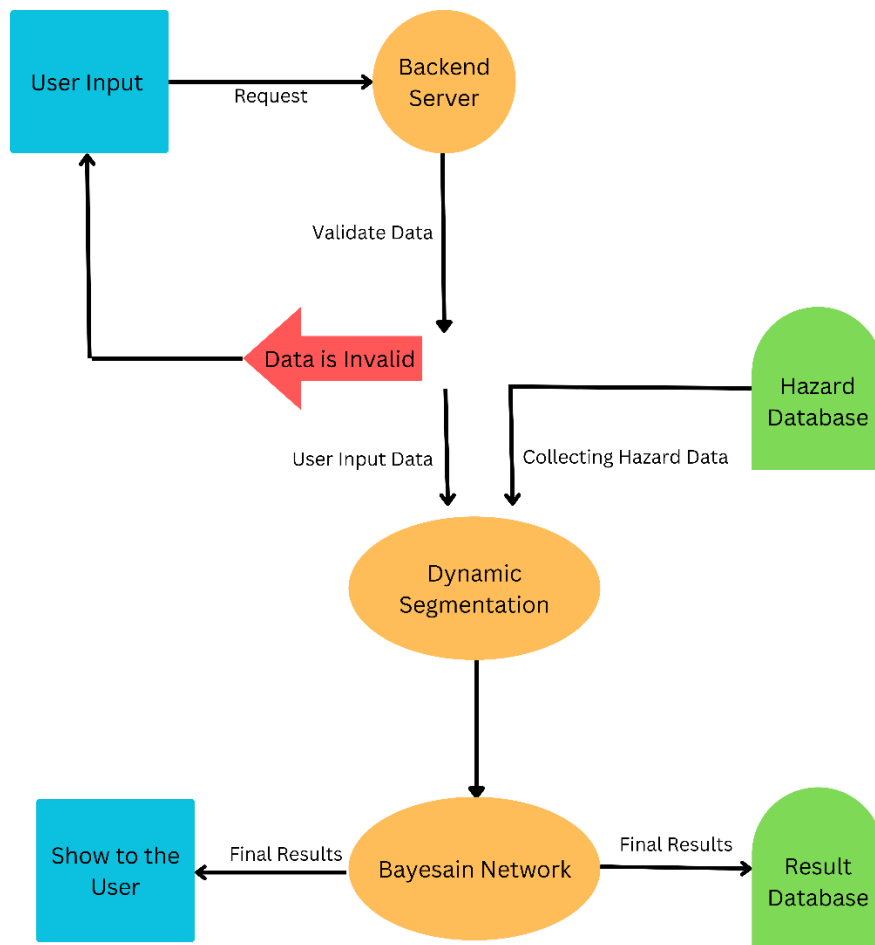
For example, for a pipeline of 10 km, the software will first partition this long pipeline into many small segments of length 25 meters. Suppose there is a segment from location A to location B, where A and B each represents the latitude and longitude location of the starting point and ending point of this pipeline segment, then, for fault displacement hazard quantification, the software will iterate over its database for all fault displacement data points and look for the datapoints that falls within the distance threshold. If there exists a fault displacement data point C near the pipeline, where the distance between C to segment AB is less than 50 meters, then the software will pick this data point C. Then, the software will input data at point C along with the user input data for pipeline and soil to quantify the probability of failure of the segment AB.

Segments of the pipeline that are not within the specified distance thresholds to any hazard data point or does not have a change in pipeline or soil data value are considered safe from these hazards. Consequently, they are excluded from the final risk quantification and will not be reflected in the quantification results.

11 End-User Guide for Using Risk Tools

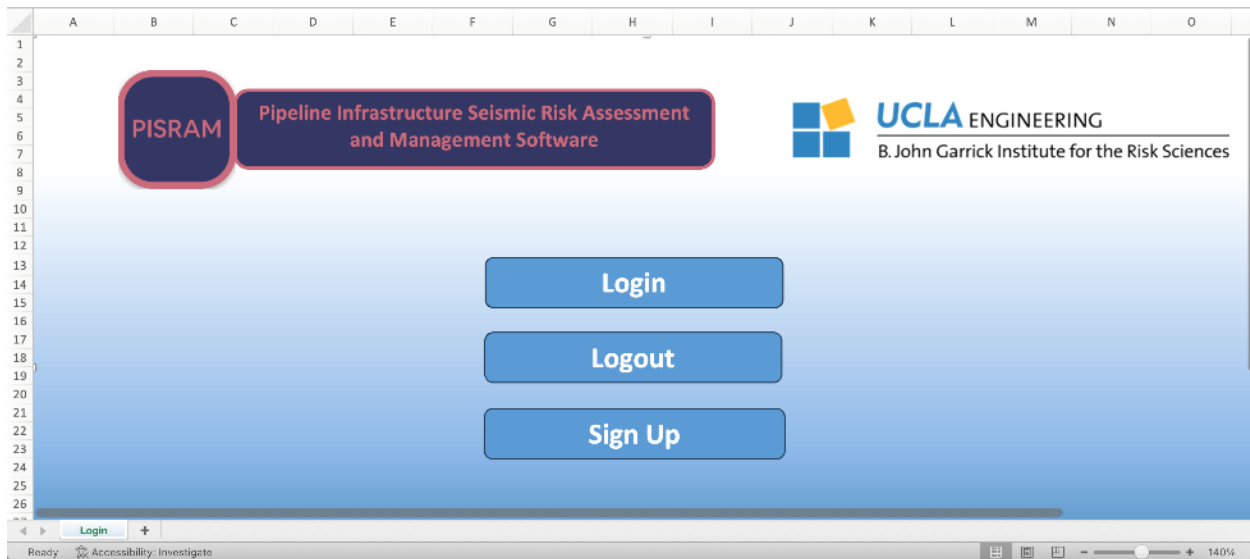
This chapter provides step by step guide and examples on how to run various analyses and use different risk management features of the software (PISRAM: Pipeline Infrastructure Seismic Risk Assessment and Management Software). PISRAM has a complex foundational architecture as shown in the Quantification Process Flow Chart (Figure 129). The blue boxes are the frontend of the software which consists of a dynamic spreadsheet which will be explained in more details in the following sections. The excel sheet is where the user can input the data and also see the results. The Backend and computational modules are hosted in a UCLA server. The modules include data validation, hazard database, dynamic segmentation, Bayesian network quantification, and results database.

Figure 129 Quantification Process Flow Chart



The frontend of the software consists of an interactive desktop excel spreadsheet, that is connected to a Backend where all the models are stored, and computations takes place. (Figure 130)

Figure 130 Software Dashboard



11.1 Software Login

The first step to use the software is to create an account as shown below in Figure 131. You should provide your name, email address, and choose a username and password. Once your account is created, you can login using your username and password as shown in Figure 132.

Figure 131 Account Creation

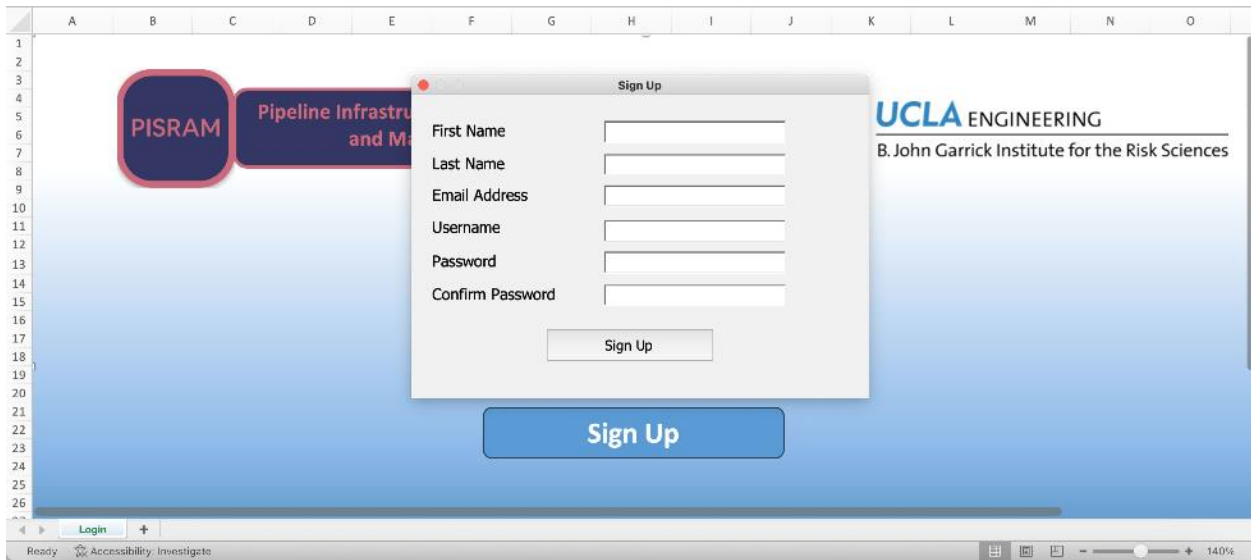
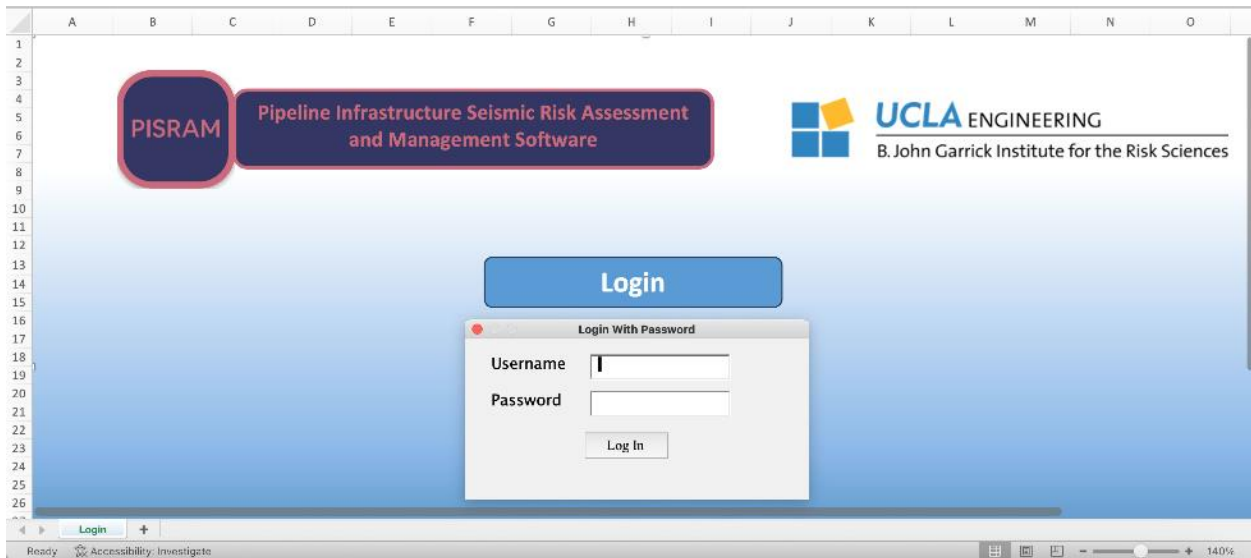


Figure 132 Software Login After Account Creation



11.2 Software Dashboard

Once signed up and logged in, you have the option to create a new quantification or load previous quantification results as shown in Figure 133 and Figure 134.

Figure 133 Option to Create a New Quantification or Load Previous Quantification Results

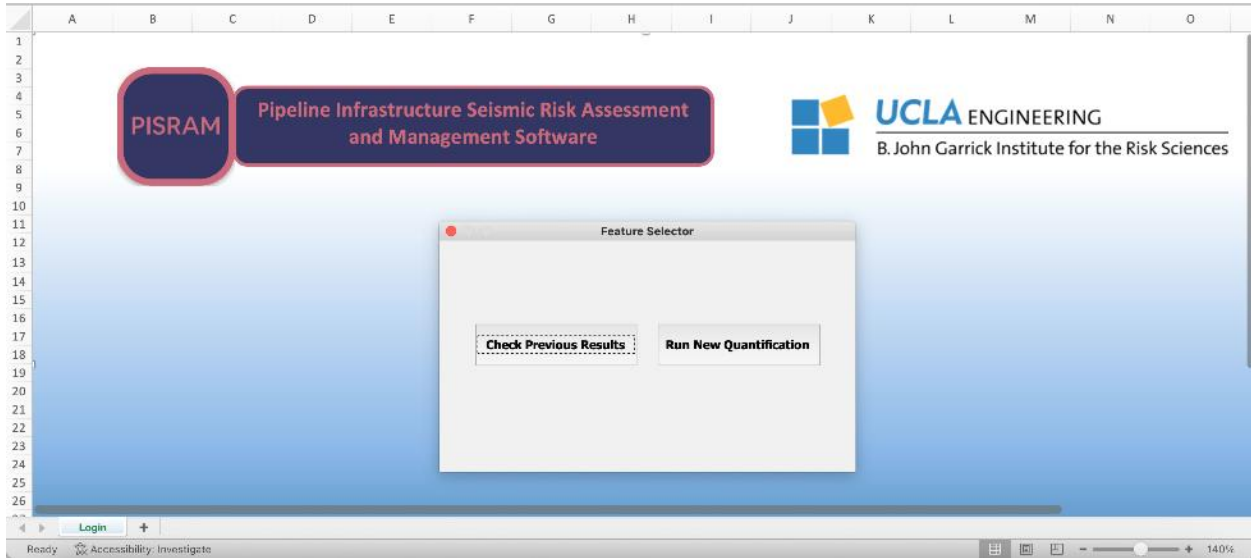
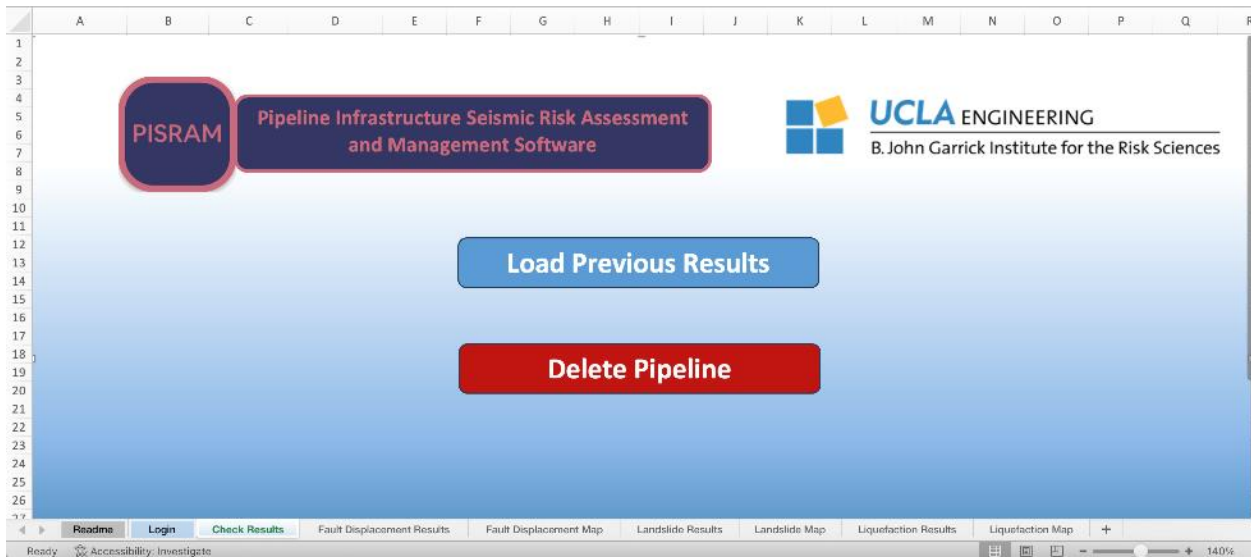


Figure 134 Load Previous Quantification Results Feature



If the user chooses to load previous quantification results, a pop up will be displayed (Figure 135) and the user needs to choose the pipeline from the dropdown menu showing the saved pipelines list. In addition, the user has the option to delete a pipeline from the list (Figure 136).

Figure 135 The User Needs to Choose the Pipeline from the Dropdown Menu Showing the Saved Pipelines List

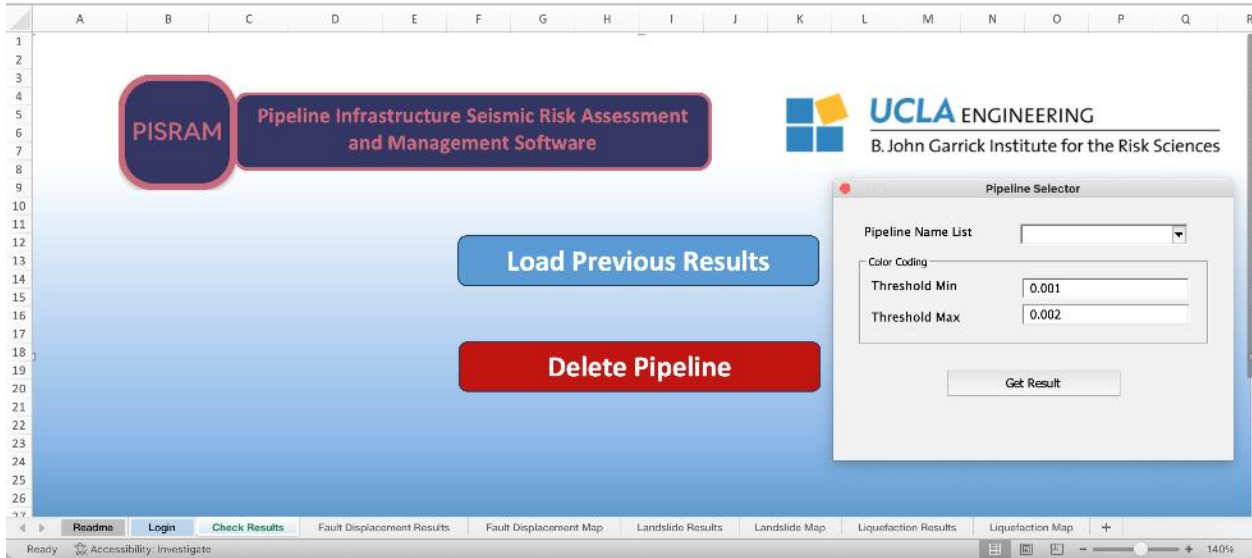
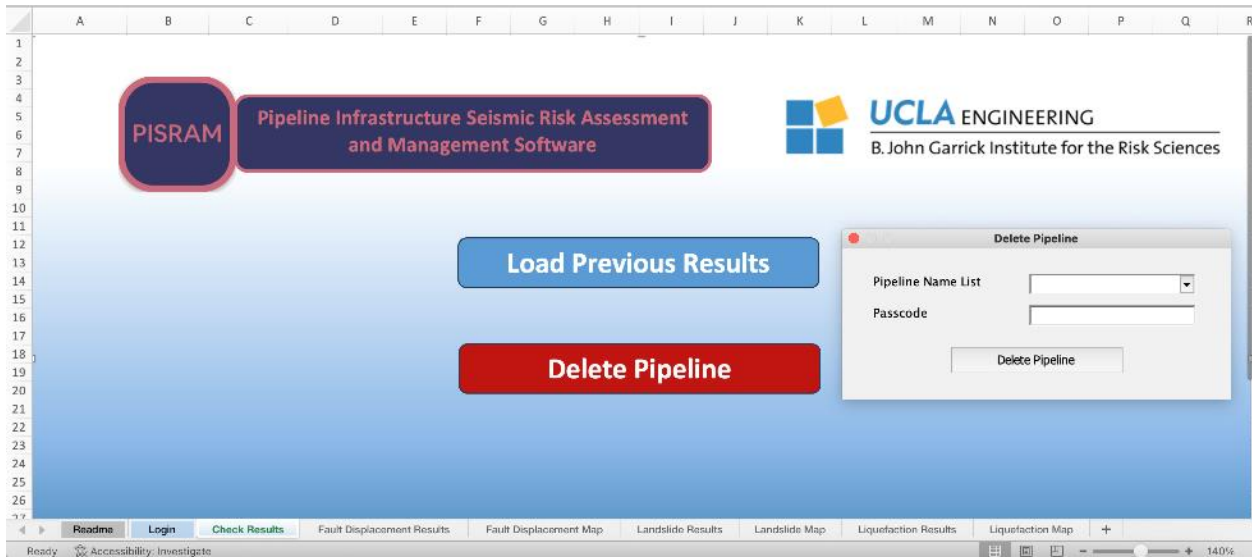


Figure 136 The User has the Option to Delete a Pipeline from the List



11.3 Creating a New Quantification

To create a new quantification the user has to follow the following steps:

1. Fill the 3 input tabs highlighted in green (GPS Data, Pipeline Data, Soil Data) with the required input data (Figure 137, Figure 138, Figure 139). The GPS Data tab should contain the pipe points in terms of latitude and longitude. The Pipeline Data tab should contain the pipe diameter, thickness, and depth of cover of the pipe segments defined based on distance (From, To). The Soil Data should contain the soil shear strength, soil friction angle, and soil type along the pipe segments defined based on distance as well (From, To). The units required are shown in Table 32.

Figure 137 The User has to Enter the GPS Data of the Pipeline

	A	B	C	D	E	F	G	H	I	J	K	L	M	N
1	Latitude	Longitude												
2	36.86390276	-121.4301665												
3	36.86088549	-121.4303094												
4	36.85783555	-121.4304808												
5	36.85777381	-121.4297724												
6	36.85614395	-121.4298096												
7	36.85594559	-121.429985												
8	36.85576248	-121.430191												
9	36.85441208	-121.4302444												
10	36.85245132	-121.430275												
11	36.85263061	-121.4296188												
12	36.85211182	-121.4292603												
13	36.85151948	-121.4305122												
14	36.85041791	-121.4326235												
15	36.85005951	-121.4334259												
16	36.84993362	-121.4339294												
17	36.85013962	-121.4340286												
18	36.85011569	-121.437336												
19	36.85011291	-121.4378128												
20	36.85020447	-121.4378204												
21	36.85021536	-121.4382991												
22	36.85036576	-121.438851												
23	36.85062935	-121.4395686												
24	36.85094971	-121.4400991												

Figure 138 The User has to Enter the Pipeline Data (Diameter, Thickness, and Depth of cover)

Pipe Diameter			Pipe Thickness			Pipe Depth of Cover		
From	To	Value	From	To	Value	From	To	Value
0	500	42	0	500	0.25	0	500	2.5
500	1000	42	500	1000	0.2	500	20000	8
1000	2000	28	1000	20000	0.2			
2000	3000	30						
3000	8000	35						
8000	20000	30						

Figure 139 The User has to Enter the Soil Data

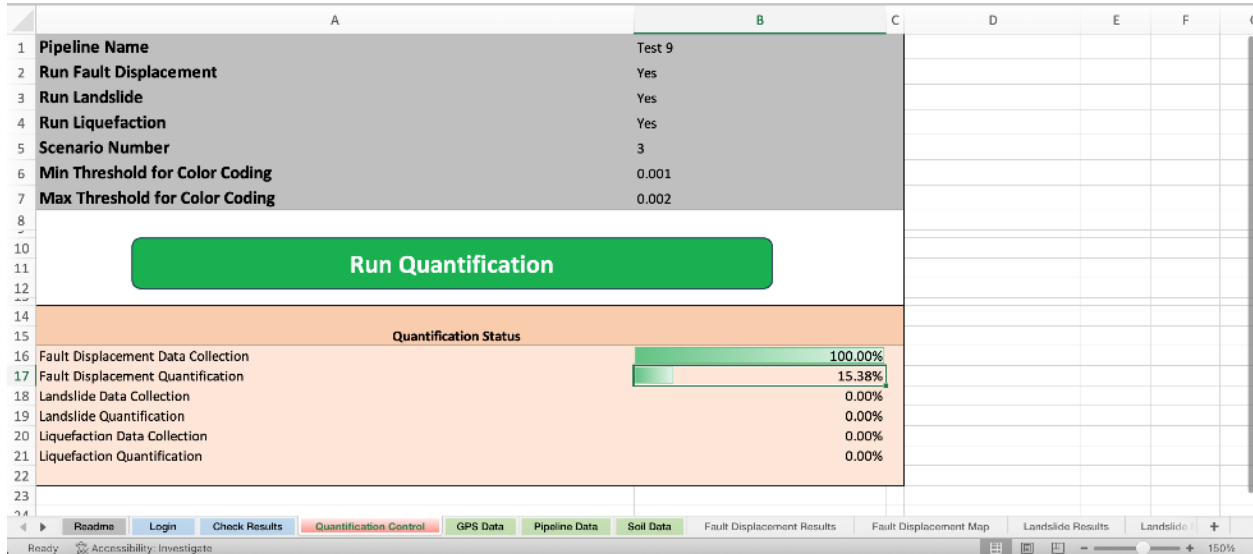
Soil Type			Soil Shear Strength			Soil Friction Angle		
From	To	Value	From	To	Value	From	To	Value
0	10000	Sand	10000	20000	520	0	1000	5
10000	20000	Clay				1000	2000	10
						2000	4000	5
						4000	8000	10
						8000	10000	10

Table 32 The Units Required in the Inputs Fields

Pipe Diameter	inch
Pipe Thickness	inch
Pipe Depth of Cover	feet
Soil Type	Clay or Sand
Soil Friction Angle (used for Sand)	degree
Soil Shear Strength (used for Clay)	psf
From, To	meter

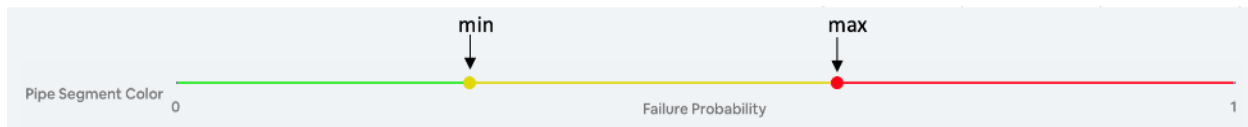
- Go to the Quantification Control tab highlighted in red (Figure 140)

Figure 140 The Quantification Control tab



- The user has to fill the following input fields:
 - choose a Pipeline name (if the name you chose was used before, an error message will appear, and you have to enter a different name)
 - choose yes/no from the dropdown menu to run Fault Displacement, Landslide, Liquefaction hazards
 - choose a scenario number from the dropdown menu (only if you chose "yes" to landslide or liquefaction)
 - enter min/max thresholds for color coding of the POF of the pipe segments. These thresholds are explained below in Figure 141. This feature enables the users to change the pipe segments color based on their POF by setting 2 thresholds that define 3 colors: green, yellow, and red. By default, if the annual failure probability is lower than 0.001, then the color is green. If it's higher than 0.001 and lower than 0.002 then the color is yellow. And if it's higher than 0.002 then it's red.

Figure 141 Thresholds for Color Coding of the POF of the Pipe Segments



- The user finally clicks on the “Run Quantification” button. The user can see the progress of the quantification in the Quantification Status window.

11.4 Pipeline Risk Assessment Results

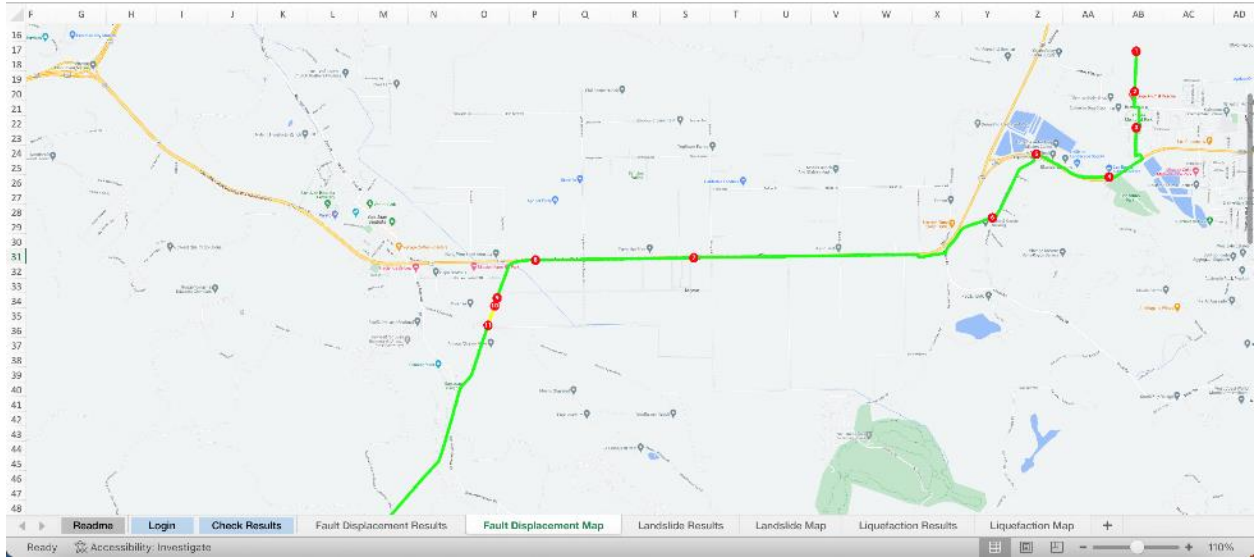
Once the quantification is done, the user will see the pipeline risk assessment results. After clicking on the Fault Displacement, Landslide, or Liquefaction “Results” tab, the user will see a table that has the detailed results (Figure 142). The results table shows the significant points along the pipeline when pipeline or soil data has changed, it also shows points that were affected by any of the hazards. The table also shows the pipe probabilities of failure (POF) at those points.

Figure 142 Results Table

Point	Latitude	Longitude	Distance from Start [m]	POF	Pipe Diameter [in]	Pipe Thickness [in]	Depth of Cover [ft]	Soil Friction Angle [deg]	Soil Shear Strength [psf]	Soil Type	Horizontal Fault Angle [deg]	Vertical Fault Angle [deg]	Fault Displacement: 0-ft	Fault Displacement: 0-1 ft
1	36.85399276	-121.4301665	0	0	42	0.25	2.5	5	NaN	Sand	NaN	NaN	1	0
2	36.85949981	-121.4303923	500	0	42	0.25	2.5	5	NaN	Sand	NaN	NaN	1	0
3	36.8553153	-121.4302202	1000	0	42	0.2	8	5	NaN	Sand	NaN	NaN	1	0
4	36.85311776	-121.4342857	2000	0	28	0.2	5	10	NaN	Sand	NaN	NaN	1	0
5	36.85278862	-121.4446523	3000	0	30	0.1	6	5	NaN	Sand	NaN	NaN	1	0
6	36.85566262	-121.4306211	4000	0	35	0.25	5	5	NaN	Sand	NaN	NaN	1	0
7	36.8412924	-121.4830656	8000	0	35	0.25	5	10	NaN	Sand	NaN	NaN	1	0
8	36.84104166	-121.513538	10000	0	30	0.3	6	10	NaN	Sand	NaN	NaN	1	0
9	36.8393086	-121.5309721	10667.94296	0.0030781	30	0.3	6	NaN	520	Clay	71.3	0	0.058248718	0.000327223
10	36.83584781	-121.5213341	10768.15812	0.001553095	30	0.3	6	NaN	520	Clay	71.3	0	0.056531772	0.000308182
11	36.83398002	-121.522278	11021.39581	0	30	0.3	6	NaN	520	Clay	NaN	NaN	1	0
12	36.81139757	-121.5412098	14047.35058	9.32468E-06	30	0.3	6	NaN	520	Clay	84.93516189	14.07357574	0.599980489	0.000008844
13	36.80759123	-121.5365164	20000	0	30	0.3	6	NaN	520	Clay	NaN	NaN	1	0

The user can also see the pipe segments color coded in green, yellow, or red based on their failure probability by clicking in the “Map” tab (Figure 143).

Figure 143 Color Coded Map Results



11.5 Storage Facilities

A separate interactive excel spreadsheet (RASf_Risk Analysis of Storage Facilities.xlsx) is provided to show the user the storage fields results (Figure 144 ~ Figure 155). The results are split into 4 sections: Hazard curve, Anchored fragility curves, Unanchored fragility curves, and probabilities of exceedance table.

Figure 144 Aliso Canyon Results

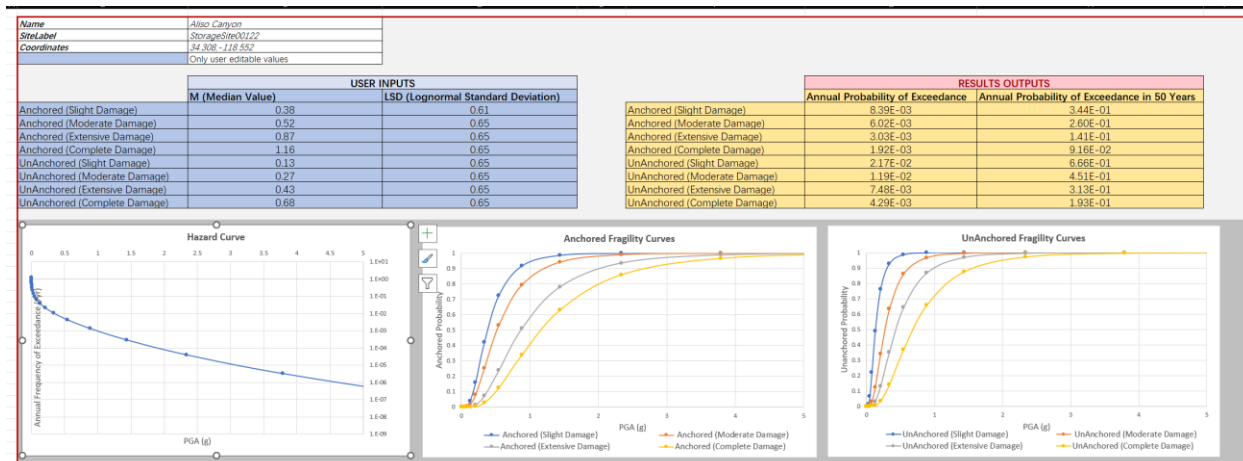


Figure 145 Honor Rancho Results

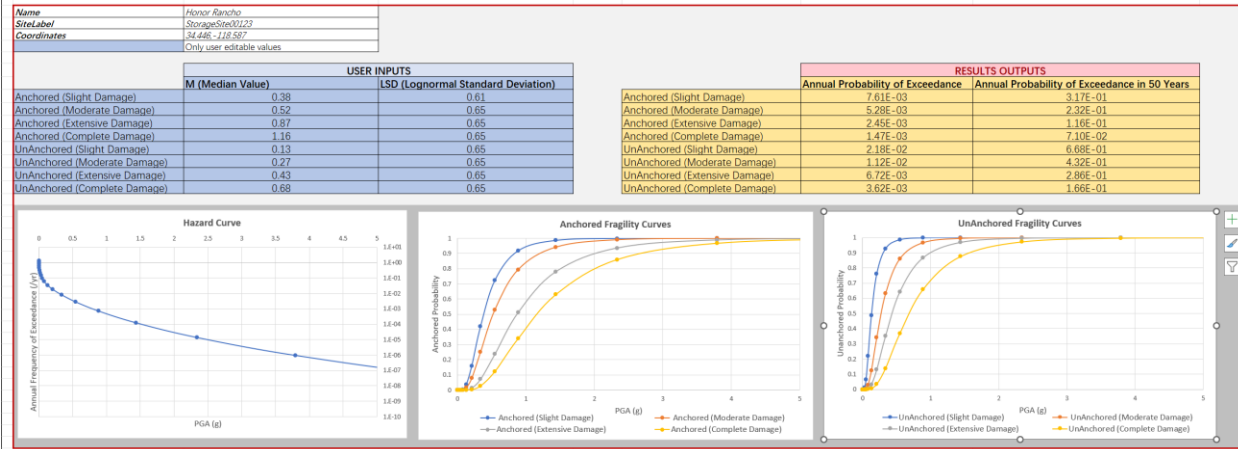


Figure 146 Playa Del Rey Results

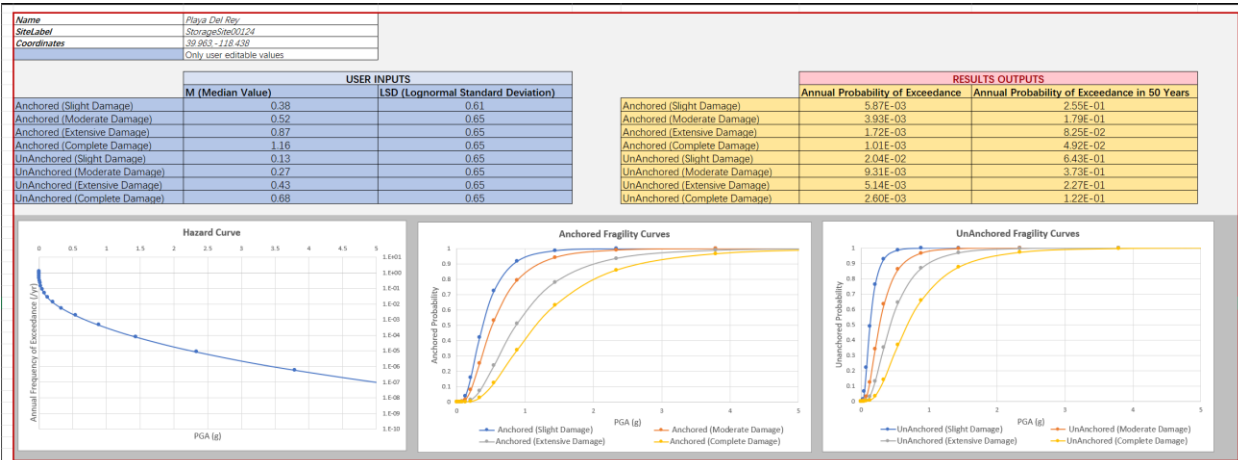


Figure 147 La Goleta Results

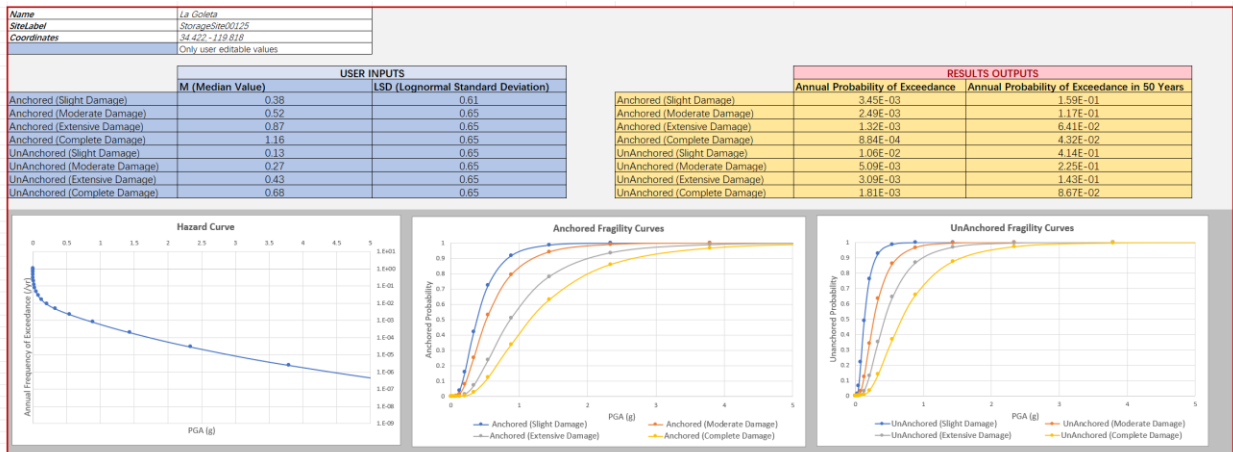


Figure 148 McDonald Island Results

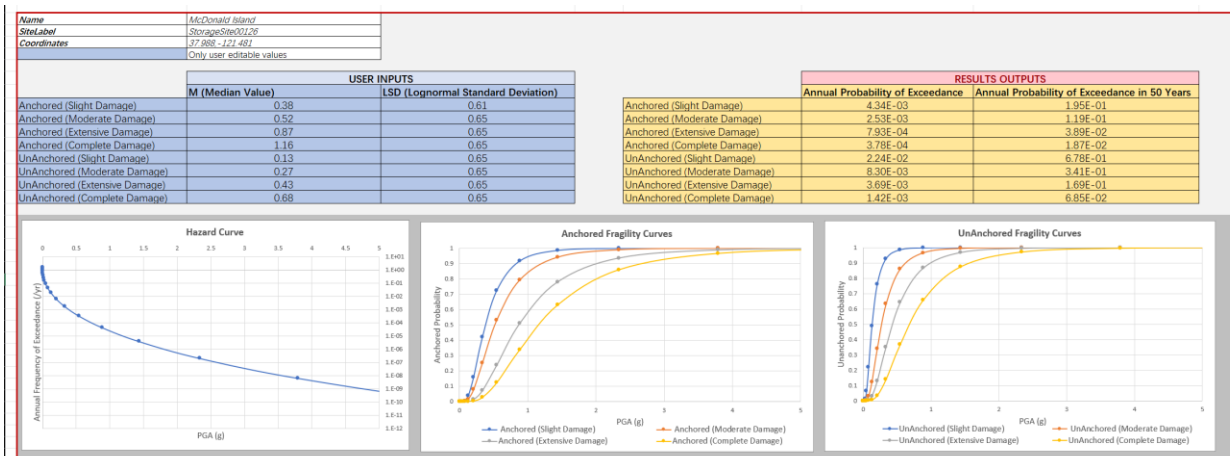


Figure 149 Los Medanos Storage Facility Results

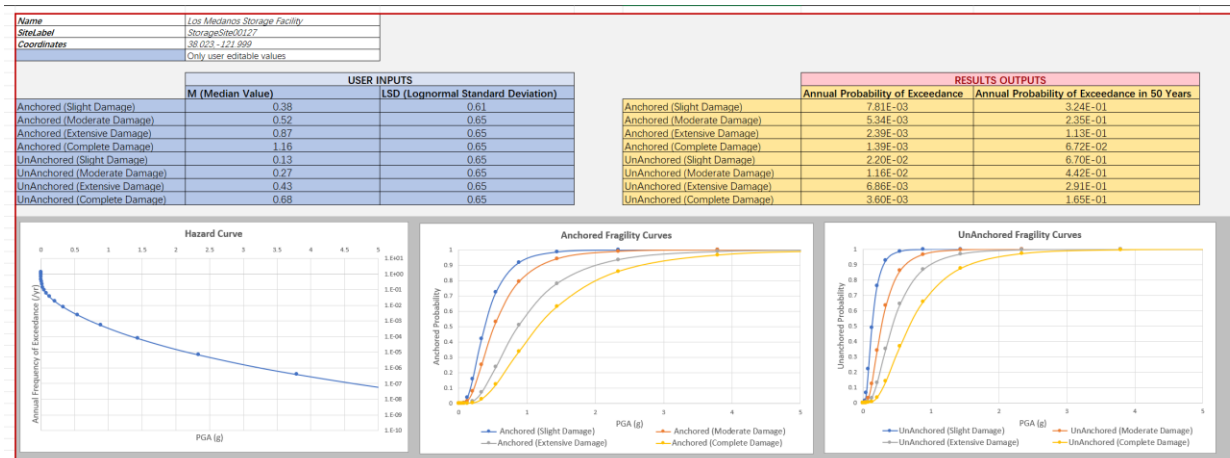


Figure 150 Pleasant Creek Results



Figure 151 Gill Ranch Results

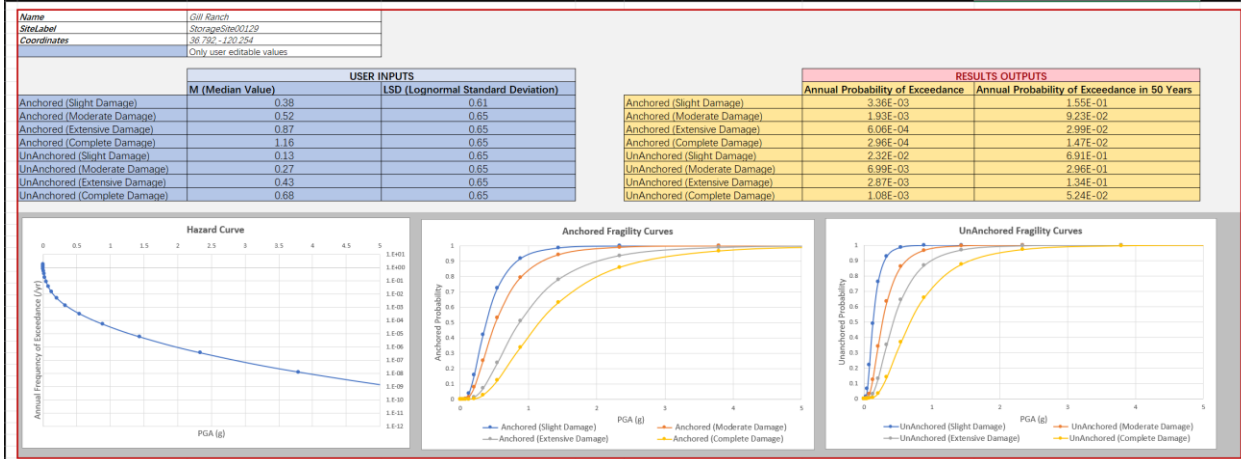


Figure 152 Kirby Hills Results

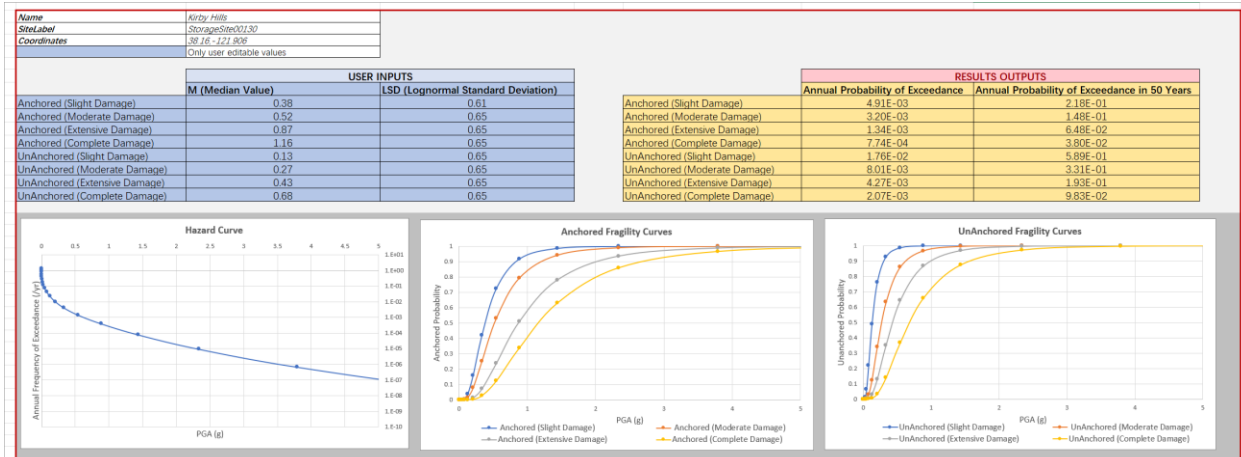


Figure 153 Lodi Storage Results



Figure 154 Central Valley Gas Storage Results

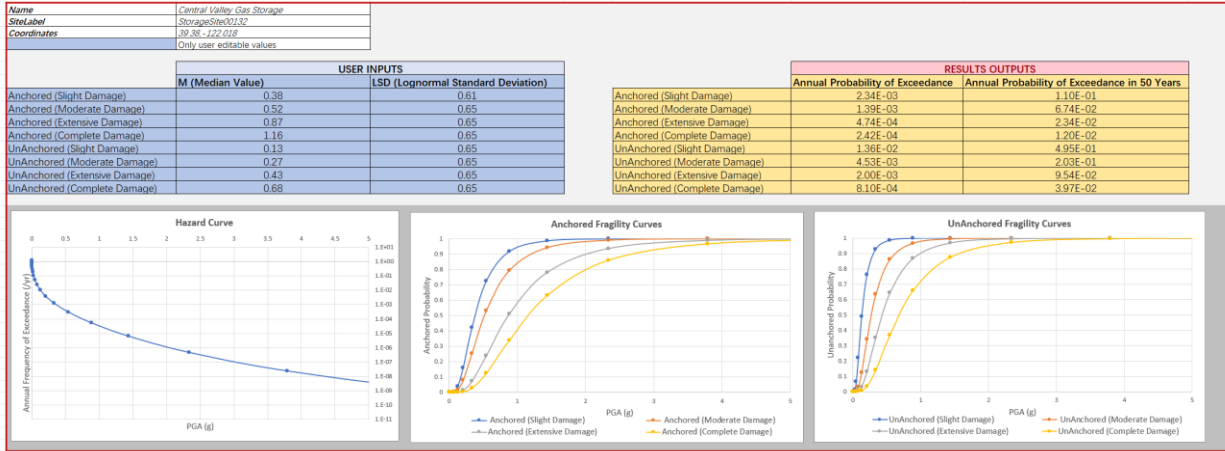
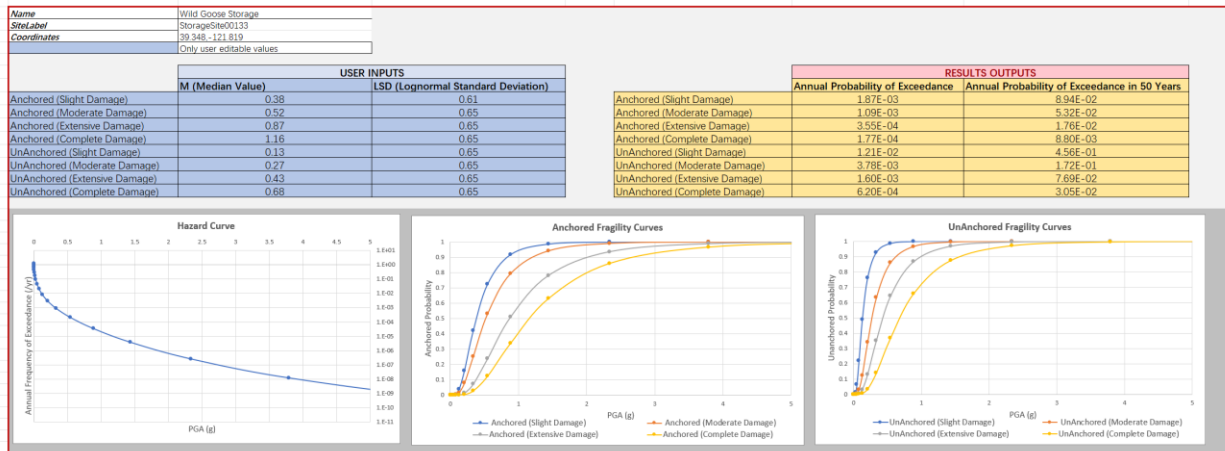


Figure 155 Wild Goose Storage Results



12 Acronyms

CPT	conditional probability table
FEA	finite element analysis
K_o	horizontal pressure coefficient
kip	1000 pounds-force
NPS	nominal pipe size
pcf	pounds per cubic foot
PGA	peak ground acceleration
PGV	peak ground velocity
PRCI	Pipeline Research Council International, Inc.
psf	pounds per square foot
SFA	friction angle
SSS	soil shear strength (SSS)
ϕ	interface friction factor
σ	standard deviation
R	total displacement
θ_v	generic vertical angle
θ_H	generic horizontal angle
ϕ	fault strike angle
δ	fault dip angle
λ	fault rake angle

13 References

- Ayello, F., Jain, S., Sridhar, N., Koch, G., “Quantitative Assessment of Corrosion Probability - A Bayesian Network Approach”. *Corrosion*. 2014; 70(11):1128-1147.
- Daiyan, N., Kenny, S., Phillips, R., and Popescu, R., 2010. “Numerical Investigation of Oblique Pipeline/Soil Interaction in Sand,” *Proceedings of the 8th International Pipeline Conference, IPC 2010*, American Society of Mechanical Engineers.
- Der Kiureghian, A., 2022. *Structural and System Reliability*, Cambridge University Press.
- Dorey, A.B., Cheng, J.J.R. and Murray, D.W., 2001. “Critical Buckling Strains for Energy Pipelines,” *Structural Engineering Report 237*, Department of Civil Engineering, University of Alberta, Canada.
- Honegger, D.G., Wijewickreme, D., and Monroy, M., 2011. “Phase II Assessment of Geosynthetic Fabrics to Reduce Soil Loads on Buried Pipelines,” *PRCI Catalog No. L52325*, Pipeline Research Council International, Inc., Chantilly, VA, 81 pgs.
- Hsu, T-W, Chen, Y-J, and Hung, W-C, 2001. “Soil Restraint of Oblique Pipelines in Loose Sand,” *Journal of Transportation Engineering*, American Society of Civil Engineers, Vol. 127, No. 1.
- Hsu, T-W, Chen, Y-J, and Hung, W-C, 2006. “Soil Restraint to Oblique Movement of Buried Pipes in Dense Sand,” *Journal of Transportation Engineering*, American Society of Civil Engineers, Vol. 132, No. 2.
- Honegger, D.G., and Nyman, D.J., 2017. *Pipeline Seismic Design and Assessment Guideline (2017 Revision)*, Pipeline Research Council International, Inc., Catalog No. L51927-R01, <https://www.prci.org/Research/DesignMaterialsConstruction/2774/ENV-5-1/4267/122225.aspx>.
- Mohareb, M.E., Elwi, A.E., Kulak, G.L. and Murray, D.W., 1994. “Deformational Behavior of Line Pipe,” *Structural Engineering Report 202*, Department of Civil Engineering, University of Alberta, Canada.
- PRCI, 2009, “Guidelines for Constructing Natural Gas and Liquid Hydrocarbon Pipelines in Areas Subject to Landslide and Subsidence Hazards,” report prepared by D.G. Honegger Consulting, C-CORE, and SSD, Inc., Catalog No. L52292.
- Wang, Y.Y., Liu, M, and Song, Y., 2011, "Second Generation Models for Strain-Based Design," *PRCI Catalog No. PR-334-064509-Z01*, August 02, 180 pgs.
- Wang, P., Al Atik, L., Gregor, N., Kuehn, N., Walling, M. A., Kottke, A. R., Liu, Z., Zimmaro, P., Bozorgnia, Y., Brandenburg, S. J., & Stewart, J. P. “Hazard-Consistent Scenario-Based

Correlated Ground Motions for California Gas Pipeline Infrastructure.” GIRS Reports. Squarespace. <https://girs.squarespace.com/girs-reports/2023/02>

Yoosef-Ghodsi, N., Kulak, G.L. and Murray, D.W., 1994. “Behavior of Girth-Welded Line Pipe,” Structural Engineering Report 203, Department of Civil Engineering, University of Alberta, Canada.

Zimmerman, T.J.E, Stephens, M.J., DeGreer, D.D. and Chen, Q., 1995. “Compressive Strain Limits for Buried Pipelines,” Proceedings of the 1995 Offshore Mechanics and Arctic Engineering Conference, American Society of Mechanical Engineers, Volume V, pp. 365-378.

Zhou, H, Wang, Y, Stephens, M, Bergman, J, & Nanney, S. "Tensile and Compressive Strain Capacity in the Presence of Corrosion Anomalies." Proceedings of the 2018 12th International Pipeline Conference. Volume 2: Pipeline Safety Management Systems; Project Management, Design, Construction, and Environmental Issues; Strain Based Design; Risk and Reliability; Northern Offshore and Production Pipelines. Calgary, Alberta, Canada. September 24–28, 2018.

APPENDIX A: Pressure Integrity Strain Capacity Formulation

Pressure Integrity Tensile Strain Capacity is ε

$$\varepsilon_t = \min(\varepsilon_u, P(f_p), G(t)\varepsilon_{t,f_p})$$

$$G(t) = \left(\frac{15.9}{t}\right)^{0.8096} \left[1 + 1.503\left(\frac{h}{t}\right)^{1.229}\right]$$

$$f_p = \frac{PD}{2t\sigma_y}$$

$$P(f_p) = P_{\max} - \frac{5f_p}{3}(P_{\max} - 1) \quad \text{if } 0 < f_p < 0.6$$

$$P(f_p) = 1 \quad \text{if } 0.6 \leq f_p < 0.8$$

$$P_{\max} = 2.25 - 2\frac{a}{t}$$

$$\varepsilon_{t,f_p} = A \frac{f(\delta_A)}{1 + f(\delta_A)}$$

$$f(\delta_A) = (C\delta_A)^{B(\delta_A)^D}$$

Formulas for Gas Metal Arc Welded (GMAW) Joints

$$A = a_1 e^{\frac{a_2}{\beta}} e^{-\frac{a_3 \eta \beta e^{-\frac{a_4}{\beta}}}{\beta}} \left[1 + a_5 \psi^{a_6} + a_7 \psi (\eta \beta)^{a_8}\right] \left(1 + a_9 \xi^{a_{10}} \phi^{a_{11}} + a_{12} \psi^{a_{13}} \xi^{a_{14}}\right)$$

$$B = \beta^{b_1} \eta^{\frac{b_2 \beta^{\frac{b_3}{\eta}}}{\eta}} \left[b_4 \phi^{b_5} (b_6 \phi^{b_7})^{\xi} + b_8 \psi^{b_9}\right]$$

$$C = e^{\frac{c_1}{\beta}} e^{\frac{c_2 \beta}{(1+c_3 \beta) \eta}} \left(1 + c_4 \psi^{c_5} + c_6 \psi e^{-\eta} + c_7 \psi e^{-\beta}\right) (c_8 + c_9 \phi^{c_{10}} + c_{11} \xi^{c_{12}} \phi)$$

$$D = d_1 \beta^{d_2} \eta^{\frac{d_3 \beta}{(1+d_4 \beta) \eta}} \left(1 + d_5 \psi^{d_6}\right) \left(1 + d_7 \xi^{d_8} + d_9 \phi^{d_{10}}\right)$$

Formulas for Flux-Cored Arc Welded (FCAW) and Shielded Metal Arc Welded (SMAW) Joints

$$A = a_1 e^{\frac{a_2}{\beta}} e^{-\frac{a_3 \eta \beta e^{-\frac{a_4}{\beta}}}{\beta}} \left[1 + a_5 \psi^{a_6} + a_7 \psi^{a_8} (\eta \beta)^{a_9}\right] \left(1 + a_{10} \xi^{a_{11}} \phi^{a_{12}}\right)$$

$$B = \beta^{b_1} \eta^{\frac{b_2 \beta^{\frac{b_3}{\eta}}}{\eta}} \left[b_4 \phi^{b_5} (b_6 \phi^{b_7})^{\xi} + b_8 \psi^{b_9}\right]$$

$$C = e^{\frac{c_1}{\beta}} e^{\frac{c_2 \beta}{(1+c_3 \beta) \eta}} \left(1 + c_4 \psi^{c_5} + c_6 \psi e^{-\eta} + c_7 \psi e^{-\beta}\right) (c_8 + c_9 \phi^{c_{10}} + c_{11} \xi^{c_{12}} \phi)$$

$$D = d_1 \beta^{d_2} \eta^{d_3} \left(1 + d_4 \psi^{d_5} + d_6 \mu \beta \psi\right) \left(1 + d_7 \xi^{d_8} + d_9 \phi^{d_{10}}\right)$$

Coefficients for Tensile Strain Capacity for GMAW Joints

a1	2.084E+00	b1	-5.005E-02	c1	1.409E+00	d1	2.209E-02
a2	2.812E-01	b2	-5.139E-03	c2	2.345E-01	d2	1.156E+00
a3	-4.950E-01	b3	4.485E-01	c3	1.125E+00	d3	1.601E+00
a4	7.373E-01	b4	1.417E+00	c4	4.181E+00	d4	8.964E-01
a5	-5.005E+00	b5	2.217E+00	c5	1.201E+00	d5	1.383E+00
a6	1.186E+00	b6	1.029E+00	c6	-5.384E+00	d6	1.333E+00
a7	1.644E+00	b7	-2.598E+00	c7	2.406E+00	d7	9.313E-02
a8	7.374E-01	b8	-2.679E+00	c8	-2.154E-01	d8	-2.240E+00
a9	-9.829E-01	b9	1.694E+00	c9	-5.237E-03	d9	8.559E+00
a10	8.655E-02			c10	9.889E+00	d10	-3.719E+00
a11	-1.029E-01			c11	3.547E-01		
a12	-1.500E-01			c12	-7.513E-01		
a13	1.025E+00						
a14	5.557E+00						

Coefficients for FCAW and SMAW Joints

a1	9.281E-01	b1	-5.578E-02	c1	1.609E+00	d1	6.822E-03
a2	9.573E-02	b2	1.112E-02	c2	1.138E-01	d2	1.014E+00
a3	-5.053E-01	b3	-1.735E-01	c3	6.729E-01	d3	1.746E+00
a4	3.718E-01	b4	1.675E+00	c4	2.357E+00	d4	2.378E+00
a5	-2.023E+00	b5	2.603E-01	c5	1.057E+00	d5	9.434E-01
a6	7.585E-01	b6	1.106E+00	c6	-4.444E+00	d6	-1.243E+00
a7	6.299E-01	b7	-1.073E+00	c7	1.727E-02	d7	3.579E+01
a8	5.168E-01	b8	-1.519E+00	c8	-1.354E-02	d8	7.500E+00
a9	7.168E-01	b9	1.965E+00	c9	-1.224E-02	d9	6.294E+01
a10	-9.815E-01			c10	8.128E+00	d10	-6.930E+00
a11	2.909E-01			c11	2.007E-01		
a12	-3.141E-01			c12	-1.594E+00		

$$\eta = a/t$$

$$\beta = 2c/t$$

$$\psi = h/t$$

$$\xi = \sigma_y / \sigma_u$$

$$\phi = \sigma_{uw} / \sigma_u$$

t is the pipe wall thickness (valid range 12.7 mm – 25.4 mm)

D is the pipe diameter (recommended range 12” – 48”)

P is the internal pressure

f_p is the ratio of hoop stress to tensile yield strength (valid range 0.0 – 0.8)

a is the flaw depth

$2c$ is the flaw length

β is the normalized flaw length (valid range 1.0 – 20.0)

ϵ_u is the maximum allowable (ultimate) tensile strain capacity

δ_a is the apparent crack tip opening displacement (valid range 0.2 mm – 2.5 mm)

η is the normalized flaw depth (valid range 0.05 – 0.5)

ψ is the normalized girth weld high-low misalignment (valid range 0.0 – 0.2)

σ_y is the tensile yield strength of the pipe metal (recommended range is 56 ksi – 100 ksi)

σ_u is the tensile ultimate strength of the pipe metal

σ_{uw} is the tensile ultimate strength of the weld metal

ξ is the base metal ratio of yield tensile strength to ultimate tensile strength (valid range 0.75 – 0.94)

ϕ is the ratio of ultimate weld metal tensile strength to base metal ultimate tensile strength (valid range 1.0 – 1.3)

Reference

Wang, Y.-Y., Liu, M, and Song, Y., 2011, Second Generation Models for Strain-Based Design,” final report to US DOT PHMSA, US DOT Contract No. DTPH56-06-T000014, <http://primis.phmsa.dot.gov/matrix/PrjHome.rdm?prj=201>.